Investigation of Potentially Toxic Elements in Selected Water Bodies in Limpopo Province: Transport, Fate and Risk Assessment, and Detection and Remediation Method Development

Report
to the Water Research Commission

by

Abayneh Ataro Ambushe, Pertunia Ramolwetsi Dikotla, Lutendo Francis Mashavha, Bennett Siphiwe Dintsi, Sifelani Dube, Vincent Masilela, Dipuo Precious Kgabi and Messai Adenew Mamo
Department of Chemical Sciences, University of Johannesburg

WRC report no. 3228/1/25
ISBN 978-0-6392-0735-3

September 2025

WATER
RESEARCH
COMMISSION

This is the final report of WRC project no. C2022/2023-00933.

EXECUTIVE SUMMARY

The alarming deterioration rate of the water quality due to pollution causes a severe global health concern to both the ecosystem and humans. One such concern is contamination of water by potentially toxic elements (PTEs), which is the most pressing environmental problem in society resulting from industrialisation. Industrial activities lead to the generation of considerable quantities of wastewater containing PTEs such as arsenic (As), cadmium (Cd), chromium (Cr), copper (Cu), lead (Pb), mercury (Hg), nickel (Ni) and vanadium (V). The information about the levels of As, Cr and Hg species, and other PTEs such as Cd, Cu, Pb, Ni and V in water bodies and their transport, and fate is important for risk assessment. In this project, PTEs and their species in water, sediment, soil, and vegetables were determined to assess the associated risks to humans *via the* food chain. The total concentrations of these selected PTEs in water and vegetable samples were quantified by inductively coupled plasma-mass spectrometry (ICP-MS). Whereas the concentrations of selected PTEs in sediment and soil samples were quantified by inductively coupled plasma-optical emission spectrometry (ICP-OES). The accuracy of the methods was confirmed by analysing standard reference materials (SRMs) of appropriate sample matrices. Total concentrations of PTEs in water were within the maximum permissible limits (MPLs) stipulated by the guidelines. The concentrations of Cd, Pb, and Hg in sediment surpassed the probable effect limit (PEL) stipulated by the Canadian Council of Ministries of the Environment (CCME) during both low and high flow seasons and this suggested adequate biological effects in aquatic organisms and the food chain. Total concentrations of Cd and Cr in all the soil used for cropping as well as of Cu in some soil (farm 1 site 2 onion, farm 1 site 3 chomolia, farm 1 site 3 pumpkin and farm 3 site 1 covi) surpassed the SQG values during the high flow season. This was attributed to the use of manure and organic fertilizers to improve the fertility of the soil used for cropping at farms 1, 2 and 3. High concentrations of As, Cr, Cd, Pb, and V that surpassed the MPLs stipulated by the WHO and Food and Agriculture Organization (FAO) were detected in vegetable samples during the low flow season. Whereas high concentrations of As, Cr, Cu, Pb, Ni and V that surpassed the maximum MPLs stipulated by WHO/FAO were detected in vegetable samples during the high flow season. The human health risk assessment (HHRA) data revealed that both the health of adults and children in Lephalale who consume these contaminated vegetables are threatened since calculated hazard index (HI) values exceed 1. The speciation analysis of Cr and As was performed using high-performance liquid chromatography hyphenated to inductively coupled plasma-mass spectrometry (HPLC-ICP-MS). The consumption of some vegetables, particularly by children, could cause serious health risks as the THQ > 10 was observed for some vegetables contaminated with Cr. The incremental lifetime cancer risk (ILCR) threshold of 1×10^{-4} was exceeded, indicating that the overall consumption of vegetables had high cancer risks for adults and children. This study suggests that the consumption of vegetable samples would lead to health risks in the population.

Water, sediment, soil, and vegetable samples were collected from Steelpoort area and analysed to determine the levels of PTEs. The levels of PTEs in most water samples, including those from the Steelpoort River and some samples from boreholes, were below the MPLs set by the WHO and South African National Standards (SANS). However, levels of PTEs in sediments exceeded probable effect limits (PEL) and probable effect concentrations (PEC) stipulated by American and Canadian SQGs, except for Ni during the high flow season. The elevated concentrations above the threshold of SQGs suggested frequent biological effects in aquatic organisms and consequently *via the* food chain. The PTEs in vegetables exceeded WHO/FAO limits. Hazard quotient (HQ) and hazard index (HI) values indicated that Cr in water exceeded safety thresholds for children

(HQ = 1.70) and adults (HQ = 1.12) during the low flow season, with HI = 1.60 and Cr in vegetables exceeded safety thresholds for Children (HQ = 140) and adults (30). The HQ trend of borehole water during the low flow season followed this order: Cr > V > As > Ni > Pb > Cd > Cu > Hg and for the high flow season, the order was Cr > V > As > Hg > Pb > Ni > Cu > Cd. The HI values for both seasons followed a similar trend, with the risks being higher during the low flow season. Long-term exposure to contaminated vegetables could pose non-carcinogenic health risks to both adults and children.

Ion imprinting technology attracted our interest to synthesise low-cost ion-imprinted polymers (IIPs) fabricated sensors for chemo-resistive detection of toxic metal ions using an electronic device that measures impedance (L), capacitance (C), and resistance (R) (LCR meter) of the sensing material. The fabricated chemo-resistive sensor has been developed with remarkable re-binding cavities predetermined by the memory effect upon removing the template ion in the polymeric matrix. A significant contribution of the sensor detection is based on the novel application of IIP-reduced graphene oxide (rGO) (IIP-rGO) based chemo-resistive sensors for the detection of metal ions in water using an LCR meter. The synthetic procedure of IIPs, IIP:rGO mass ratio performance, stability, reusability, and selectivity of fabricated sensors were thoroughly investigated and optimised to develop a rapid response fabricated sensor for the detection of the selected metal ions in water. A chemoresistance-based sensor for detecting Cd(II) using a hybrid material of rGO and IIP was developed. Various rGO to IIP ratios were investigated to balance conductivity and ion recognition capabilities, with the 1:3 (IIP:rGO) configuration showing the highest sensitivity and wide dynamic range across analyte concentrations. The sensor exhibited rapid response times and sensitivity (1.765 µg/L), excellent reproducibility, and a strong linear response up to 600 µg/L with a LOD = 0.704 µg/L, validating its applicability for ultra-trace level detection. Percentage recoveries of 91.6% to 105% in real water samples confirmed the accuracy of the method. Therefore, the results highlight the effectiveness of combining rGO's conductive properties with IIP's selective recognition to create a scalable, versatile sensor for environmental and analytical applications.

This study further aimed to investigate agricultural byproducts, such as sugarcane bagasse and orange peels as adsorbents for de-contamination of PTEs in water and wastewater and assess bio-reactive organoclays for transformation of toxic elemental species into less toxic ones. The potential of low-cost and reusable bio-sorbents: calcined orange peels (OPs) and sugarcane bagasse (SCB) for the removal of Ni(II) and Cd(II) from simulated aqueous solutions and real wastewater was investigated. Batch bio-sorption studies were conducted under various experimental conditions to optimise the removal efficiency (RE) of calcined OPs, SCB, and OPs: SCB composite. The solid: liquid ratio of 0.1:100 (0.1 g/100 mL – w/v ratio) was applied at a stirring rate of 200 rpm for contact time ranging from 10 to 300 minutes, and the results revealed that calcined OPs could remove over 98% of 20 mg/L Ni(II) and 20 mg/L Cd(II) at an optimum contact time of between 60 and 90 minutes, while calcined SCB could remove over 97% at an optimum contact time of 120 minutes. The OPs: SCB composite were able to remove over 92% of Ni(II) and Cd(II) at a 5:5 ratio at an optimum contact time between 60 and 120 minutes. The corresponding adsorption capacities for Ni in AMD water were 32 mg/g for calcined OPs, 26.5 mg/g for calcined SCB, and 30.6 mg/g for the composite, while for Cd, the adsorption capacities were 40 mg/g for calcined OPs and 20 mg/g for both calcined SCB and their composite.

This work also focused on the removal of Pb(II) from aqueous solution using kaolin and bentonite clays modified with hexadecyl trimethyl ammonium bromide (HDTMA). The clays were characterized using a zetasizer, scanning electron microscopy (SEM), powder X-ray diffraction (PXRD), Brunauer-Emmet-Teller (BET), Fourier-transform infrared (FTIR) spectroscopy and thermal gravimetric analysis (TGA). Factors that

influence the adsorption of Pb(II) from aqueous solution, namely pH, contact time, adsorbent mass, ionic strength, temperature and initial Pb(II) concentration were investigated. The results show that HDTMA was successfully incorporated into the kaolin and bentonite clay structures. The most favorable parameters for the adsorption of Pb(II) ions onto all adsorbents was pH of 6.0, temperature of 25 °C and adsorbent mass of 200 mg. Maximum adsorption capacity of organobentonite was 18.75 mg/g, which is higher than that obtained for the unmodified bentonite (14.71 mg/g); while for organokaolin it was 2.26 mg/g, which is less than that of the unmodified kaolin (4.19 mg/g). The adsorbents also revealed good removal efficiency for up to four regeneration cycles.

ACKNOWLEDGEMENTS

The project team wishes to thank the following people for their contributions to the project.

Reference Group	Affiliation
Dr Eunice Ubomba-Jaswa	Water Research Commission (Chairperson)
Dr Bridget Shaddock	WSP Africa Pty Ltd
Prof Olatunde Olatunji	University of KwaZulu-Natal
Prof Ntebogeng Mokgalaka-Fleischmann	Tshwane University of Technology
Ms Penny Jaca	Water Research Commission (Project Administrator)

CONTENTS

LIST OF FIGURES

LIST OF TABLES

ACRONYMS & ABBREVIATIONS

AAS	Atomic absorption spectrometry
BOD	Biological oxygen demand
CSF	Cancer slope factor
COD	Chemical oxygen demand
DMA	Dimethylarsinic acid
DOM	Dissolved organic matter
DO	Dissolved oxygen
EDI	Estimated daily intake dose
HHRA	Human health risk assessment
HPLC-ICP-MS	High-performance liquid chromatography–inductively coupled plasma–mass spectrometry
LCR	Impedance, capacitance, and resistance
ILCR	Incremental Lifetime Cancer Risk
ICP-MS	Inductively coupled plasma-mass spectrometry
ICP-OES	Inductively coupled plasma–optical emission spectrometry
IARC	International Agency for Research on Cancer
IUPAC	International Union of Pure and Applied Chemistry
IIP	Ion-imprinted polymer
MIP	Molecularly imprinted polymer
MIT	Molecular imprinting technology
MMA	Monomethylarsonic acid
NIP	Non-imprinted polymer
PTEs	Potentially toxic elements
THQ	Target hazard quotient
TOC	Total organic carbon
TMAO	Trimethylarsine oxide
TUI	Tolerable upper intake
WRC	Water Research Commission
WHO	World Health Organisation

CHAPTER 1: BACKGROUND

1.1 INTRODUCTION

The scarcity and pollution of water remain two of the most significant challenges in the 21st century. In South Africa, particularly, the deterioration of water quality due to water pollution places stress on the availability of potable water (Letsoalo et al., 2018). South Africa is a water scarce country, and with the current urbanisation and industrialisation growth, water demand is likely to exceed supply in the near future (Ochieng et al., 2010). Although industrial developments have substantially contributed to the growth of the economy, such activities have resulted in severe environmental pollution, of which contamination of water by the potentially toxic elements (PTEs) is of the utmost concern. Global climate change has also contributed to the growing water crisis since the rain that usually supplies the water has become sporadic. Due to a shortage of potable water supply, groundwater has been the most reliable water supply option for meeting the daily water needs of rural communities in South Africa. This is partly due to the fact that most rural communities are geographically located in hard-to-reach areas due to their dispersed nature and bad terrain (Nkuna et al., 2017). These conditions have made it particularly expensive and difficult for water service providers to provide services to rural communities. Such communities have no option but to rely on hand-dug wells and springs for their daily water needs (Nkuna et al., 2017). Rural communities regard springs as a sustainable and reliable means of obtaining water compared to a formal water supply from the relevant service providers. In Sub-Saharan Africa, groundwater is the most appropriate and commonly used source of drinking water for many rural communities (Gitari et al., 2015). However, groundwater is becoming increasingly contaminated because of natural and anthropogenic activities (Obijole et al., 2019). The communities in rural areas rely on these sources without knowing the imposed effects of PTEs in these systems because of no physical alteration of water by some of the toxic elements (Kumar and Riyazuddin, 2010; Nkuna et al., 2017). The anthropogenic activities, such as industrial activities, mining, and power stations, which operate in the proximity of rural communities and rivers, elevate the levels of PTEs in the aquatic ecosystem and the environment.

A large quantity of PTEs associated with anthropogenic activities have been released into the atmosphere from where they can reach the soil environment and aquatic ecosystem through both dry and wet deposition processes (Constantine et al., 2014). Apart from soil environment and aquatic ecosystem, atmospheric inorganic contaminants of natural origin or anthropogenic sources that contained PTEs such as arsenic (As), cadmium (Cd), chromium (Cr), copper (Cu), lead (Pb), mercury (Hg), nickel (Ni) and vanadium (V) at high concentrations could lead to serious ecological consequences and pose human health risks (Neeti and Prakash, 2013). The PTEs are hazardous to humans and various ecological receptors because of their toxicity, persistence, bio-accumulative and non-biodegradable nature. Therefore, monitoring, evaluation of their transportation and fate in the environment as well as removal of PTEs in water are imperative to identify hazards to human health to prevent bioaccumulation in the food chain and further degradation of the ecosystem.

Waste generated from mining and industrial activities are a major concern. This waste may contain high levels of PTEs that may have an adverse effect on humans and animals living in the vicinity or downstream of the contaminated site. The presence of PTEs in water bodies has been a source of worry to

environmentalists, government agencies and health practitioners. With the deterioration of water quality, humans are at an increasing risk of exposure to PTEs.

Water pollution requires ongoing monitoring of pollutants. Water contamination occurs when pollutants are discharged directly or indirectly into water bodies without adequate treatment to remove harmful compounds. Pollution of water affects plants, fish, and other organisms in water bodies. The effect damages the natural biological communities. The contamination of water by PTEs poses a serious concern to public health and is a serious environmental problem.

The PTEs in the environment could contaminate different environmental compartments. These include water used for human consumption and irrigation, sediment, fish, soil and crops (Dokou et al., 2016). Potentially toxic elements in the environment can seriously affect human health *via* the food chain. Thus, understanding the transport and fate of PTEs and their species in the biota is vital to conducting the risk assessment. The accumulation of PTEs in the kidney and liver of humans leads to cardiovascular, nervous, kidney and bone diseases, whereas in plants, the accumulation may lead to biochemical pathway disorders mostly related to photosynthesis (Reboredo et al., 2019).

1.2 TRANSFER OF POTENTIALLY TOXIC ELEMENTS THROUGH THE FOOD CHAIN

In aquatic food webs, the food chain is regarded as a major pathway for the transfer of PTEs through biological interrelationships, such as prey relationships, namely, the toxic element in water bodies is absorbed and accumulated into organisms. Then, the organism is eaten by its predator, which could result in the transfer of the toxic element into the predator. Subsequently, the toxic element is transferred into a final predator, including humans (Wang et al., 2018). The toxic elements ingested by humans lead to insidious biological effects that indirectly affect health and disease risk (Bost and Sanchez, 2018).

Food is the main source of PTEs for humans. Among food types, vegetables are the most exposed food to environmental pollution due to the aerial burden. Vegetables take up PTEs and accumulate them in different parts at concentrations high enough to cause clinical problems to both animals and human beings (Jolly et al., 2013). Fresh vegetables are very imperative because they include vitamins, minerals and other components that promote healthier eating and help to prevent different diseases (Shaheen et al., 2016). Nonetheless, essential and non-essential elements may be present in vegetables. The concentrations of PTEs in vegetables are influenced by pollution in the environment, seasonal variation, and the composition of soil (Scott et al., 1996; Shaheen et al., 2016). The transfer of PTEs from soil to vegetables is very imperative in their distribution along the food chain trophic levels. Vegetables take up PTEs from soils that are polluted, and they are then passed along the food chain to humans, who consume these plants (Alloway, 2013). It has been reported that increased levels of Cd and Pb are found in vegetables that are irrigated with wastewater compared to those irrigated with groundwater (Nica et al., 2012). It has also been reported that leafy vegetables such as spinach have higher concentrations of these metals compared to stem vegetables such as tubers, because leafy vegetables have high abilities to uptake and accumulate PTEs (Nica et al., 2012). Thus, ingestion of vegetables contaminated with PTEs may expose humans to serious health risks.

1.3 HEALTH RISKS CAUSED BY POTENTIALLY TOXIC ELEMENTS

Currently, the health risk assessment associated with contamination of PTEs has become one of the hot topics globally due to increasing public awareness of health risks posed by PTEs. Prolonged consumption of high concentrations of PTEs *via* contaminated food may cause chronic PTEs accumulation in humans' liver, kidney, and bones, resulting in kidney, cardiovascular, nervous, and bone diseases (Anwar et al., 2016; Gupta et al., 2022). The accumulation of PTEs in vegetables poses long-term risks to the ecosystem and human health (Khairiah et al., 2006). The PTEs, like Pb, are known to be carcinogenic and their accumulation in edible vegetables poses long-term risks to the ecosystem and human health. High Pb and Cd concentrations in food have been linked to the development of gastrointestinal cancer (Sharma et al., 2008). Most significantly, unveiling the health risk of the PTEs is important in children, who are more prone to PTEs toxicity than adults.

1.4 HEALTH RISK ASSESSMENT

The human health risk assessment (HHRA) is a tool that involves an estimation of the nature and the adverse health effects in populations that may be exposed to environmental media contaminated with chemicals (Li et al., 2014; Oosthuizen et al., 2015). Scientific data is evaluated to yield a scientific basis that can be utilized to reduce chemical risks brought upon the environment or human health (Beronius and Vandenberg, 2015). Therefore, it is considered to be the crucial initial step in assessing the need for risk management strategy developments or the need for a regulation to be introduced (Rasheed et al., 2016). The HHRA has been popularly conducted to identify hazards towards the labour force, consumers and the general public who may be exposed to different kinds of potential hazards in the workplace, by consuming products containing potential hazards or by hazards released in the environment (Gentry et al., 2017).

The HHRA comprises three parts: hazard assessment, exposure assessment, and risk characterization. The hazard assessment involves reviewing toxicological data to identify the adverse effects that could result from the compound. It also characterizes the dosage response and concludes a safe dose by calculating a human reference dose. The exposure assessment determines the sources of exposure to a certain compound. It estimates the exposure levels in populations such as certain workers, a certain age group or the general population. The risk characterization step combines the outcomes of the hazard and exposure assessments in order to draw conclusions concerning the risk, e.g., if the determined safe dosage is exceeded by the estimated exposure (Beronius and Vandenberg, 2015).

The HHRA involving chemicals can be qualitative or quantitative. The assessment can be utilized to evaluate exposures from the past, present, and future. These exposures include chemicals present in food, water, consumer products, soil, air and other materials. It is used to identify high risks that result from chemical exposures; to assess risks of drinking water; to assess a chemical spillage; to assess old hazardous sites to see if contaminated soil needs to be cleaned before the development of property; to impose limits on chemical exposures in occupational environments, environmental media, food and consumer products; and to limit chemical emissions from various human activities such as agricultural and industrial (WHO, 2010).

1.5 HEALTH RISK ASSESSMENT MODELING AND INDICES

There are several exposure pathways associated with the PTEs, primarily dependent on pollution media such as water, soil, air, food, and the exposed population. However, among these pathways, exposure *via* vegetable consumption and drinking contaminated water is critical for PTEs entering the human body (Hoaghia et al., 2022; Muchuweti et al., 2006; Caussy et al., 2003). The human health effects of PTEs ingestion through vegetable consumption are divided into carcinogenic and non-carcinogenic health effects.

The most applied HHRA method is based on the evaluation of non-carcinogenic effects, particularly by estimation of the target hazard quotient (THQ). The THQ is not only limited to the metal intake parameter but also includes other parameters such as exposure duration, exposure frequency, oral reference doses and body weight (Manea et al., 2020). The method of estimating risk by calculating THQ based on the following equation (Amwele et al., 2017).

$$TTTTTT = \frac{FF_{IIII} \times EE_{F\,F} \times EE_{DD} \times CC}{RRRRRR \times AAAAAA \times AA_{TT}} \qquad \text{Equation 1}$$

Where E_F is the frequency of exposure or the number of exposure events per year of exposure (365 days/ year for adults and 350 days/year for children), E_D is the duration of the exposure (30 years for adults and 6 years for children) which is equivalent to the average lifetime (Manea et al., 2020; Dadar et al.; 2017: Fakhri et al., 2017); F_{IR} is the rate of food ingestion (114.77 g/person/day), C is concentration of element in vegetables, RfD is the oral reference dose (for example: 0.0003 mg/kg/day for As and 0.003 mg/kg/day for Cr) which is defined as the daily oral exposure to a substance that will not result in any harmful effect in a life time for a given population; ABW is the average body weight (for South Africa ABW is 68.1 kg for adults and 13.8 kg for children), and A_T is the average exposure time for non-carcinogens (365 days/year× number of exposure years (10950 days for adults and 2190 days for children)) (Manea et al., 2020; Fakhri et al., 2017).

The level of non-carcinogenic health risks can be evaluated using the calculated THQ values. The THQ < 1 reveals that the exposed population is safe (Manea et al., 2020) or is not under potential health risk (Fakhri et al., 2017). Whereas, THQ > 1 indicates potential health risks, and THQ > 10 indicates a serious chronic health risk (Fakhri et al., 2017).

The carcinogenic risk assessment is regarded as the probability of an individual developing any kind of cancer in their lifetime due to exposure to carcinogenic hazards (Sun et al., 2017). The carcinogenic risk assessment is determined using the Incremental Lifetime Cancer Risk (ILCR) (Sharafi et al., 2019), as shown by equation 2.

$$IIIIIIII = EEEEII \times IICCCC \qquad \text{Equation 1}$$

where EDI is the estimated daily intake (mg/kg/day).

The CSF is the cancer slope factor (mg/kg/day) (Sharafi et al., 2019. For example, CSF for As is 1.5 mg/kg-day (Rockafellow-Baldoni et al., 2018), whereas for Cr, the CSF is 0.5 mg/kg-day (Sharma, 2020; Onyedikachi et al., 2019). The tolerable or acceptable carcinogenic risk ranges between 10^{-6} to 10^{-4}; whereby if ILCR < 10^{-6}, the cancer risks are negligible and denotes that 1 cancer case would occur per

1 000 000 population exposures, whereas an ILCR > 10^{-4} indicates that the risks are unacceptable by most international regulatory agencies and denotes that 1 cancer case would occur per 10 000 population exposures (Sharafi et al., 2019).

The daily intake of PTEs mainly depends on the concentration of PTEs in food and the quantity of regular food consumption (Antoniadis et al., 2019). Furthermore, human tolerance for particular PTEs may also depend on the person's body weight. The EDI of PTEs through vegetable consumption (mg/kg/day) can be calculated by using the following equation (Antoniadis et al., 2019).

$$EEEEII = \frac{FF_{IIII} \times EE_{FF} \times EE_{DD} \times CC}{AAAAAA \times AA_{TT}}$$ Equation 3

1.6 SPECIATION ANALYSIS OF SELECTED POTENTIALLY TOXIC ELEMENTS

According to the International Union of Pure and Applied Chemistry (IUPAC), chemical speciation is defined as the distribution of a specific form of an element amongst defined chemical species in a system (Kiss et al., 2017). Chemical species identification in various environmental matrices such as food, water, sediment, soil and air allows us to set a benchmark against ecosystem health based on the forms of chemical species present (Van Vuuren, 2014). The toxicity, bioavailability and transport properties of the elements depend on the specific form in which the element is present in the environment. Speciation of As, Cr and Hg is of particular interest because these elements exhibit acute toxicity at low concentrations (Jagtap and Maher, 2015). The inorganic As species are highly toxic, with As(III) being the most toxic of As species and a human carcinogen. The As(V) exhibits relatively high toxicity, whereas monomethylarsonic acid (MMA) and dimethylarsinic acid (DMA) are least toxic species and occur rarely because they are produced through activities of microbial metabolism (Chen et al., 2014; Schmidt et al., 2017). The Cr speciation is more complex with Cr(III) being a necessary nutrient for humans, and Cr(VI) reported as very mobile in the environment, carcinogenic and mutagenic (Markiewicz et al., 2015). The World Health Organisation (WHO) and International Agency for Research on Cancer (IARC) have classified As(III), As(V) and Cr(IV) as group 1 carcinogens and genotoxic species based on findings that these species may cause bladder, lung and skin cancers (IARC, 2004; WHO, 1996).

Exposure to Hg, even in very low concentrations, may cause serious health problems. Mercury has toxic effects on the nervous, digestive, and immune systems, as well as lungs, kidneys, skin, and eyes. Mercury is considered by the WHO as one of the top ten chemicals or groups of chemicals of major public health concern (Menon, 2016). The United States Comprehensive Environmental Response, Compensation, and Liability Act lists Hg and its species in third place on the "Priority List of Hazardous Substances" (Jagtap and Maher, 2015). The toxicity of Hg also depends upon its chemical form. Its organic form (methyl Hg) is more toxic than the inorganic form (Hg(II)) (Jagtap and Maher, 2015).

The strong affinity of Hg to natural particles allows this toxic metal to ultimately settle down and accumulate in sediments (Chakraborty et al., 2012). Thus, sediments act as a major sink for Hg and other PTEs. However, the polluted sediment can be a potential source of Hg in the aquatic environment (Randall & Chattopadhyay, 2013). Changes in the distribution and speciation of Hg in sediment can alter the bioavailability of Hg in the system. The inorganic Hg can accumulate in sediments where it can be converted into methyl Hg, which is generally considered to be the most concerning form of Hg due to its neurotoxicity to humans (Wang et al., 2012).

Speciation analysis has become an irreplaceable tool in human health risk assessment, environmental monitoring, or food quality control. For instance, a reliable assessment of human exposure to some elements requires knowledge of the chemical species in which they occur, their bioavailability and metabolic pathways in living organisms (Marcinkowska and Barałkiewicz, 2016). Due to significant differences in the biochemical properties of As, Cr and Hg species, there is an obvious need for their accurate quantification (Markiewicz et al., 2015). Relatively few studies have been conducted in South Africa dealing with the levels of PTEs, particularly their speciation in surface waters (Letsoalo et al., 2018). Limited reports dealing with the speciation of PTEs in South African rivers and a lack of information on transport and fates of PTEs and their species in water, sediment, soil, and biota make it difficult to assess the potential health risks associated with contaminated water. Thus, it is necessary to assess their transport accompanied by fates and chemical forms in water, sediment, soil, and biota.

The risk of contaminated sediment by PTEs is strongly related to their specific chemical fraction and binding state; thus, analysing the total concentration alone is insufficient. Furthermore, speciation analysis of PTEs in sediment is helpful to understand their source, mode of occurrence, mobility, and bioavailability related to the realistic risk assessment (Yang et al., 2014).

If not properly controlled, PTE pollution could pose serious challenges to the community, particularly in the mining areas. Frequent monitoring of the levels of PTEs and their sources will help in policy making and easy management of water bodies. This will also assist in preventing disasters and in saving lives. Therefore, the main objective of this project is to assess selected PTEs (As, Cd, Cr, Cu, Fe, Hg, Mn, Ni, Pb, V and Zn) and their species in water, sediment, soil and vegetables or edible crops collected from selected rivers in Limpopo Province, South Africa. Our previous Water Research Commission (WRC) funded project (K5/2515/1) results revealed that the concentrations of most of the selected PTEs, particularly in Blood River, exceeded the permissible limits of drinking water by the WHO. The high levels of PTEs in water and sediment samples, particularly from Blood River, show the impact of anthropogenic activities in the river. Furthermore, the findings showed the potential of high mobility of Cr, Cu, and Pb from sediments to water (Matabane et al., 2021). Thus, there is an increased possibility of risks of these PTEs to the biota and humans.

Accumulation of PTEs and their species in sediments threatens ecosystems due to the potential mobilisation of these species and their subsequent uptake into food webs. Thus, this study follows very well our previous successfully completed WRC-funded project (K5/2515/1) and focuses on assessing the transfer of PTEs to humans through the food chain since it is important to monitor the presence and effects of PTEs in the sediment/water-plant-animal-human chain. The impact of toxic elements on the aquatic system and potential health risks to humans will be investigated.

After successful completion of the WRC-funded project (K5/2515/1), we continued the project focusing on multi-elemental speciation of As and Cr in sediments and water using high-performance liquid chromatography–inductively coupled plasma–mass spectrometry (HPLC-ICP-MS), which substantially reduced analysis time, reagent consumption, and waste production (Letsoalo et al. 2021a; Letsoalo et al. 2021b). The speciation of Hg(II) and MeHg(I) in river sediments by HPLC-ICP-MS was also conducted (Kgabi and Ambushe, 2021). The hyphenated techniques have the advantages of exceptional sensitivity and selectivity for the separation and detection of elemental species in a single analytical run. However, instruments such as HPLC and ICP-MS are expensive techniques with high maintenance costs, labour-intensive, and require experienced personnel for operation. Therefore, developing an alternative detection technique for the quantification of toxic elemental species is necessary.

1.7 ION-IMPRINTED POLYMERS FOR DETECTION OF POTENTIALLY TOXIC ELEMENTS IN WATER

The recent advances in the development of nanotechnology and polymeric scientific areas have emerged as newly developed analytical techniques that attracted significant interest, counteracting conventional techniques (Cui et al., 2015). Molecular imprinting technology (MIT) has established procedures for synthesising molecular imprinted polymer (MIP) and ion-imprinted polymer (IIP) based on designing an artificial receptor macro porous three-dimensional polymeric network. The IIP inherits similar features as MIP except that IIP specifically recognises metal ions and is in the development stage, whereas MIP has been studied extensively. The MIPs have been used for various applications that include separation science, purification, recognition for peptides or biomolecules, sensors, biosensors, catalysis, and drug delivery (Branger et al., 2013; Kusumkar et al., 2021).

As an alternative detection technique for toxic elemental species, ionic imprinting technology attracted our interest to synthesise low-cost IIPs fabricated sensors for chemo-resistive detection of toxic metal ions using an electronic device that measures impedance (L), capacitance (C), and resistance (R) (LCR meter) of the sensing material. Ion/Molecularly imprinting technology is a technology that utilises the advantages of molecular lock to match a molecular key function to recognise a specific molecule ion or in a matrix. This can be achieved by synthesising ion or MIPs with tailor-made binding sites complementary to the template molecule or ion in specific size, shape, charge, and functional groups. Ion-imprinted polymer and MIP are used in various application areas, although they are most frequently used in the extraction of precious metals and as a stationary phase in chromatographic separation, they have been used in the detection of active molecules, pharmaceuticals, environmental pollutants, and toxic metal ions in sensors.

The high physical strength and resistance capability of the imprinted polymers to a variety of adverse conditions, such as high pressure, high temperature, and various chemicals (organic solvents, acids, and bases), can sustain the lifespan for several years (Wackerlig & Schirhagl, 2016). Moreover, they can be re-reusable without loss of selectivity and specificity with low production costs (Kibechu et al., 2014; Kusumkar et al., 2021). The large surface area embedded in the IIP matrix exhibits sufficient ionic recognition cavities per unit area, which is critical for binding the target analyte. In addition, their macro-porous structure allows the recognition of the target analyte diffusion during the binding and re-binding processes (Kibechu et al., 2014). The imprinted polymer's imprinting effect and efficient binding capacity can be evaluated by monitoring the non-imprinted polymer (NIP) performances, which is commonly known as a control material. The NIP bears similar virtues as IIP but lacks distinct recognition cavities.

Application of IIP/MIP in chemical and biological sensing has made considerable progress since the synthesis method is well developed and most of them follow one-pot synthesis methods or require minimum steps, which adds cost efficiency in the production. More importantly, IIP/MIP are easy to manipulate or tunable for a specific target by changing the template and functional group. In addition to this, it has high stability and excellent selectivity, and wide practicality of sensing performance. In the past few decades, several scientific reports have been published on the application of the IIP/MIP based sensors in detecting inorganic ions, drugs, nucleic acids, proteins, and viruses using different templates for specific target molecules and modifying imprinting structures. The characteristic future of the IIP/MIP based sensors has the ability to recognise the specific targets that bind the cavity since it has predetermined selectivity toward recognising particular targets and can also be used as a transducer that can send an output signal to the process. The change in the output signal is due to the interaction between the sensing materials, IIP/MIP

and the target analyte, when the target analyte binds the cavity, it changes the electrical property of the sensor, either in impedance (L), capacitance (C) or resistance (R). This change in electrical property could be either an increase or a decrease, depending on the type of target analytes or the templates, which is usually proportional to the target analyte that binds to the cavities.

In chemo resistive sensor, the sensor performance is measured in terms of the change of resistance. It has advantages such as quick response, low power consumption, low-cost effectiveness, portability, and simple fabrication methods were used to fabricate the devices. In this project, we will be focusing on the fabrication of sensors for the detection of Pb(II), As(III), As(V), Cr(VI), Hg(II) and Cd(II) ions in river and groundwater at very low concentrations. The fabricated sensors will be cost-effective, portable and with excellent sensitivity, stability, and reliability.

1.8 UTILISATION OF LOW-COST ADSORBENTS FOR REMOVAL OF SELECTED POTENTIALLY TOXIC ELEMENTS FROM WATER AND WASTEWATER

Several agricultural activities contribute a large amount of waste that could potentially cause environmental problems in the soil, water, and air. Agricultural waste materials are generally produced in the processing of agricultural and forestry products and livestock breeding. If these waste products are not disposed of appropriately, environmental disputes will arise. Most of the available disposal measures are complex, economically impractical, and could potentially create secondary pollution. The environmental issues could be addressed by finding a conceivable usage of these waste products (Mo et al., 2018). Adsorbents from agricultural wastes are easily collected, prepared, applied, and recovered without causing environmental problems (Kwikima et al., 2021). The concept of applying agricultural waste materials in wastewater treatment is innovative, effective, and sustainable (Kwikima et al., 2021). Agricultural by-product adsorbents are easily acquired; hence, their wide application in the removal of PTEs is highly relevant. Agricultural by-product adsorbents have been applied to remove a wide range of PTEs due to the abundance of binding sites on the surface of adsorbents. These binding sites create a strong affinity and high selectivity for PTEs in wastewater (Kwikima et al., 2021). In general, modified agricultural adsorbents exhibit higher removal efficiencies than unmodified agricultural adsorbents (Baig et al., 2015). Fruits and vegetables produce several by-products and wastes during several industrial processes and secondary product manufacturing. The potential environmental impacts may be reduced by finding promising and renewable industrial applications for them (Baig et al., 2015). Fruit waste products contain structural components such as pectin, cellulose, and hemicellulose, which contain hydroxyl and carboxylic functional groups. These structural components are involved in the adsorption of PTEs such as Pb, Cr, As, Cu, and Ni (Baig et al., 2015).

Waste collected from agriculture may be modified by pyrolysis to produce highly efficient biochar (carbon material) with high PTEs adsorption efficiencies (Baig et al., 2015). Agricultural waste adsorbents release highly soluble organic compounds, contributing to chemical oxygen demand (COD), biological oxygen demand (BOD), and total organic carbon (TOC). An increase in COD, BOD, and TOC release results in the depletion of dissolved oxygen (DO), which threatens all life underwater (Wan Ngah et al., 2008). Adsorbents may be modified for the purpose of reducing soluble organic compounds. Modifying agents such as NaOH and $Ca(OH)_2$, Na_2CO_3, several organic acids and compounds, and oxidising agents are used to remove soluble organic compounds, eliminate aqueous solution colour changes, and improve removal efficiencies (Wan Ngah et al., 2008). Agricultural waste sorbent material may be modified using different chemicals to

enhance adsorption capacities and removal efficiencies of surface functional groups. Modification may also increase physical components of adsorbents such as pore volume, pore distribution, and surface area (Baig et al., 2015).

This study further aims to investigate agricultural by-products such as sugarcane bagasse (SCB) and orange peels (Ops) as adsorbents for the decontamination of PTEs in water and wastewater. An adsorption using low-cost adsorbents has received extensive attention since it is simple, easy to operate and highly effective (Sarkheil & Tavakoli, 2015). In the past decade, the search for low-cost, easily accessible, abundant, and efficient bio-sorbents has received a great deal of attention (Montero et al., 2018). The low-cost bio-sorbents are produced using natural and agricultural waste products (Bajpai & Katoch, 2017). The use of agricultural by-products is economically favoured, and most importantly, they are a good representation of green chemistry due to the ease in handling, storing and safety of the waste materials during operation. In addition, the use of agricultural by-products in wastewater treatment creates a noble destination for organic load that has been deemed agriculturally futile.

Some examples of agricultural by-product adsorbents are sugarcane bagasse, coconut shells, rice husk, sawdust, maize cob, and orange peels (Bajpai & Katoch, 2017; Montero et al., 2018). In this study, the low-cost, green adsorbents, namely, sugarcane bagasse and orange peels, will be investigated for the removal of selected PTEs. Sugarcane bagasse, a bio-sorbent, is a low-cost residue (by-product) of the sugar industry remaining after sugar has been extracted (Esfandiar et al., 2014). On the other hand, one of the most valuable biomass wastes is orange peels. Despite the high removal capacity for PTEs that may be achieved using these agricultural by-products, it is highly advantageous to find industrial usage for them as their disposal is usually significantly problematic (Lasheen et al., 2012; Sarker et al., 2017). The use of these agricultural by-products, which are abundant and easily accessible in South Africa with minimal consumption of energy in the removal of PTEs from contaminated water, responds to the global call to raise awareness and capacities on applicable green chemistry approaches.

Another alternative low-cost adsorbent to be investigated for the removal of PTEs from water and wastewater, in this study, is bio-reactive organoclay. Commercial applications of the organoclay materials have steadily increased in recent years, but mainly for the remediation of organic contaminants. Unlike organic contaminants, limited studies focused on the investigation of whether inorganic contaminants immobilised onto organoclays are available to microorganisms or not. Organoclays have shown promising efficiency as an adsorbent due to their high adsorption capacities, relatively low cost, simple preparation, and efficiency for re-use after regeneration. To date, fewer studies have investigated the ability of bio-reactive organoclays for the transformation of PTEs into less toxic ones. The discovery of viable bio-reactive organoclays for PTEs remediation can be used to overcome the challenge of costly and less effective techniques. Furthermore, the use of low-cost materials will help in improving the quality of our water resources, particularly in vulnerable communities.

There are two main reasons why clay minerals are frequently selected as starting materials for the development of important adsorbents. Firstly, the clay minerals usually have a very large surface area. Secondly, the clay mineral’s expansive surface often has an electrical charge that results in the accumulation of inorganic and organic cations (Sarkar et al., 2012). Clay surface charge is caused by isomorphic substitution within the crystal structure, defects, and broken edges of clay minerals (Sarkar et al., 2012; Xu et al., 2018). Both factors are very important, and they have made clays very suitable to be developed as sorbents in many areas.

It is evident from several studies that organoclays are highly efficient in cleaning up organic and inorganic contaminants from the environment, and sorption is the guiding principle for this. However, a remediation technology or material that is based on the sorption of contaminants has some basic disadvantages in its long-term use. For example, a sorbent reaches its maximum adsorption capacity in due course of time, after which it should be either regenerated for further use or replaced with fresh material (Sarkar et al., 2012). Total replacement of a whole lot of spent sorbents might need additional infrastructure, which would require more time, work, and cost. There is also the chance that contaminants may re-disperse from spent organoclay at a new site, depending on environmental conditions such as pH, redox conditions, temperature, ionic strength, and dissolved organic matter (DOM). One economically viable and environmentally sustainable solution to these problems is the sorption of the contaminants followed by their degradation on the organoclay surface. Degradation can be achieved by imparting either chemical or biological activity to the organoclays. Chemically reactive organoclays, which are capable of sorption and degradation of contaminants, basically act as catalysts (Kapahi and Sachdeva, 2019). These materials have received huge attention and popularity in recent years. On the contrary, biologically reactive organoclays remain largely unexplored. Organoclays imparted with biological degradation properties can be termed bio-reactive organoclays. If microorganisms thrive well on an organoclay, they can take part in the degradation of adsorbed contaminants (Witthuhn et al., 2005, 2006). Thus, combining sorption and degradation by bioreactive organoclays could facilitate the regeneration of this remediation material (Yang et al., 2003). Microorganisms that use a particular organic contaminant as the sole carbon and energy source and are capable of mineralising the organic contaminant completely into CO_2 and water can be combined with organoclays to obtain the best results. Even inorganic pollutants such as arsenite and chromate can be targeted by microorganisms thriving on organoclays to bio-transform them into less toxic forms. However, the degradation performance of the introduced microorganisms depends on many factors. The growth and proliferation of the microbes should not be prohibited by any kind of toxicity from the organoclay or the contaminant in question. Also, the contaminants sorbed on the organoclay should be available to the microbes for degradation (Sarkar et al., 2012). The microbes may need additional nutrient sources as well. However, information on these in the literature is very scarce because it is a very recently emerging technology that combines material science and microbiology (Sarkar et al., 2012).

Unlike organic contaminants, little attempt has been made to date to investigate whether inorganic contaminants (e.g., toxic metals and metalloids) immobilised onto organoclays are available to microorganisms. A bioremediation approach utilising specific microorganisms may be employed to degrade organoclay-immobilised PTEs, given that those become bioavailable to microbes. In addition to adsorption by modified organoclays, remediation by reduction of toxic form to a less toxic oxidation state is the focus of this project. Conversion of carcinogenic Cr(VI) to Cr(III), As(III) and As(V) to the less toxic organic forms, namely monomethylarsonic acid (MMA), dimethylarsinic acid (DMA), and trimethylarsine oxide (TMAO) and more toxic vanadium(V) to other less toxic oxidation states will be investigated. This will combine remediation with speciation studies to identify the different oxidation states before and after treatment. Some extra nutrients may need to be added to the system for the proper functioning of the microbes. So, this study saw it essential to understand the possibility of integrating microbial degradation/transformation of inorganic toxic metals and metalloids held on organoclays. Thus, the bio-reactive organoclays will be employed for the transformation of more toxic elemental species to less toxic forms.

This project will focus on Steeelpoort River in Steelpoort, which is heavily affected by mining activities in the area and the Mokolo River in Lephalale, which is situated close to Grootegeluk coal mine as well as Medupi and Matimba power stations. In addition to these study areas, which were selected in the first cycle of the WRC project, particularly, borehole water in the Sekhukhune district will be investigated to evaluate the impact of mines such as the Tubatse Ferrochrome mine on the groundwater. Thus, a survey of the groundwater quality of these areas on a large scale is vital as a first step in the development of a

groundwater management strategy for the communities residing in these areas.

1.9 PROJECT AIMS

The following are the aims of the project:

1. To conduct a literature review that focuses on levels of PTEs and their speciation in South African water bodies, transport, fate, and risk assessment of PTEs via the food chain, IIP-based sensors application for detection of toxic metal ions, agricultural by-products such as sugarcane bagasse and orange peels as adsorbents for de-contamination of PTEs in water, and bio-reactive organoclays for transformation of toxic chemical forms into less toxic species.
2. To quantify the total concentrations of As, Cd, Cr, Cu, Hg, Mn, Ni, Pb, and V in water, sediment, soil, and vegetable samples using atomic absorption spectrometry (AAS), inductively coupled plasma-mass spectrometry (ICP-MS) and inductively coupled plasma–optical emission spectrometry (ICP-OES).
3. To optimise method(s) for simultaneous determination of As and Cr species in water, sediment, soil and vegetable samples using HPLC hyphenated to ICP-MS as well as a method for quantification of Hg species (methyl mercury [MeHg(I)] and inorganic Hg [Hg(II)] in sediment, soil and vegetable samples using HPLC hyphenated to ICP-MS.
4. To compare the mobility of PTEs and their species through the food chain and determine fate by identifying steps where in the food chain transfer of PTEs and their species may be enhanced or constrained.
5. To evaluate concentrations of PTEs and their species in water, sediment, soil, and vegetables collected from selected areas and conduct risk assessment for human health, which will be addressed through the determination of the estimated daily intake dose (EDI) and the tolerable upper intake (TUI).
6. To fabricate ion-imprinting polymer-based sensors for the detection of selected toxic metal ions in water.
7. To investigate agricultural by-products, such as sugarcane bagasse and orange peels, as adsorbents for decontamination of PTEs in water and wastewater, and assess bio-reactive organoclays for transformation of toxic elemental species into less toxic ones.

CHAPTER 2: METHODOLOGY

2.1 CHEMICALS, STANDARDS, AND CERTIFIED REFERENCE MATERIALS

Ultrapure water with a resistivity of 18.2 MΩ.cm was obtained using a Milli-Q System (Millipore, France) and used for dilutions and washing glassware. Chemicals of high purity were utilized throughout this study. These include 65% suprapur HNO_3 (Merck, Germany), 40% HF (Merck, RSA), and H_3BO_3 (Sigma-Aldrich, Germany), which were utilized for sample digestion. Stock solutions of 1000 mg/L PTEs (Inorganic Ventures, USA), 500 mg analytical grade MMA (Supelco, USA), and 500 mg analytical grade DMA (Supelco, USA) were utilized to prepare standard solutions. An ACS reagent > 98% NH_4NO_3 (Thembane chemicals, RSA), 28-30% NH_3 basis NH_4OH (Sigma Aldrich, Germany), 99% dibasic $(NH_4)_2HPO_4$ (Merck, Germany), analytical grade> 99% EDTA (Merck, RSA) for preparation of mobile phase and extraction of As and Cr Species. Standard reference materials (SRMs) of trace elements in natural water (SRM 1640a) (NIST, USA), San Joaquin soil (SRM 2709a) (NIST, USA), and tomato leaves (SRM 1573a) (NIST, USA) were used to evaluate methods utilized for the determination of trace elements in water, sediments, soil, and vegetables, respectively. The test of interference by polyatomic ions was carried out using NaCl (Promark chemicals, RSA).

The rGO, IIP and NIP were synthesised and purified using the following chemical reagents. A $<$20 μm graphite (G) powder, hydrogen peroxide (H_2O_2) (30%), sulfuric acid (H_2SO_4) (98.0%), potassium permanganate ($KMNO_4$) (99.0%) and phosphoric acid ($H3PO_4$) (85%) were used in the preparation of GO from G. Ascorbic acid ($C_6H_8O_6$) (99.0%) was used in the reduction of GO to rGO. For the synthesis of IIP and NIP, a mixture of acetonitrile (ACN) (99.9%) and dimethyl sulfoxide (DMSO) (99.9%) was used as a porogen to dissolve the source of template ion; cadmium(II) nitrate ($Cd(NO_3)_2.4H_2O$) (98.0%), the monomer methacrylic acid (MAA) (99%) and the cross-linker; ethylene glycol dimethylacrylate (EGDMA) 98.0%. Azobisisobutyronitrile (AIBN) (98%) was used as an initiator for polymerisation. The synthesised GO and polymers were purified in ethanol (EtOH) (97.2%) and hydrochloric acid (HCl) (30%). The nanocomposites (rGO-Cd-IP and rGO-NIP) were composed using a polysulfone membrane (used as a binder) with an average MW = 3500 and dissolved in 1,2-dichloroethane (DCE) (99.8%). A potassium bromide (KBr) salt (≥99%) was used to prepare samples for FTIR spectroscopy analysis.

All high-density polyethylene bottles, microcentrifuge tubes, and glassware were cleansed with detergent, rinsed with de-ionized water, and soaked for 24 h in an acid bath solution composed of 10% HNO_3. Analytical grade lead nitrate ($Pb(NO_3)_2$), hexadecyl trimethyl ammonium bromide (HDTMA), nitric acid (HNO_3, 65%), sodium hydroxide (NaOH, 98%), all purchased from Sigma-Aldrich (Darmstadt, Germany); hydrochloric acid (HCl, 37%) purchased from Chemistore (Kempton Park, South Africa); as well as silver nitrate ($AgNO_3$) purchased from Rochelle Chemicals (Johannesburg, South Africa) were used without

further purification. Natural kaolin (CEC = 13.1 meq/100 g) and bentonite (78.6 meq/100 g) clays were purchased from Micronized (Johannesburg, South Africa) and Imerys (Pretoria, South Africa), respectively.

2.2 INSTRUMENTATION AND APPARATUS

All synthesised materials for sensor fabrication were ground using an Agate mortar and pestle and sieved through a 0.045 mm mesh wire. These materials were then characterised using various instrumental techniques. A Witec 300 Confocal Laser Raman spectrometer (Witec Focus Innovations, Germany) was used for Raman shifts identification, and a Frontier FTIR spectrometer (PerkinElmer, Germany) was used to identify and monitor functional group changes using a potassium bromide (KBr) pellet. The KBr was preferred since carbon-based materials like graphite have reduced sampling depths and weaker signals in the Attenuated total reflectance (ATR) mode (Tseng et al., 2024). Brunauer-Emmett−Teller (BET) analysis was used for nitrogen (N_2) adsorption/desorption studies using a surface and pore analyser (Micromeritics Instrument Corporation, USA). An Empyrean powder X-ray diffractometer (P-XRD) (Malvern Panalytical, UK) with a Cu-Kα radiation source of 0.154184 nm wavelength was used for characterising crystallinity and amorphousness of the materials for morphological studies and elemental composition, a Tescan Vega 3 scanning electron microscope (SEM) (Tescan, Czech Republic) equipped with an energy dispersive X-ray spectrometer (EDS) and a Joel-Jem 2100F transmission electron microscope (TEM) (Joel, Japan) were used. The concentrations of PTEs were determined using Spectro Arcos ICP-OES (Spectro, Germany) and NexION 300 ICP-MS (Perin Elmer, Canada). Sensor performance testing was monitored using an E4980AL Precision inductance, capacitance, and resistance (LCR) meter from Keysight, USA, operating using LabVIEW 21.0 software.

The flame atomic absorption spectrometer AAS-7000 from Shimadzu (Kyoto, Japan) was used to measure the concentrations of Pb(II) in solutions before and after adsorption. The surface morphology of the clays was investigated using the TESCAN VEGA 3 LMH SEM (TESCAN, Brno-Kohoutovice, Czech Republic); the zeta potential of the clays was determined using the Malvern Zetasizer (Malvern Panalytical, Randburg, South Africa). The functional groups present were identified by means of an IR Affinity-1S FTIR spectrophotometer (Shimadzu, Kyoto, Japan). An STA 6000 TGA (TA Instruments, New Castle, DE, USA) was used to determine the thermal stability of the clays. The solutions were stirred on an RS Pro stirrer plate (RS Components, Midrand, South Africa).

2.3 STUDY AREAS

This study is based on the Mokolo River, which is in Lephalale, Limpopo Province, South Africa. The Mokolo River serves as a water source for activities that are industrially, recreationally, and agriculturally based, as well as a water source for domestic use. Lephalale is home to various industrial activities, including mining (Grootegeluk Coal Mine) and the production of electricity (Matimba and Medupi Power Stations) (Letsoalo et al., 2018). The coal contains PTEs such as U, Pb, Mn, Cr, As, and Cu, some of which are released through combustion when utilized in power stations (Cui et al., 2019). The combustion of coal is reported to release PTEs such as As and Cr in the form of atmospheric particles, which are dispersed by wind (Cui et al., 2019; Letsoalo et al., 2018). The dust particles released through coal mining and power stations' operation can highly impact the ecosystem, resulting in high concentrations of Cd, Pb, Cu, Ni, Hg, V, Cr, and As in water, sediment, soil and vegetables. These particles often end up in water sources, putting water

sources like the Mokolo River at risk of being exposed to toxic elements. There are various activities which were observed during sampling, including sand mining and water abstraction pumps used for irrigation purposes. Therefore, there is a need to assess the different environmental samples in the Mokolo River and its surroundings to determine their distribution and the levels of the PTEs.

This study also focused on the Steelpoort River, a prominent tributary of the Olifants River in Limpopo province, which is a critical watercourse with significant ecological and economic importance. Originating in the northern part of the province, the river flows eastward before joining the Olifants River. Its catchment area is characterized by a mix of natural landscapes and intensive human activities, which are significantly impacted by both mining and agricultural activities. Key tributaries of the Steelpoort River include the Elands River, which joins from the northwest, the Dikgatlong River from the north, and the Jubilee Creek from the west. Each of these tributaries contributes to the river's flow and influences its water quality, reflecting the varying degrees of local anthropogenic impacts.

The Steelpoort River and its tributaries are essential for local communities, agriculture, and industry, providing water for domestic use, irrigation, and industrial processes. However, the river system faces considerable environmental challenges due to extensive mining operations, particularly for ferrochrome and platinum, and intensive agricultural practices (Department of Cooperative Governance and Traditional Affairs, 2019). These activities lead to the release of pollutants, including PTEs such as V, Cr, Ni, As, Cu, Cd, Pb, and Hg, alongside pesticides and organic matter. These PTEs can accumulate in sediments and adversely affect both water quality and aquatic ecosystems.

2.4 SAMPLE COLLECTION

Sampling from the Mokolo River was carried out in August 2022 and May 2023 for low and high flow seasons, respectively. Fifteen sampling sites were identified, of which ten (10) are in the Mokolo River, two (2) are in Mokolo Dam and three (3) are the farms in the vicinity. From Mokolo River and Mokolo Dam, water and sediment samples were collected and from the farms, irrigation water, soil and vegetable samples were collected. However, for the high flow season, only twelve sampling sites were identified, of which eight are in the Mokolo River, two are in Mokolo Dam, and two are from the farms. Figure 2.1 displays a map with different sampling sites that were chosen in the Mokolo River and Mokolo Dam. One litre (1 L) of water samples was collected into polyethylene bottles. Sediment samples of 500 g were collected at a depth of 30 cm with an auger sampler. Vegetable samples were collected from the 3 farms. Similarly, soil samples were collected at a depth of 30 cm with an auger sampler from the farms. The important water quality physicochemical parameters like pH, electrical conductivity (EC), dissolved oxygen (DO), salinity, resistivity, oxidative reduction potential (ORP), and total dissolved salts (TDS) were recorded on site.

The samples were kept in a cooler box with ice. The water, sediment, and soil samples were collected in high-density polyethylene bottles of 1000 mL, 500 mL, and 500 mL, respectively, which were previously soaked for 24 h in 10 % HNO_3. The vegetable samples were collected into a plastic bag. The global positioning system (GPS) coordinates were documented at each sampling point.

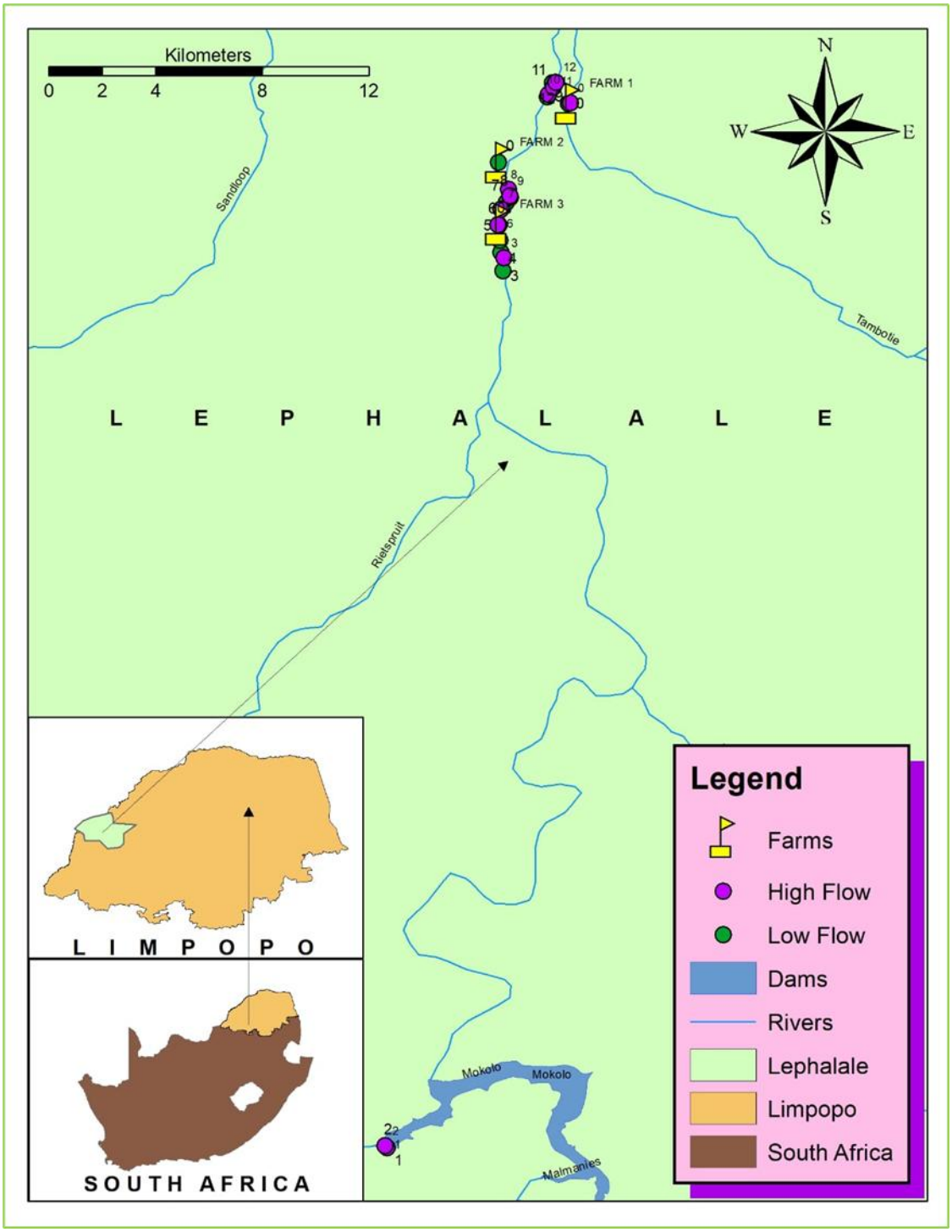

Figure 2.1. Map displaying water and sediment sampling sites from Mokolo Dam and Mokolo River together with the farms in the vicinity of Mokolo River, Limpopo Province.

Some of the vegetables collected and activities observed from the farms and along the river are displayed in Figures 2.2 and 2.3.

Figure 2.2. Images showing vegetables grown on farms, which include pumpkin (left), chomolia (middle), and a water system (right) used to irrigate the vegetables.

Figure 2.3. Images showing site 9 (left), site 10 (middle) and a board (right) indicating that sites 9 and 10 are mining sites.

Figure 2.4 shows a map indicating the study area of the Steelpoort River and Greater–Tubate/Fetakomo region.

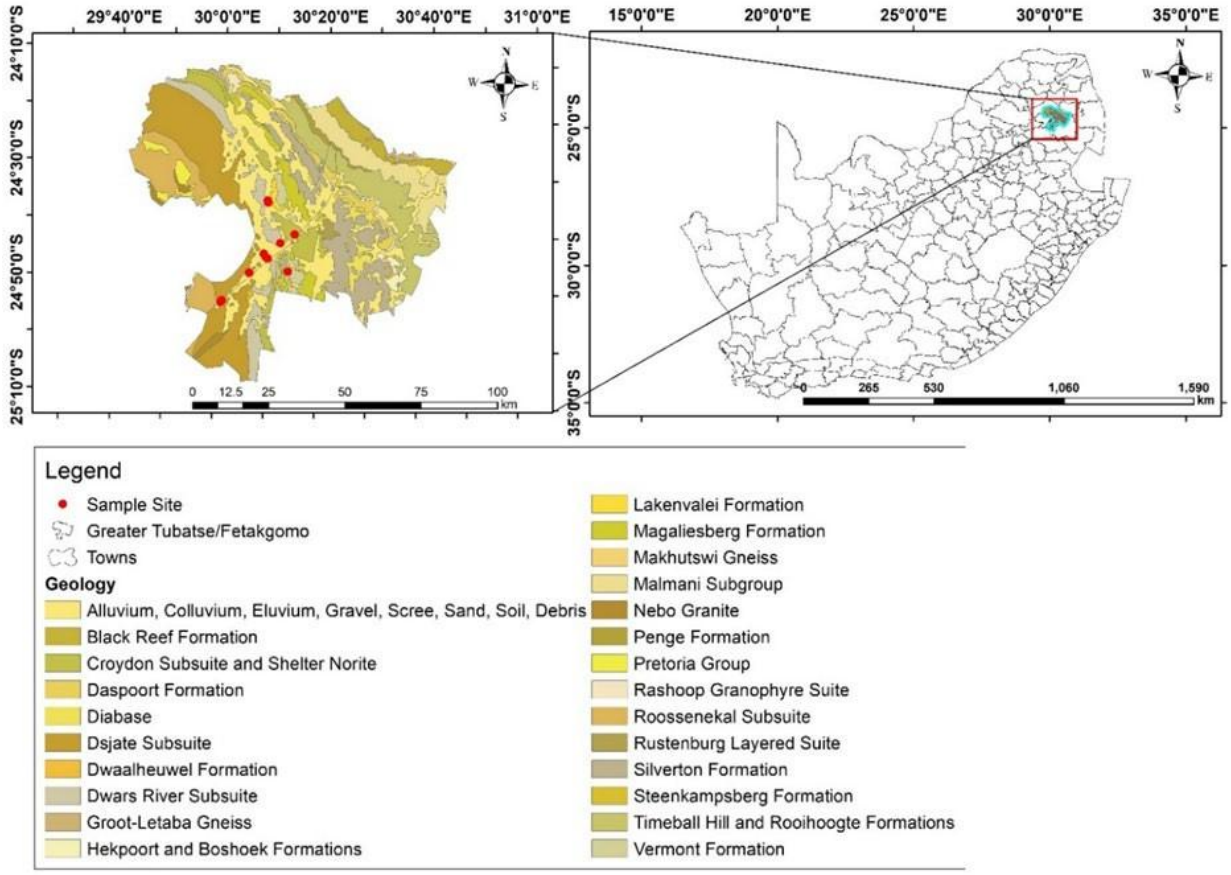

Figure 2.4. Geographical area of sampling sites.

The detailed map is colour-coded to represent various geological formations, each denoted by distinct shades of yellow, brown, and green. These formations include significant geological features such as the Malmani Subgroup, Nebo Granite, and Magaliesberg Formation, among others. The legend provides a comprehensive list of these formations, which range from alluvial deposits to various types of bedrock, highlighting the diverse geological landscape of the region. The geology of Sekhukhune District is dominated by ultramafic substrate, which is known as serpentine soil of Rustenburg-layered suited bushveld complex (Kgaphola et al. 2023).

The maps in Figures 2.5 and 2.6 present a detailed overview of the Steelpoort River and borehole water sampling sites located in Limpopo province. The map also highlights the surrounding towns, such as Steelpoort, Driekop, and Tubatse, and identifies significant industrial landmarks, including the Lion Smelter for ore smelting and Tubatse Ferrochrome for Cr mining. Major roads like the R555 have been marked for reference.

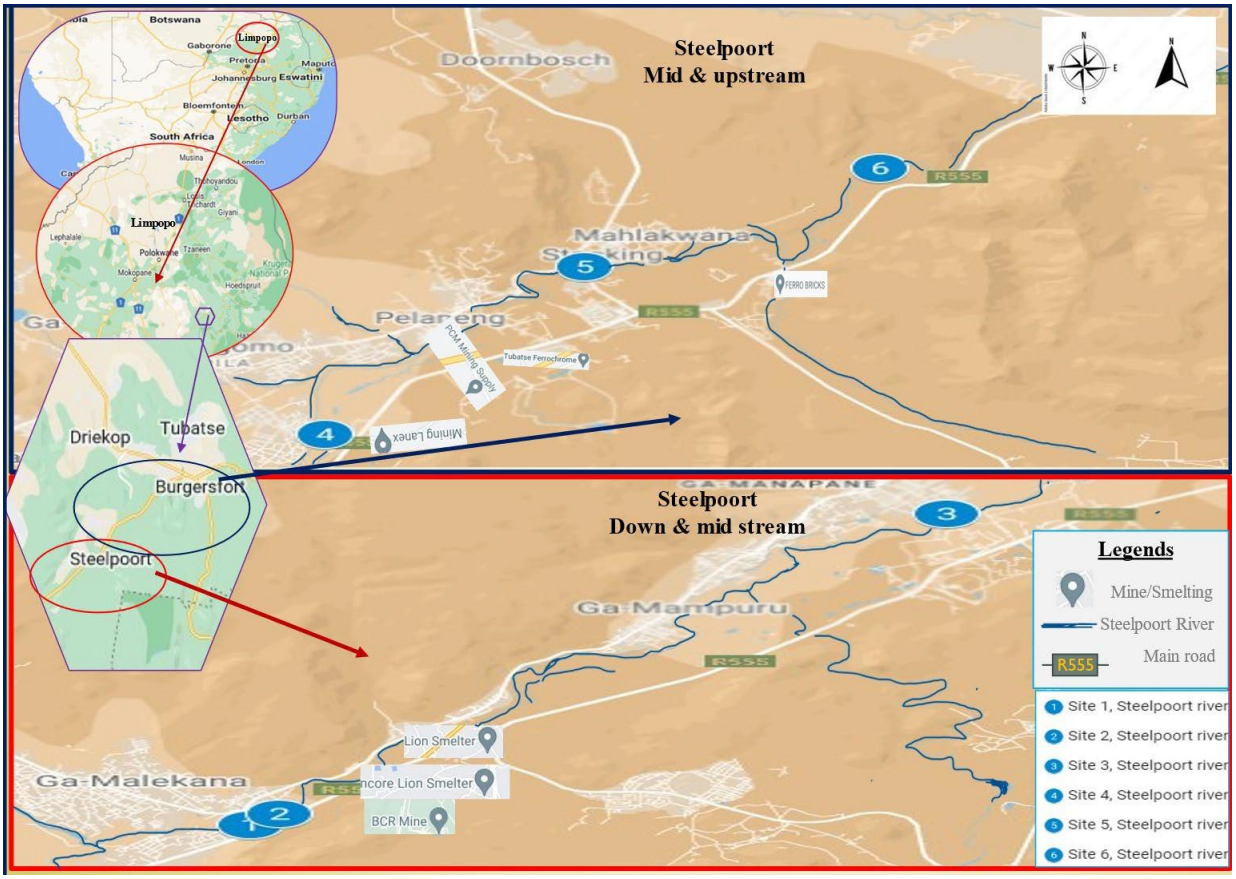

Figure 2.5. Map of Steelpoort River sampling sites.

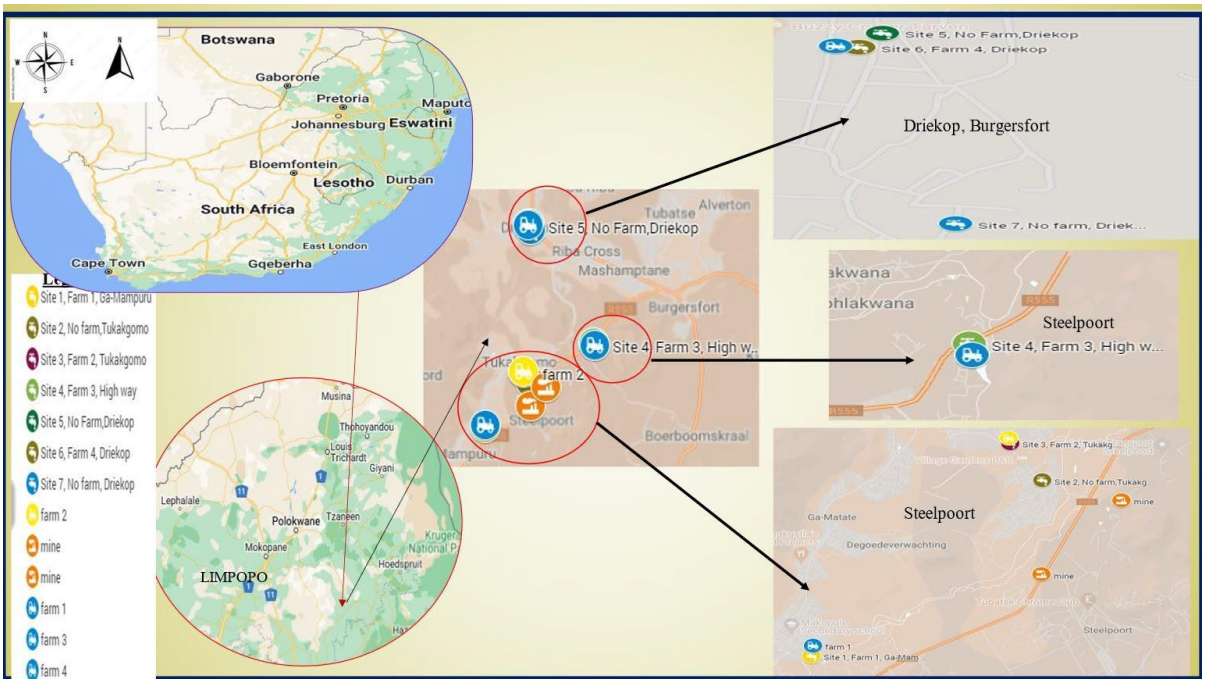

Figure 2.6. Sampling sites for borehole water and vegetables in the Steelpoort and Driekop areas.

Sampling sites 1, 3, 4 and 6 are associated with farms where both borehole water and vegetables were collected. At sites 2, 5 and 7, there were no farms, and only borehole water samples were collected for analysis. Sampling was conducted during the low flow season from 13 to 14 September 2023 and during the high flow season from 24 to 25 April 2024.

During the low and high flow seasons, the vegetables collected included chomolia (Brassica *oleracea acephala*), spinach (Spinacia *oleracea*), welsh onion (Allium *cepa L.*), spring onion (Allium *fistulosum L.*), okra leaves (Abelmoschus *esculentus*), beetroots (Beta *vulgaris L.*), baby spinach (Spinacia *oleracea L.*), yellow spinach (Spinacia *oleracea L.*), rape (Brassica *napas*), covo (Brassica *oleracea var. capitata L.*), mochina (Brassica *perviridis*), cabbage (Brassica *oleracea var. capitata*), carrots (Daucus *carota subsp. sativus*), and tomatoes (Solanum *lycopersicum*). Agricultural topsoil samples were taken from the same sites where vegetables were collected, providing representative samples of the farm's soil.

2.5 SAMPLE PRESERVATION, PRE-TREATMENT, AND PREPARATION

Upon return to the laboratory, the filtration of water samples was executed through a filtration system fitted with 0.45 µm disk filter paper and were kept in a refrigerator set at 4 °C. A 100 mL of the samples was acidified with 1% HNO_3 for use during total concentration measurements, while the unacidified portion of water was kept for use in speciation analysis. The water was kept in the refrigerator. The vegetable samples were rinsed three times with deionised water, and all solid samples (sediment, soil, and vegetable) were dried using a freeze dryer. After drying, the samples were ground with an agate mortar and pestle into fine particulate matter and sieved using a sieve with a 100 µm aperture opening.

The digestion of sediment and soil samples was executed prior to the determination of total concentrations. Ahead of digestion, a supersaturated solution of H_3BO_3 was freshly prepared by dissolving 7 g of H_3BO_3 in about 60 mL of de-ionised water and topped up to 100 mL. After that, the solution was filtered with a 0.22 µm syringe filter. A 100 mg of homogenised sediment, soil, and SRM 2709a were weighed and transferred to Teflon vessels of the microwave digestive system. The digestion of homogenised samples involved two stages. The first stage entailed the introduction of 4 mL of 65% HNO_3 and 500 µL of 40% HF to each vessel containing a 100 mg sample and allowing the vessels to stay open for 20 minutes. The vessels were sealed and correctly positioned in the microwave digestion system, and the first digestion stage was allowed to run. After the first stage, 1 mL of a supersaturated solution of H_3BO_3 was added to each vessel and allowed to proceed with the second stage on the microwave digestion system. The digestion was done in triplicate. This method was adapted with slight modifications from Mekonnen *et al.* (2015).

The plant samples were also digested prior to quantification of total concentrations of analytes. 200 mg of homogenised vegetable samples and SRM 1573a were transferred to Teflon vessels of the microwave digestive system, and only 6 mL of 65% HNO_3 was added to the vessels. The vessels were allowed to stand with constant swirling after 5-minute intervals for 20 minutes. The vessels were placed on the microwave digestion systems rotor, and digestion was allowed to proceed with only one stage at 40.0 bar pressure control of 10 minutes power ramping, 10 minutes power holding, maximum power of 700 W with an IR temperature of 210 ℃ and an internal temperature of 240 ℃.

After digestion, the solutions were topped up to 50 mL with de-ionised water and filtration of the solutions was executed with a syringe fitted with a 0.45 µm syringe filter. Ten reagent blanks were prepared for each digestion method (10 for the sediment/soil digestion method and 10 for the vegetable digestion method) following the digestion methods. All samples were prepared in triplicate and concentrations of all the analytes in the samples were quantified using ICP-MS.

The extraction method adopted from Letsoalo et al. (2021) was used for the extraction of elemental species in vegetable and soil samples for speciation analysis. Briefly, a buffer prepared using 0.375 M $(NH_4)_2HPO_4$ and 50 mM EDTA was used for the extraction of As and Cr species in soil, and vegetables collected during high and low flow seasons from the Mokolo River. A 500 mg sample was transferred into Teflon vessels, and 15 mL of extraction solution was added to each vessel. The extracts were filtered with a syringe fitted with a 0.22 µm syringe filter without further dilutions. Filtered water samples were injected into an HPLC column without any further pre-treatment. A gradient mode of elution using 10 mM NH_4NO_3 and 70 mM $NH_4H_2PO_4$ at pH 8.7 mobile phase solutions was adopted for the simultaneous separation of As(III), DMA, MMA, As(V), and Cr(VI) (Letsoalo et al., 2021). Prior to speciation analysis, a test solution of 50 mg/L Cl^- was prepared and injected for monitoring of polyatomic ion interferences. The HPLC -ICP-MS operating conditions are presented in Table 2.1.

Table 2.1. Operating conditions for HPLC-ICP-MS.

Parameter	Setting
Analytical column	Hamilton PRP-X100
Column dimension	4.6 ×250 mm, 5 µm
Guard column	4.6 × 150 mm, PEEK
Pump flow rate	1 mL/min
Pump pressure	2520 psi
Injection volume	100 µL
Mobile phase A	NH_4NO_3 (10 mM) and $NH_4H_2PO_4$ (0.5 mM) at pH 8.7
Mobile phase B	NH_4NO_3 (70 mM) at pH 8.7
Nebuliser gas flow	1.18 L/min
Auxiliary has flow	1.20 L/min
Plasma gas flow	15 L/min
ICP RF Power	1450 V
Lens voltage	12

2.6 PROCEDURES FOR DETERMINATION OF ANALYTICAL FIGURES OF MERIT

2.6.1 Determination of limit of detection and limit of quantification

After the analysis of the reagent blanks by ICP-MS, the standard deviations (**σ**) were determined from the concentrations observed. The products of 3 times the standard deviation (3σ) and 10 times the standard deviation (10σ) were used as the limit of detection (LOD) and limit of quantitation (LOQ) for each sample, respectively.

2.6.2 Linearity

The linearity was determined for each analyte using 5-point calibration curves, which contain 4 standards and a blank. The coefficient of determination (R^2), along with linear equations, was determined from calibration curves plotted on Excel.

2.6.3 Method accuracy and precision

The accuracy of the method was confirmed by analysing standard reference materials (SRMs). Tomato leaves SRM 1573a, trace element in water SRM 1640a and San Joaquin soil SRM 2709a were used to confirm the accuracy of the methods. The measured concentrations were compared with the certified concentrations to obtain a percentage recovery. The obtained percentage recoveries were used to confirm the accuracy of the method. In speciation analysis, the accuracy of the method was evaluated by spiking soil and vegetable samples at 3x LOQ and 20x LOQ with As(III), As(V), MMA, DMA, and Cr(VI) before extraction and the extracts were analysed using HPLC-ICP-MS. The percent relative standard deviation (%RSD) was utilised to assess the precision of the methods utilised in this study.

2.7 HEALTH RISK ASSESSMENT

The health risk assessment (HRA) to the communities who consume vegetables was assessed by calculating the targeted health quotient (THQ) and hazard Index (HI). The HHRA was employed to determine the possibility that consuming vegetables would result in carcinogenic health effects for adults and children. The estimation of carcinogenic health effects was determined using the ILCR, a product of EDI and CFS expressions presented in Equations 1 and 2. The EDI parameters employed were ingestion rate, exposure frequency and duration, oral reference dosage, average body weight, and exposure time.

$$IIIIIIII = EEEEII \times IICCCC \qquad \text{Equation 1}$$

$$EEEEII = \frac{EE_{FF} \times EE_{DD} \times FF_{IIII} \times CC}{AAAAAA \times AA_{TT}}$$ Equation 2

2.8 PREPARATION OF MATERIAL COMPOSITES

2.8.1 Synthesis of NIPs and Cd(II)-IPs

The polymers were used as a source of support matrix to imprint the target Cd(II). The bulk polymerisation process was used to synthesise the polymers imprinted with Cd(II) and the non-imprinted ones (Letsoalo et al., 2021). A 0.5 mmol of Cd(II) source was dissolved in a 10 mL porogen solvent mixture of DMSO and ACN in a 1:9 ratio. 4 mmol of the MAA monomer and 20 mmol of the crosslinker EDGMA were added to the dissolved mixture. The mixture was stirred at room temperature for 10 min before adding AIBN (0.3 mmol) to initiate the polymerisation. After the initiator had dissolved, the reaction flask was sealed and placed in a preheated oil bath at 65 ℃. The reaction was left to proceed for 24 h under a nitrogen atmosphere while stirring at 1000 rpm. Nitrogen gas was used to remove any potential oxygen gas in the reaction mixture that could impair the polymerisation process. Polymerisation would usually set in the first few hours of reaction. The same procedure was employed in synthesising NIPs without the Cd(II) imprint. A white solid polymer was ground into a fine powder and sieved before repeatedly washing and rinsing it in EtOH and de-ionised water to purify impurities. The same process was applied to the NIPs. The purified polymer was dried, and some of the dry product was leached with 0.01 M HCl solution for several 24 h cycles to remove the Cd(II) ions and produce a leached IIP. Leachate solutions were collected after each cycle and analysed for the presence of Cd until it was no longer detected using ICP-OES and ICP-MS. The dry leached Cd-IP was stored for further reaction with rGO to form nanocomposites.

2.8.2 Synthesis of GO

Reduced graphene oxide was used to improve the conductivities of polymer nanocomposites. The rGO was synthesised from GO, which was synthesised following the improved Hummer's method as reported by Marcano and colleagues (Marcano et al., 2010) with slight modifications. A 1 L round bottom flask was pre-cooled in an ice bath. A 3.004 g of graphite powder synthetic was added to the cold flask, followed by 360 mL of conc. H_2SO_4 (slowly) while stirring. After 30 min, 40 mL of conc. H_3PO_4 was slowly added with continuous mixing. The mixture was left to cool before 18 g of the oxidising $KMNO_4$ was added. The oxidant was added cautiously, and the spatula was full at a time with continuous stirring for at least 30 minutes until it reached room temperature. The graphite-oxidising reaction flask was transferred to a preheated 50 ℃ oil bath under slow stirring. The mixture was allowed to react while monitoring the temperature for 24 h. After 24 h, the purple reaction mixture was removed from heating, carefully poured into 400 mL of ice, and allowed to cool. A 5 mL of 30% H_2O_2 was slowly added to react with the unreacted $KMNO_4$, forming a brown paste solution. The mixture was sonicated for 4 h at 4000 rpm to exfoliate the formed GO layers while discarding the supernatant. The resultant pellet was washed with centrifugation twice in each solution of 200 mL absolute EtOH to purify it, 200 mL of 30 % HCl to remove the sulphate and 200 mL of de-ionised water continuously until the supernatant pH was neutral. The produced GO was dried in a vacuum oven at 50 ℃ for 72 h, ready for characterisation and synthesis of rGO.

2.8.3 Synthesis of rGO

Some of the produced GO was used to synthesise rGO. About 0.5 g of GO and 1.0 g of ascorbic acid were added to 250 mL of de-ionised water in a 500 mL round-bottom flask. The mixture was sonicated for 30 min and placed in a preheated oil bath at 50 ℃ for 24 h. The synthesised rGO was washed and rinsed repeatedly with de-ionised water before drying in the oven, ready for characterisation and synthesis of rGO-based nanocomposites for sensor fabrication.

2.8.4 Sensor fabrication

The synthesised rGO was mixed with leached Cd-IPs and NIPs to form rGO-Cd-IPs and rGO-NIP nanocomposites. To make the nanocomposite mixture, 100 mg of polysulfone was dissolved in 3 mL of DCE. Polysulfone acts as a binder for placing the nanocomposite onto the electrode. This mixture added leached Cd-IP with rGO in varying ratios of 0:3, 1:1, 1:3, 3:0 and 3:1 for optimisation with continuous stirring for at least 48 h to form different sensors. After 24 h, 50 μL of the homogenous nanocomposite mixture was drop cast on a gold interdigitated electrode to form a sensor film and dried in a vacuum desiccator. The same process was followed for the control rGO-NIP.

2.9 ELECTROCHEMICAL SENSOR MEASUREMENTS

2.9.1 FABRICATION OPTIMISATION AND CALIBRATION

The fabricated sensors were tested for their response sensitivity towards Cd(II) in solution. During testing, the sensor was dipped in a Cd(II) test solution for 300 s, removed, rinsed and placed in a leaching solution (blank) of 0.1 M HCl for another 300 s to leach out the ions while recording the signal continuously. The process continued while the blank and test solutions were interchanged. A series of Cd(II) standard solutions was prepared from 5 μg/L to 200 μg/L. These were used to calibrate the sensor to determine the limit of detection, linearity, and sensitivity for method validation. The NIP sensor was used as a control. The sensor's sensitivity, selectivity, stability, repeatability, reproducibility, and performance in real water samples were evaluated.

2.9.2 Real water sample analysis

Upon calibration, real water samples from Driekop and Steelpoort, Limpopo, South Africa, were used to test the sensor’s analytical performance. Two samples were borehole water (BW), and the other was river water (RW). Since ICP-OES results indicated a Cd concentration of <0.1 μg/L for the real samples, target concentrations of 1 and 2 μg/L were used for spiking. 45 mL of each water sample was initially spiked with 0.45 mL of a 100 μg/L Cd(II) solution. The percentage recoveries were to evaluate the method’s accuracy.

2.10 SEM-EDS ANALYSIS

A scanning electron microscope coupled to an energy dispersive X-ray spectrometer was employed in studying the surface morphology and chemical composition of polymers. Samples were prepared by dispersing a small amount of fine powder over a double-sided sticky black tape. The tape was mounted on an aluminium sample holder (20 mm diameter). To coat the samples, a carbon rod source was mounted in a vacuum system between two high-end current terminal points of an electric sputter coater. Samples were

then coated with a fine stream of evaporating carbon upon heating. The coated samples were analysed for surface morphology using a VEGA 3 LMH SEM spectrometer (Tescan, Czech Republic) operating at 20 kV coupled to an EDS spectrometer (X-max 500 mm2, Oxford Instruments, Buckinghamshire, UK). The EDS spectra were obtained to determine the elemental composition.

2.11 FT-IR ANALYSIS

To identify the functional groups in polymers and graphene, FT-IR spectra were recorded in the range of 4000 cm^{-1} to 300 cm^{-1} using a TL 8000 FT-IR EGA Balanced (Perkin Elmer, Canada) flow system spectrometer. All samples were diluted (100:1 mass ratio) by grinding in KBr using a mortar and pestle to thoroughly mix them and pelletized using a die at 40 psi. Up to 32 scans were run for each sample at a resolution of 16 cm^{-1}. The obtained spectra were matched to a library of databases to check compounds with similar functional groups.

2.12 BET ANALYSIS

The pore size, pore volume, surface area analysis and isotherms of leached and unleached Cd(II)-IPs were determined after N_2 adsorption-desorption analysis following a method by Brunauer et al. (1938). A 0.2 g sample was degassed at 80 °C for 6 h under a continuous nitrogen flow using the Flow Prep 060 Sample Degas System (Micrometrics, USA). A low temperature was used to prevent changes in the structure of the samples from heating. Degassed samples were analysed using an ASAP 2460 N_2 adsorption-desorption analyser (Micrometrics, USA).

2.13 TGA ANALYSIS

Only GO and rGO were analysed for thermal stability using an SDT Q600 TGA Thermobalance analyser (TA Instruments, USA). The TGA analysis was performed by carefully adding sample material into a sample holder until it was almost 80% full. The sample holder was introduced into the analyser and calcined up to 1000 ^oC at 10 ^oC/min increase rate using lab forceps.

2.14 POWDER X-RAY DIFFRACTION ANALYSIS

A 0.3 g powder sample was pressed to compact in an aluminium sample holder in preparation for PXRD analysis. Samples were analysed in the range of 5 to 90^o (2θ) at 0.033^o/s intervals. A diffractometer equipped with an 8.04 keV X-ray radiation from a Cu-Kα source with a wavelength of 0.15406 nm was utilised, scanning continuously at a stepwise increase rate of 0.0170/s. The diffractometer operated at a generator current of 40 mA with a voltage of 40 kV.

2.15 ACQUISITION AND PREPARATION OF BIO-SORBENTS

Sugarcane sticks were obtained from a sugarcane farm in Mpumalanga, while orange fruits were purchased from a recognized vegetable market. Sugarcane sticks were peeled, and the fibrous parts were crushed to remove the juice and produce SCB. Orange fruits were peeled to obtain OPs. Then, the obtained SCB and OPs were washed with tap water, followed by deionized water. They were then left to dry naturally in a controlled environment before being dried at 105 °C in the oven until their weight was constant. The SCB and OPs were then ground using a Nama electric grinder (Nima YK, Osaka, Japan) and sieved to obtain a

powder form of SCB and OPs. The pure SCB and OPs were activated for use in this project. These bio-sorbents were heated in a furnace to a temperature of 400 °C at a heating rate of 2 °C min^{-1} and under an inert atmosphere of argon gas to produce the activated forms of SCB and OPs.

2.16 BATCH ADSORPTION AND OPTIMIZATION OF EXPERIMENTAL PARAMETERS

Batch adsorption and optimization studies are already completed for Ni(II) removal, while the lab work for Cd(II) removal is still ongoing. Following the optimization study of each bio-sorbent, the combination study will follow.

2.16.1 Investigation of the removal of 20 mg/L Ni(II) and Cd(II) with a change in pH

The effect of pH was studied at pH 3, 4, 5, 6, 7 and 8. A few drops of 65% HNO_3 were added in situations where the pH exceeded the required pH value. Similarly, a few drops of 0.50 M NaOH were added to increase the pH of the solution. The bio-sorbent dosage of 0.1 g was used and agitated for an hour. The calcined OPs and SCB were added to the solutions in steady doses of 0.1 g each, and the mixture was allowed to react for 1 h. Beyond pH 9, a precipitate was seen for both elements. Hence, the effect of pH could not be investigated. The solutions were then filtered using filter paper with a 0.45 µm pore size and put through a FAAS analysis utilising an air/acetylene flame. An analytical wavelength of 232 nm for Ni and 228.8 nm for Cd and a slit width of 0.5 nm were used. The optimum pH for removing Ni(II) and Cd(II) with calcined SCB and OPs was subsequently obtained.

2.16.2 Investigation of the removal of 20 mg/L Ni(II) and Cd(II) with a change in contact time

Investigations into the effect of contact time were conducted for contact times of 10, 30, 45, 60, 90, 120, 150, 180, 210, 250 and 300 min. The pH of the solutions was adjusted to the optimum pH. The calcined OPs and SCB were added to the solutions in steady doses of 0.1 g each. The filtrate was then subjected to FAAS analysis. The ideal contact time for the remediation of water contaminated by Ni(II) and Cd(II) using calcined SCB and OPs was determined.

2.16.3 Investigation of the removal of Ni(II) and Cd(II) with a change in bio-sorbent dosage

The following dosages of calcined OPs and SCB were utilized to examine the impact of adsorbent dosage on the percentage removal of Ni(II) and Cd(II): 0.05 g, 0.1 g, 0.25 g, 0.5 g, 0.75 g, 1.0 g, 1.25 g, 1.5 g, 1.75 g and 2 g. The pH of the solution was adjusted to the optimum pH for the determined optimum contact time. The ideal dosage of calcined OPs and SCB for Ni(II) and Cd(II) removal was determined.

2.16.4 Investigation of the removal of Ni(II) and Cd(II) with a change in initial metal ion concentration

To investigate the influence of initial metal ion concentration, the optimum bio-sorbent dosage was added to 100 mL of metal ion concentrated solutions, varying in concentrations at the optimum pH. After that, the solution was stirred for the optimum contact time. This process was used for concentrated metal ion solutions of 10, 20, 40, 60, 80, 100, 120 and 150 mg/L. The solutions were filtered, and FAAS was used to determine the remaining metal ions.

2.16.5 Investigation of the removal of Ni(II) and Cd(II) with a change in solution temperature

To determine the effect of the solution temperature on the adsorption of Cd and Ni ions, all parameters were held constant while the temperature of the solutions was varied, set at 25 ^{o}C, 30 ^{o}C, 35 ^{o}C, 40 ^{o}C, 45 ^{o}C and 50 ^{o}C. The solutions were filtered and analysed using FAAS to determine the concentration of remaining metal ions. The optimum temperature for the remediation of water contaminated by Ni(II) and Cd(II) was obtained.

2.17 REAL WASTEWATER SAMPLE

Acid mine drainage (AMD) wastewater was collected from the discharge point of a coal mine, Mpumalanga province, South Africa. This water was treated with pure and calcinated SCB and OPs to investigate the potential of SCB and OPs in the presence of competitor ions.

2.18 CHARACTERISATION OF SCB AND OPS

Characterisation studies were performed using different characterisation techniques as highlighted in the aims and objectives section. The bio-sorbents were characterised before and after adsorption using FTIR spectroscopy, TGA, SEM, PXRD, and Zeta potential. The efficacy of calcinated SCB and OPs separately has been investigated for the removal of Ni(II) and Cd(II) from water. For both metal ions, the effects of adjusting pH, contact time, initial metal ion concentration, adsorbent dosage, and temperature have been evaluated. The metal ion concentration before and after treatment with bio-sorbents was determined using FAAS. For every parameter, the removal efficiency (RE) of bio-sorbents for Ni and Cd removal was calculated. For Ni(II) and Cd(II) independently, adsorption isotherm, kinetics, and thermodynamic investigations have been conducted to gain more insight into the adsorption process.

All parameters were studied in triplicate during batch adsorption studies for pH, contact time, adsorbent dosage, initial metal ion concentration, and solution temperature for both metal ions.

2.19 DESORPTION AND REGENERATION

The used bio-sorbents will be repeatedly cleaned with 0.1 M HNO_3 acting as the desorbing reagent in order to regenerate the adsorbents. The adsorbents will be filtered and equilibrated using 20 mL of 0.1 M HNO_3 for an hour after each adsorption cycle. The adsorbents will be utilized for the regeneration adsorption cycles after being thoroughly cleaned with deionized water.

2.20 PREPARATION OF THE ORGANOCLAYS

A mass of 30.0 g of the clay samples was annealed at 500 °C to remove any organic material and increase the clay's stability Dinh et al., 2022. After annealing, the organoclays were prepared according to a procedure reported in the literature Chanra et al., 2019. A mass of 20.0 g of each clay was dispersed in 1500 mL Millli-Q water, the solution was stirred with a high-speed stirrer for 2 h until the clay was homogenously dispersed in the water. Hexadecyl trimethyl ammonium bromide was weighed (based on the clay's 0.5 x CEC) and dissolved in 500 mL Milli-Q water until completely dissolved. The amount of HDTMA used was calculated based on the CEC of the clay as follows:

WWWWWWWWhtt oooo TTEETTHHHH (WW) = mm xx IIEEII xx HH xx BB (1)

where A = weight of the clay (g) and B = is molecular weight of HDTMA (g/mol); n = ratio to be used (0.5). The amounts of HDTMA used for the surface modification, calculated based on equation 1 is given in Table 2.2.

Table 2.2. Amount of HDTMA calculated for organoclay preparation.

Clay	Weight of clay (A) (g)	Molecular weight of HDTMA (B) (g/mol)	Ratio used (n)	Clay's CEC (meq/100 g)	Amount of HDTMA required (g)
Bentonite	20.0	364.45	0.5	78.6	**2.86**
Kaolin	20.0	364.45	0.5	13.1	**0.48**

The dissolved HDTMA solution was poured into the clay's solution and stirred for 24 h at room temperature. The mixed solution was then precipitated at 4000 rpm in a centrifuge. The precipitate was washed several times with Milli-Q water until it was free of bromide ions (tested with 0.1 M $AgNO_3$ solution). The resulting precipitate was then dried overnight in an oven at 60 °C. The dried organoclay samples were then ground using a mortar and pestle, sieved through a 100 µm sieve, and stored in a desiccator until use.

2.21 BATCH ADSORPTION STUDIES USING CLAYS AND ORGANOCLAYS

Batch adsorption studies were performed by stirring the solutions on a magnetic stirrer plate at a speed of 300 rpm. The effects of pH (2 - 6), contact time (30 - 300 minutes), temperature (25 – 70 °C), adsorbent mass (0.05 - 0.3 g), initial Pb(II) concentrations (5 - 100 mg/L) and the concentration of KCl (0.0 – 0.5 mol/L) on the adsorption were investigated. The adsorption studies were done in triplicate. The percentage removal (%) and adsorption capacity Q_e (mg/g) were calculated using equations described by Castro-Castro et al. (2020):

$$TTWW = \frac{CCCC - CCCC}{mm} xx\ VV \quad (2)$$

$$\%\ rrWWrroorrrrrr = \frac{CCCC - CCCC}{CCCC} xx\ 100 \quad (3)$$

where Q_e (mg/g) is the adsorption capacity, m is the adsorbent mass (g), V is the volume (L) of the solution, C_o (mg/L) is the Pb(II)concentration before adsorption, and C_e (mg/L) is the Pb(II) concentration after adsorption.

2.22 REAL WATER APPLICATION AND REGENERATION STUDIES

Borehole water was used to study the applicability of the clay adsorbents in removing Pb(II) from real water samples, as well as for the regeneration-reuse studies. The concentration of Pb(II) in borehole water was significantly lower than the highest Pb concentration that can be removed by the adsorbents; as such, the borehole water was spiked with 30 mg/L of Pb for adsorption onto bentonite and organobentonite, as well as 10 mg/L of Pb for adsorption onto kaolin and organokaolin. The usage of borehole water ensures the presence of matrix effect and, as such, can be used as a real water sample. The experiments were all performed in triplicate at a solution pH of 6, and an adsorbent mass of 1.0 g at room temperature. The best contact times for adsorption onto bentonite, kaolin and organokaolin were 120 minutes and 300 minutes for

organobentonite. After adsorption, the clay and Pb solution mixtures were filtered through a 0.45 µm filter papers and the clear solution was analysed using FAAS.

To regenerate the spent adsorbents, the residues, i.e., the clay-adsorbed materials, were agitated in 100 mL of 0.01 M HCl solution for 60 min. After agitation, the mixture was filtered and the obtained residue was rinsed with Milli-Q water and oven dried overnight at 60 °C Mudzielwana (2019), ground to a fine powder using a pestle and mortar and sieved through a 100 µm sieve. The recovered clays were used again to treat the real water samples. The regeneration-reuse process was repeated 3 more times.

2.23 STATISTICAL ANALYSIS

The analysis of variance (ANOVA) incorporated into Microsoft Excel as an add-in was used to evaluate variations occurring seasonally. The variations were determined using one-way ANOVA. The variation was considered statistically insignificant if $p > 0.05$ and significant if $p < 0.05$ at a 95% confidence level.

CHAPTER 3: RESULTS AND DISCUSSION

3.1 PHYSICOCHEMICAL PARAMETERS

Physiochemical parameters of water, such as pH, temperature, EC, DO, salinity, resistivity, ORP and TDS, were measured for all samples collected from the Mokolo River and the farms in the vicinity of the river. These physicochemical parameters are mostly used as water quality parameters. These parameters were measured in situ and their relationships are shown in Figures 3.1 and 3.2.

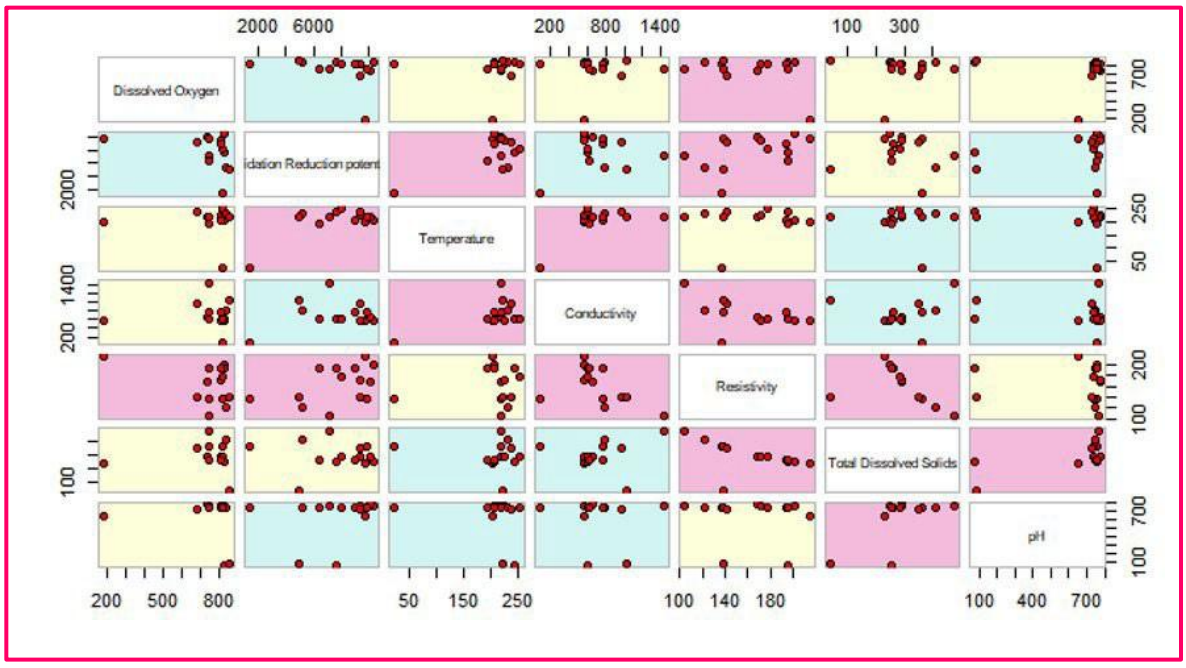

Figure 3.1. Correlation plot of all the physicochemical parameters during low-flow season.

According to Wang (2021), water with a TDS value that does not exceed 600 mg/L satisfies the water quality guidelines and is recommended for drinking and irrigation purposes (DWAF, 1996b; SANS, 2015; WHO, 2019). The TDS of water from the Mokolo River during the low flow season ranged from 23.1 to 47.8 mg/L, and it could be deduced that this water is of good quality. The ORP indicates the relationship between the reductants and oxidants, mainly focusing on the oxidants, which is the quality of water. Positive ORP readings indicate the sanitary state of water, while negative ORP readings indicate the presence of contaminants in water (US Environmental Protection Agency, 2021). The presence of elements such as DO and chlorine promotes high levels of ORP and indicates increased contamination in water. However, increasing levels of ORP indicate higher levels of water quality and sanitation. The ORP is dependent on DO. As the temperature increases, DO decreases, and ORP decreases as well. Other factors that influence DO are pressure and salinity. Dissolved oxygen decreases with a decrease in pressure as well as an increase in salinity. Decreased levels of DO indicate decreased levels of ORP. It is reported that positive ORP values that range between 650 and 750 mV indicate good sanitation (US Environmental Protection Agency, 2021). In this study, positive ORP values of 80.5 and 13.3 mV were observed in sites 8 and 11, respectively, and these ORP values indicate good sanitation. Negative ORP values were observed in all other sites except sites 8 and 11, which indicated increased contamination.

Salinity increases with an increase in EC. Thus, an increase in salinity and EC implies that the water contains high concentrations of minerals and ions. This was not the case with water samples from the Mokolo River since a constant relationship between salinity was observed. Indicating that the water from the Mokolo River does not contain high concentrations of ions. From the plot it is observed that water with lower resistivity had a high EC. There is an inverse proportionality relationship between EC and resistivity. The water samples from the Mokolo River indicated lower values of resistivity and high values of EC during low-flow season (US Environmental Protection Agency, 2021).

The TDS values of the water collected from the Mokolo River during high flow season did not exceed 600 mg/L with the exception to farm 3, which had a high TDS value of 639 mg/L. This clearly indicates that the water from this farm is not safe for consumption and irrigation purposes. It is also noted that the TDS value is extremely high as compared to the ones obtained during low flow season. This could be due to high levels of water were observed during high flow season as compared to low flow season. Additionally, it is observed that there is no clear relationship between TDS and temperature as the TDS values are scattered. Salinity and resistivity are not shown on the correlation plot for high flow season. This is because they were not measured due to the defaulting of the multi-meter during sampling.

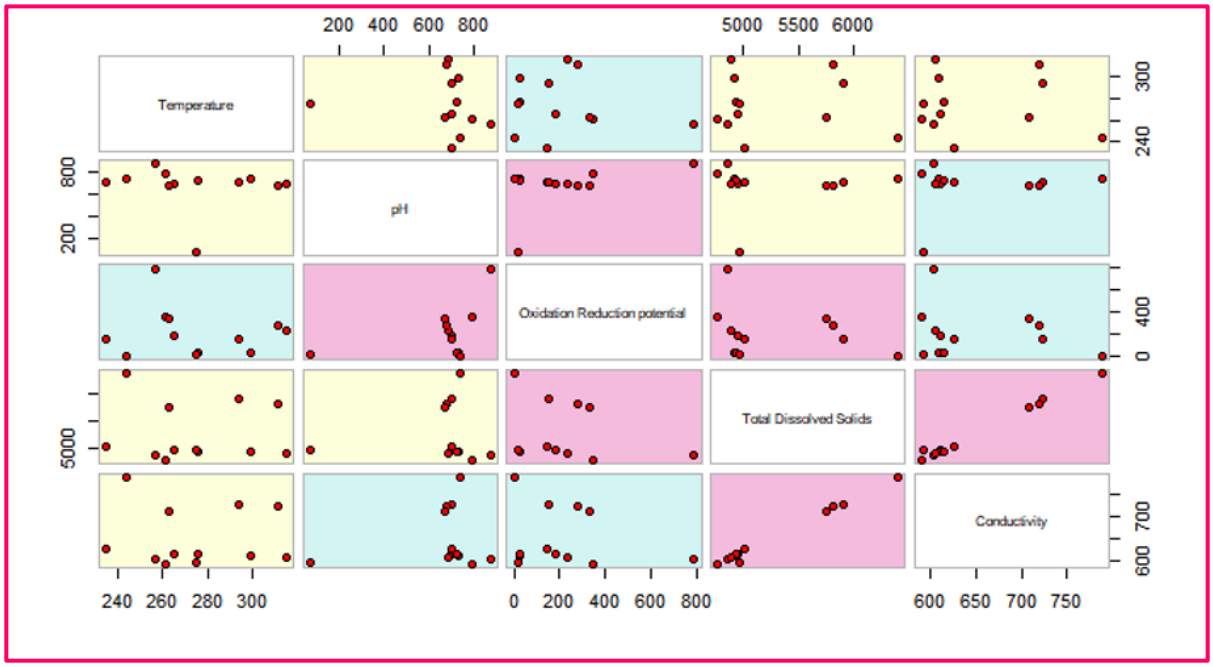

Figure 3.2. Correlation plot of all the physiochemical parameters during high flow season.

Positive ORP were observed at sites 5, 6, 8, 10, 11 and 12 as well as farm 1. This clearly indicates that the water from these sites and farm is of good quality. However, negative ORP were observed at sites 1, 2, 7, 9 and farm 3, indicating increased contamination.

A pH serves as a measurement of the alkalinity and acidity of the solution, influenced by chemicals present in water. Assessing the pH of water is crucial as it can reveal potential contamination or chemical impacts. Accurate pH assessment is particularly vital in treating both potable water and wastewater. Acceptable pH range for drinking and irrigation water falls within the range of 6.5 to 8.5 as recommended by guidelines (DWAF, 1996b; WHO, 2017). Drinking water that usually has a lower pH may lead to corrosion of pipes, resulting in the release of harmful metals such as Cu and Pb into the water supply. Conversely, water with

excessively high pH can have an unpleasant taste and be overly salty. In wastewater treatment, pH is regulated to facilitate the prompt occurrence of desired chemicals and microbial reactions.

3.2 CALIBRATION CURVE

Five (5) point calibration curves that contained 4 standards and 1 blank were constructed for quantification of all PTEs in samples by ICP-MS. These calibration curves had shown an excellent linearity with coefficient of determination (R^2) values greater than 0.999.

3.3 DETERMINATION OF LOD AND LOQ

In this study, the LOD and LOQ values obtained for the determination of selected PTEs in water samples in µg/L are 0.00720 and 0.0218 (V), 0.0114 and 0.0344 (Cr), 0.00449 and 0.0136 (Ni), 0.0213 and 0.0646 (Cu), 0.0198 and 0.0600 (As), 0.0364 and 0.110 (Cd) and 0.00696 and 0.0211 (Hg) as well as 0.0477 and 0.145 (Pb). Similarly, the LOD and LOQ obtained for the determination of vegetable samples in µg/g were found to be 0.0526 and 0.175 (V), 0.175 and 0.585 (Ni), 0.226 and 0.754 (Cu), 0.0334 and 0.111 (As), 0.00951 and 0.0317 (Cd), 0.0188 and 0.0628 (Hg), as well as 0.0534 and 0.178 (Pb). The obtained LODs for all the analytes, both in water and vegetable samples, are below 1 µg/L and 1 µg/g, respectively. The LOD of Hg, V and Pb in water samples are comparable with those reported by Nsaka, Mccrindle and Ambushe (2018). The authors reported the LOD values of 0.01, 0.05 and 0.015 µg/L for Hg, Pb and V, respectively. The obtained LOD of Cr and Cu were lower than 0.030 and 0.040 µg/L, reported by the same authors except Cd, which was above 0. 0038 µg/L reported by the authors using ICP-MS. The LOD obtained for As in this study is comparable with 0.22 µg/L reported by Letsoalo *et al.* (2018), with the employment of ICP-MS. The LODs obtained in this study show great sensitivity of the ICP-MS instrument used for analysis.

3.4 ACCURACY OF THE METHODS

Various SRMs suitable for the sample matrices were used to evaluate the accuracy of analytical methods employed for quantification of selected PTEs in water, sediment, soil, and vegetable samples using ICP-MS and ICP-OES. The percentage recoveries were computed by comparing the measured values with the certified values, as shown in Tables 3.1 to 3.4. In general, the percentage recoveries ranged from 97.5 to 115% for SRM 1640a, 76.4 to 113% in tomato leaves SRM (SRM 1573f) and tea leaves (INCT-TL-1) SRMs, 75.5 to 89.8% in SRM 2709a and SRM 2589 as well as 84.3 to 94.1 in AMIS 0373 SRM. The obtained percentage recoveries of the selected analytes in water, vegetable, soil, and sediment samples are within the acceptable range of 75-125%, which confirms a good percentage recovery as it falls within the acceptable range set by the United States Environmental Protection Agency (US EPA) (2010). Therefore, the

quantitative percentage recoveries obtained confirm the accuracy of the methods employed for the quantification of selected PTEs in the specified matrices. The precision of the method was evaluated by determining the relative percentage standard deviations (%RSDs) from triplicates of each sample. Lower %RSD that ranged from 0.0881 to 12.5% was obtained. The repeatability of these methods was proven by %RSD below 10%, falling within the acceptable range recommended by the US EPA. This aligns with the recommended %RSDs of less than or equal to 15% for each analyte, confirming the reliability and repeatability of the method employed (US EPA, 2017).

However, the percentage recovery of Hg in water was not determined due to a lack of water SRMs with established certified values for Hg. A spiking technique was introduced for the determination of Hg, but it did not produce a good percentage recovery for Hg. This was also observed with the use of SRMs that had certified values for Hg in vegetables, sediment, and soil. Though the ICP-MS is a highly effective instrument extensively employed in environmental sample analysis, detecting Hg is very challenging. This is because Hg adheres to the walls of the spray chamber and introductory system, which requires prolonged rinsing. As a result, it causes a memory effect and affects the sensitivity of the method. Therefore, the use of Hg Zeeman analyser is recommended for the successful determination of Hg in water, sediment soil and vegetables (Nsaka et al., 2018).

Table 3.1. Percentage recoveries of analytes in water SRM 1640a.

	Analytes						
	As	Cd	Cr	Cu	Pb	Ni	V
Measured Value (µg/L)	9.30	3.80	41.2	88.6	11.8	26.0	15.4
Certified Value (µg/L)	8.075	3.992	40.54	85.75	12.101	25.32	15.05
Percentage Recovery (%)	115	95.2	102	103	97.5	103	102

Table 3.2. Percentage recoveries of analytes in tomato leaves (SRM 1573f) and tea leaves (INCT-TL-1) SRM.

	Analytes						
	As	Cd	Cr	Cu	Pb	Ni	V
Measured Value (µg/g)	0.100	1.46	1.79	4.75	1.36	1.78	0.654
Certified Value (µg/g)	0.1126	1.517	1.998	4.70	1.78	1.582	0.835
Percentage Recovery (%)	88.8	96.2	89.6	101	76.4	113	78.3

Table 3.3. Percentage recoveries of analytes in SRM 2709a and SRM 2589 for soil and sediment.

	Analytes						
	As	Cd	Cr	Cu	Pb	Ni	V
Measured Value (µg/g)	10.4	1.51	98.2	26.6	2775.02	64.4	85.9
Certified Value (µg/g)	12.2	1.80	130	33.9	3091	85.0	110
Percentage Recovery (%)	85.3	83.9	75.5	78.5	89.8	75.8	78.1

Table 3.4. Percentage recoveries of analytes in AMIS 0373 SRM for soil and sediment.

	Analytes						
	As	Cd	Cr	Cu	Pb	Ni	V
Measured Value (µg/g)	78.7	< 0.072	88.7	16.1	17.5	14.6	42.5
Certified Value (µg/g)	83.6	0.09	109	20.0	20.9	16.4	47.6
Percentage Recovery (%)	94.1	-	84.3	80.5	83.7	89.0	89.3

3.5 QUANTIFICATION OF TOTAL CONCENTRATIONS OF PTEs IN WATER SAMPLES COLLECTED FROM THE MOKOLO RIVER

The total concentrations of PTEs in water samples from the Mokolo River during the low flow season are presented in Figure 3.3. The total concentrations of all the analytes in water samples were detected using ICP-MS and they varied from site to site. This might be due to different sources that contributed to the PTE levels in the Mokolo River at different sampling sites.

The total concentrations of analytes in water samples collected during the low flow season followed this trend: Ni > Cu > Cr > As > Cd > V > Pb > Hg. The total concentrations of Ni in water samples from the Mokolo River ranged from 0.557–1.22 µg/L, of which the lowest and the highest total concentrations of Ni have been detected in irrigation water samples collected from farms 1 and 2, respectively. Farm 2 is located near the main road and the two power stations located in Lephalale. Therefore, high total concentrations of Ni detected in the irrigation water from this farm could be derived from combustion of coal, diesel and fuel oils used in vehicles (Genchi, Carocci, et al., 2020). Farm 1 is located far from the power stations and the main road, so lower total concentrations of Ni were detected. High total concentrations of Cu and Pb were detected in water collected from farm 2 and site 4. During sampling, two main activities that could

contribute to high total concentrations of PTEs at this site and farm were observed. It was observed that at farm 2, they were fixing cars and welding steel. The crude oil from cars and steel produces PTEs, contributing to high total concentrations of PTEs such as Ni, Pb and Cu. Site 4 is one of the sand mining sites; hence, high total concentrations of PTEs in water collected from this site were observed.

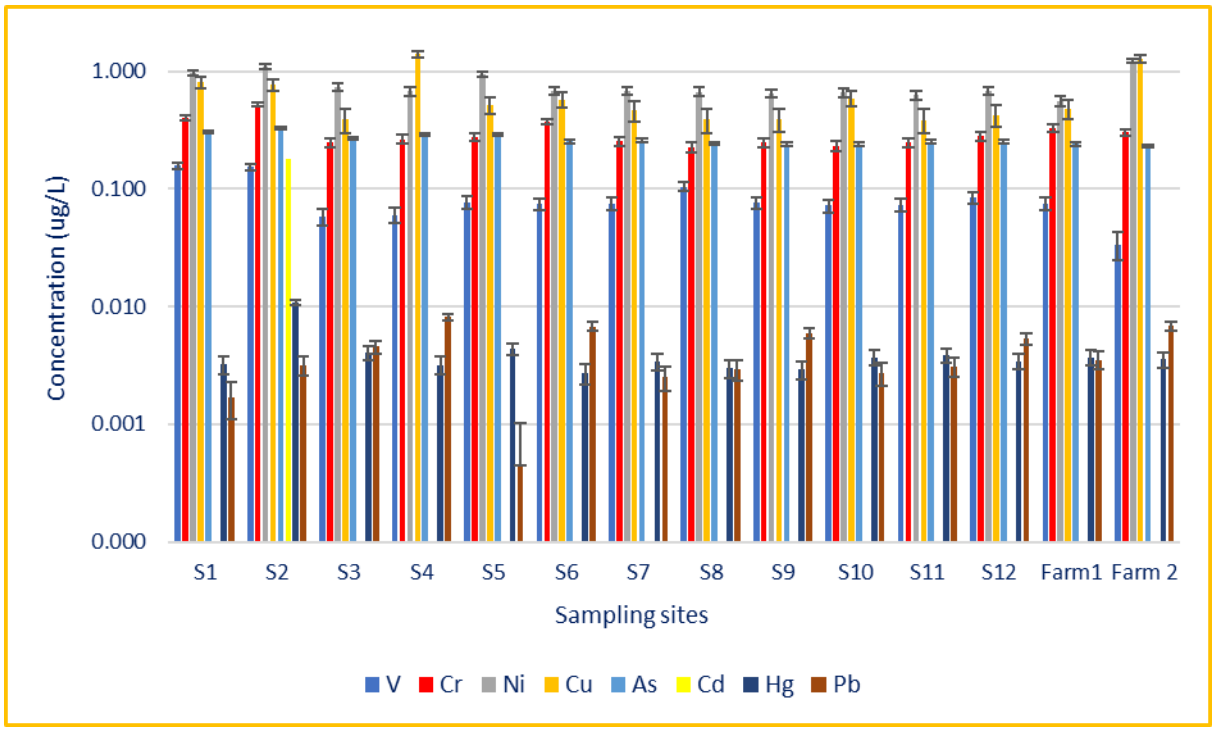

Figure 3.3. Total concentrations of PTEs in the water samples from the Mokolo River during low flow season.

Addo-Bediako (2020) assessed pollution by PTEs in the Blyde and Steelpoort Rivers of the Olifant River system, South Africa. The author reported Ni total concentrations that ranged from 26 µg/L to 100 µg/L in river water samples employing ICP-OES. The source of high metal total concentrations in the water could be due to sedimentation, environmental change, or from untreated industrial effluents. The more contaminated the sediment is, the higher the total concentrations of PTEs in water, as the water and the sediment layers are in direct contact with each other. In this study, it is evident that Cd was not detected in Mokolo River water in all the sites, with the exception of site 2, which contained a total Cd concentration of 0.180 µg/L. However, the detected Cd total concentration in site 2 could be due to agricultural activities taking place in the vicinity of this site. The total concentrations of Cd in other sites, as well as farms 1 and 2, were below the LOD value of 0.0364 µg/L. The results obtained for Cd in this study can be compared with those reported by Nsaka, McCrindle and Ambushe (2018). The authors reported that Cd total concentrations in most of the samples were below the LOD value of 0.0038 µg/L with the employment of ICP-MS. They

also reported the highest Cd total concentration of 0.946 µg/L, which was detected in water collected from Wonderfonteinspruit Dam. The Cd total content obtained in this study is 249 times greater than that obtained by Nsaka, McCrindle and Ambushe (2018).

The total concentrations of PTEs in water samples collected during the high flow season followed the following trend: Pb > Ni > Cu > As > Cr > V > Cd > Hg. As shown in Figure 3.4, it is evident that lower total concentrations of Cu, Cr, As, V, and Hg were detected in the majority of the sites. However, Cd was not detected in almost all the sites, with the exception of sites 5 and 6 that showed Cd total concentrations of 0.0380 and 0.0379 µg/L, respectively. On average, it is observed that high total concentrations of Pb were detected in water from site 5 (located near the R518 bridge) and site 8 (located near the bridge on R33 road), as well as from farm 1. Various activities were spotted at site 5, which include fishing and dumping of waste. At farm 1, they connected a pipe collecting water directly from the river, which they use for irrigation. Therefore, high total concentrations of Pb from these sites and farms could be attributed to anthropogenic activities observed, emissions from vehicle traffic, pipe rust, and burning of coal from mining and industrial activities. Maximum total concentrations of Ni (13.5 µg/L) were detected. The total concentrations of Pb in water from the Mokolo River ranged from 0.0168 to 9.95 µg/L, of which the lowest and highest total concentrations were observed in water from sites 8 and 1, respectively. High total concentrations of Ni were observed from site 11, and this could be attributed to anthropogenic activities, such as illegal dumping and untreated industrial effluents observed at this site during sampling.

The results obtained in this study are comparable to those reported by Shanbehzadeh et al. (2014). The authors carried out a study to investigate the total levels of PTEs in both water and sediment samples at upstream and downstream of the Tembi River, where sewage is discharged in Iran. They reported high total concentrations of PTEs in water at sites located downstream from sites located upstream. They further reported the highest total concentration on the downstream for Pb (1950 µg/L) in water. However, this was not the case in this study. The highest Pb total concentration reported in this study was 9.95 µg/L upstream. The highest Pb concentration in this study is 196 times lower than the one reported by the authors in their study for water and it was suggested that it is due to the effect of the entry of sewage, including untreated municipal sewage, run-offs, wastewater and leachate of solid wastes around the river (Shanbehzadeh et al., 2014).

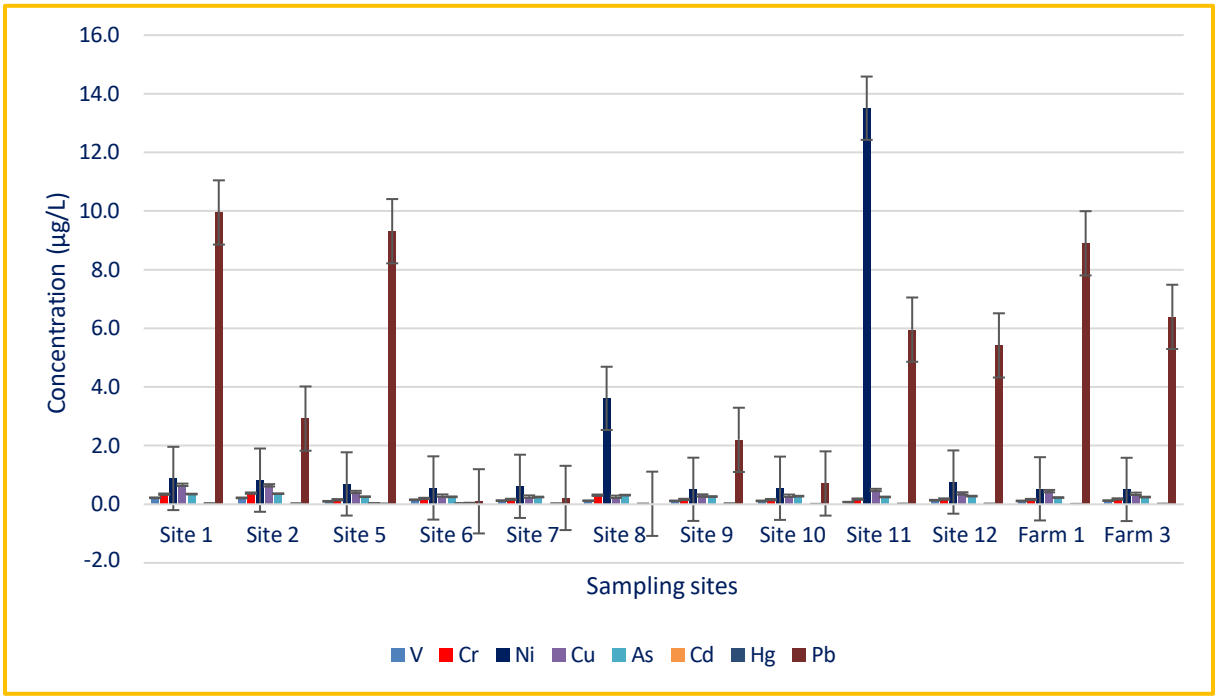

Figure 3.4. Total concentrations of PTEs in the water samples from Mokolo River during high flow season.

The overall total concentrations of all the selected PTEs quantified in water from the Mokolo River and Dam for both low and high flow seasons were compared with the guideline values established by water quality standard guidelines for safe drinking and irrigation water. Guidelines are typically used to evaluate the safety of drinking and irrigation water, with the concern to ensure water quality (DWAF, 1996b, 1996a; SANS, 2015; WHO, 2017). Table 3.5 illustrates the maximum permissible levels (MPLs) stipulated by WHO, SANS and DWAF for drinking water and Table 3.6 illustrates the target water quality range for irrigation water.

Table 3.5. Maximum permissible levels (MPLs) stipulated for drinking water.

Analyte	Standard Guidelines			Maximum Concentrations	
	WHO (µg/L)	DWAF (µg/L)	SANS (µg/L)	Low flow season (µg/L)	High flow season (µg/L)
As	10	10	10	0.325	0.362
Cd	3	5	3	0.180	0.0380
Cr	50	50	50	0.519	0.380
Cu	2000	1000	2000	1.39	0.665
Pb	10	10	10	0.00810	9.95
Hg	6	6	6	0.0107	0.0290
Ni	70	-	70	1.22	13.5
V	100	100	-	0.157	0.220

Table 3.6. Target Water Quality Range (TWQR) stipulated for irrigation water (DWAF, 1996a).

Analyte	Irrigation water guideline	Maximum Concentrations	
	TWQR DWAF (µg/L)	Low flow season (µg/L)	High flow season (µg/L)
As	100	0.325	0.326
Cd	10	0.180	0.0380
Cr	100	0.519	0.380
Cu	200	1.39	0.665
Pb	200	0.00810	9.95
Hg	-	-	-
Ni	200	1.22	13.5
V	100	0.157	0.220

As recommended by the guidelines set by DWAF, WHO and SANS, the total concentrations of the selected PTEs in drinking and irrigation water are presented in Tables 3.5 and 3.6, respectively. Total concentrations of the selected PTEs in water samples collected from the Mokolo River and Dam during low and high flow seasons were below the MPLs stipulated by DWAF, WHO and SANS. The results showed that the water quality of the Mokolo River and Dam is at an acceptable level. Therefore, the water can be recommended as safe or suitable for drinking and irrigation purposes with respect to the specified analytes. The statistical seasonal variation was insignificant ($P > 0.05$) for As and Ni and significant ($P < 0.05$) for Cd, Cr, Cu, Pb, Hg, and V at 95% confidence level. The significant variation could be attributed to increased runoffs, untreated industrial wastes and sewage discharged observed during the high flow season.

3.6 QUANTIFICATION OF TOTAL CONCENTRATIONS OF PTEs IN SEDIMENTS COLLECTED FROM MOKOLO RIVER

This study measured the total concentrations of the selected PTEs in sediments obtained from the Mokolo River and Dam during high and low flow seasons. The quantification of PTEs in sediment samples was conducted to evaluate the extent of water contamination in the Mokolo River and Dam. The polluted sediment could represent an additional source, given its capability to retain metals over extended periods and serves as a potential pollutant to surface water pollution under specific physicochemical conditions. Total concentrations of all the PTEs in sediments from the Mokolo River and Dam during low-flow season are illustrated in Figure 3.5.

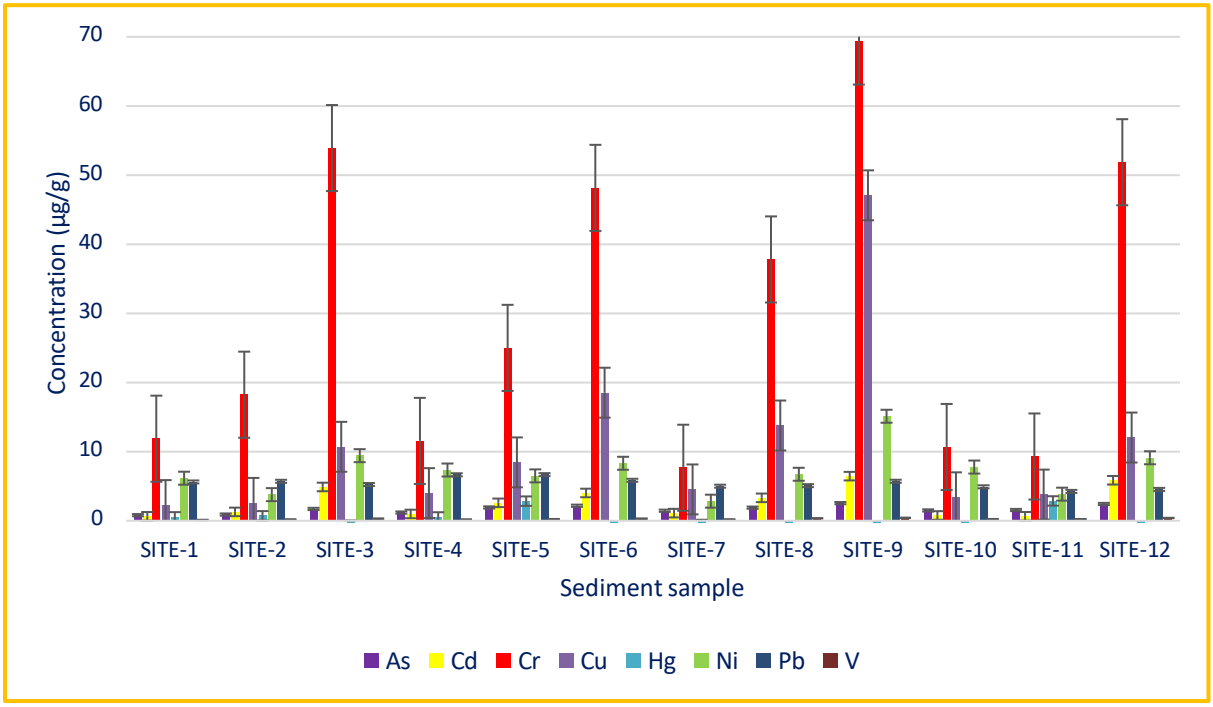

Figure 3.5. Total concentrations of analytes in sediments from Mokolo River and Dam during low flow season.

The total concentrations of analytes in sediments collected during the low flow season followed this trend: Cr > Cu > Ni > Pb > Cd > As > V. The highest total concentration of Cr (69.3 µg/g) was detected in sediment from site 9. From Figure 3.5, it is also evident that maximum total concentrations of Cu (47.1 µg/g), Ni (15.1 µg/g), Cd (6.45 µg/g), As (2.55 µg/g), and V (0.425 µg/g) were detected in the sediment sample from site 9. Site 9 is located next to the bridge or main road; these maximum total concentrations could be attributed to particulates released from vehicles as reported by Luo *et al.* (2019). The authors reported that the primary source of pollution by PTEs is predominantly attributed to vehicle exhaust-related activities. Particularly, the release of Cu and Pb into the environment occurs due to the wear and subsequent degradation of materials from automotive components, along with the use of lubricants and gasoline. Additionally, Kumar *et al.* (2020) reported that traffic emissions contribute to the pollution of Pb and Ni. Anthropogenic activities such as runoffs, waste disposal, and sewage sludges were observed at this site. The mentioned activities as well as the industrial and agricultural activities taking place in Lephalale are also potential contributors to these high total concentrations of Cr, Cu, Ni, Cd, As, and V at this site. The industries in Lephalale release their wastewater directly into the Mokolo River without any basic treatment and fly ash is deposited into the river through dry and wet depositions, leading to the accumulation of PTEs in sediments (Jin et al., 2022). The results obtained in this study are similar to those reported in the literature (Sojka, 2022). In their study, they examined the spatial arrangement, pollution levels, potential ecological hazards, and quantities of pollutants origins for Cr, Cu, Ni, Pb, Cd and Zn within the sediment of 47 rivers in Poland. They reported high total concentrations of Cr, Cu, Ni and Pb following the same trend as in this study, with Cd not being detected in some regions. Their findings revealed that the primary source of Cr, Cu, Ni and Pb in water and sediment is

attributed to both point and non-point origins, whereas the prevalence of Cd total concentrations is mainly derived from natural and point sources. Among these factors, they further concluded that urban pollution contributes to the transportation of Cu and industrial pollution is responsible for the delivery of Cr and Ni.

The total concentrations of PTEs in sediment collected during the high flow season followed this trend: Pb > Cr > Cu > Ni > Cd > As > V > Hg, as shown in Figure 3.6. This trend is like the one obtained for the low flow season, although Pb total content was observed to be the highest, followed by Cr, Cu and Ni, respectively. This also correlates with the trend obtained for water during the high flow season, whereby Pb total content was the highest. The high flow season was observed to have the highest Pb total content of 157 µg/g, detected in sediment from site 10. High Pb total concentrations were observed at sites located downstream and low Pb total concentrations were observed at sites located upstream. Sojka (2022) reported that it is expected that PTE content should increase from upstream to downstream, which is in harmony with the findings from this study. This was also confirmed by Jin *et al.* (2022). The authors reported that the highest levels of pollution with Cr, Cd, Cu, Ni, Pb, and Hg were identified at sites located midstream and downstream of the river. The High Pb levels from these sites could be attributed to various anthropogenic activities taking place closer to these sites. Sites 9, 11, and 12 also displayed high Pb total concentrations of 139, 151, and 142 µg/g, respectively. This trend is observed at sites located near the bridge and main road and the high Pb total concentrations at these sites could be attributed to vehicle exhaust and the dust from the road. In opposite sites 11 and 12, the land is being used for agricultural activities. Therefore, the high levels of Pb from these sites could be attributed to manure and fertilizers used for agricultural purposes. And as mentioned before, some of the activities observed at site 9 included waste disposals, sewage discharge and runoffs. These activities were also spotted at site 10, which could have contributed to the high total concentrations of Pb at both sites 9 and 10. However, previous studies reported that industrial operations significantly contribute to the presence of Cu and Pb (Luo et al., 2019). Similar studies indicated that industrial activities are the primary sources of contamination involving Cr, Cu, Ni, and Hg (Chen et al., 2016; Liang et al., 2017). Furthermore, Ji *et al.* (2019) reported that industrial production, particularly the discharge of industrial wastewater from factories, is linked to contamination of Pb and Ni. In this study, conducted within the industrial district of Waterberg, the Mokolo River experienced substantial impacts due to industrial operations in Lephalale area, although other sources are not ruled out. Mokolo River is also situated in a tributary of sedimentation. Therefore, it is proposed that the presence of these PTEs could be attributed to geogenic sources as well (Dong et al., 2019; Tian et al., 2020).

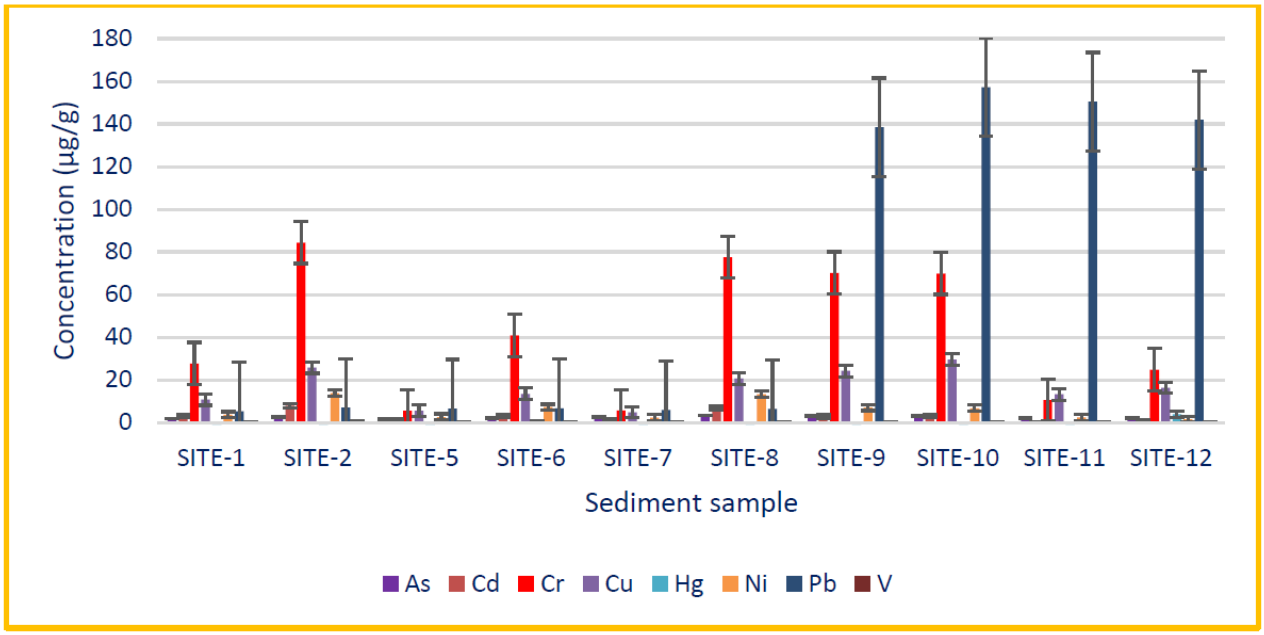

Figure 3.6 Total concentrations of all analytes in sediments from Mokolo River and Dam during high flow season.

South Africa has not set national Threshold Effect Concentration (TEC), Probable Effect Level (PEL), and the Interim Sediment Quality Guidelines (ISQGs) for freshwater ecosystems. As a result, the ISQGs and PELs proposed by the Canadian Council of Ministries of the Environment (CCME) were used in this study to assess the extent of negative health impacts resulting from the presence of PTEs in sediment exposure. These Sediment Quality Guidelines (SQGs) were formulated using ecotoxicological and ecological information sourced from various global regions, making them suitable for application in areas lacking local SQGs. Values may fall either below ISQG, within the range of ISQG and PEL or exceed PEL. These variations can result in diverse outcomes, including infrequent, periodic, and frequent occurrences of adverse biological effects. The ISQG and PEL of selected PTEs investigated in this study are presented in table 3.7, except for Ni and V as their thresholds are not provided in guidelines.

Table 3.7 The ISQGs and PELs for selected PTEs in sediment (Canadian Sediment Quality Guidelines, 1998).

Analyte	Canadian Sediment Quality Guideline	
	ISQG (µg/g)	PEL (µg/g)
As	5.90	17.0
Cd	0.600	3.50
Cr	37.3	90.0
Cu	35.7	197
Pb	35.0	91.3
Hg	0.170	0.486
Ni	-	-
V	-	-

The ISQG and PEL values of selected PTEs in sediment as stipulated by the CCME (1998) are 5.90 - 17.0 (As), 0.600 – 3.50 (Cd), 37.3 –90.0 (Cr), 35.7 –197 (Cu), 35.0 – 91.3 (Pb) and 0.170 – 0.486 µg/g (Pb). It was noted that the total concentrations of As during low and high flow seasons were below the ISQG and PEL in all sites. The Cd total content in majority of the sites were observed to be within the ISQG and PEL values except for sites 3, 6, 9, and 12 for low flow season as well as sites 2 and 8 for high flow season, which surpassed the PEL value of 3.50 µg/g. The Pb total content during low and high flow seasons were observed to be below the ISQG value in majority of the sites, apart from sites 9, 10, 11, and 12 for high flow season, which surpassed the PEL value of 91.3 µg/g. The Cr total content in majority of the sites were observed to be within the ISQG and PEL values, whereas in some of the sites it was observed to be below the ISQG value both for low and high flow seasons. The Cu total content during both high and low flow seasons were observed to be below the ISQG value, except for site 9 that surpassed the ISQG value of 35.7 µg/g during low flow season. The Hg total content in majority of the sites were below the ISQG value both for low and high flow seasons, with the exception of sites 1, 2, 4, 5, and 11 (low flow season) and site 12 (high flow season), which surpassed the PEL value of 0 486 µg/g. Total concentrations below the ISQG value suggest that harmful impacts on aquatic species and the food chain are infrequent, as the recorded total concentrations of As (in all the sites), Pb, Cr, Cu, and Hg in some of the sites are below the ISQG values. In contrast, total concentrations within the ISQG and PEL range will result in moderate biological effects towards the aquatic species and the food chain with respect to Cd, Cr and Cu total content in some of the sites. However, sites which surpassed the PEL value suggest that adverse biological effects will occur frequently on the aquatic species and the food chain with respect to Cd, Pb, and Hg. In general, the obtained results revealed that Cd, Pb, and Hg are of concern. This poses a serious threat to the food chain since the elevated total concentrations adversely impacts crucial components of the food chain (plant and bacteria). Consequently, posing an increased risk to consumers of the affected aquatic species. The statistical evaluation of seasonal variation revealed that Cd, Cr, Cu, Ni, and V were insignificant ($P > 0.05$) at 95% confidence level. However, As and Pb revealed significant variation ($P < 0.05$) at 95% confidence level. The significant variation could be due to increased runoffs and high-water levels observed during high flow season.

Nickel and V total concentrations were not examined as they do not have any ISQG and PEL values provided by the CCME. However, the results obtained for Ni in this study were compared with those reported by Mohajane and Manjoro (2022). The authors assessed the potential ecological risk of an urban

river in South Africa, and they used the TEC and PEC reported elsewhere (Vivien et al., 2020). The TEC was referred to indicate the threshold of PTEs concentration at which it is anticipated that there will be no negative ecological effects. It was reported that concentrations equal to or surpassing the TEC but falling below the PEC indicate a range where ecological effects are rarely observed. In contrast, concentrations exceeding the PEC suggest a range where ecological effects are likely to occur frequently. The reported TEC and PEC for Ni by the authors are 22.7 and 48.6 µg/g, respectively. The maximum total concentrations obtained for Ni in this study are 13.8 and 15.1 µg/g for high and low flow seasons, respectively. The obtained Ni total concentrations in this study are below the TEC and PEC values reported by the authors. Thus, this suggests that there will be no negative biological effects likely to occur towards the aquatic species and food chain with respect to Ni in the current study. However, the results obtained in this study are different to those reported by the authors in their study. They reported minimum total concentrations that are higher than the maximum total concentrations obtained in this study for Ni in both high and low flow seasons. They reported the minimum and maximum Ni total concentrations of 20.88 and 64.58 µg/g and Ni was recognized as having the potential to cause adverse impacts on aquatic animals and food chain in their study area.

3.7 QUANTIFICATION OF TOTAL CONCENTRATIONS OF PTES IN SOIL SAMPLES COLLECTED FROM LEPHALALE

In this study, PTEs in soil samples were quantified to evaluate the quality of the soil used for crop cultivation and to assess the pathways through which the selected PTEs are transported to vegetables. A total of thirteen (13) soil samples were successfully analysed during low flow season and the total concentrations of PTEs are presented in figure 3.7.

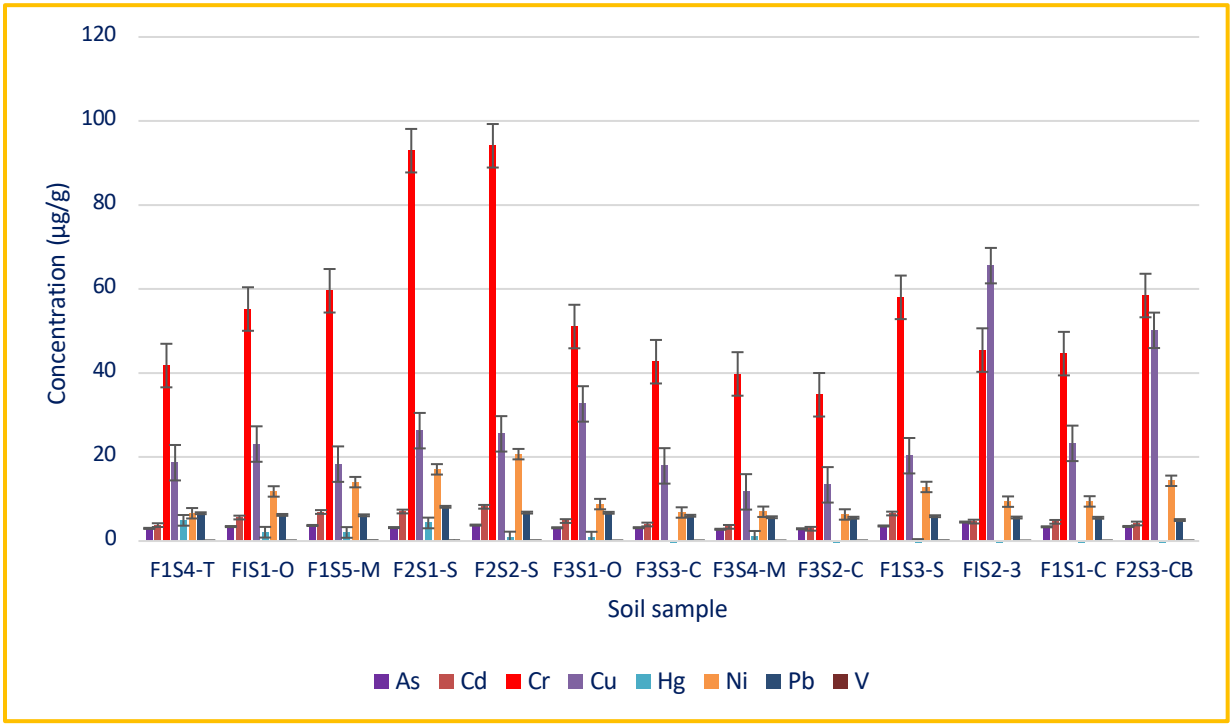

Figure 3.7. Total concentrations of PTEs in soil during low flow season.

The total concentrations of all the analytes in soil collected during low flow season followed this trend: Cr > Cu > Ni > Pb > Cd > As > V > Hg as shown in figure 3.7. The soil samples were observed to contain the highest total concentrations of Cr ranging from 34.8 – 94.1 µg/g and lowest total concentrations of Hg ranging from 0.929 – 4.90 µg/g. The highest total concentration of Cr was observed in soil (F2S2-S) collected from farm 2 and the highest total concentration of Hg was observed in soil (F1S4-T) collected from farm 1. Similarly, the highest total concentrations of Cd (8.15 µg/g) and Ni (20.7 µg/g) were observed in soil collected from farm 2. Whereas, the highest total concentrations of As (4.52 µg/g), Cu (65.6 µg/g), Pb (8.15 µg/g) and V (0.149 µg/g) were observed in soil collected from farm 1. These highest total concentrations of Cr, Cd and Ni at farm 2 could be attributed to the various activities taking place at this farm, which include panel beating steel, use of manures, petrol chemicals and vehicle exhaust. Alternately, the highest total concentrations of As, Cu, Pb, Hg and V at farm 1 could be attributed to the mining industries taking place in Lephalale, burning of coal from the power stations, use of manure and water from Mokolo River for irrigation purposes (Hasnine et al., 2017; Obinnaa & Christian, 2019; Rashid et al., 2023). The results for the soil are in consistent to those obtained for vegetables during low flow season. It was observed that the soil (F2S2-S) that contained high total concentrations of Cr is the same soil that was used for cropping the spinach vegetable (F2S2-S) that contained the highest total concentration of Cu during low flow season. Therefore, this clearly shows that when PTEs accumulate in agricultural soil, the non-biodegradable PTEs are taken up by plants, resulting in contamination of the food chain.

The measured total concentrations of As, Pb, Ni, Hg, and V in all the soils that were used for cropping the 13 vegetables were below the MPLs of 12, 70, 50, 6.6 and 130 µg/g, respectively, as stipulated by the Canadian soil quality guidelines shown in table 3.8 (Canadian Council of Ministries, 1999). However, the total concentrations of Cd in all the soils that were used for cropping the 13 vegetables surpassed the MPL of 1.4 µg/g stipulated by the Canadian soil quality guideline. Additionally, the highest total concentrations of Cr only surpassed the MPL of 64 µg/g with respect to the soil that was used for cropping spinach vegetables from farm 2 site 1 (F2S1-S) and farm 2 site 2 (F2S2-S). Whereas, the highest total concentration of Cu surpassed the MPL of 63 µg/g with respect to the soil that was used for cropping the spinach vegetable from farm 1 site 2 (F1S2-S). The introduction of the highest total concentrations of Cr and Cu could be due to the use of manures to improve the fertility of the soil used for cropping. Livestock manures primarily derived from poultry, cattle, and pig manures, serve as organic fertilizers and they contain elevated total concentrations of PTEs such as As, Cd, Cr, Cu, Pb, Ni, Hg, and V as pollutants. The prevalent agricultural practice involves applying these manures and the resulting compost to farmlands for crop production, hence highest total concentrations of Cd, Cr and Cu in these soils (Liu et al., 2020; Zhuang et al., 2020). Overall, it can be deduced that majority of the soils used for cropping the 13 vegetables during low flow season were not contaminated with high levels of As, Cd, Cr, Cu, Pb, Hg, Ni, and V. The results obtained from soil analysis are also in agreement with those obtained for water in this study. The water used for irrigation in all the farms was found to be safe for irrigation and drinking regarding the investigated PTEs, in this study. Therefore, the soil used for cropping in the three different farms is suitable for commercial and agricultural practices.

Table 3.8. Canadian Soil Quality Guidelines for selected PTEs.

Analyte	CCME	Maximum Concentrations	
	SQG (µg/g)	Low flow season (µg/g)	High flow season (µg/g)
As	12	4.52	3.25
Cd	1.4	8.15	29.1
Cr	64	94.1	92.6
Cu	63	65.6	89.9
Pb	70	8.15	81.7
Hg	6.6	4.92	< 0.0387
Ni	50	20.7	12.1
V	130	0.149	0.145

Similar to vegetables collected during high flow season, a total number of seven (7) soil samples used for cropping the respective vegetables were successfully analysed and the total concentrations of all the analytes are presented in Figure 3.8. It is also important to note that only soil collected from farms 1 and 3 were analysed due to not getting access to farm 2 during high flow season.

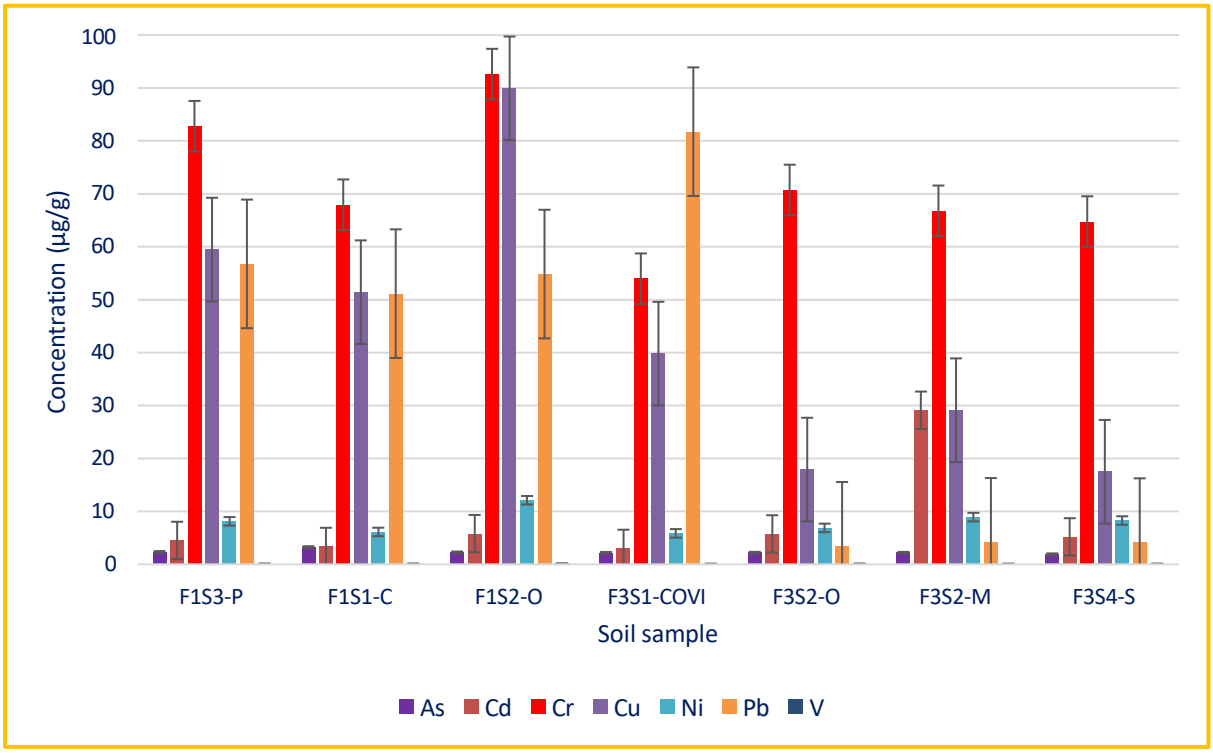

Figure 3.8. Total concentrations of all the analytes in soil during high flow season.

The total concentrations of all the PTEs in soil collected during high flow season followed this trend: Cr > Cu > Pb > Cd > Ni > As > V. Similar to the trend observed during the low flow season, Cr was found to be the highest, with total concentrations ranging from 54.0 to 92.6 µg/g followed by Cu. However, Cd and Pb total concentrations are higher than Ni total concentration as compared to the low flow season. The results obtained are comparable to those reported by Balkhair and Ashraf (2016). The authors reported high total concentrations of Cr ranging from 0.87 to 1.00 mg/kg in soil from the Western region of Saudi Arabia, which is lower than the highest total concentration of Cr reported in this study. Additionally, they also reported lower total concentrations of Cd, Cu, Pb, and Ni than those reported in this study. This could be due to soil from Lephalale being more contaminated with the selected PTEs than soil from the Western regions of Saudi Arabia. From Figure 4.20, it is also evident that Hg was not detected in all the analysed soil samples. Soil used for cropping in farm 1 accumulated the highest total concentrations of the selected PTEs than the soil used for cropping in farm 3. The highest total concentrations of As (3.25 µg/g), Cr (92.6 µg/g), Cu (89.9 µg/g), Ni (12.1 µg/g), and V (0.145 µg/g) were observed in soil used for cropping vegetables in farm 1. Whereas, the highest total concentrations of Cd (29.1 µg/g) and Pb (81.7 µg/g) were observed in soil used

for cropping vegetables in farm 3. At both farms they use water from the river for irrigation and manure for increased soil fertility, of which attributes to high total concentrations of the selected PTEs in soil from these farms. It is also evident that high total concentrations of Cr, Cu, and Ni were observed in soil sample where onion sample collected from farm 1 site 2 (F1S2-Onion), Covi soil sample from farm 3 site 1 (F3S1-Covi), and pumpkin soil sample from farm 1 site 3 (F1S3-Pumpkin), respectively. The results obtained are in consistent with those obtained for vegetables during high flow season. It was observed that the soil (F3S1-Covi) that contained the highest total concentrations of Cu is the same soil that was used for cropping the Covi vegetable (F3S1-covi) that contained highest total concentration of Ni during high flow season. As compared to the low flow season, the total concentrations of As and Ni decreased with 68.9 and 72.0 %, respectively from high to low flow season in relative to all the soil used for cropping. However, total concentrations of Cd, Cr, Cu, Pb, and V increased with 63.0, 77.5, 61.2, 16.8, and 98.8 %, respectively from low to high flow season in relative to all the soil samples used for cropping. The statistical analysis revealed that Cd, Cr, Cu, Ni, and V were insignificant ($P > 0.05$) at 95% confidence level. However, As and Pb were significant ($P < 0.05$) at 95% confidence level. This variation is due to higher water levels in seasons of higher precipitations or rainfall as well as use of organic fertilizers to improve the fertility of soil.

The total concentrations of As, Pb, Hg, Ni, and V in all the soil used for cropping the 7 vegetables were below the soil quality guideline values of 12, 70, 6.6, 50, and 130 µg/g, respectively with the exception to Cd and Cr, which surpassed the soil quality guidelines of 1.4 and 64 µg/g, respectively. However, the highest total concentration of Cu surpassed the soil quality guideline of 63 µg/g with respect to the soil that was used to crop the onion vegetable from farm 1 site 2 (F1S2-O), chomolia vegetable from farm 1 site 3 (F1S3-C), pumpkin vegetable from farm 1 site 3 (F1S3-P) and Covi vegetable from farm 3 site 1 (F3S1-Covi). Luo *et al.*(2011) also reported Cd total concentrations that surpassed the action values of the Dutch standard in soil near E-waste processing site in China. The results are in harmony with those reported for soil during low flow season. They revealed that the soil used for cropping at farm 1 and farm 2 during high flow season is suitable for commercial and agricultural use regarding As, Pb, Hg, Ni, and V.

3.8 QUANTIFICATION OF TOTAL CONCENTRATIONS OF PTEs IN VEGETABLES COLLECTED FROM LEPHALALE

The PTEs may enter the human body through consumption of contaminated food. In this study, the total concentrations of the PTEs were quantified to assess if the vegetables collected from the farms, irrigated with water from Mokolo River are safe for consumption. Total concentrations of all the PTEs in these vegetable samples collected from the vicinity of Mokolo River during low flow season were successfully quantified and are presented in Figure 3.9.

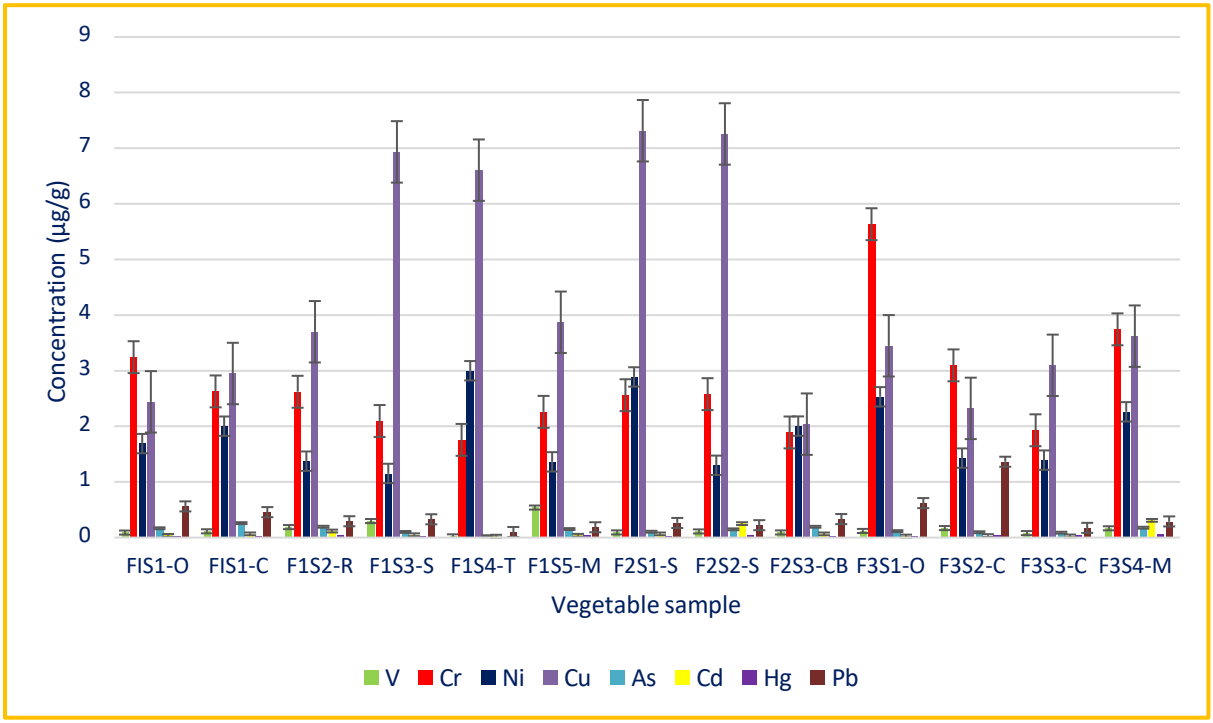

Figure 3.9. Total concentrations of all the PTEs in vegetables during low flow season.

The total concentrations of the PTEs in vegetables during low flow season followed this trend: Cu > Cr > Ni > Pb > V > As > Cd > Hg. This shows that these vegetable samples contained high total concentrations of Cu, which ranged from 2.04 to 7.31 µg/g, of which the lowest and highest total concentrations of Cu were detected in vegetable samples collected from farm 2 site 3 and farm 2 site 1, respectively. The lowest Cu total concentration of 2.04 µg/g was detected in cabbage sample (F2S3-CB) and the highest Cu total concentration of 7.31 µg/g was detected in spinach sample (F2S1-S). High total concentrations of Cu were detected from the vegetables collected from farm 2. As mentioned above, at farm 2 there was panel beating of steel. Hence, high total concentrations of Cu, Cr, Ni and Pb in these vegetable samples could be linked to the panel beating activity. Copper is one of the elements found in fertilizers, high total concentrations of Cu in vegetables from this farm might be due to the use of fertilizers to enhance plants growth. Although, Cu is regarded as one of the essential macronutrients for plants because of its role as activators of numerous enzymes and cofactors for oxidative enzymes, excessive absorption of it may inhibit numerous metabolic functions, resulting in plant retardation and damage, which, in turn, results in lower yields (Malan et al., 2015). Due to the fact that plants serve as significant sinks for both essential and non-essential PTEs within the terrestrial ecosystem, elevated levels of PTEs in agricultural soil would consequently raise the absorption of these PTEs by crops cultivated in such soils. Consequently, this heightened uptake would contribute to an increase in PTEs content in the human diet (Malan et al., 2015).

The results obtained in this study are comparable to those reported by Bvenura and Afolayan (2012) in their study of PTEs contamination of vegetables cultivated in home gardens in the Eastern Cape. They

reported high Cu total concentrations that ranged from 0.62 to 8.70 µg/g. The Cu total concentration range of 2.04 to 7.31 µg/g that was detected in vegetables, in this study, falls within the same range reported by the authors in their study. The authors also reported that high total concentrations of Cu were obtained in onion, followed by tomato and spinach, whereas low total concentration of Cu were obtained in cabbage samples. In this study, high total concentrations of Cu were detected in spinach followed by tomato and low total concentration of Cu were detected in cabbage. The results obtained in this study provide clear evidence that leafy vegetables accumulate high total concentrations of PTEs than fruity and stem vegetables (Mekonnen et al., 2015).

Low total concentrations of Hg that ranged from 0.00561 to 0.0637 µg/g were detected in vegetable samples, of which the lowest total concentration (0.00561 µg/g) of Hg was detected in tomato sample from farm 1 site 4 (F1S4-T) and the highest total concentration (0.0637 µg/g) of Hg was detected in Mo'china sample from farm 3 site 4 (F3S4-M).

The vegetable samples collected from the farms in the vicinity of Mokolo River contained varying total concentrations of all the analytes. These total concentrations were compared with those recommended by the World Health Organisation and the Food and Agriculture Organization (WHO/FAO) as well as those used by other authors in other studies as shown in table 3.9 (Codex Alimentarius Commission Joint FAO/WHO, 1995; Gebeyehu & Bayissa, 2020; Li et al., 2018; Mekonnen et al., 2015; Shaheen et al., 2016).

Table 3.9. The MPLs stipulated by WHO/FAO in vegetables.

Analyte	Standard Guideline	Maximum Concentrations	
	WHO & FAO (µg/g)	Low flow season (µg/g)	High flow season (µg/g)
As	0.1	0.260	0.273
Cd	0.2	0.309	0.0825
Cr	2.3	5.63	7.72
Cu	10	7.31	26.3
Pb	0.3	1.36	8.75
Hg	0.03	0.0637	0.0255
Ni	10	3.00	54.7
V	0.03	0.540	0.630

From this study, it is evident that the concentrations of Cu, Hg and Ni were below the MPLs stipulated by the WHO/FAO of 10, 0.03 and 10 µg/g, respectively (table 3.9). Concentration of Cd in almost all the vegetable samples were observed to be below the MPL of 0.2 µg/g, except for F2S2-S and F3S4-M, which

surpassed with concentrations of 0.251 and 0.309 µg/g, respectively. Whereas Cr concentrations in almost all the vegetable samples exceeded the MPL stipulated by the WHO/FAO of 2.3 µg/g, apart from F1S3-S (2.10 µg/g), F1S4-T (1.76 µg/g), F2S3-CB (1.89 µg/g), and F3S3-C (1.93 µg/g). It is also evident that V concentrations in all the vegetable samples exceeded the MPL stipulated by WHO/FAO of 0.03 µg/g, except for tomato sample (FIS4-T), which had low concentration of 0.02 µg/g (Shirkhanloo et al., 2015). Whereas As concentrations in 8 vegetable samples were below the MPL stipulated by WHO/FAO of 0.1 µg/g except for onion (F1S1-O), chomolia (FIS1-C), rape (F1S2-R), cabbage (F2S3-CB) and mo'china (F3S4-M), which had concentrations of 0.167, 0.260, 0.195, 0.194 and 0.178 µg/g, respectively. Concentrations of Pb in 9 vegetable samples were also observed to be below the MPL of 0.3 µg/g, with the exception to onion (F1S1-O and F3S1-O) and chomolia (FIS1-C and F3S2-C) samples, which surpassed with 0.560 to 0.620 µg/g and 0.457 to 1.36 µg/g, respectively. Therefore, it can be deduced that the vegetable samples collected from the farms in the vicinity of Mokolo River during low flow season are contaminated with high concentrations of As, Cr, Cd, Pb, and V.

Vegetables collected during high flow season are fewer as compared to those collected during low flow season. This is due to not getting access to farm 2 and some of the vegetables were unavailable at local farms as they grow different vegetables each season. In general, seven vegetables were collected during high flow season and the total concentrations of all the PTEs in each vegetable sample are illustrated in figure 3.10.

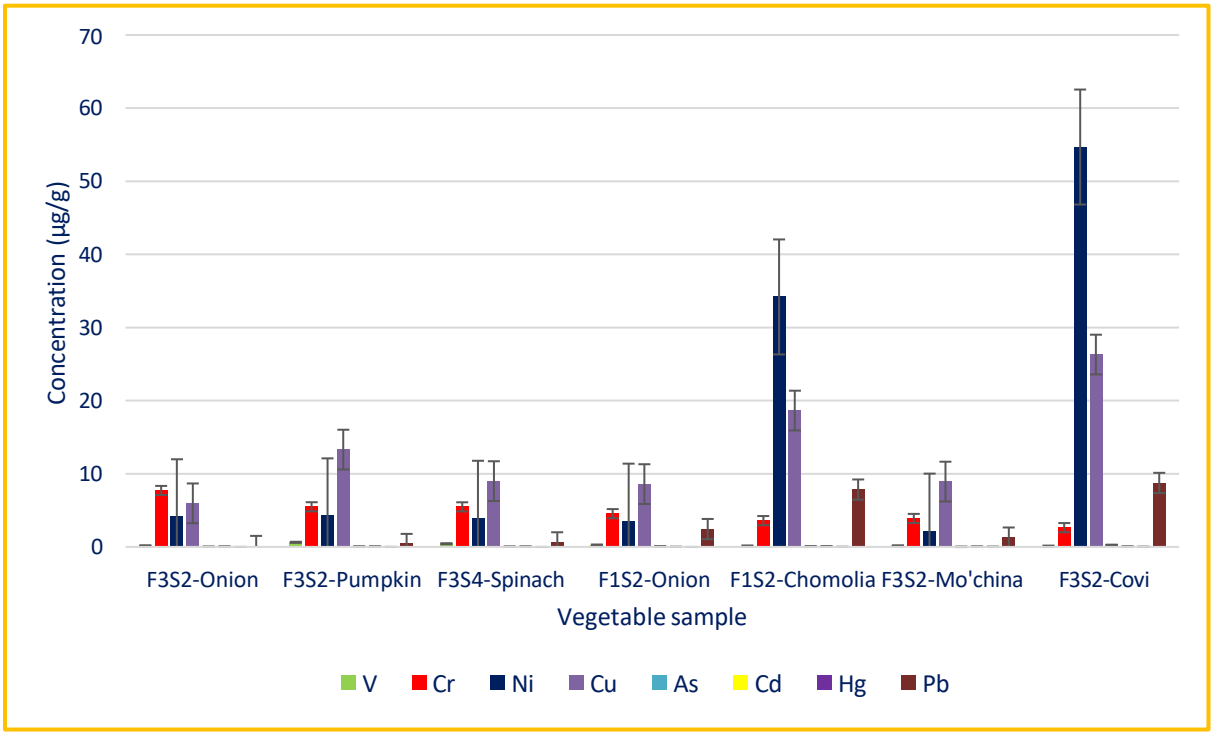

Figure 3.10 Total concentrations of all the analytes in vegetables during high flow season.

The total concentrations of all the PTEs in vegetables collected during high flow season followed this trend: Ni > Cu > Cr > Pb > V > As > Cd > Hg as shown in figure 3.10. This vegetable samples contained highest total concentrations of Ni, which ranged from 2.16 to 54.7 µg/g. This trend is similar to the one obtained for low flow season, although Ni level was observed to be the highest, followed by Cu, Cr and Pb, respectively. The lowest and highest Ni total content were observed in vegetable samples from Farm 3 site 2. The lowest Ni level was observed in Mo'china vegetable sample (F3S2-M), and the highest Ni level was observed in covi vegetable sample (F3S2-Covi). It is evident that Hg total concentration was the lowest in all the vegetable samples as it was also observed during low flow season, with a range of 0.00420 to 0.0254 µg/g. The lowest Hg total content was observed in spinach (F3S4-S) sample from farm 3 site 4 and the highest Hg total content was observed in Mo'china (F3S2-M) sample from farm 3 site 2. The highest total concentrations of Cu (26.3 µg/g), As (0.273 µg/g) and Pb (8.75 µg/g) were observed in the covi (F3S2-Covi) sample collected from farm 3 site 2, which is the same covi sample that contained the highest Ni total concentration. The highest Cr (7.72 µg/g) and V (0.630 µg/g) total concentrations were observed in onion (F3S2-O) and pumpkin (F3S2-P) samples from farm 3 site 2, respectively. However, the highest Cd (0.0825 µg/g) total concentration was observed in chomolia sample (F1S2-C) from farm 1 site 2. The results revealed that highest total concentrations of Ni, Hg, As, Pb, Cu, Cr, and V were observed in vegetable samples collected from farm 3. At farm 3, they were burning wood next to the vegetable garden and use it to cook food. Burning of wood results in the generation of a significant quantity of ash. This ash contain varying concentrations of PTEs such as As, Cd, Cr, Pb, and Hg, though these total concentrations can be highly variable (Etchie et al., 2020). Ash can be transported by wind, spread out and deposited in surface water and soil and alternately accumulated by plants from the soil resulting in contamination of the food chain. Since the ash may contain elevated total concentrations of PTEs, it poses a potential risk to humans and other animals that come into contact with airborne particles or consumes the contaminated vegetables (Pacifico et al., 2023).

The total concentrations of Cr and V in all the vegetable samples during high flow season surpassed the MPLs stipulated by WHO/FAO of 2.3, and 0.03 µg/g, respectively except for Cd and Hg which were below the MPLs stipulated by WHO/FAO of 0.2 and 0.03 µg/g, respectively. Alternately, it is observed that the total content of Cu in F3S2-Onion, F3S4-Spinach, F1S2-Onion, and F3S2-Mo'china were below the MPL of 10 µg/g stipulated by WHO/FAO apart from its concentrations in F3S2-Pumpkin, F1S2-Chomolia and F3S2-Covi, which were higher than 10 µg/g stipulated by WHO/FAO with concentrations of 13.3, 18.6, and 26.3 µg/g, respectively. Similarly, it was observed that the total concentration of As in F3S2-Covi (0.273 µg/g) as well as Ni in F1S2-Chomoila (34.2 µg/g) and F3S2-Covi (54.7 µg/g) surpassed the MPL stipulated by WHO/FAO of 0.1 and 10 µg/g, for As and Ni, respectively. However, the total concentration of Pb in almost all the vegetable samples surpassed the MPL of 0.3 µg/g, except for F3S2-Onion, which was below the MPL with concentration of 0.122 µg/g. Therefore, the obtained results for high flow season revealed that majority of the vegetable samples are contaminated with high concentrations of As, Cr, Cu, Pb, Ni, and

V posing a serious threat to the people who consumes them. The statistical seasonal variation was insignificant for As, Cd, and V ($P > 0.05$) and significant for Cr, Cu, Pb, Hg, and Ni ($P < 0.05$) at 95% confidence level. The difference in variation could be attributed to agricultural activities observed during high flow season.

The results obtained in this study can be compared with those reported by Malan *et al.*(2015) in the Phillippi horticultural area in the Western Cape province, South Africa. The authors reported maximum total concentrations of 0.06, 4.48, 9.24, 1.66, and 0.14 mg/kg for Cd, Cr, Cu, Ni, and Pb, respectively in vegetables during high flow season. However, the maximum total concentrations obtained in this study are higher than those reported by the authors in their study. The authors further reported that maximum total concentrations of these PTEs were detected in leafy vegetables such as lettuce and cabbage. This was also confirmed in this study since the maximum total concentrations of selected PTEs were mostly observed in leafy vegetables such as Mo'china and Covi. Additionally, the authors reported high total concentrations of Pb and Cd, which surpassed the MPLs stipulated by South African legislation and regulations made for cosmetics, and disinfectant act during winter than summer, whereas Cu and Ni were reported to be high during summer than winter, but within the MPLs stipulated. However, in this study high total concentrations of the selected PTEs were observed during high flow season than low flow season. This could be because Cape Town experiences lower temperature and most rainfall during winter, whereas Lephalale experiences high temperature and most rainfall during summer. They further reported that Cd and Pb surpassed the MPLs stipulated, whereas Cu and Ni were below MPLs.

3.9 HUMAN HEALTH RISK ASSESSMENT

In performing the human health risk assessment for both the adult and child population of Lephalale that consumes the contaminated vegetables, the THQ was used to determine the non-carcinogenic human risk associated with consumption of these contaminated vegetables (Gebeyehu & Bayissa, 2020). The obtained THQ values for adult and children population of Lephalale for both seasons are presented in Figures 3.11 to 3.14.

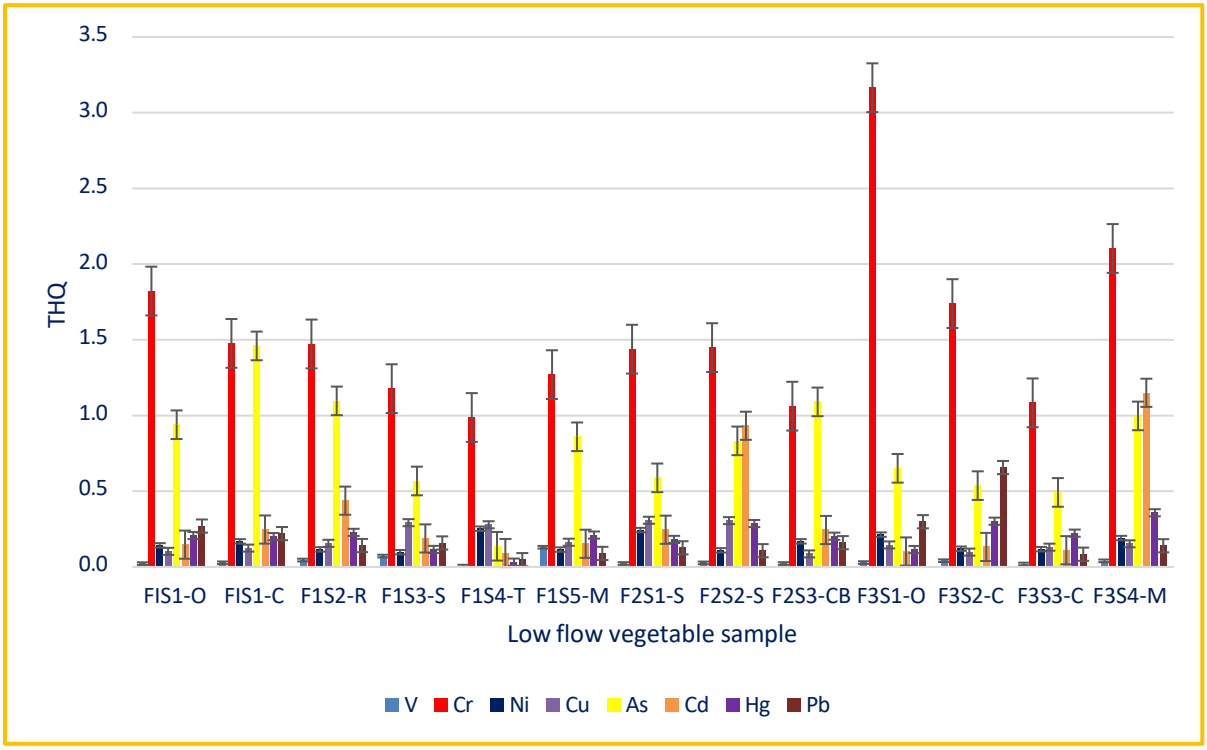

Figure 3.11 THQ values for adult during low flow season.

From Figure 3.11, it is evident that the THQ values of the adult population that consumes the contaminated vegetables are below 1, with consumption of all the vegetables contaminated with Cu, Pb, Hg, Ni, and V. Consumption of almost all the vegetables contaminated with Cd showed THQ values less than one, with the exception to Mo'china vegetable (F3S4-M) from farm 3 site 4, which showed THQ value (1.15) greater than 1. This clearly indicates that consumption of these vegetable samples will pose no risk to human health, with the exception to F3S4-M contaminated with Cd. However, Cr showed the highest THQ of 3.17 with consumption of onion (F3S1-O) from farm 3 site 1. There are possible high risks associated with consumption of almost all the vegetables contaminated with Cr with the exception to consumption of these vegetables (F1S4-T) from farm 1 site 4, which had THQ value (0.987) less than 1. Additionally, it is also observed that consumption of chomolia (F1S1-C), rape (F1S2-R), and cabbage (F2S3-CB) vegetables that had THQ values (1.46, 1.10, and 1.09, respectively) greater than 1 pose serious risks to the adult population with respect to As. The majority of the vegetable samples showed THQ values less than 1, indicating that there will be no risks threatening the health of the adult population that consumes these contaminated vegetables, with respect to Cu, Pb, Hg, Ni, and V during low flow season. However, consumption of all the vegetables contaminated with Cr and some of the vegetables contaminated with As and Cd is of serious concern.

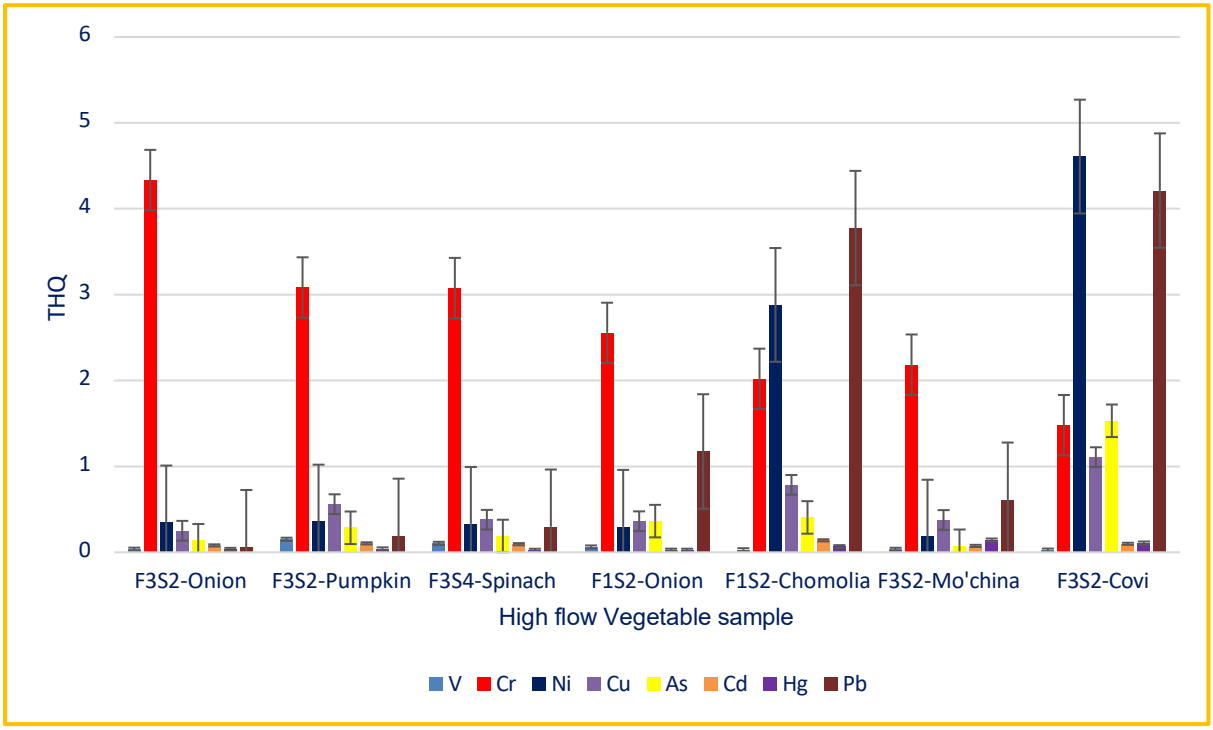

Figure 3.12. THQ values for adult during high flow season.

The THQ values of the adult population that consumes the contaminated vegetables during high flow season were less than 1, with consumption of all the vegetables contaminated with Cd, Hg, and V. Consumption of almost all the vegetables contaminated with As and Cu showed THQ values less than 1 apart from Covi vegetable (F3S2-Covi) from farm 3 site 2, which had THQ values of 1.53 and 1.11 for As and Cu, respectively. However, the THQ values of all vegetables contaminated with Cr were greater than 1 with the highest THQ of 4.33 observed in onion (F3S2-O) from farm 3 site 2. It is also evident that consumption of chomolia (F1S2-chomolia) and Covi (F3S2-Covi) will result in possible health risks with respect to Ni (2.88 and 4.61) and Pb (1.17 and 4.21). The results revealed that THQ values obtained during high flow season are greater than THQ values obtained during low flow season. Consumption of Covi (F3S3-Covi) will result in higher possible risks to the adult population as compared to 6 other vegetables. However, consumption of all vegetables contaminated with Cr and some of the vegetables contaminated with As, Cu, Pb, and Ni threatens the health of the adult population during high flow season. The results obtained are similar to those reported by Duan et al. (2017). The authors reported Cr as one of the PTEs that accumulated high THQ values for both the adult and children population. In this study, Cr accumulated highest THQ values than other PTEs in almost all the vegetables for both adult and child population.

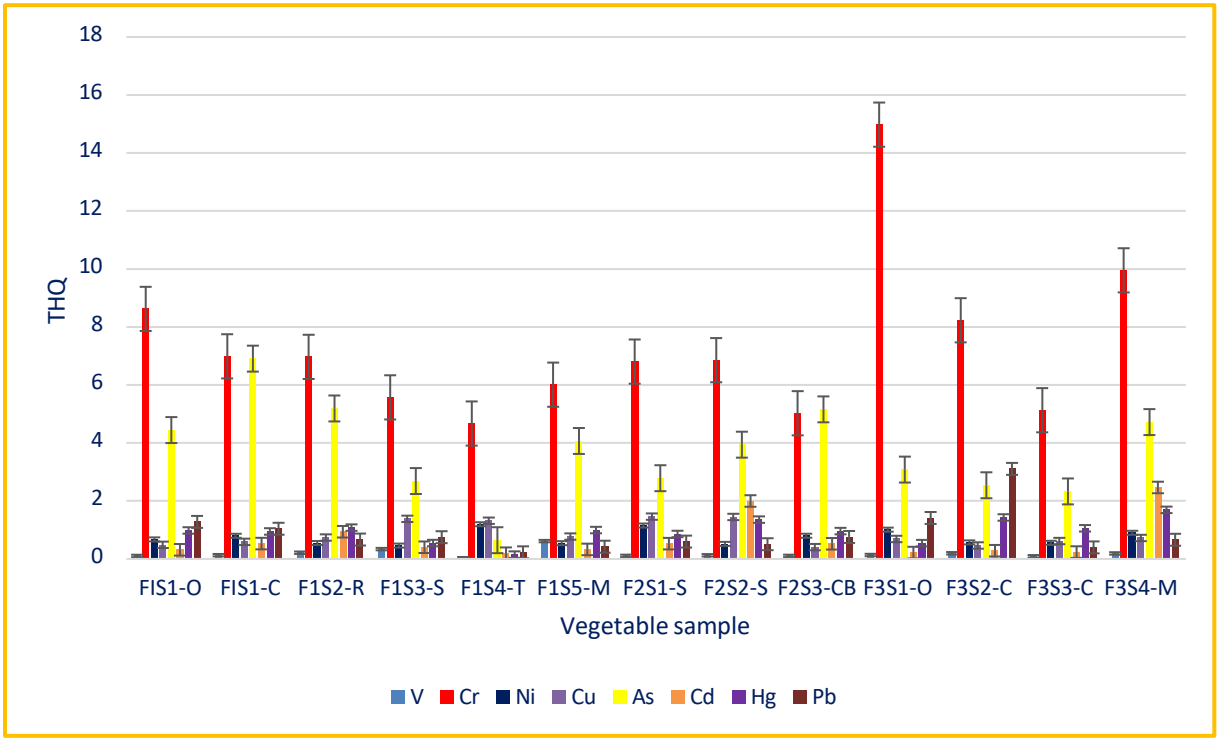

Figure 3.13. THQ values for children during low flow season.

The THQ values for children population that consumes the contaminated vegetables were observed to be greater than 1 with consumption of all the vegetables contaminated with Cr. The highest THQ value was observed to be 15.1 with consumption of onion (F3S1-O) contaminated with Cr from farm 3 site 1 as displayed in figure 3.13. Consumption of almost all the vegetables contaminated with As showed THQ values greater than 1 with the exception to consumption of thepe (F1S4-T) from farm 1 site 4, which had a THQ value (0.646) less than 1. Additionally, it is observed that vegetables contaminated with Cd (F2S2-S and F3S4-M), Cu (F1S3-S, F1S4-T, F2S1-S, and F2S2-S), Pb (F1S1-O, F1S1-C, F3S1-O, and F3S2-C), Ni (F1S4-T, F2S1-S, and F3S1-O) and Hg (F1S2-R, F2S2-S, F3S2-C, F3S3-C, and F3S4-M) had THQ values greater than 1. The results revealed that the health of the children population is threatened with exposure to As, Cd, Cr, Cu, Pb, Ni, and Hg. However, it is observed that the THQ values of all vegetables with exposure to V were less than 1, indicating that there are no possible health risks associated with consumption of these vegetables to the children population.

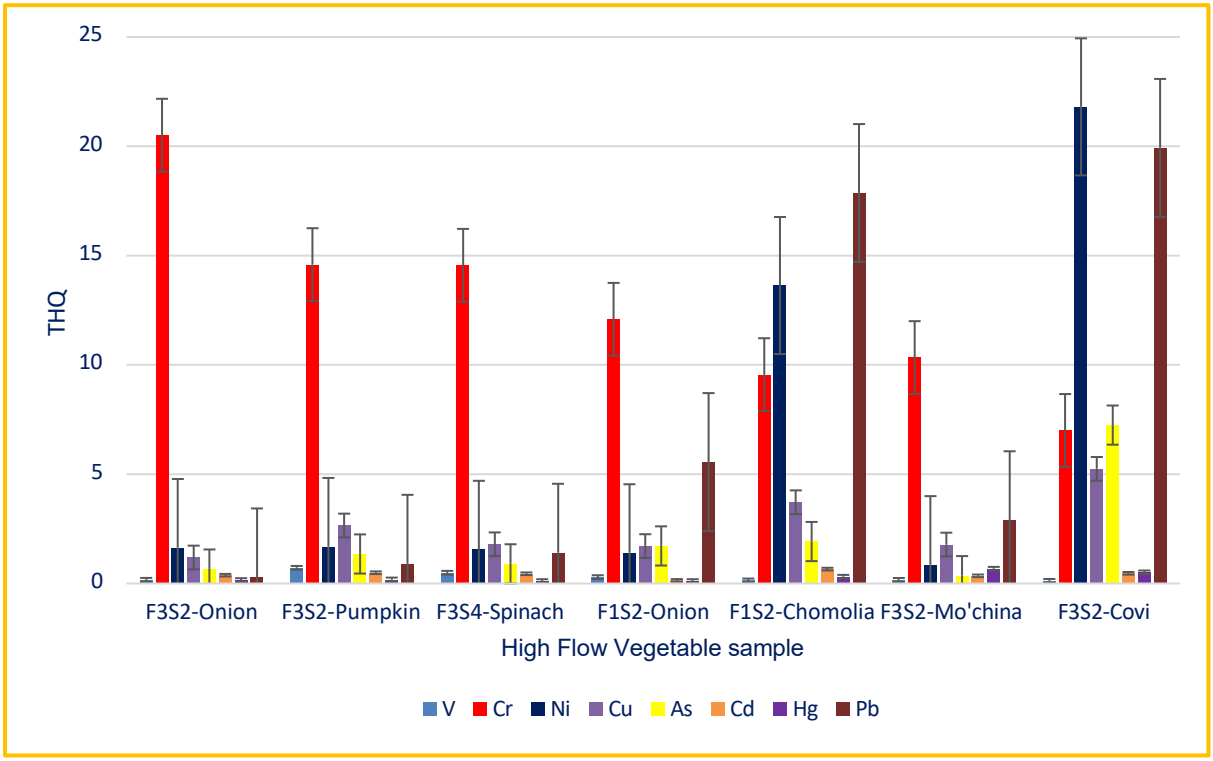

Figure 3.14. THQ values for children during high flow season.

The THQ values for the child population that consumes the contaminated vegetables during high flow season are observed to be less than 1, with consumption of all the vegetables contaminated with Cd, Hg, and V. However, consumption of all the vegetables contaminated with Cr and Cu will result in possible health implications to the children population. The highest THQ value was observed to be 21.8 for Ni with respect to consumption of F3S2-Covi as shown in Figure 3.14. Consumption of Covi (F3S2-Covi) pose serious health risks to the children population as compared to other vegetables. Similar results were observed for adult population during high flow season. The health of the child population is threatened with consumption of majority of vegetables contaminated with As, Pb, and Ni. Therefore, the results have revealed that the health of the children population is more threatened than the health of the adult population during both low and high flow seasons. This could be because the average body weight and exposure durations of children are lower than those of adults. Similar results were reported by Xu et al. (2016) and it was proposed that it could be attributed to the fact that children have lower body weight as compared to adults.

The hazard index (HI), which considers the cumulative effect of ingesting numerous PTEs from various vegetables, has also been determined and the results are shown in figure 3.15 (low flow season) and 3.16 (high flow season). For each vegetable, the HI was computed by finding the sum of all the analytes in each vegetable sample.

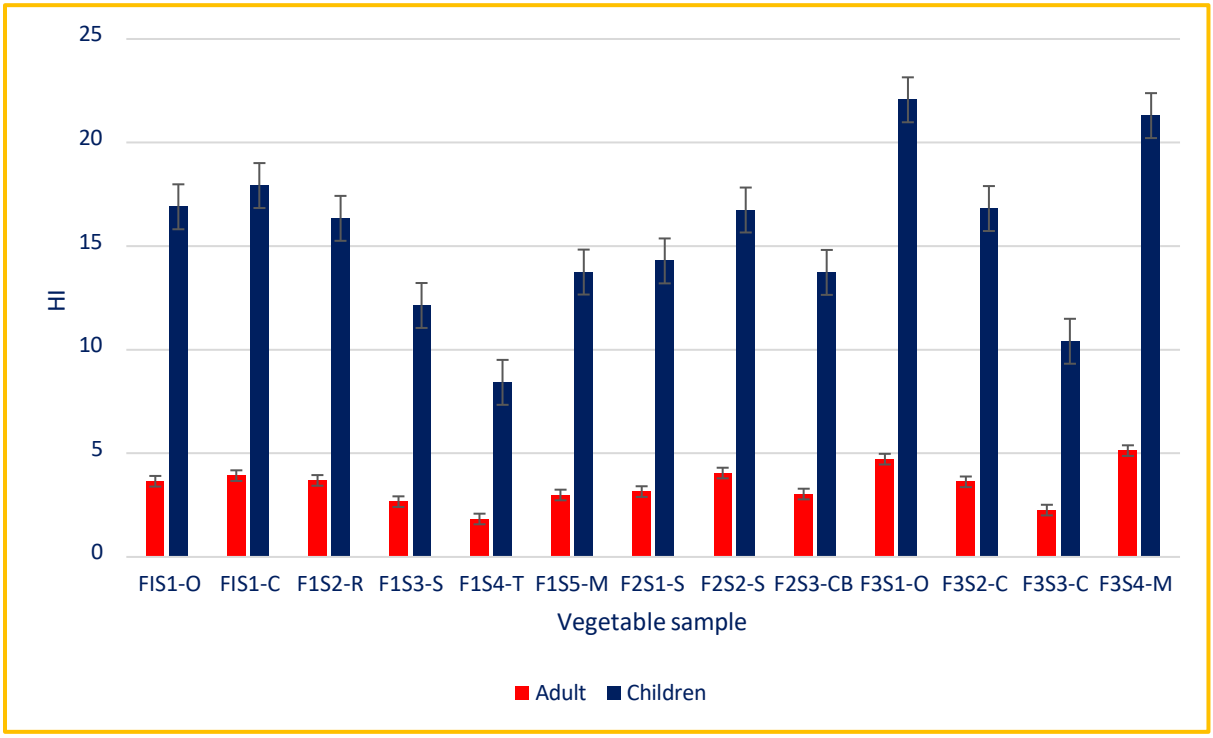

Figure 3.15. The HI values for adult and children population of Lephalale during low flow season.

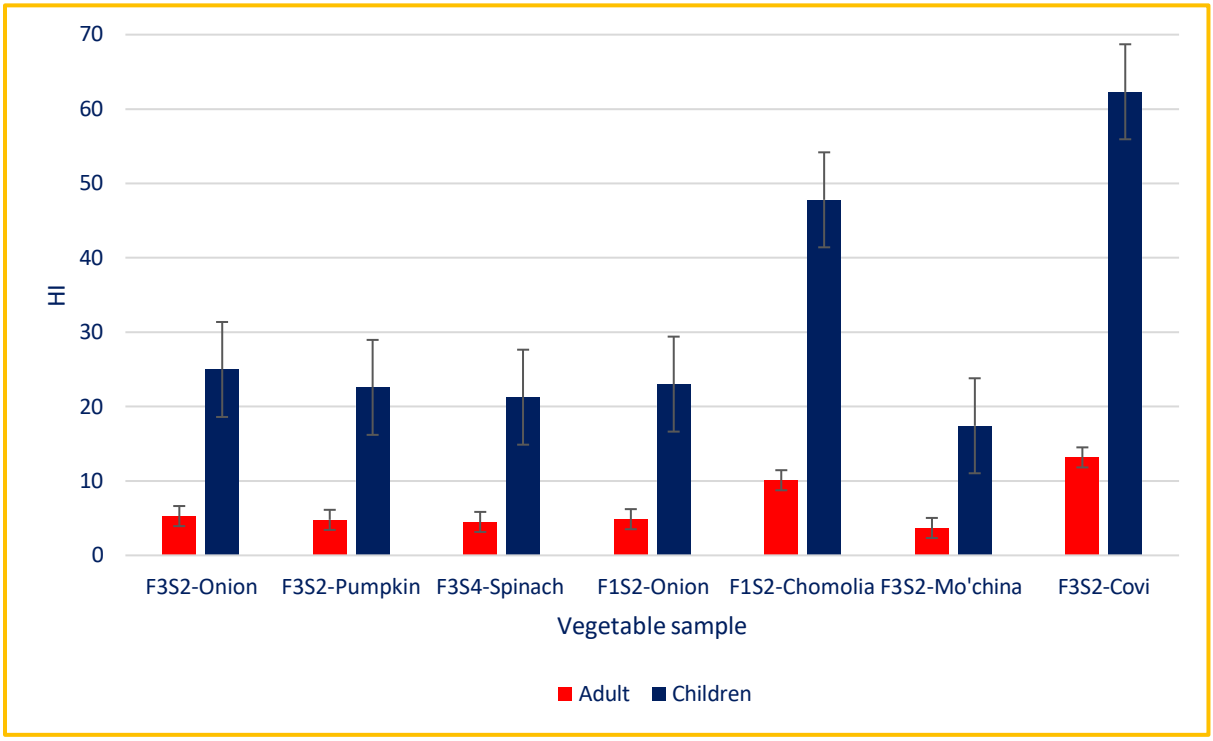

Figure 3.16. The HI values for adult and children population of Lephalale during high flow season.

From Figures 3.15 and 3.16, it is observed that the HI values for the children and adult population during both low and high flow seasons are greater than 1. The highest HI values obtained during low flow season are 5.13 and 21.3 (observed in F3S4-M) for adult and children's population, respectively. Alternately, the highest HI values obtained during high flow season are 13.2 and 62.3 (observed in F3S2-Covi) for adult and children's population, respectively. Therefore, this confirms that there are potential health implications threatening both the health of the adult and children population with consumption of all the vegetables during both low and high flow seasons in relative to the PTEs considered in this study. The results obtained in this study are similar to those reported by Jiménez-Oyola et al. (2021). The authors reported that both the adult and children's exposure were above the exposure safety limit.

3.10 TOTAL CONCENTRATIONS OF PTEs IN WATER SAMPLES FROM STEELPOORT AREA

River water (RW) and borehole water (BW) samples were analysed to determine the total concentrations of the selected PTEs. The variation in concentrations of PTEs reflected the diverse activities occurring within the sampling areas. Table 3.10 provides the total concentrations of PTEs during the low-flow season. The detailed summary of PTEs concentration during low-flow season showed that most elements were within MPL of the WHO and SANS except V in RW4 and Cr in BW5 to BW7. The overall average observed concentrations of PTEs in BW and RW samples followed the trend: Cr > V > Ni > Cu > Pb > As > Cd > Hg. The highest total concentrations of Cr from Steelpoort River and boreholes ranged from 1.69 to 114 µg/L and an average of 24.5 µg/L with about 23% above MPL. The lowest concentration was observed in RW1 (1.69 µg/L), while the highest concentration was in BW6 (114 µg/L). The total concentrations of V ranges from 1.66 to 31.1 µg/L with an average of 18.8 µg/L. The total concentrations of V in about 8% of the total sampling sites exceeded the MPL stipulated by the WHO. The value of Ni ranged from 0.741 to 14.2 µg/L and was within the permissible limit. The concentrations of Cu ranged from 0.703 to 7.05 µg/L, which is negligible when compared to MPL of 2000 µg/L stipulated by the WHO and SANS. Munyangane et al. (2017) reported that As is mostly found bearing within various mineralization, especially gold mineralization. The concentration of As ranged from 0.16 to 1.12 µg/L, which was also below the MPL of 10 µg/L. Cadmium is not abundant when compared to other minerals in earth crust and mostly exist in groundwater naturally (Panda et al. 2022). Low concentrations of Cd were also observed from the study conducted by Nsaka et al. (2018). Cadmium was found to be the second least dominant at the range of 0.0385 to 0.107 µg/L. The concentrations were within MPL, which indicates that the Cd-bearing rocks and pollutants were not dominant in the region compared to V and Cr-bearing rocks. Mercury was least dominant element with total concentrations ranging from 0.00737 to 0.0248 µg/L in water. The total concentrations of Pb in water ranged from 0.134 to 1.80 µg/L, which was also found to be within acceptable limit.

The sampling site RW1 (Figure 3.17), located upstream and distant from anthropogenic activities, showed minimal PTEs contamination, confirming its relatively pristine condition. In contrast, the borehole where BW6 sample was collected, has been operating for over 36 years, may also be a factor contributing to the

elevated levels of PTEs, as shown in Figure 3.18. Other boreholes have been operating for 10-20 years, and also reflected these factors in their levels of PTEs. The prominent level of Cr concentration in BW was also observed from the study conducted by Munyangane et al. (2017) from Greater Giyani, with the average concentration of 33.1 µg/L for the low-flow season. The authors also reported one borehole with the highest concentration of 69.5 µg/L, which is above the MPL established by SANS (SANS, 2015). Munyangane et al. (2017) related the increase of Cr level in BW in their study with the Cr-bearing mineral chromite, evapotranspiration effects due to hot climate changes, and high pH, which could also be related to the current observation of Cr concentration in samples BW5 to BW7. Elsewhere in India, the study by Panda et al. (2022) reported high concentrations of Cr in BW with a range of 38.5–256.1 µg/L during the low-flow season. The authors related the increase of Cr contamination with the opencast mine within the region and soil erosion in relation to the geological process.

Table 3.10. Total concentrations of PTEs in water during the low-flow season.

Samples	V (µg/L)	Cr (µg/L)	Ni (µg/L)	Cu (µg/L)	As (µg/L)	Cd (µg/L)	Hg (µg/L)	Pb (µg/L)
RW1	1.80 ± 0.0692	1.69 ± 0.0971	0.741 ± 0.0364	0.933 ± 0.0229	0.142 ± 0.00589	0.0397 ± 0.00831	0.00855 ± 0.0000234	0.516 ± 0.00424
RW2	1.66 ± 0.0777	1.78 ± 0.0665	1.00 ± 0.0788	1.55 ± 0.0884	0.157 ± 0.0238	0.0385 ± 0.00482	0.00744 ± 0.000286	0.355 ± 0.0190
RW3	2.44 ± 0.108	2.66 ± 0.116	0.860 ± 0.0133	0.960 ± 0.0496	0.189 ± 0.0102	0.0547 ± 0.00395	0.00853 ± 0.000180	0.421 ± 0.0133
RW4	31.1 ± 0.326	8.38 ± 0.131	0.633 ± 0.00423	1.13 ± 0.0468	0.226 ± 0.0234	0.0626 ± 0.00298	0.00797 ± 0.000337	0.491 ± 0.00161
RW5	24.6 ± 0.557	4.36 ± 0.105	0.774 ± 0.0356	1.07 ± 0.0458	0.208 ± 0.0242	0.0636 ± 0.00851	0.00846 ± 0.000517	0.375 ± 0.0175
RW6	28.1 ± 3.39	5.74 ± 0.554	1.19 ± 0.0861	1.33 ± 0.115	0.318 ± 0.0325	0.107 ± 0.0655	0.0248 ± 0.00182	1.10 ± 0.209
Bw1	29.3 ± 1.31	8.37 ± 0.606	1.15 ± 0.0502	1.64 ± 0.178	0.327 ± 0.0209	0.0954 ± 0.0109	0.00832 ± 0.000864	0.327 ± 0.0490
Bw2	29.4 ± 1.08	3.20 ± 0.192	9.22 ± 0.292	1.21 ± 0.0863	1.03 ± 0.0208	0.0592 ± 0.00365	0.00737 ± 0.000220	0.719 ± 0.0442
Bw3	22.8 ± 1.36	3.14 ± 0.358	3.47 ± 0.259	0.761 ± 0.0184	0.377 ± 0.0344	0.0703 ± 0.00922	0.00837 ± 0.000292	0.380 ± 0.0785
Bw4	13.2 ± 1.74	4.28 ± 0.0262	13.4 ± 0.0597	0.703 ± 0.00219	1.10 ± 0.158	0.0639 ± 0.00149	0.00885 ± 0.000652	0.134 ± 0.0209
Bw5	20.8 ± 0.812	91.6 ± 4.62	1.99 ± 0.0679	1.33 ± 0.0186	0.224 ± 0.0344	0.0721 ± 0.0101	0.00776 ± 0.000526	1.62 ± 0.0801
Bw6	20.2 ± 0.458	114 ± 2.92	14.2 ± 0.670	3.69 ± 0.0560	0.279 ± 0.0304	0.0675 ± 0.00889	0.00743 ± 0.000213	1.80 ± 0.00889
Bw7	19.1 ± 0.763	68.9 ± 2.73	0.404 ± 0.0334	7.05 ± 0.272	0.259 ± 0.0249	0.0687 ± 0.00371	0.0074 ± 0.000369	0.719 ± 0.0972
Min	1.66	1.69	0.404	0.703	0.142	0.0385	0.00737	0.134
Max	31.1	114	14.2	7.05	1.10	0.107	0.0248	1.80
Average	18.8	24.5	3.77	1.80	0.372	0.0664	0.00933	0.689
SANS[a]	-	50	70	2000	10	3	6	10
WHO[b]	30	50	70	2000	10	3	6	10

a (DWAF, 1996; SANS, 2015), b (WHO, 2017)

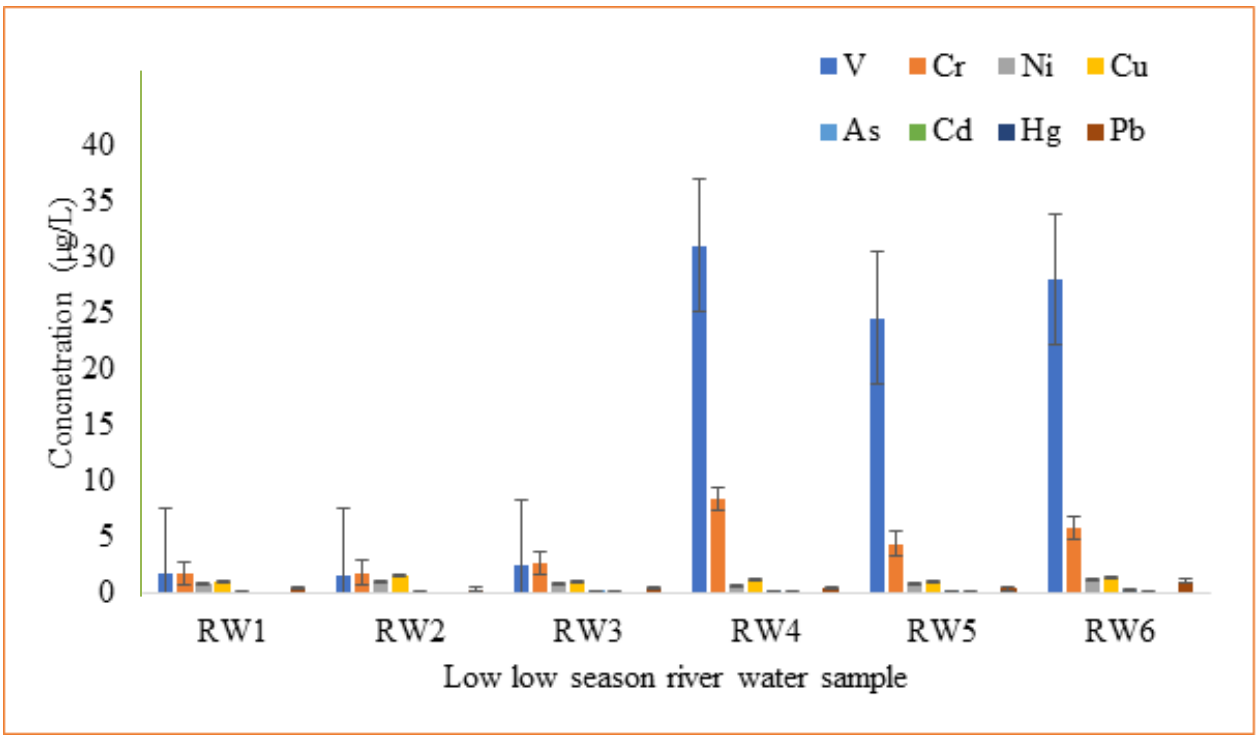

Figure 3.17. Total concentrations of PTEs in Steelpoort River water samples during low-flow season.

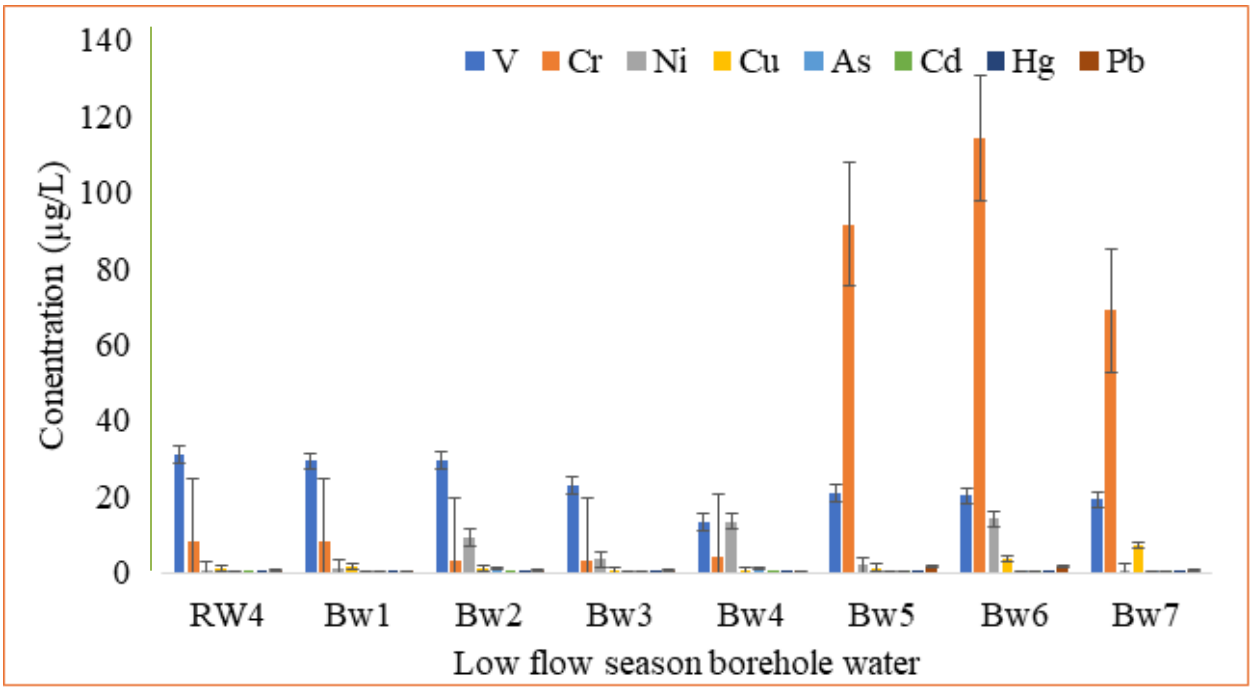

Figure 3.18. Total concentrations of PTEs in borehole water samples during low-flow season.

The trend in RW samples followed the order: V > Cr > Cu > Ni > Pb > As > Cd > Hg. Vanadium concentrations in RW ranged from 1.16 to 31.1 µg/L. The RW1 had the lowest V concentrations due to its distance from possible contamination sources. The observation was evident when Makgoale et al. (2022)

conducted the study in Steelpoort River; the authors reported species of vertebrates that are sensitive to pollution adapting to live at sites where pollutants are not prominent. The sites where this pollution-sensitive vertebrate was obtained were within the proximity of RW1, confirming the least contamination by pollution. Sample collected from site RW4, located under a bridge, near a main road, and close to a smelting area, exhibited the highest V concentration, which could be related to emissions from the smelting industry and frequent gas emissions by vehicles. The water samples from RW5 and RW6 also showed prominent V and Cr levels, which could be associated with industrial activities.

High levels of V were consistently observed in BW samples from Steelpoort and Driekop areas. The total concentrations of Cr and V in RW3–6 could be attributed to nearby mining, smelting, and human activities observed during sample collection. The sampling site where RW3 was collected is located directly across from a smelting industry and a sub-power station. Additionally, due to the absence of a bridge at the site, vehicles frequently drive through the river, as illustrated in Figure 3.19. This could contribute significantly to the levels of PTEs. At RW4, a scrap yard, mining activities, road, and brick-making processes were close to the site, contributing to PTE levels through oil spillage, grease, and particulate distribution from cement, including constant gas emissions from mines and vehicles. Similarly, the effect of greases and oil spillage was observed by Dikotla and Ambushe (2024) from the study conducted in Mokolo River, Lephalale of Limpopo province. The authors reported high levels of PTEs associated with the bridge over the river and human activities such as welding and scrapyard.

Figure 3.19. Images showing vehicles and animals passing through site 3 of Steelpoort River.

Sampling site RW5, located under a bridge, showed contamination from the discharge of the domestic sewer and possible mining effluent, as observed from the water's colour and odour in Figure 3.20. Concentrations of PTEs for most samples were within the MPLs set by SANS, DWAF, and WHO (DWAF 1996; SANS 2015; WHO 2017), except for V in RW4 and Cr in BW5-BW7. The V concentrations in RW6, BW1, and BW2 were close to the MPL threshold, making them potentially unsafe for drinking, as levels could increase over time.

Figure 3.20. Image showing the colour of the water and pollution around site 5 of Steelpoort River.

The observed concentrations of PTEs from different sites were within safe levels, except for RW4 and BW5 to BW7. Regular monitoring and mitigation measures are essential to ensure the safety and reliability of these water sources. The results of the current study are comparable with those reported by Nsaka, McCrindle & Ambushe (2018). The authors reported high levels of Cr and V in surface and groundwater, which were found to be higher than 1 and 0.763 µg/L, respectively, than world average concentrations in unpolluted water.

High levels of V and Cr in RW and BW samples in the study area were anticipated since the production of high-quality steels involves the use of ferrous materials containing V, making smelting and ferrochrome industries prominent sources of V and Cr contamination. These industries, located near sampling sites RW3-RW6 in Steelpoort, could contribute significantly to the elevation of levels of PTEs, including V levels, due to industrial waste and metallurgical slags (Moskalyk and Alfantazi, 2003).

The abundance of V in the Earth's crust, being 1.2 times that of Cr and 66.7 times that of As, also explains the higher V concentrations in water. Moderate levels (25-49 µg/L) of V were reported by Wright & Belitz (2010) in California, USA, similar to the moderate contamination observed in three RW and six BW samples. Existence of V in RW could have resulted from the by-product of the smelting industry near the river and geological position for BW due to the black reef belt in the Sekhukhune District (Moskalyk and Alfantazi, 2003). This suggests a combination of anthropogenic sources and natural geological contributions.

In BW samples, V concentrations can be influenced by ORP and pH, which affect the dissolution/precipitation and adsorption/desorption of V-bearing rocks such as carnotite, roscoelite, vanadinite, mottramite, patronite, and descloizite ores in South Africa. Vanadium readily reacts with oxygen across various pH ranges. According to Wright & Belitz (2010), V(III) and V(V) species are dominant at pH 7-8. The findings of polluted water by V align with the study conducted by Nsaka et al. (2018), where borehole and river water were observed to exceed the world average concentration in an unpolluted river. Meanwhile, the study conducted by Dikotla & Ambushe (2024) in Mokolo River reported a low concentration of V in water, which was below 0.763 µg/L, which confirms the unpolluted river water by V.

Chromium levels in river water were expected to exceed permissible limits due to nearby chromite mines. However, the total concentrations were below MPL, possibly due to effective waste effluent control to the river. Adhikari et al. (2022) reported high Cr levels in Steelpoort River from smelting and mining industries, which were anticipated in the current study. The low-flow rate during sampling likely caused Cr particles to settle into sediments and river tailings, as observed by Adhikari et al. (2022) in Sekhukhune land. A study by Addo-Bediako et al. (2018) at De Hoop Dam and Steelpoort River reported increased Cr downstream compared to upstream, with concentrations of 30-80 µg/L using ICP-OES. This increase was attributed to mine waste washing off riverbanks. Another study by Addo-Bediako (2020) found that the Steelpoort River was more contaminated than the Blyde River, with Cr concentrations ranging from 0.2-0.9 µg/L, lower than previous and current studies. Kgaphola et al. (2023) suggested that land use and cover could influence Cr contamination levels.

The total concentrations of Ni, Cu, and Pb in RW samples were found to be low when compared with other studies conducted on similar locations and Limpopo province. Previous studies conducted by Addo-Bediako (2020) and Addo-Bediako et al. (2018) reported higher concentrations of Ni, Cu, Pb, and As in Steelpoort River. The current study found Ni concentrations ranging from 0.76 µg/L in RW1 to 1.20 µg/L in RW6, significantly lower than the 10–30 µg/L and 26–100 µg/L reported in studies conducted in 2015 and 2018 by Addo-Bediako et al. (2018, 2020), respectively. The observed 98.8% decrease in Ni concentration could be due to improved waste control and reduced industrial activity during the COVID-19 lockdown (2020-2022).

Similarly, Cu concentrations in the current study ranged from 0.94–1.34 µg/L, lower than the 20 µg/L reported by Addo-Bediako et al. (2018), indicating a 93.3% decrease between 2015 and 2023. As concentrations showed a slight decrease, ranging from 0.16-0.35 µg/L compared to the 0.3-0.6 µg/L reported by Addo-Bediako (2020), reflecting a 41.7–46.7% decrease between 2018 and 2023. Lead concentrations ranged from 0.355–1.10 µg/L, higher than those reported by Addo-Bediako (2020), with an increase of over 80%. Sedimentation could be a major factor contributing to the increased Pb levels, as observed further in this chapter.

The samples collected during the high-flow season were obtained from the same locations as those collected during the low-flow season. However, it's important to note that Farm 1, corresponding to BW1, was not accessible during the high-flow season. As a result, any comparison between the low and high-flow season variations for samples from Farm 1 will be omitted from the analysis.

The concentrations of PTEs in water samples during the high-flow season were measured for the samples obtained from the same sources and locations to compare the variation of PTE concentrations between the two seasons. Twelve water samples were collected, comprising six samples each for RW and BW, as indicated in Table 3.11 for MPLs for drinking water and Table 3.12 for irrigation water. The elevated levels of Cr and V in both RW and BW remained high in both seasons, whereas the concentration of Hg was below the LOD value of 0.00357 µg/L in some samples.

Table 3.11. The statistical summary of PTEs concentration in BW and RW obtained from Steelpoort River and surrounding areas.

Sample	V (µg/L)	Cr (µg/L)	Ni (µg/L)	Cu (µg/L)	As (µg/L)	Cd (µg/L)	Hg (µg/L)	Pb (µg/L)
RW1	1.48 ± 0.00933	0.167 ± 0.00779	0.455 ± 0.0107	0.780 ± 0.00761	0.134 ± 0.0108	0.176 ±0.0183	0.0743 ± 0.001407	0.508 ± 0.0296
RW2	1.37 ± 0.0140	0.0755 ± 0.00193	0.659 ± 0.0224	2.47 ± 0.0207	0.165 ± 0.0122	0.00293 ± 0.00942	<0.00357	0.605 ±0.0247
RW3	2.03 ± 0.0205	0.167 ± 0.00231	0.479 ± 0.0144	0.642 ± 0.0106	0.183 ± 0.0127	0.00269 ± 0.00000679	0.0544 ± 0.00422	0.191 ± 0.0237
RW4	14.5 ± 0.321	2.53 ± 0.0826	0.503 ± 0.0154	0.713 ± 0.0250	0.214 ± 0.00667	0.115 ± 0.00970	0.0265 ± 0.0127	0.402 ± 0.0152
RW5	12.7 ± 0.719	2.33 ± 0.150	0.544 ± 0.375	0.716 ± 0.0418	0.188 ± 0.0149	0.0395 ± 0.00510	<0.00357	0.345 ± 0.0179
RW6	12.4 ± 0.478	2.34 ± 0.103	0.506 ± 0.0162	0.661 ± 0.0369	0.197 ± 0.0273	0.0189 ± 0.00255	<0.00357	0.320 ± 0.0213
BW2	22.8 ± 0.332	2.60 ± 0.0628	0.425 ± 0.0100	0.819 ± 0.00933	0.654 ± 0.0223	0.0161 ± 0.00255	<0.00357	0.224 ± 0.00635
BW3	20.1 ± 0.184	1.40 ± 0.00805	0.851 ± 0.0253	0.616 ± 0.0205	0.427 ± 0.0169	0.0240 ± 0.00511	<0.00357	0.192 ± 0.00670
BW4	11.3 ± 0.150	1.78 ± 0.00766	9.85 ± 0.135	1.32 ± 0.00954	1.09 ± 0.0538	0.0398 ± 0.00255	<0.00357	0.0392 ± 0.00367
BW5	15.8 ± 0.564	73.6 ± 2.91	0.124 ± 0.00943	0.537 ± 0.0116	0.280 ± 0.0372	0.0280 ± 0.00306	<0.00357	0.25 ± 0.0121
BW6	15.8 ± 0.277	90.2 ± 1.42	0.159 ± 0.00579	10.3 ± 0.0822	0.345 ± 0.0226	0.0298 ± 0.00153	0.05 ± 0.0229	1.18 ± 0.116
BW7	17.1 ± 0.354	32.0 ± 0.638	0.128 ± 0.00100	4.76 ± 0.118	0.473 ± 0.0406	0.0269 ± 0.00357	0.04 ± 0.0267	0.44 ± 0.0103
Min	1.37	0.0755	0.12	0.54	0.13	0.00269	<0.00357	0.0392
Max	22.8	90.2	9.85	10.3	1.09	0.18	0.07	1.18
Average	12.3	17.4	1.22	2.03	0.363	0.0433	0.00648	0.392
SANS	-	50	70	2000	10	3	6	10
WHO	30	50	70	2000	10	3	6	10

Table 3.12. Target water quality range (TWQR) stipulated for irrigation water (DWAF, 1996a).

Irrigation water guideline		Maximum Concentrations	
Analytes	TWQR DWAF (µg/L)	Low-flow season (µg/L)	High-flow season (µg/L)
V	100	31.1	22.8
Cr	100	114	90.2
Ni	200	14.2	9.85
Cu	200	7.05	10.3
As	100	0.107	1.09
Cd	10	0.107	0.176
Hg	-	-	-
Pb	200	1.80	1.18

The data in Table 3.11 presents the concentrations of PTEs during high-flow seasons, including V, Cr, Ni, Cu, As, Cd, Hg, and Pb, in RW and BW samples from various locations. The observed values are compared against the MPLs stipulated by SANS, DWAF, and WHO. The high-flow season trend was as follows: Cr > V > Cu > Ni > Pb > As > Cd > Hg. During high-flow season, Cr was a dominant pollutant in BWs; meanwhile, V was dominant in RWs.

Vanadium ranged from 1.37 µg/L (RW2) to 22.8 µg/L (BW2) with an average of 12.3 µg/L, which is below the MPL stipulated by the WHO. The V concentrations were generally higher in BW samples compared to RW samples. The highest concentration was observed in BW2, which may be attributed to natural geological sources as well as industrial activities related to steel production. The higher levels in BW samples could also be influenced by the dissolution of V-bearing minerals (carnotite, roscoelite, vanadinite, mottramite, patronite, and descloizite ores) due to changes in ORP and pH. The concentration of V decreased significantly when compared to the low-flow season, as expected from previous studies. The observed concentration during the low-flow season ranged from 1.66 µg/L (RW2) to
31.1 µg/L (RW4) with an average of 18.8 µg/L. The decrease in concentration shows that climate conditions and seasonal variation play a pivotal role in PTEs distribution across the environment.

Chromium levels for drinking exceeded the MPL of 50 µg/L in BW5 and BW6, indicating significant contamination possibly from ferrochrome production and smelting industries. The irrigation water MPL, as recommended by DWAF, was low except for Cr during the low-flow season, with 114 µg/L. Therefore, the water obtained from Steelpoort River and borehole water can be recommended as safe for irrigation and drinking purposes, except for water obtained in BW6. In contrast, RW samples had much lower Cr concentrations, suggesting effective control of waste effluents into rivers or sedimentation processes that trap Cr particles in riverbeds. The range of 0.0755 µg/L (RW2) to 90.2 µg/L (BW6) was observed during high-flow season compared to 1.75 µg/L (RW1) to 114 µg/L (BW6) during low-flow season. As expected, the decrease in Cr concentration shows high levels of water, which results in dilution of PTEs that were distributed during the low-flow season (Paerl et al. 2018). The BW6 showed high levels of Cr in both seasons, which suggests that dissolution of Cr containing minerals dominates throughout the seasons. Similar dominance of Cr was reported by Panda et al. (2022) for groundwater of an industrial city in eastern India, which was related to opencast mining. Additionally, Munyangane et al. (2017) reported high levels of Cr in some regions and related it to Cr-bearing mineral chromite. Sekhukhune District contained various rocks, including alluvium and black reef formations. Black reef formation is rich in gold and uranium, which is also associated with the chromate minerals (Fuchs et al. 2016; Nwaila et al. 2022). Therefore, elevated concentrations of Cr in water from BW5, 6, and 7 could be attributed to geological sources.

The concentrations of other PTEs, such as Ni, Cu, As, Cd, Pb, and Hg in water samples were found to be below their respective MPLs. Nickel concentrations indicated relatively low contamination, ranging from 0.12 µg/L at BW5 to 9.85 µg/L at BW6, with an average concentration of 2.03 µg/L. The elevated Ni concentration observed at BW6 may be attributed to localised geological sources or specific industrial discharges. Copper concentrations were also low, ranging from 0.54 µg/L at BW5 to 10.3 µg/L at BW6, suggesting minimal contamination from industrial sources. The high Cu concentration could be due to natural mineral dissolution. Copper levels were negligible in comparison to the MPL for Cu (2000 µg/L). The highest As concentrations in both water samples, ranging from 0.13 µg/L at RW1 to 1.09 µg/L at BW4, are relatively low and suggest that contamination may stem from natural geological sources with minor contributions from anthropogenic activities.

The concentration of Cd in the samples ranges from 0.00269 µg/L at RW3 to 0.176 µg/L at RW1, with an average of 0.04 µg/L. These values are significantly lower than the MPL set by both the SANS and the WHO, which are 3 µg/L. The low levels of Cd across the samples suggest minimal contamination and indicate that the sources of Cd, whether natural or anthropogenic, are either absent or very limited in the area. The highest detected Cd concentration (0.176 µg/L) remains well below regulatory limits, indicating that the water quality in terms of Cd contamination is within acceptable safety standards. The results obtained in this study are comparable to those reported by Munyangane et al. (2017) and Nsaka et al. (2018). The authors found Cd below 0.200 and 0.0038 µg/L, respectively.

Mercury was detected at very low concentrations across the samples, ranging from <0.00357 in RW2, RW5, and BW1 to BW5 to 0.07 µg/L in RW1, with an average concentration of 0.00648 µg/L. Both the SANS and WHO guidelines establish the MPL for Hg at 6 µg/L. The measured Hg concentrations are significantly below this threshold, indicating that Hg pollution is not a concern in the study area. The presence of Hg at such low levels suggests the absence of prominent local sources of Hg contamination, such as industrial discharges, mining activities, or the use of Hg-containing products. This finding is positive for both the aquatic environment and public health, as Hg is a highly toxic element capable of bioaccumulating in aquatic organisms such as fish, leading to serious health risks. Figures 3.21 and 3.22 summarised the concentrations of BW and RW during high-flow seasons.

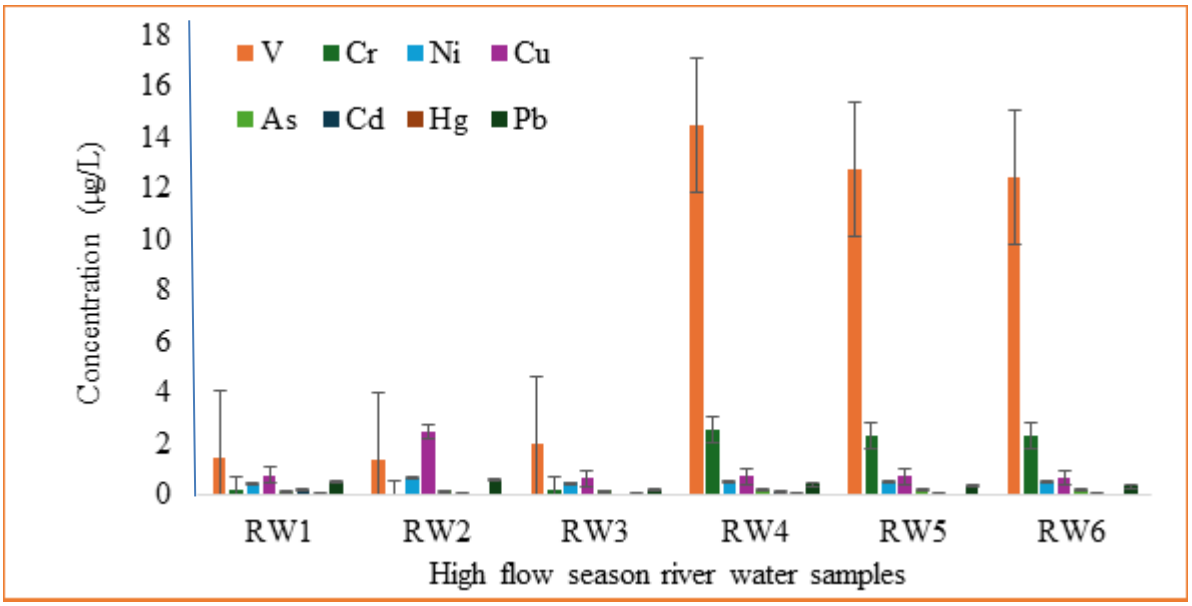

Figure 3.21. Concentrations of PTEs in RW samples during high-flow seasons.

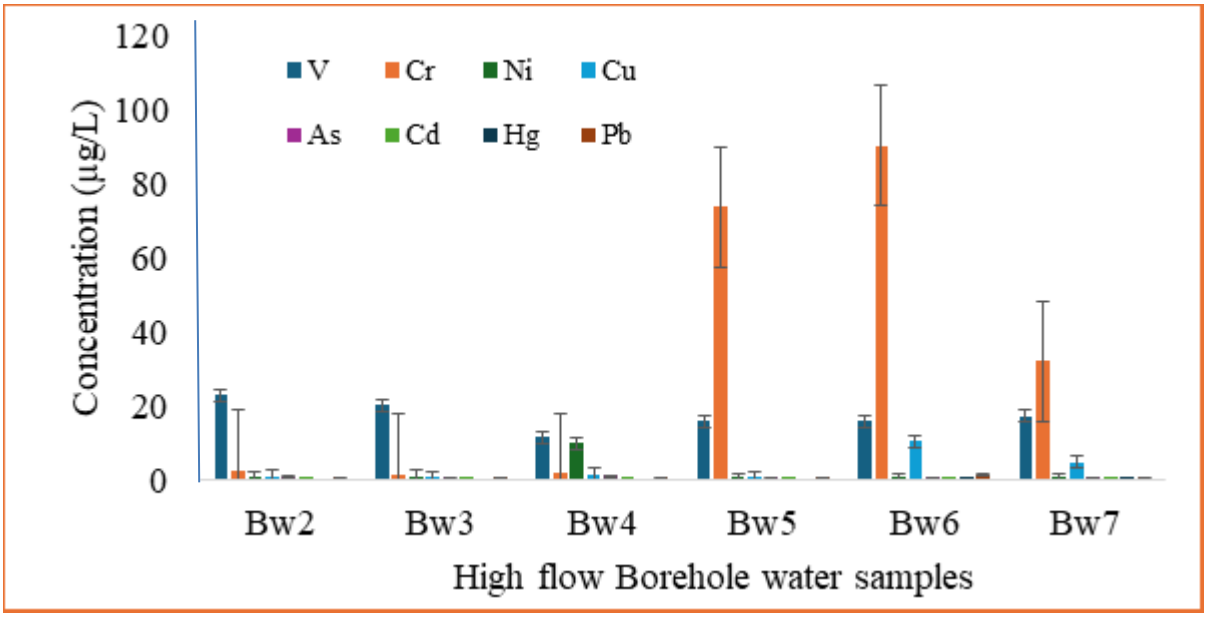

Figure 3.22. Concentrations of PTEs in BW samples during high-flow seasons.

A comparable study conducted by Aralu et al. (2024) in Awka, Nigeria, demonstrated similar seasonal variations between rainy and dry seasons. Contrary to the current study, which observed a slight decline in pollutant concentration from the low to the high-flow season, Aralu et al. (2024) reported an increase in PTEs such as Pb, Cd, and Ni during the transition from low to high-flow seasons. These elevated concentrations, particularly during the dry season, were attributed to reduced dilution effects from rainfall. The study highlighted significant health risks, especially for children, due to the elevated levels of toxic PTEs like Cd, which exceeded the WHO thresholds and are considered highly toxic. The decline of concentration between low and high flow seasons is commonly observed in many studies, in South Africa and worldwide (Aralu et al. 2024; Bhuyan & Bakar, 2017; Edokpayi et al. 2018; Munyangane et al. 2017; Panda et al. 2022; Pant et al. 2021). In South Africa, the study by Dintsi et al. (2023) for As and Cr in Mokolo River, Lephalale found that the concentration of Cr and As showed a significant increase in the high-flow season than in the low-flow season, which contradicts the findings in the current study, where the concentration was decreasing from low to high-flow season.

3.11 TOTAL CONCENTRATIONS OF PTEs IN SEDIMENT SAMPLES FROM STEELPOORT RIVER

The total concentrations of PTEs in the sediments from Steelpoort River are presented in Figure 3.23. The origin of contamination in the sediments is the mixture of nearby pollution and weathering of rocks, which influences the elevation of PTEs (Martínez et al. 2024). The total concentrations of selected PTEs in sediments collected from the Steelpoort River during the low-flow season followed a distinct trend: Pb > As > V > Cr > Cu > Cd > Ni. Site 3 exhibited the highest concentrations of V, Cr, Cu, As, and Pb, with values of 1581, 1566, 1065, 6227, and 9932 µg/g, respectively. These PTE concentrations patterns differ from those observed in water during the same season, where V and Cr were more prevalent than Pb and As. The maximum Pb concentration in sediments was detected at site 3, whereas in water, it peaked at RW6 (corresponding to site 6 in the sediments). The elevated Pb levels at RW6 are likely influenced by the second-highest Pb concentration found in sediments at site 6. Similar discrepancies between sediment and water PTEs concentrations were reported by Bhuyan and Bakar (2017), which supports the findings of this study. The highest concentrations of Ni and Cd were observed at site 6, with values of 253 and 664 µg/g, respectively.

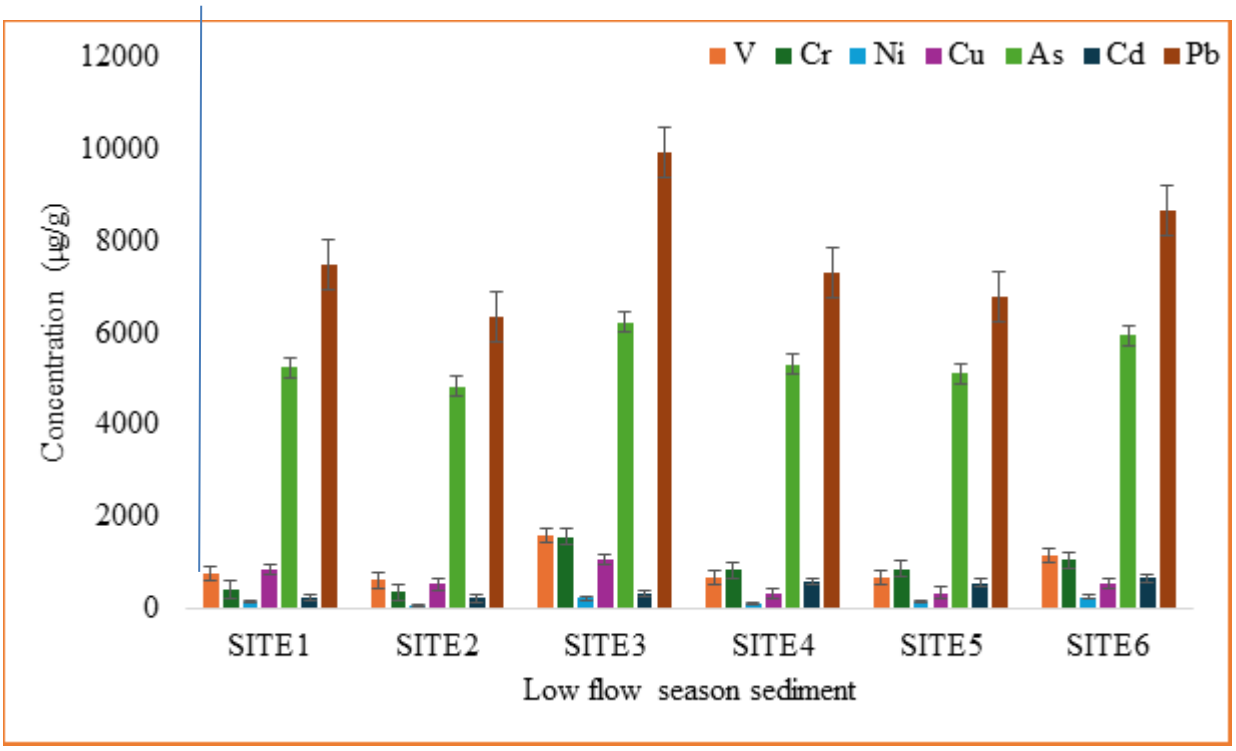

Figure 3.23. Total concentrations of PTEs in sediments from Steelpoort River during the low-flow season.

The significant Pb concentration (9932 µg/g) at site 3, located near a smelting industry, mining activities, a main road, dust, and vehicle exhaust, could be a primary source of contamination. This study's results align with those of Kien et al. (2010), who found high concentrations of PTEs in sediments, particularly Cr (10 428 µg/g) and Ni (4 200 µg/g), near mining tailings. Similarly, McConnell et al. (2018) documented Pb pollution stemming from mining activities, highlighting a historical pattern of sediment contamination. In the Steelpoort area, activities such as construction (building of bridges), heavy vehicular traffic (mining trucks), and dust from mining (coal, chrome, and platinum group metals) could contribute to elevated levels of V, Cr, Ni, Cu, Cd, Pb, and As in the environment, especially in far areas. Addo-Bediako (2020) also reported high Ni and Cr concentrations in Steelpoort River sediments, particularly near ferrochrome mines. The proximity of site 3 to a ferrochrome mine in this study further corroborates these findings. While no significant waste pollution from communities or industries was observed along the Steelpoort River, site 2 revealed evidence of construction activity and discarded liquor bottles.

The distribution of V observed in this study is consistent with findings by Tulcan et al. (2021, 2023), who linked high V concentrations in surface sediments along China's central coast and Shandong Peninsula to industrial activities such as coal power plants, petrochemicals, and oil fields, reporting V concentrations ranging from 35.1 to 135 µg/g. Similarly, da Silva Junior et al. (2022) found the highest concentrations of Pb, Ni, Cr, Cu, and V in Brazil to be 18.7, 48.6, 6.50, 13.3, and 12.9 µg/g, respectively, attributing these levels to anthropogenic sources. The current study suggests that the levels of Pb, Ni, Cr, Cu, and V released by nearby industries such as coal mines and smelting in the Steelpoort area are significantly higher than those reported in similar studies worldwide. This suggests a substantial impact from local industrial activities on the levels of PTEs in sediments in the Steelpoort River.

The observed concentrations of PTEs in sediments collected during the high-flow season followed the trend: Pb > As > Cr > V > Cu > Cd > Ni. This trend was similar to the low-flow season, where Pb had

the highest concentration and Ni the lowest. However, during the low-flow season, Cr was found to be lower than V, whereas in the high-flow season, V was lower than Cr. The highest Pb concentration, 8350 µg/g, was recorded at site 3, consistent with observations during the low-flow season. The highest level of Pb was also observed in the study conducted by Martínez et al. (2024), when measuring the concentration of sediments near an abandoned mine. Bedrock and soil weathering were dominated by Alluvium rocks in the province of Jaen (Andalusia, Spain), where the high content of Pb over 2000 µg/g was distributed from across stream bed sediments, floodplain sediments, and riverine soils (Martínez et al. 2024). Similar to the current study, the authors reported arsenic as the second-highest concentration from sediments. Therefore, the deposition of Alluvium soil content from mines and rock-weathering influences the elevation of Pb and As concentrations.

Figure 3.24 indicates that sediment concentrations did not correlate consistently with the concentration observed in RW samples. A similar finding was reported by Nsaka et al. (2018) when observing the concentration of PTEs in sediment, where the concentration of water did not follow the same trend as sediment concentration. Typically, higher concentrations of PTEs are expected downstream compared to upstream. Addo-Bediako (2020) reported variations in concentrations of PTEs from upstream to downstream, noting the highest As concentrations upstream and the lowest midstream to downstream, which aligns with this study's findings, where As was highest upstream and lowest at midstream sites 4 and 5. Similarly, V, Cr, Ni, Cu, and Pb concentrations were higher upstream compared to midstream sites, except for Cr. Nickel concentrations decreased from upstream to downstream in both seasons, a trend also reported by Addo-Bediako et al. (2018). They also noted a decrease in Cu concentrations midstream. The consistency of PTEs gradients between upstream and downstream was unclear for both water and sediment, likely due to localised pollution sources rather than upstream-to-downstream effluent flow (Addo-Bediako et al. 2018; Bhuyan & Bakar, 2017).

Total concentrations of PTEs varied from site to site, influenced by local pollution sources. Sites 1 and 2 upstream experienced minimal activities, with potential pollution from bridge construction, human activities, and vehicle exhaust. Site 3, near a smelting area, likely had pollution from atmospheric particulates from the smelting industry. Sites 4 and 5, located midstream near a main road, had PTEs likely from vehicle exhaust and road dust. Site 6, downstream, was close to manufacturing industries and urban areas, which could be contributing to higher levels of PTEs compared to sites 4 and 5.
Previous studies have identified various activities contributing to the concentrations of PTEs in sediments and water, including mining, agriculture, topography, road dust, and smelting (Adhikari et al. 2022b; Niu et al. 2023; Teng et al. 2009). The topography of the Sekhukhune District along the Steelpoort River influences PTEs distribution in water, plants, and sediments (Adhikari et al. 2022). While natural sources of PTEs cannot be ruled out since the high levels of PTEs observed could suggest a combination of anthropogenic and geogenic sources.

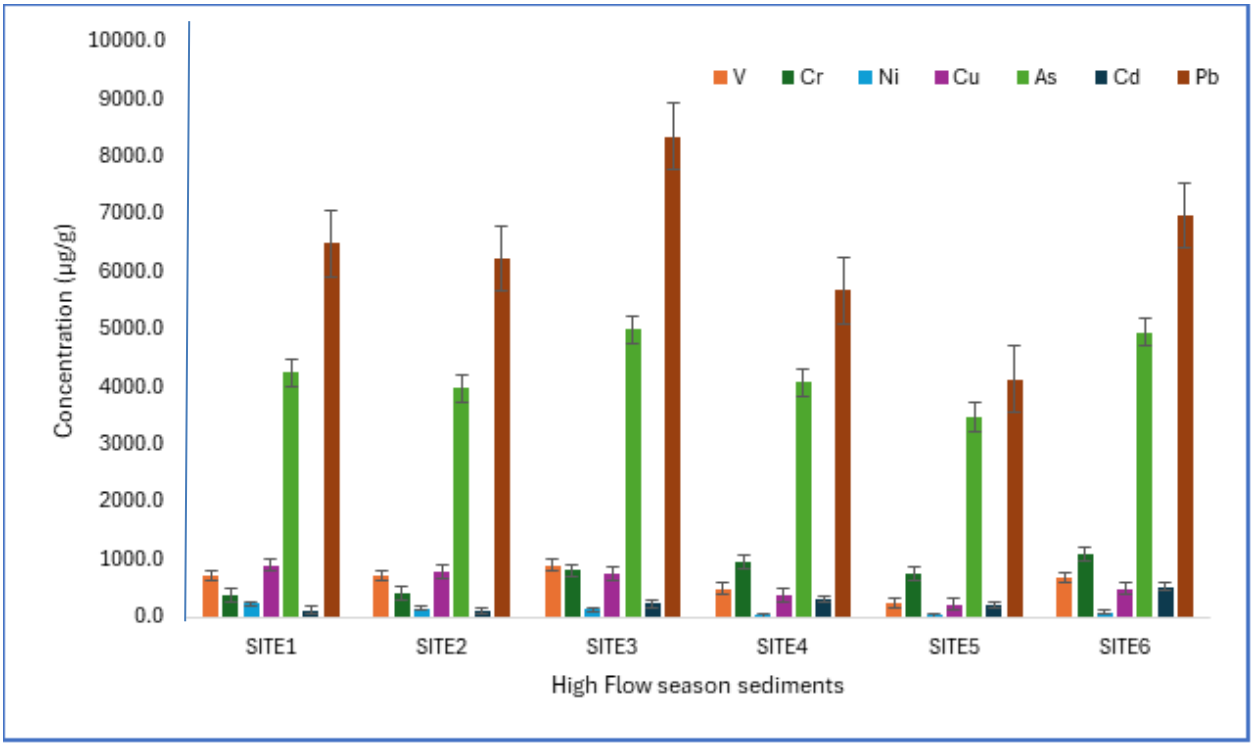

Figure 3.24. Total concentrations of PTEs in sediments from Steelpoort River during high-flow season.

In South Africa, there are no established guidelines specifying the MPLs for PTEs in sediments of freshwater ecosystems, such as the Probable Effect Level (PEL) and the Interim Sediment Quality Guidelines (ISQGs). Consequently, the proposed PELs and ISQGs adopted from the CCME were used to assess the safety of the aquatic ecosystem and freshwater. The maximum concentrations of PTEs in river sediments are compared against these PEL and ISQG benchmarks, as indicated in Table 3.13, except for Ni and V, which are not included in these guidelines.

Table 3.13. The ISQGs and PELs with the maximum concentrations of PTEs in sediments.

Analyte	Canadian Sediment Quality Guidelines		Current study Maximum	
	ISQG (µg/g)	PEL (µg/g)	low-flow (µg/g)	High-flow (µg/g)
As	5.90	17.0	6227	4990
Cd	0.60	3.50	664	527
Cr	37.3	90.0	1566	1083
Cu	35.7	197	1065	897
Ni	NA	NA	253	238
Pb	35.0	91.3	9932	8350
V	NA	NA	1581	899

NA: not available

The ISQGs and PEL for sediments were established by the CCME in 2002. It was found that all detected concentrations of PTEs during both low and high-flow seasons exceeded the ISQG and PEL values. The concentrations of PTEs can be categorized based on their occurrence of adverse biological effects. None of the total concentrations of PTEs were below ISQG or PEL, suggesting a frequent occurrence of adverse biological effects, which could harm aquatic species and food chains. The observed

concentrations of V, Cr, Cd, Cu, Pb, Ni, and As across all sites were several times higher than the PEL and ISQG values, indicating frequent biological effects on aquatic species.

The CCME did not provide ISQG and PEL thresholds for Ni and V for comparison with the current study. However, the Ni results from this study can be compared with other studies conducted on the Steelpoort River, such as the one by Addo-Bediako et al. (2018). The ISQG and PEL values are typically used in ecological studies to investigate the toxic effects of PTEs on vertebrates, which might also affect human health. A study by Mohajane and Manjoro (2022) reported total concentrations of PTEs in sediments and compared them against the threshold effect concentration (TEC) and probable effect concentration (PEC) to assess potential ecological risks in Mahikeng, North–West province of South Africa. In the current study, all selected PTEs were above TEC and PEC, except for Ni at sites 4 and 5 during the high-flow season, where levels were below PEC.

Table 3.14 shows the minimum and maximum concentrations of PTEs measured during low and high-flow seasons compared with the TEC and PEC values. The minimum concentration of Ni during the high-flow season was above TEC but below PEC, indicating rare ecological impacts. Higher concentrations than PEC observed in sediments suggest frequent negative impacts (Mohajane & Manjoro, 2022). Conversely, concentrations below TEC and PEC suggest no expected ecological impacts. The selected PTE concentrations are expected to cause significant ecological impacts, except for Ni at sites 4 and 5 during the high-flow season.

Table 3.14. Comparison of measured concentrations of selected PTEs in sediments and SQGs.

Analytes	SQGs (µg/g)		Minimum (µg/g)		Maximum (µg/g)	
	TEC	PEC	Low-flow	High-flow	Low-flow	High-flow
As	9.79	33.0	4824	3476	6227	4990
Cd	0.990	4.99	221	109	664	527
Cr	43.4	111	352	391.5	1566	1083
Cu	31.6	149	324	215	1065	900
Ni	22.7	48.6	49.2	33.5	253	238
Pb	35.8	128	6361	4132	9932	8350
V	NA	NA	612	241	1581	899

Similarly, a study by Vallius (2015) on the Gulf of Finland in the Baltic Sea revealed a comparable trend of sediment toxicity. The author noted that the Gulf of Finland has been subjected to prolonged anthropogenic activities, leading to widespread pollution, particularly in the sediments. In the study, American SQGs were applied, which differ from the Canadian SQGs, as highlighted in Table 3.15. This distinction underscores the variation in environmental standards used to assess sediment contamination across different regions. The distinction between American and Canadian SQGs is the references used in determining the toxicity level of PTEs in sediment. Americans add effects range-low (ERL) and effect range-medium (ERM), which refer to lower and upper reference values, respectively. Meanwhile, Canadians use ISQG and PEL, where ISQG is also considered TEL (Vallius 2015).

Table 3.15. Distinction of the various environmental standards used to assess contamination of sediment across different regions.

Analytes	Canadian SQGs		American SQGs	
	ISQG (µg/g)	PEC (µg/g)	ISQG (µg/g)	PEL (µg/g)
As	5.90	33	7.24	41.6
Cd	0.60	4.99	0.7	4.2
Cr	37.3	111	53.3	160
Cu	35.7	149	18.7	108
Pb	35	128	30.2	112
Hg	NA	NA	0.13	0.70

3.12 TOTAL CONCENTRATIONS OF PTEs IN SOIL SAMPLES FROM STEELPOORT AREA

The present study also investigated the total concentrations of PTEs in soil samples where vegetables were cultivated during the low-flow season. A total of nine soil samples were successfully analysed using ICP-OES for quantification of total concentrations of selected PTEs, as illustrated in Figure 3.25. The average total concentrations of selected PTEs in the agricultural soil obtained during the low-flow season followed this trend: Pb > As > Ni > Cr > Cu > Cd > V.

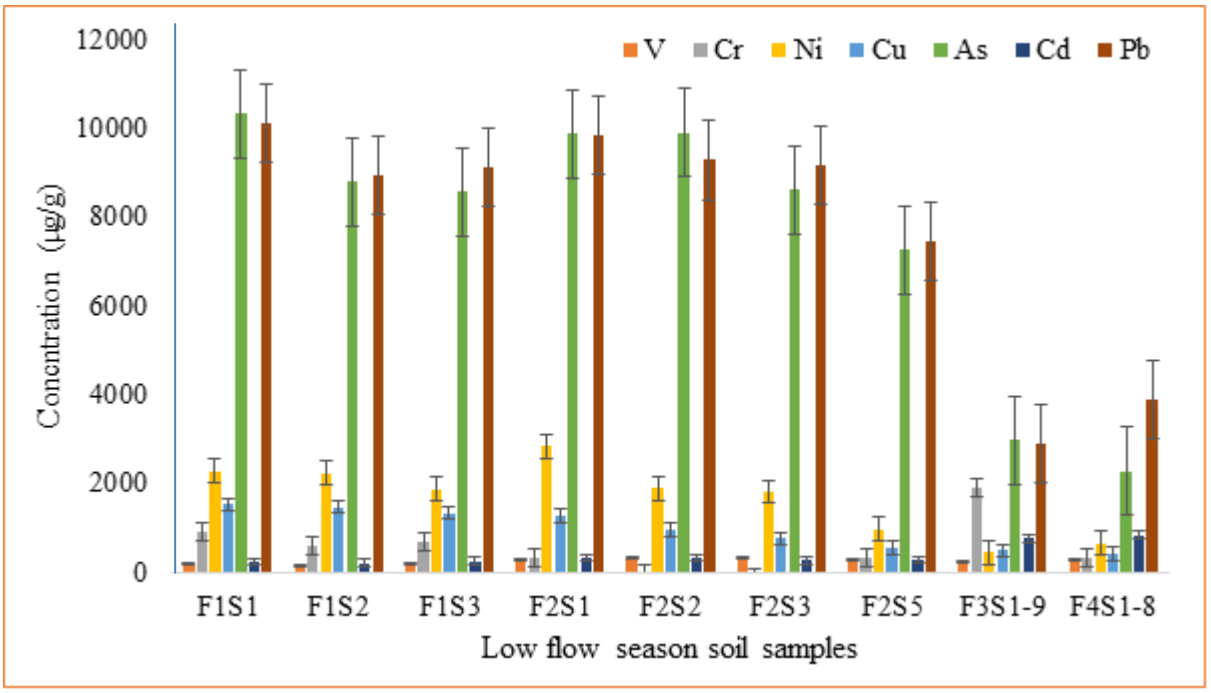

Figure 3.25. Total concentrations of selected PTEs in the soil during the low-flow season.

The results indicated that most collected soil samples exhibited high total concentrations of Pb, except for samples from F1S1 and F2S2. When comparing the concentrations of Pb in the soil and the vegetables planted in it, substantial differences in Pb accumulation were observed among various species. Leafy vegetables, such as spinach in F1S1, F2S2, F3S1, and F4S8, showed lower concentrations of Pb compared to other leafy vegetable varieties, namely Mochaina, Chomolia, Covo, and Beetroot leaves. Further analysis of different plant parts, including leaves, fruits, and roots from

species such as beetroot, carrot, tomato, and spring onions revealed noticeable variations in the total concentrations of Pb accumulated in the tissues. Specifically, tomatoes from farm 2 (F2S5-T) and cherry tomatoes from farm 4 (F4S3-CT) exhibited elevated concentrations of Pb, found to be above 12.0 µg/g in both farms, despite their geographic separation. This finding suggests that Pb is more likely to reside on the fruit of the plants than leaves and roots. Interestingly, the total concentration of Pb in the soil where tomato plants were cultivated was lower compared to other sites within the same farm where leafy and root vegetables were grown. This observation indicates that when the soil concentration of Pb is high, the concentration found in the vegetables cultivated in such soil may be reduced, demonstrating the transfer effect of Pb from the water, soil to plant tissues. The low movement of Pb to leafy parts of spinach was also observed in a study conducted by Gupta et al. (2019) where spinach accumulates less Pb compared to other leafy vegetables. The total concentration of Pb across the samples ranged from 2893 to 10139 µg/g, while the lowest total concentration of V ranged from 157 to 329 µg/g. Notably, the highest total concentration of Pb was recorded in the soil sample collected from farm 1 (F1S1-S), whereas the highest total concentration of V was observed in soil from farm 2 (F2S3- O/Ch).

When observing the concentrations of PTEs in vegetables during the low-flow season, Cu, Cr, and V were amongst the prominent PTEs in vegetable species. However, when observing the concentration of Cu in the soil across all farms and vegetables, it is noticeable that the soil had an influence in transferring of Cu from soil to plant tissues for leafy vegetables, roots, and fruits. Gupta et al. (2019) reported higher Cu translocation when comparing the concentration of Cu in water and soil with Cu in vegetables, both in roots and leaves. The evidence supports the essentiality of Cu in plants for functioning, where it absorbs high levels of Cu from soil to maintain itself for growth. The presence of lower levels of Cr in the soil and prominent levels of Cr in vegetables is similar to Cu and Pb translocation. Chromium and Cd ions can compete with essential elements such as calcium and phosphate ions, therefore leading to plants accumulating more Cr and Cd in instances where soil had high levels of Cr or Cd (Oliveira, 2012).

Chromium had the highest concentration of 1892 µg/g in the soil sample from farm 3 F3S1-9. The soil samples collected from farm 1 had the highest concentrations of Cu (1531 µg/g) and As (10340 µg/g). Cadmium was the highest in soil samples collected from farm 4 F4S1-8, with a total concentration of 844 µg/g. In farms 3 and 4, soil samples were collected separately from various locations within each farm to ensure a comprehensive representation of the soil's characteristics. The samples from each farm were then combined into a single composite sample for each location. This approach provides an average concentration of PTEs across the farms while accounting for spatial variability. By mixing the individual samples, the aim is to obtain a more uniform and representative assessment of soil contamination, particularly in areas where vegetables are grown, as these vegetables are directly influenced by the surrounding soil conditions and the size of the farm (Saini et al. 2015; Pelcová et al. 2021).

.

The highest concentrations of Cu, As, and Pb at farm 1 could be attributed to the smelting industry situated directly opposite the farm. The highest concentration of Cr in farm 3 could be due to the manufacturing industry and the proximity of the main road, which contributes waste products from fuel combustion and particulates from mining, concrete, and cement users near the farm. The highest total concentration of V from farm 2 (F2S2-O/Ch) could also be linked to the smelting industry situated opposite the farm. The highest total concentration of Cd from farm 4 might be due to the type of soil and the nearby mining industry. Studies have found that soils such as mafic and ultramafic soils can have high Cd contamination levels, up to 100 µg/g (Khan et al. 2017), which is similar to the present study's soil types (alluvium and colluvium), ranging from 5.00 to 1050 µg/g (Ozunu, 2015).

It was observed that soil collected from farms 1 and 2, which was used to cultivate vegetables such as spinach (F1S1-S), spring onion (F1S2-SO), okra (F1S3-Ok), spinach (F2S1-S), beetroot (F2S2-BL), chomolia (F2S3-Ch), spring onion (F2S4-SOL), and tomato (F2S5-T), had high Pb concentrations during the low-flow season. This suggests that accumulated PTEs are transferred to plants. The present study showed that the elevated concentrations of PTEs in the soils could have been taken up by plants. Khan et al. (2017) reported that highly contaminated soils result in highly contaminated vegetables, which supports the findings that vegetables cultivated in contaminated soils contribute to a contaminated food chain. The study by Dintsi et al. (2023) showed low concentrations of As across all farms where vegetables were obtained, and that was reflected by the amount of As detected in the vegetables, which coincided with the Khan et al. (2017) suggestion of PTEs transferable from soil to vegetables.

Total concentrations of V, Cr, As, Cd, Pb, Ni, and Cu in all soil samples collected during the low-flow season were above the MPLs stipulated by the Canadian Council of Ministers of the Environment (CCME) of 130, 64, 12, 1.4, 70, 50, and 63 µg/g, respectively (Canadian Council of Ministers of the Environment, 1999). The MPL and maximum concentration of soil detected between the low and high-flow seasons are shown in Table 3.16. The lowest and highest concentrations of V are 1.22 to 2.53 times more than the MPL stipulated by the CCME. The high concentration of V in the soil increases its prevalence in vegetables, as observed in Figure 4.12. Vanadium is more accumulated in roots and shoots than leaves, as reported by Chen et al. (2021). The current study corroborates findings where V concentrations in beetroot roots and leaves were measured at 1.42 µg/g and 0.967 µg/g, respectively. Similarly, spring onion roots and leaves contained 0.273 µg/g and 0.210 µg/g of V, respectively. These results highlight a higher accumulation of V in the roots compared to the leaves for both vegetables, consistent with trends observed in previous studies.

The total concentrations of Cr are 5.03 to 30 times more than the MPL, with the highest Cr concentration in farm 3 (F3S1-9(all)) surpassing the MPL by 30 times. Elevated Cr concentrations in farm 3 soils and vegetables could be due to the proximity to the main road and the use of inorganic manure and compost. Other PTEs were 862, 603, 145, 57, and 24 times more than the MPLs for As, Cd, Pb, Ni, and Cu, respectively. The elevated Cd levels could be attributed to the use of inorganic manure, particularly in farms 3 and 4 (Haider et al. 2021). Mining, smelting, proximity to main roads, and manufacturing industries around the Steelpoort area may have enriched many parts of the region with PTEs from atmospheric deposition. The soil used to grow vegetables is unsafe for agricultural, residential, commercial, and industrial purposes due to high levels of PTEs, which are above the CCME MPLs. The borehole water (BW6) used for irrigation could also contribute to the increase of Cr and V in the soil, and subsequently in the vegetables.

Table 3.16. Canadian Soil Quality Guidelines (SQGs) for the protection of environmental and human health.

Analyte	CCME	Maximum Concentration	
	SQG (µg/g)	Dry-season (µg/g)	Wet-season (µg/g)
As	12	10340	3713
Cd	1.4	844	744
Cr	64	1892	4014
Cu	63	1531	131
Ni	50	2850	375
Pb	70	10139	5026
V	130	329	181

The total concentrations of seven soil samples obtained from Steelpoort and Driekop farms were analysed and illustrated in Figure 3.26. Collected soil samples were used to grow crop vegetables obtained during the high-flow season. It is important to notice that when compared to the low-flow season, high-flow is missing farm 1 results due to no access to the farm since the owner was not available during the sampling period.

The observed total concentrations of PTEs during the high-flow season followed the trend: Pb > As > Cr > Cd > Ni > V > Cu. Conversely, during the low-flow season, the trend was: Pb > As > Ni > Cu > Cr > Cd > V. The consistent dominance of Pb and As in both seasons highlights the prevalence of these toxic elements in the environment. Lead concentrations ranged from 3421 to 5027 µg/g during the high-flow season, while during the low-flow season, its concentration ranged from 2893 to 7862 µg/g. Similarly, As concentrations ranged from 2626 to 3713 µg/g during the high-flow season and 2278 to 7628 µg/g during the low-flow season.

The decrease in concentrations of PTEs between the low- and high-flow seasons aligns with the findings of Rahman et al. (2012), who reported a decrease in As concentrations from 4073.1 µg/g in the low-flow season to 2326.2 µg/g in the wet season in Depz, Bangladesh. They also observed a wide range of As concentrations (0-14307 µg/g) during the high-flow season, higher than the current study's findings. Rahman et al. (2012) also reported trends for Cu, Cr, Pb, Ni, and Cd, which followed Cu > Cr > Ni > Pb > Cd in the low-flow season and Cu > Ni > Cr > Pb > Cd in the high-flow season, with concentrations lower than those in the present study due to varying point sources of contamination. Figure 4.19 indicates that soil had the lowest total concentration of Cu. The highest total concentrations of PTEs were observed in soil from farm 4, with V (182 µg/g), Cr (4015 µg/g), Ni (375 µg/g), Cu (132 µg/g), As (3713 µg/g), Cd (744 µg/g), and Pb (5027 µg/g). The soils from these farms rely on borehole water and rainfall for irrigation, potentially increasing PTE concentrations, particularly at farm 4. The use of animal manure to fertilize the vegetables could also add a significant amount of PTEs in the soils, such as Cd from phosphate fertilizers, which could be seen by elevated levels of Cd in farm 4 (Niño-Savala et al. 2019; Suciu et al. 2022). The increase in composition mineral hosting Cr could be attributed to the increase of Cr and As, which could be comparable with that conducted by Dintsi et al. (2023), where total concentrations of As and Cr were high when compared to the acceptable value by the FAO/WHO.

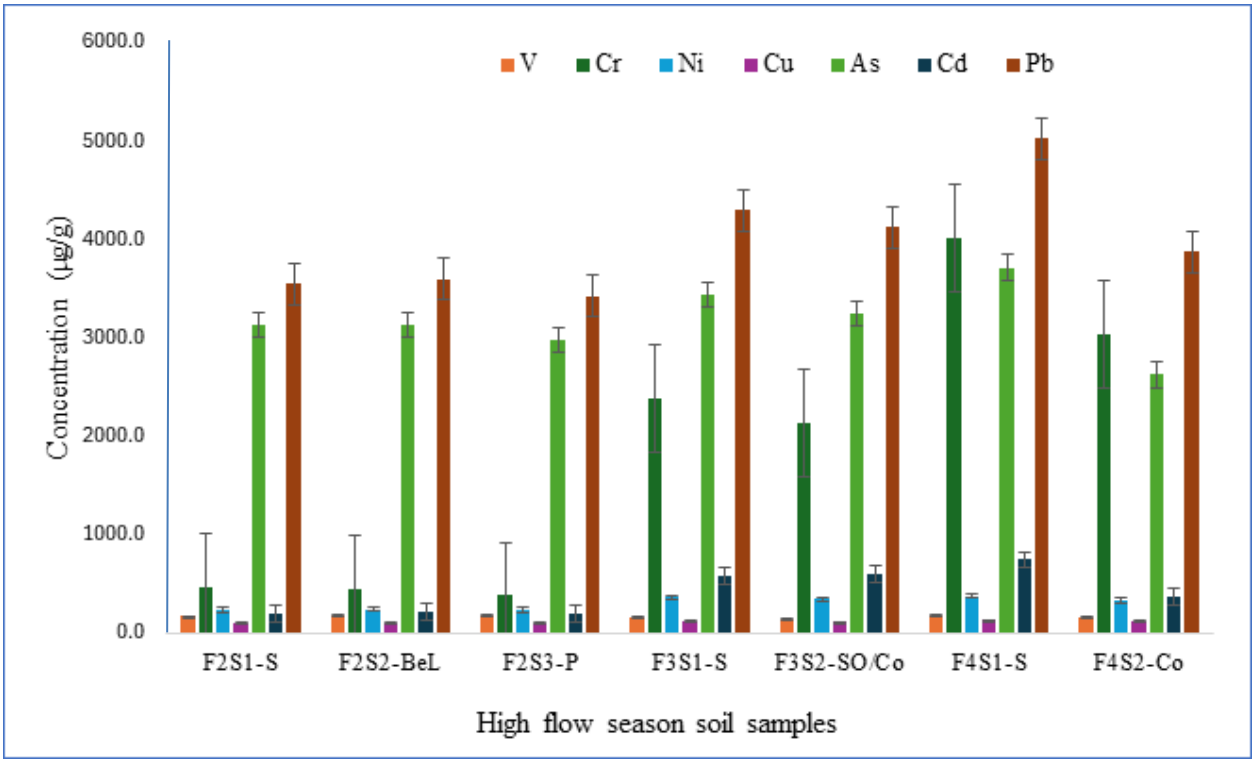

Figure 3.26. Total concentrations of selected PTEs in soil collected during high-flow season.

The decrease in PTE concentrations during the high-flow season compared to the low-flow season might be due to the continuous uptake by vegetables grown in the sampled areas (Rahman et al. 2012), and infiltration by rainfall, which results in PTEs carried into the groundwater. During high-flow season, increased growth of weeds, vegetables, and other plants could result in higher PTE uptake, reducing soil concentrations. Additionally, rainfall can wash away topsoil, further lowering PTE concentrations. Compared to the low-flow season, there was a decrease in total concentrations of V, Ni, Cu, As, and Pb by 32.9%, 81.8%, 88.4%, 58.3%, and 49.3%, respectively. Conversely, Cr and Cd concentrations increased by 153.6% and 7.91%, respectively, due to high concentrations at farms 3 and 4. Nde et al. (2021) reported similar differences in soil PTEs concentrations between pre- and post-cultivation periods, noting decreases in PTEs concentrations post-cultivation. The study also highlighted elevated concentrations of As, Cu, Pb, Cd, and Cr in soils that were used for the cultivation of spinach, cabbage, and onions, exceeding Canadian Council of Ministries of the Environment (CCME) thresholds.

In the current study, total concentrations of V, Cr, Ni, Cu, As, Cd, and Pb in all soil samples collected during the high-flow season from farms exceeded the CCME MPLs of 130, 64, 50, 63, 12, 1.4, and 70 µg/g, respectively. The highest concentrations observed were 182, 4015, 375, 132, 3713, 744, and 5027 µg/g for V, Cr, Ni, Cu, As, Cd, and Pb, exceeding the guideline values by 1.4, 62.7, 7.5, 2.1, 309, 532, and 71.8 times, respectively. Rahman et al. (2012) also reported Cu concentrations exceeding the CCME limits, consistent with the current study's results. These findings, corroborated with various studies (Addo-Bediako, 2020; Addo-Bediako et al. 2018; Dintsi et al. 2023;Khan et al. 2008), indicate that the collected soils remain unsuitable for agricultural purposes, as evidenced by both high- and low-flow season results.

3.13 TOTAL CONCENTRATIONS OF PTEs IN VEGETABLES FROM STEELPOORT AREA

One of the routes of human exposure to PTEs is through the consumption of contaminated vegetables. In this study, the total concentrations of PTEs in vegetables irrigated with borehole water from various farms were analysed using ICP-MS to assess their safety. Samples were collected from four small-scale commercial farms: Farm 1 (BW1), Farm 2 (BW3), Farm 3 (BW4), and Farm 4 (BW6). The results were categorized by farm number, sample number, and vegetable species. Some vegetables exhibited higher concentrations of PTEs than others, which is consistent with their differing capacities to absorb nutrients and contaminants from soil and water.

Figures 3.27 to 3.30 present the total concentrations of selected PTEs in vegetables across all four farms during the low-flow season. The observed concentration trends followed the order: Cu > Cr > Pb > Ni > V > As > Cd > Hg. The trend observed in the current study is similar to the findings observed by Dikotla & Ambushe (2024) from Mokolo River in Lephalale, Limpopo, which was as follows: Cu > Cr > Ni > Pb > V > As > Cd > Hg. Copper concentrations were notably high in both studies, ranging from 5.27 to 76.9 µg/g for the current study, with the lowest detected in Chomolia (F4S5-Ch) and the highest in cabbage (F4S7-Cb). High levels of Cu were detected in vegetables from all farms, except for Farm 2. Dikotla & Ambushe (2024) reported Cu ranging from 2.04 to 7.31 µg/g during the low-flow season.

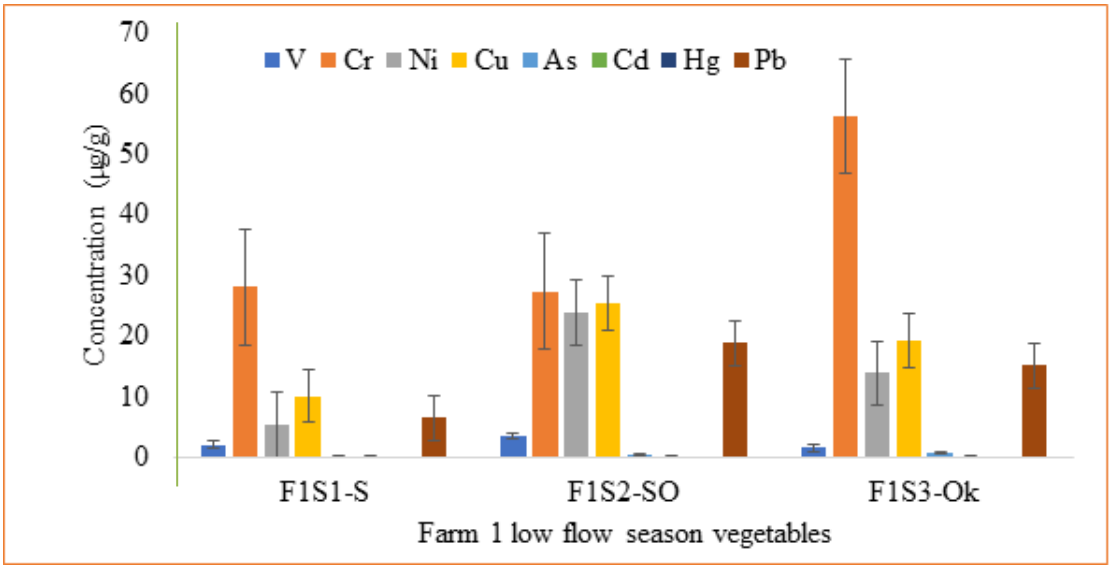

Figure 3.27. Total concentrations of PTEs in vegetables from farm 1 during low flow season.

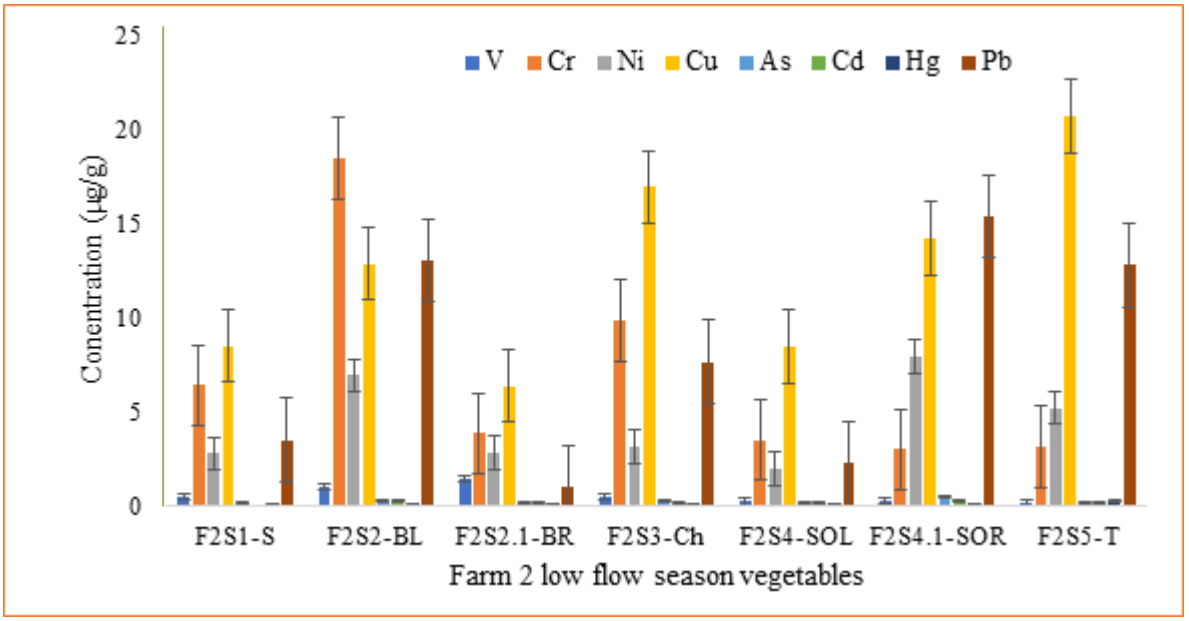

Figure 3.28. Total concentrations of PTEs in vegetables from farm 2 during low flow season.

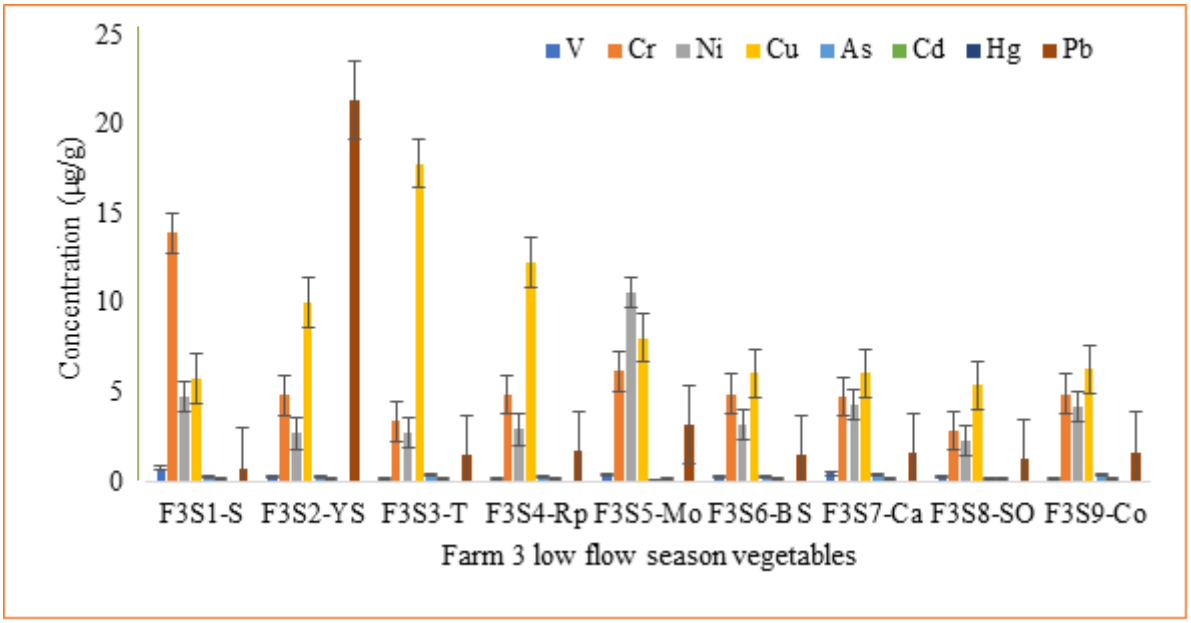

Figure 3.29. Total concentrations of PTEs in vegetables from farm 3 during low flow season.

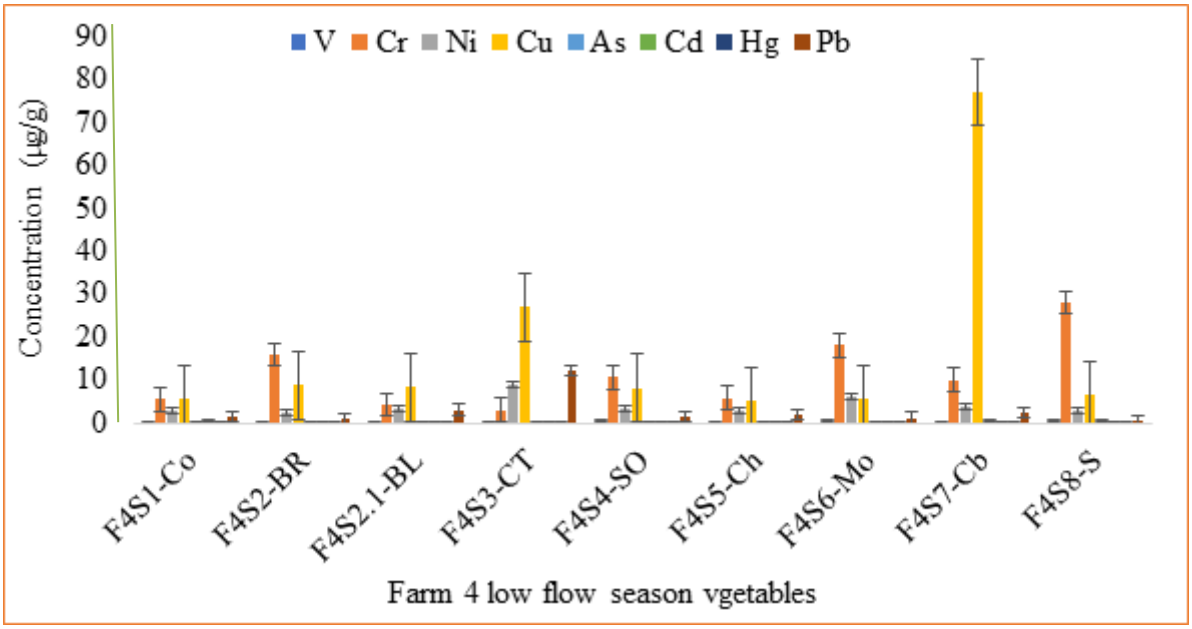

Figure 3.30. Total concentrations of PTEs in vegetables from farm 4 during low flow season.

The elevated levels of Cu across all farms in edible parts such as leaves and roots of vegetables may be attributed to atmospheric deposition from nearby mining activities. Although there was no direct evidence of pesticide use contributing to vegetable or soil Cu levels, the proximity of Farm 3 to a major road and industrial activity likely contributed to the high PTE concentrations observed there. Road dust, which is known to contain elevated levels of PTEs, particularly Cu, can settle on nearby farmland, increasing contamination in soils and leaves of the vegetables. Similar findings were reported by Du et al. (2013) in Beijing, China, where Cu levels in road dust reached 72.1 µg/g, which was deposited in nearby farms. In the current study, the concentration of Cu in soil from farm 3 reached 490 µg/g, which could be influenced by road dust, mining dust, and other industries nearby.

Copper, an essential micronutrient for plants, plays a crucial role in photosynthesis, respiration, and oxidative stress protection (Yruela, 2009). However, excessive Cu can hinder plant growth by affecting root and shoot development and interfering with the uptake of other essential nutrients, such as iron (Fe) and calcium (Ca). Plants are unable to differentiate between essential and non-essential elements, leading to the accumulation of PTEs in agricultural soils and, consequently, in crops. This increases the risk of human exposure to elevated levels of PTEs through dietary intake.

The results of this study align with findings from other regions. For example, Singh & Kumar (2006) reported Cu concentrations ranging from 15.3 to 29.4 µg/g in vegetables grown in the peri-urban areas of New Delhi, India. Similarly, Gupta et al. (2019) documented Cu concentrations between 0.03 and 71 µg/g in various vegetables worldwide. The Cu levels observed in this study (5.27 to 76.9 µg/g) are within the range reported in these previous studies, although the highest Cu concentration in this study was found in cabbage (76.9 µg/g), contrasting with the 430 µg/g reported by Mohamed et al. (2003) for cabbage from Al-Taif, Saudi Arabia. These results also highlight the point source of pollutants, the type of pollutants, and the different geological settings between the two countries. Al-Taif District consists of mountainous and desert areas with few anthropogenic activities (Bishta et al., 2015) when compared to Sekhukhune District (Kgaphola et al., 2023). The difference in concentration between different countries could be due to soil composition, as reported in the literature (Mohamed et al., 2003).

Hg concentrations were the lowest among the targeted PTEs, ranging from 0.02 to 0.31 µg/g, with the lowest detected in spring onion (F1S2-SO) and the highest in cabbage (F4S7-Cb). The variations in

PTE concentrations across the sampled vegetables reflect the influence of environmental factors, including proximity to mines, smelters, roads, industrial activities, and the type of rock formations in which soils are planted. The total concentrations detected were compared to the MPLs set by the WHO and the Food and Agriculture Organization (FAO), as well as other studies, as detailed in Table 4.6 (Codex Alimentarius Commission joint FAO/WHO, 2002; WHO, 1988; Zondo, 2021). The results of Cr and As in the current study are comparable to those reported elsewhere in vegetables planted in Lephalale, Limpopo province (Dintsi et al. 2023). The authors reported a range of 0.0205 to 0.106 µg/g of As using ICP-MS during the low-flow season, which is comparable with the current range of 0.0749 to 0.788 µg/g. Furthermore, the range of Cr reported by the authors was 1.02 to 4.15 µg/g, which is lower than 2.90 to 56.2 µg/g of the current study. The reported results showed that vegetables obtained from Lephalale had lower concentrations of Cr when compared to the vegetables obtained from the Steelpoort District. The authors outline various industries, which could be involved in contamination of vegetables in Lephalale, including Grootegeluk coal mine and Matimba and Medupi power stations. The study conducted by Dikotla & Ambushe (2024) coincides with findings obtained by Dintsi et al. (2023), where the concentration of various vegetables showed high levels of Cr.

The total concentrations obtained from the current study revealed that all PTEs, except for Ni, had maximum concentrations higher than the MPLs stipulated by the WHO/FAO, as shown in Table 3.17. The total concentration of Ni was below the 67.0 µg/g limit set by WHO/FAO. The total concentration of As was generally below the recommended limit of 0.5 µg/g, except in F1S3-Ok (Okra), F4S7-Cb (Cabbage), and F4S8-S (Spinach), which had concentrations of 0.764, 0.555, and 0.788 µg/g, respectively.

Table 3.17. The MPLs of PTEs in vegetables stipulated by WHO/FAO.

Analyte	Guideline limits	Maximum concentration in the study	
	WHO/FAO (2002, 2011) µg/g	Dry season (µg/g)	wet season (µg/g)
Cu	73.0	76.9	33.8
Ni	67.0	23.9	13.2
Hg	0.100	0.314	<0.0234
Pb	0.300	21.4	7.00
Cr	1.30	56.2	40.1
Cd	0.200	0.674	0.50
As	0.500	0.788	0.42
V	0.0300	3.62	1.38

Most vegetables exceeded the MPL for Cd (0.20 µg/g), except for eight samples that were below the MPL. These samples include F1S3-Ok (Okra), F2S1-S (Spinach), F2S2.1-BR (Beetroot roots), F2S4-SOL (Spring Onion Leaves), F3S2-YS (Yellow Spinach), F3S6-BS (Baby Spinach), F3S7-Ca (Carrots), and F3S8-SO (Spring Onion), with concentrations of 0.179, <0.234, 0.170, 0.177, 0.187, 0.185, 0.190, and 0.174 µg/g, respectively.

Mercury concentrations in vegetable samples were mostly below the MPL of 0.100 µg/g, except for ten samples: F2S5-T (Tomato), F4S1-Co (Covo), F4S2-BR (Beetroot Roots), F4S2.1-BL (Beetroot Leaves), F4S3-CT (Cherry Tomato), F4S4-SO (Spring Onion), F4S5-Ch (Chomolia), F4S6-Mo (Mochaina), F4S7-Cb (Cabbage), and F4S8-S (Spinach), with concentrations of 0.251, 0.257, 0.175, 0.211, 0.235, 0.273, 0.211, 0.271, 0.314, and 0.207 µg/g, respectively.

All vegetable samples had total Cu concentrations below the MPL of 73.0 µg/g, except for F4S7-Cb, which had 76.9 µg/g. The total concentrations of V, Cr, and Pb were above the MPLs of 0.03, 1.3, and 0.30 µg/g, respectively. From the obtained results, it can be explained that vegetables collected in the vicinity of mines, main roads, and industrial activities are contaminated with high concentrations of V, Cr, and Pb. The data also indicate that vegetables from Farm 1 in the Steelpoort area were highly contaminated with V, Cr, Ni, Cu, As, and Pb compared to other farms, which could be associated with the dominant anthropogenic activities in the area. Farm 4 in Driekop was highly contaminated by Cd and Hg compared to the other three farms in the study. The contamination could be attributed to the geological setting and anthropogenic sources, especially atmospheric deposition from mining industries in the area (Ao et al. 2020; Zhang et al. 2023).

Similar to the water samples, vegetable samples during the high-flow season were collected from the same farms as those during the low-flow season. A total of eight vegetable samples were collected during the high-flow season, which is fewer than the number collected during the low-flow season. This reduction in the number of vegetable samples during the high-flow season is attributed to seasonal variations and weather conditions. Specifically, the low-flow season coincided with spring, a period known for promoting vigorous plant growth and increased agricultural yield due to favourable temperatures and longer daylight hours. In contrast, the high-flow season occurred during autumn, a time when cooler temperatures and shorter days generally result in reduced plant growth and lower agricultural productivity. This seasonal difference likely influenced the availability of plant samples during the respective sampling periods. Figure 3.31 represents the PTE concentrations in different vegetable samples, which were collected during the high-flow season.

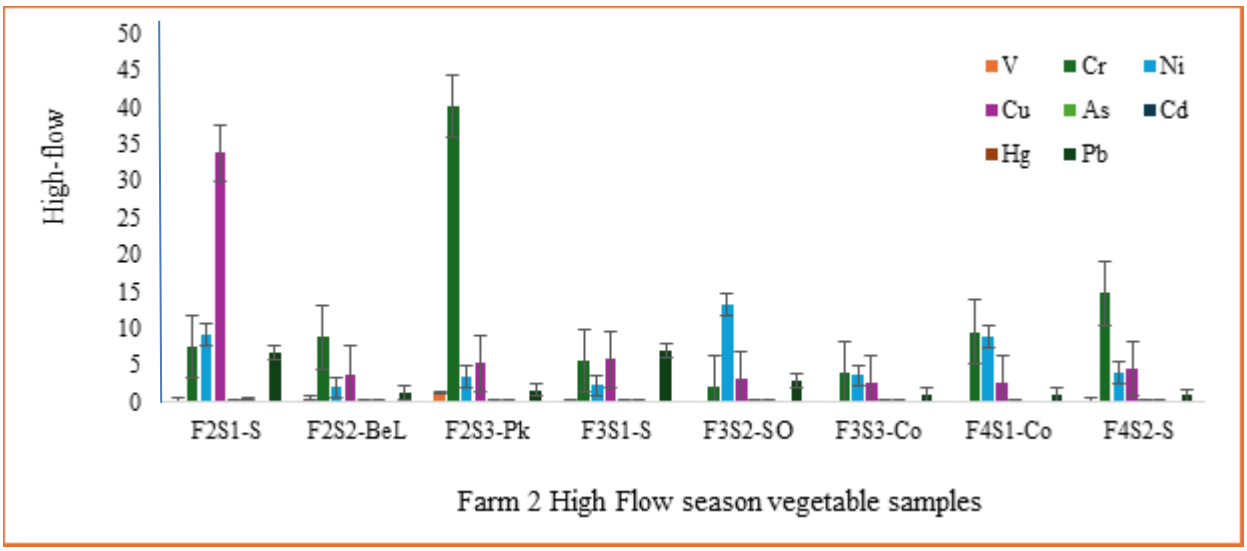

Figure 3.31 Concentrations of PTEs in vegetables collected during high-flow season from Sekhukhune District.

The results showed the following trend for vegetable contaminations with PTEs: Cr > Cu > Ni > Pb > As > V > Cd > Hg. As observed during both flow seasons, Cr and Cu are dominant contaminants, meanwhile Cd and Hg remain the lowest contaminants in vegetables. Amwele et al. (2017) observed the dominance of Cr in spinach samples collected in Mafikeng, South Africa, with Cr concentrations exceeding 1.150 µg/g and a minimum concentration of 0.005 µg/g.

Vanadium concentration was observed to be consistently exceeding the guidelines limits of 0.03 µg/g set by the WHO/FAO. The samples of spinach obtained from farms 3 and 4 were found to be above the

limit with values of 0.342 µg/g (F2S1-S) and 0.314 µg/g (F4S2-S), respectively. This finding suggests significant contamination, which could potentially lead to toxic effects in both plants and consumers. Therefore, as V is not a nutrient for plants or consumers, it can become highly toxic at elevated levels. Chromium was also observed to exceed the MPL stipulated by the WHO/FAO of 1.3 µg/g in all samples collected during the high-flow season. Notably, the higher concentration than guidelines was also observed in the soils where vegetables were planted. The highest concentration of Cr was observed in pumpkin leaves (F2S3-Pk) from farm 2, showing a concentration up to 40.1 µg/g. The lowest concentration was observed in spring onion (F3S2-SO) from Farm 3, showing 2.10 µg/g due to its thick cuticular, which could resist the sinking of PTEs into the plant's system. Similarly, low Cr level in onions was reported by Amwele et al. (2017), with the highest concentration reaching 0.021 µg/g. This significant exceedance points to high contamination, which is concerning given the Cr toxicity, especially in its hexavalent form, which is carcinogenic.

The concentrations of Ni and Cu were observed to be below guidelines across all samples, respectively. Copper was most concentrated in spinach (F2S1-S) at 33.8 µg/g, while Cu is an essential trace element for plants and animals, its excessive concentration can cause phytotoxicity and health issues in humans (Kopittke et al. 2010). Though the concentrations of the current study are not at concerning levels, which ranged from 2.56 µg/g to 33.8 µg/g when compared to the guideline value of 73.0 µg/g by FAO/WHO, constant accumulation of these PTEs can cause a serious health risk. The highest concentration of Ni was observed in F2S1-S, with 9.09 µg/g. Although this concentration level is relatively low, chronic exposure, even at these concentrations, could still pose a risk of sensitization or allergic reaction in vulnerable individuals (Das et al. 2008; Genchi et al. 2020).

3.14 NON-CARCINOGENIC HUMAN HEALTH RISK ASSESSMENT

The current study assessed ingestion of PTEs as the primary pathway of exposure to toxic elements through the ingestion of contaminated vegetables and drinking of contaminated water. This study assessed the total concentrations of PTEs in water and vegetables to evaluate the associated human health risks. The HQ and HI values calculated for both water and plants indicated a health hazard linked to the consumption of BW and vegetables. The HQ is a risk assessment metric used to evaluate the non-carcinogenic risk posed by individual elements when ingested through water, with an HQ value greater than 1 suggesting a potential health risk (Birch et al. 2023; Panda et al. 2022).

3.14.1 Human health risk assessment of borehole water

The HHRA of RW was not presented in the current study due to its low concentrations of PTEs, which resulted in low HQ when compared to levels of PTEs in BW samples. The elevated levels of Cr in BW necessitated the need to assess the human health risk of the water to evaluate the risk associated with the consumption of such water. Based on HQ for children and adults, the trend for HHRA followed this order: Cr > V > As > Ni > Pb > Cd > Cu > Hg.

Figure 3.32 presents the HQ for adults based on low-flow season BW samples (BW1 to BW7) for various PTEs: V, Cr, Ni, Cu, As, Cd, Hg, and Pb. The figure highlights that adults consuming water from BW6 face an elevated risk of developing Cr-related health issues. The health risk assessment across the BW samples indicates that the HQ values for V, Cr, Ni, Cu, As, Cd, Hg, and Pb are generally below 1. However, the water sample from BW6, collected from Driekop village, exhibits a Cr HQ value of 1.12, surpassing the safety threshold of 1. This indicates that consuming water from BW6 could pose a significant health risk due to the elevated Cr concentration.

Observations show consistently low HQ values for V across all borehole water samples, indicating negligible health risk from V exposure through these water sources. While Cr HQ values are elevated in BW5 and BW7, they remain below 1, suggesting a moderate risk from Cr exposure in these water sources. The HQ values for Ni, Cu, As, Hg, Pb, and Cd are low across all samples, indicating negligible health risks from exposure to these PTEs through the BW. The results found elsewhere by Belew et al. (2024) on a similar study found that Pb, Cd, Ni, and Cu were the main PTEs contributing to HQ of adults and child population; meanwhile, the current results found Cr as the main contributor to the HQ of adults and children in BW samples. The findings suggested the difference in the geological setting of the two countries and the source of pollution.

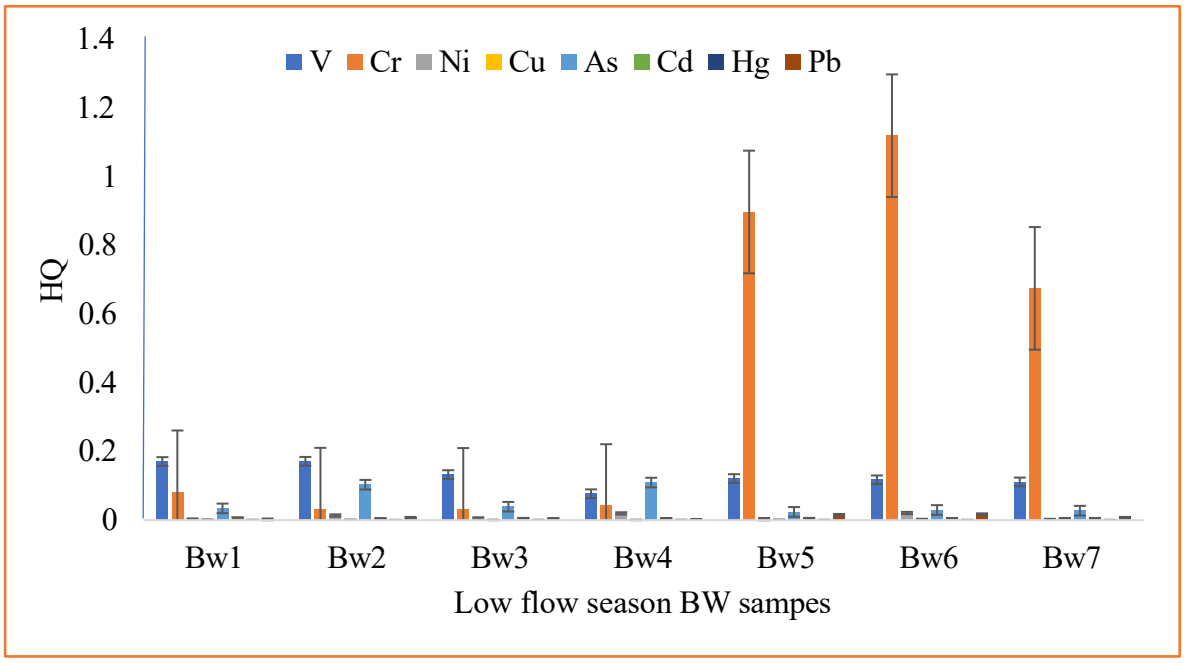

Figure 3.32. Adult HQ assessment from borehole water during the low-flow season.

Therefore, the results suggest that BW is generally safe for adult consumption regarding V, Ni, Cu, As, Cd, Hg, and Pb during low-flow seasons. However, the elevated Cr levels in BW5, 6, and 7, particularly in BW6, raise significant concerns. Targeted interventions are recommended to address Cr contamination in these specific water sources to mitigate potential health risks.

Figure 3.33 indicates that the HQ for children exposed to Cr in BW5, 6, and 7 exceeds the safety threshold of 1, with values of 1.36, 1.70, and 1.02, respectively. This suggests that these BW sources pose a significant health risk to children, more than to adults. It was observed that the total Cr concentrations in water exceeding 70 µg/L and 65 µg/L for adults and children, respectively, result in HQ values above the safety threshold. This observation was also confirmed by the study conducted by Panda et al. (2022), where most samples were Cr surpassed the 70 and 65 µg/L for adults and children, respectively, resulted in HQ greater than 1.

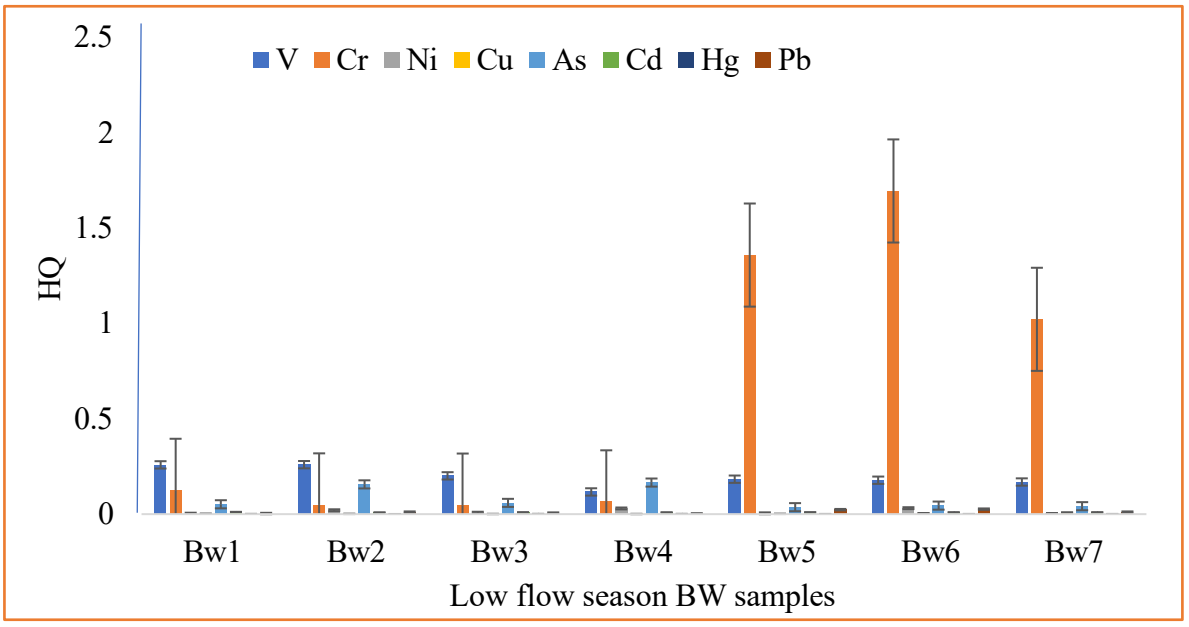

Figure 3.33. Children HQ assessment from BW during the low-flow season.

The results obtained in this study are consistent with the findings of Atangana & Oberholster (2021), who investigated borehole water from the Limpopo and Mpumalanga provinces of South Africa. Their study investigated PTEs such as Cu, Ni, Fe, Ba, Zn, and Mn, and concluded that all PTEs, including Cu and Ni, were safe for adults, children, and infants. Similarly, a study by Mallongi et al. (2022) on Pb, Cr, and Cu in groundwater from the Maros Karst area reported HQ of less than one for both adults and children during high-flow and low-flow seasons. The Maros Karst area, like the Steelpoort and Burgersfort regions, is characterized by illuvial soils. It was also noted that the concentrations of Cu, Cr, and Pb in groundwater from the Maros Karst were comparable to those observed in the current study. These findings suggest that groundwater contamination can be attributed to both natural processes and anthropogenic activities. Therefore, no health risk is expected for V, Ni, Cu, As, Cd, Hg, and Pb during the low-flow season. However, the elevated Cr levels in BW5, 6, and 7 require attention due to their potential health hazards, particularly for children.

The HI values are calculated for all measured PTEs. The dashed line represents the safety threshold (HI = 1), above which there is a potential health risk. Figure 3.34 illustrates the HI for both adults and children across seven BW samples collected during the low-flow season. For BW1 to BW4, the HI values for both adults and children are below 1, indicating a low risk of adverse health effects due to PTEs. However, in BW5 and BW6, the HI values exceed the safety threshold of 1, with children showing higher HI values than adults. Specifically, BW6 exhibits the highest HI values, with children reaching an HI of approximately 2, suggesting a significant health risk, particularly for children. The BW7 also shows elevated HI values of 1.26 in children; though it remains closer to the threshold for adults, it was a significant risk for children.

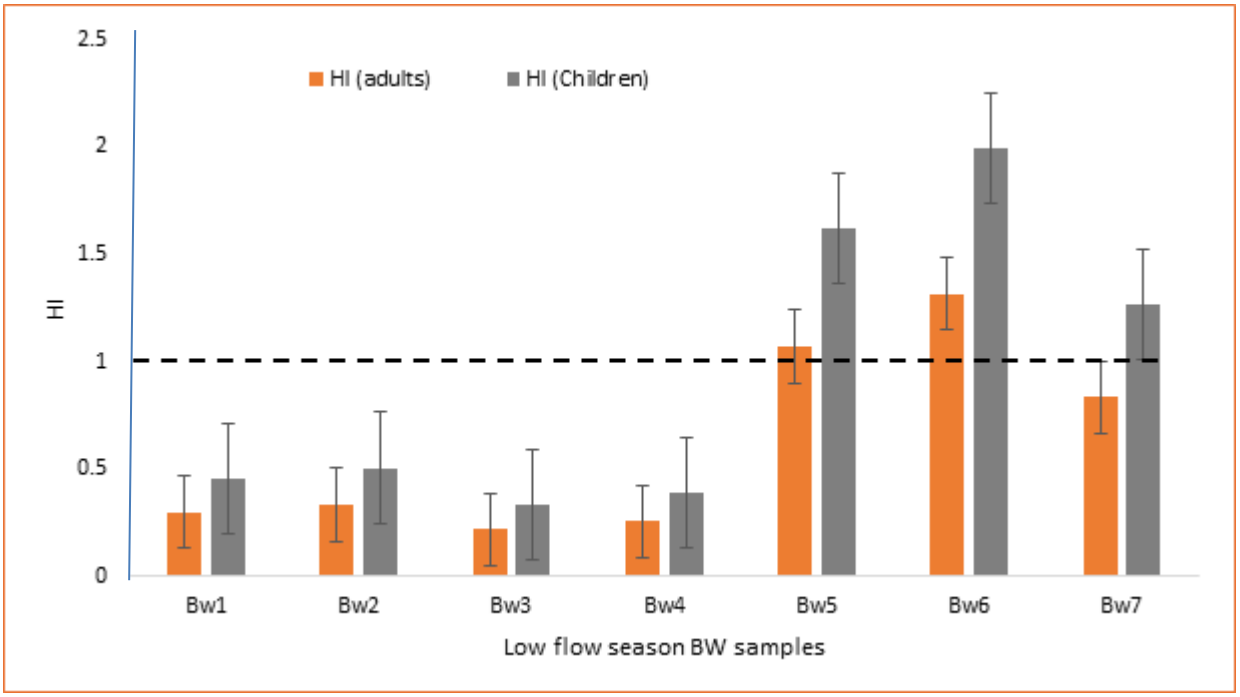

Figure 3.34. Comparative analysis of the HI for adults (orange bars) and children (grey bars) based on low-flow season BW samples (BW1 to BW7).

Overall, the data suggest that borehole water samples BW5, 6, and 7 pose a potential health risk, particularly for children, due to the elevated levels of PTEs. The results highlight the need for targeted interventions to reduce exposure to these contaminants, especially in vulnerable populations such as children.

The risk assessment of BW quality during the high-flow season is critical for understanding potential contamination risks posed by increased surface water runoff and groundwater infiltration. During this period, the elevated flow of rivers and streams can transport pollutants from agricultural, industrial, and urban sources into groundwater systems (Datry et al. 2004; Singh et al. 2018). This may lead to uncertainty of PTEs and microbial contaminants in BW. Evaluating the health risks associated with consuming or using this water is essential for developing mitigation strategies, ensuring safe water use, and protecting community health, particularly in regions dependent on BW as a primary source of drinking water.

During high-flow season, Cr continues to be a dominant pollutant and emerges to be more unsafe amongst other measured PTEs. Based on the HQ values measured during the high-flow seasons indicated the order was indicated: Cr > V > As > Hg > Pb > Ni > Cu > Cd, for both adults and children. The decrease of HQ values between low and high-flow seasons was also observed in the current study, as observed by Panda et al. (2022). The decrease in concentrations of PTEs in water influences the decrease in HQ, as HQ and concentrations of PTEs are directly proportional to each other.

Figure 3.35 illustrates various HQ values for adults. During the high-flow season, the HQ values for adults across all BW samples (BW2, BW3, BW4, BW5, BW6 and BW7) remained below the threshold of 1. This indicates that the exposure to PTEs in these water samples does not pose a significant health risk to adults. The results suggest that the natural dilution effect during the high-flow season effectively reduces the concentration of contaminants, thereby lowering the HQ values. The most notable reduction was observed for Cr in BW5 and BW6, where the HQ values were significantly higher during the low-

flow season than the high-flow season. This reduction highlights the importance of seasonal variations in the assessment of water quality and associated health risks.

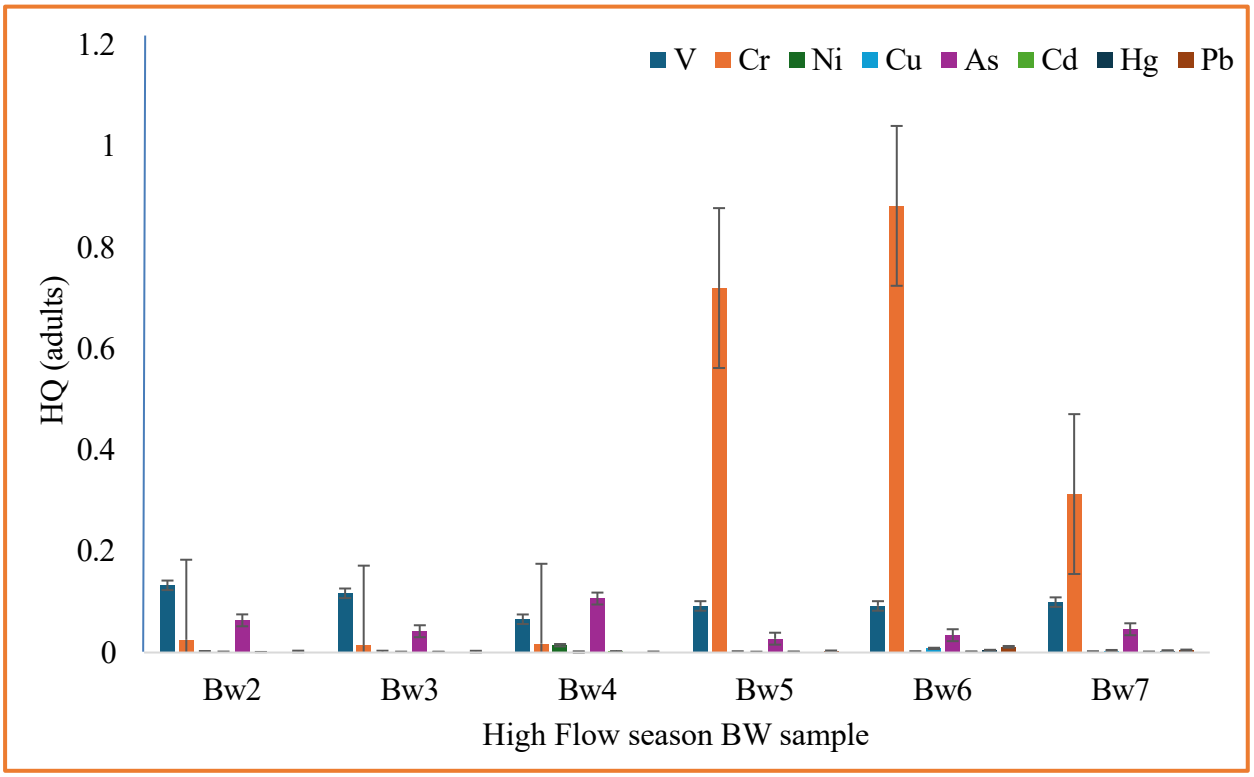

Figure 3.35. The HQ for adults from BW samples during the high-flow season.

The elevated HQ values for Cr in BW5 and BW6 suggest that Cr contamination poses a substantial risk during the high-flow season. Chromium, particularly in its hexavalent form (Cr(VI)), is highly toxic and carcinogenic, though the study did not conduct the speciation of Cr. The presence of Cr at these levels could be linked to geogenic sources other than anthropogenic sources. Additionally, increased runoff during the high-flow season likely exacerbates the leaching of Cr into groundwater, elevating the contamination in these boreholes, which is likely to be observed during the low-flow season.

Other elements, such as V and As showed lower HQ values than Cr, but their presence in samples like BW5 and BW6 still raises public health concerns. While their HQ values remain below 1, the moderate levels of V and As suggest that these elements, though not the primary contaminants, may contribute to the overall health risk. The V levels, particularly in Bw6, are still notable but do not exceed the HQ threshold in any sample, suggesting that V contamination may not be as prevalent during this season. Copper, Pb, Ni, Cd, and Hg exhibit HQ values well below 1 in all borehole water samples, indicating minimal health risks during the high-flow season. However, the detection of these elements, particularly Cd, should not be overlooked, as chronic exposure even at low levels can result in long-term health effects (Suciu et al. 2022). The relatively low HQ values could be due to the dilution effect during the high-flow season or reduced contamination sources affecting these specific PTEs (Paerl et al. 2018). There is considerable variation in HQ values across the different BW samples, with BW5 and BW6 showing significantly higher Cr levels compared to other sites like BW2 and BW3. This suggests localized sources of contamination near BW5 and BW6, possibly due to geogenic and opencast mines on the opposite side of the village, which could introduce higher concentrations of Cr into the groundwater system. These localized variations highlight the importance of site-specific monitoring and targeted interventions.

The high HQ values for Cr in BW5 and BW6 indicate a pressing need to address Cr contamination in these boreholes, particularly during the low-flow season. The potential health risks associated with Cr exposure, especially in its toxic hexavalent form, warrant immediate attention and remediation efforts. While other elements, including V and As, present moderate risks, Cr clearly dominates as the primary contaminant of concern.

Figure 3.36 presents the HQ values for children during the high-flow season. The HQ values are generally higher than those for adults, reflecting the increased vulnerability of this population group with exposure to PTEs. However, during the high-flow season, the HQ values for children also showed a significant decrease compared to the low-flow season. In particular, the HQ values for Cr and V in BW5 and BW6, which were previously concerning during the low-flow season, were substantially reduced during the high-flow season. Despite the higher HQ values for children compared to adults, the decrease during the high-flow season suggests a reduced health risk due to the dilution of contaminants. Nonetheless, the HQ values for children, especially in BW5 and BW6, still approach the threshold of 1, indicating the need for continued monitoring and potential intervention during periods of low water flow.

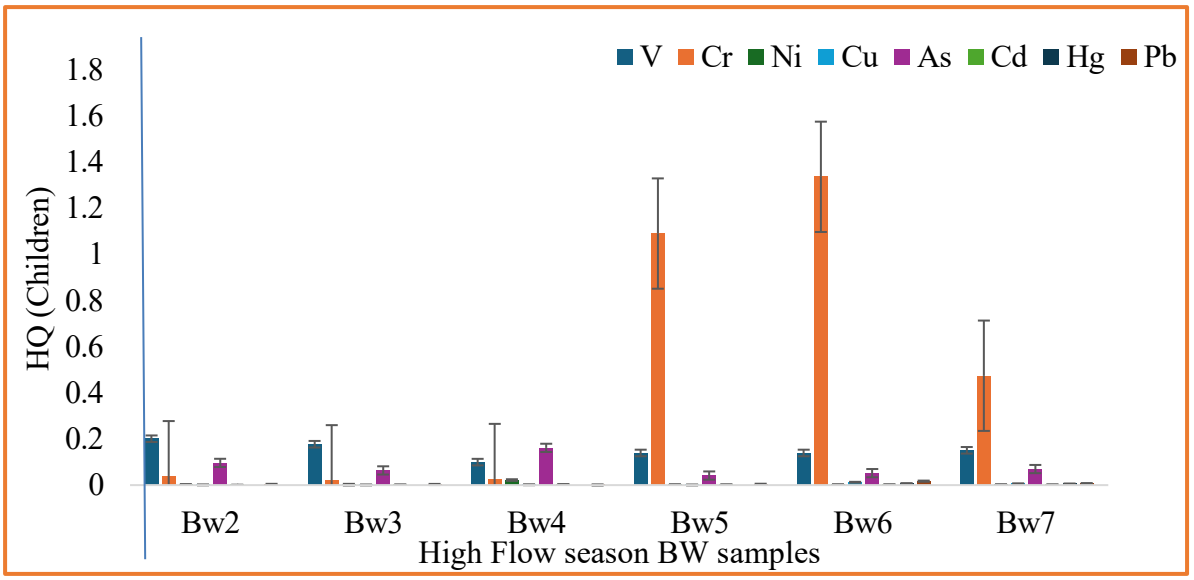

Figure 3.36. The HQ values for children from BW samples during the high-flow season.

Similar to adults, the persistent toxic elements such as V and As showed a moderate health risk to humans. With V and As noticeable from BW1 to BW6, it aids a strategy to reduce the risk of continuous exposure to such elements, as the consumers may develop diseases related to such contaminants.
Figure 3.37 displays the HI values, which represent the cumulative risk from exposure to multiple PTEs, and shows a significant decrease during the high-flow season for both adults and children when compared to the low-flow season. For adults, the HI values across all BW samples were well below the threshold of 1, except for BW6 with 1.04, indicating that the combined exposure to all measured PTEs does not pose a significant health risk. The reduction in HI values in the high-flow season compared to the low-flow season reflects the overall decrease in contaminant concentrations due to the natural dilution effect.

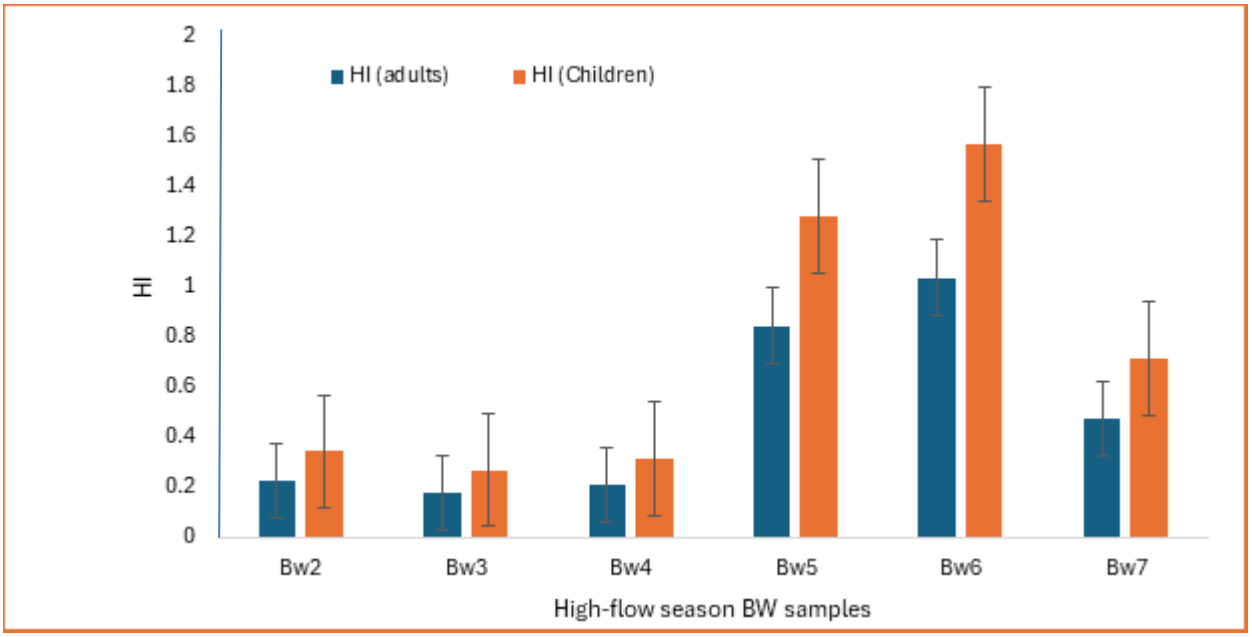

Figure 3.37. Comparative analysis of the HI for adults (blue bars) and children (orange bars) based on high-flow season BW samples (BW2 to BW7).

For children, the HI values were also reduced during the high-flow season but remained higher than those for adults. The HI values for BW5 and BW6 were of particular concern during the high-flow season, as they approached or exceeded the threshold of 1. However, during the high-flow season, these values decreased significantly, reducing the cumulative health risk for children. Despite this reduction, the HI values for children in BW5 and BW6 still warrant attention, as they are closer to the threshold compared to other BW samples, emphasizing the importance of ongoing risk assessments and possible interventions, particularly during the low-flow season.

In contrast, during the low-flow season, the HQ and HI values were notably higher, particularly for Cr and V. The higher values during the low-flow season could be due to the reduced dilution of contaminants, as water levels are generally lower, leading to higher concentrations of PTEs in the borehole water. This seasonal variation suggests that during the low-flow season, there is an increased risk of exposure to these contaminants, which is subsequently alleviated during the high-flow season when water levels rise and dilute the concentrations of PTEs. The observed decrease in HQ and HI values during the high-flow season indicates a seasonal mitigation of health risks, likely due to natural dilution processes that reduce the concentrations of PTEs in the water.

3.14.2 Human health risk assessment of vegetables

Figure 3.38 illustrates the HQ for children due to various PTEs in low-flow season vegetable samples from three different vegetables in farm 1 (F1S1-S, F1S2-SO, and F1S3-Ok). The elements investigated include V, Cr, Ni, Cu, As, Cd, Hg, and Pb. The results indicated that children who consume most vegetables from farm 1 are exposed to the HQ of less than 1, except for Cr in all vegetable samples. Chromium levels showed significantly high HQ values across all three vegetable samples, with F1S3-Ok having the highest HQ of approximately 180, followed by F1S1-S and F1S2-SO with HQs of around 100. This indicates a severe risk to children from Cr exposure *via* vegetable consumption in these areas. The F1S3-Ok shows a notable HQ for As, indicating a considerable risk, though not as high as Cr. The HQ for As in F1S1-S and F1S2-SO is lower but still of concern. Lead shows significant HQ values in all samples, with F1S3-Ok and F1S1-S having higher values, indicating a considerable risk for children. HQ values suggest lower immediate health risks compared to Cr, As, and Pb. The Pb

and Cd of F1S1-S have HQ greater than 1, which indicates the possibility of being hazardous to adults who consume spinach vegetables planted in farm 1. Cadmium is comparatively lower than those for Cr and Pb, but still presents a risk, especially in F1S2-SO and F1S3-Ok. Nickel, Cu, V, and Hg exhibit relatively low HQ values across all samples.

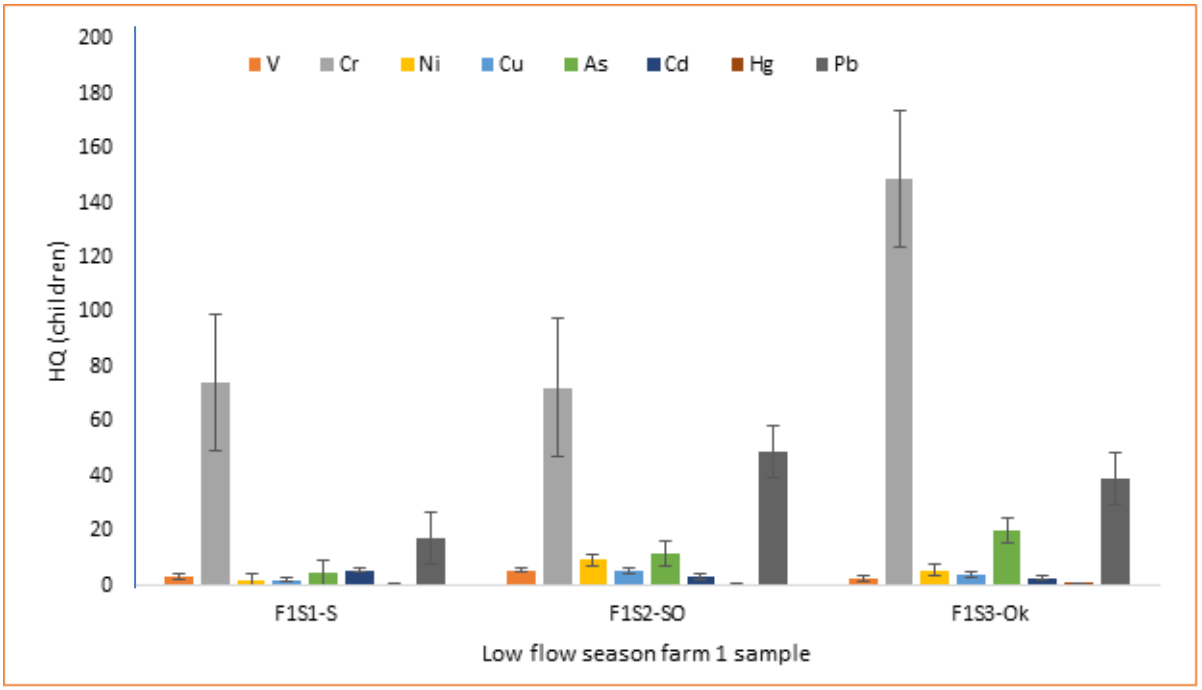

Figure 3.38. The HQ assessment of vegetables obtained from farm 1 for children.

The data reveals that Cr poses the highest risk to children, with HQ values significantly exceeding the threshold of 1, indicating a potential for adverse health effects. Lead and As also present notable risks, particularly in F1S3-Ok, where both elements show elevated HQs. The presence of these high-risk elements in the vegetables is alarming, especially since these farms are likely to sell them to small markets, which could lead to further exposure through dietary intake. The current results are similar to those reported elsewhere (Dintsi et al. 2023). The authors reported elevated HQ of greater than 1 in the child population for vegetables such as spinach, mochaina, and onion. The current results showed HQ greater than 1 for all samples collected at farm 1. The authors also noted that the high level of HQ when compared to adults was similar to the current study.

Figure 3.39 presents the HQ of adults for various PTEs in vegetable samples collected from different sections of Farm 1 (F1S1-S, F1S2-SO, F1S3-Ok) during the low-flow season. Similarly, an HQ greater than 1 indicates a potential health risk for adults who consume vegetables planted in farm 1. The elements quantified include V, Cr, Ni, Cu, As, Cd, Hg, and Pb. The HQ values indicate the potential health risk posed by these elements to adults. The Cr exhibits the highest HQ values across all three sampling sites. Figure 3.39 shows that F1S3-Ok contains the highest HQ value for Cr, exceeding 30, which indicates a significant potential health risk to adults who consume okra from farm 1. The F1S1-S and F1S2-SO also showed elevated levels of HQ for Cr exceeding 15.

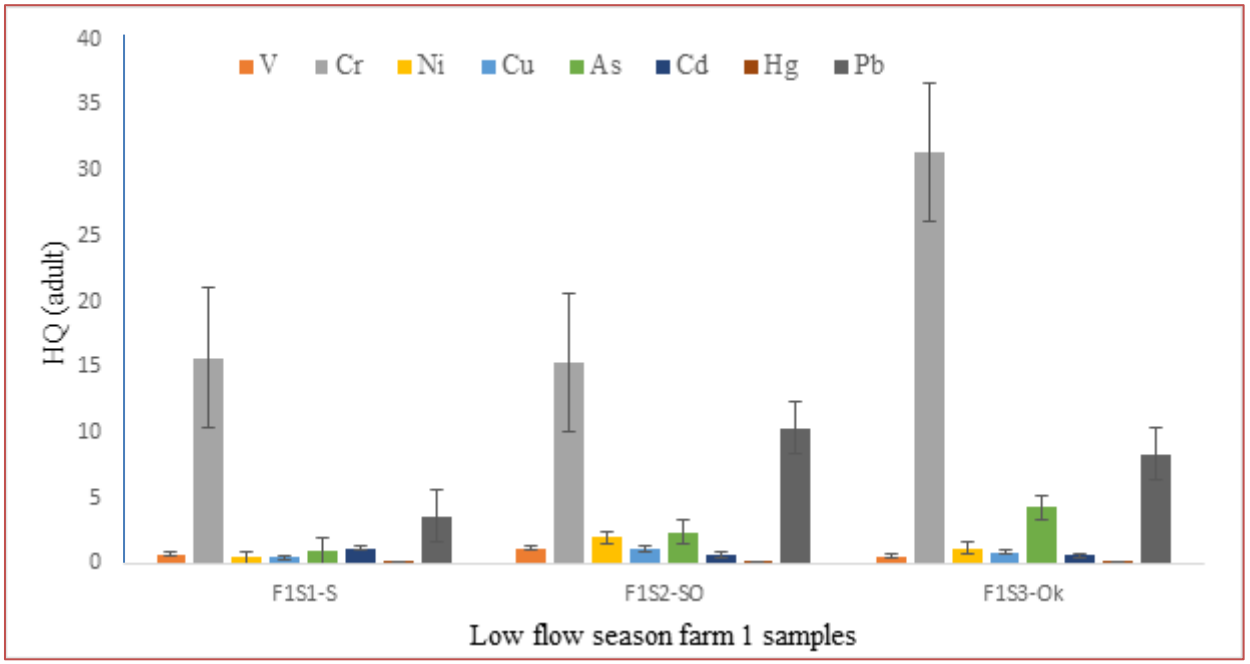

Figure 3.39. The HQ assessment of vegetables obtained from farm 1 for adults.

In the low-flow season for farm 2 samples, the HQ values for adults in Figure 3.40 reveal that Cr and Pb contribute significantly to the risk profile, with Cr showing the highest HQ across multiple samples, especially in F2S2-BL (Beetroot leaves) and F2S3-Ch (Chomolia). The HQ values for Cr range from 1.7 (F2S4.1-SOR) to 10.3 (F2S2-BL), indicating a higher potential health risk for adults in these samples compared to other metals, such as V, Ni, Cu, Cd, As, and Pb, which were below 1 except As in F2S1-S, F2S2-BL, F2S3-Ch, and F2S4.1-SOR with 1.01, 1.38, 1.61, and 2.62, respectively. Lead also presents substantial HQ values over 4.0, particularly in F2S2-BL, F2S3-Ch, F2S4.1-SOR, and F2S5-T, however, these are still significantly lower than those for Cr. Overall, the adult HQ for low-flow season indicates that Cr is the predominant risk factor among the measured PTEs, followed by As and Pb.

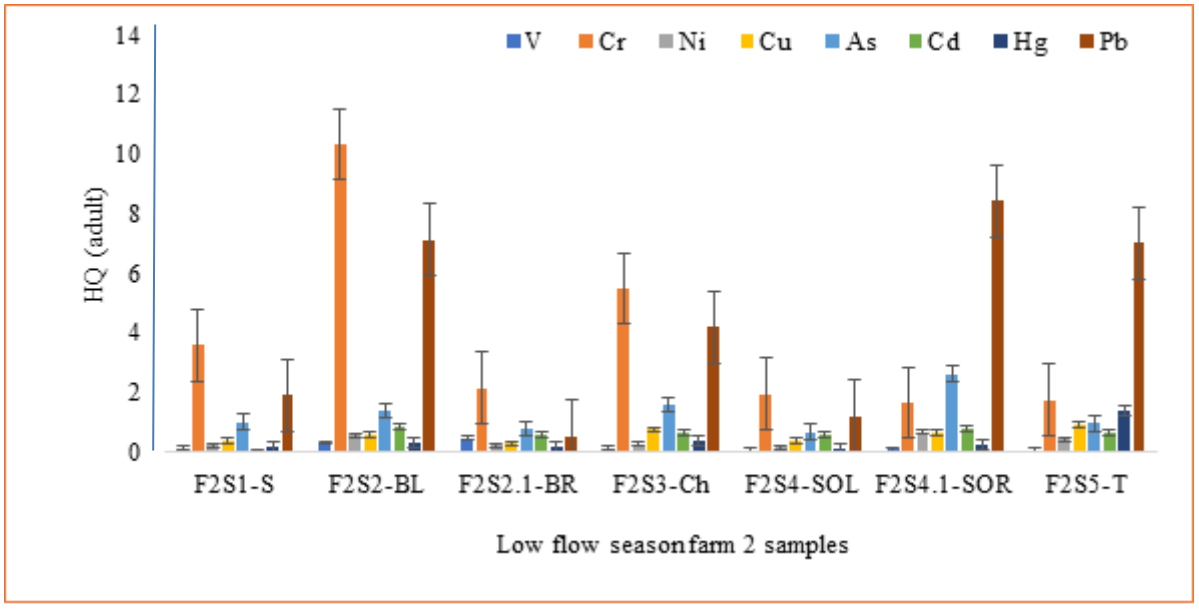

Figure 3.40. The HQ assessment of vegetables obtained from farm 2 for adults.

The results presented in Figure 3.41 highlight significant variations in the HQ values for children during the low-flow season across Farm 2 samples. Chromium is the dominant PTEs at most sites, with HQ

values exceeding 50 at F2S2-BL and F2S5-T, indicating a severe health risk. Lead also shows elevated HQ values, particularly at F2S2-BL and F2S5-T, further contributing to the potential risk. The HQ values for other PTEs, including V, Cd, and Cu, are moderate but still contribute to the overall risk at certain sites. Notably, F2S2.1-BR exhibits lower HQ values for all PTEs, suggesting reduced contamination at this part of the vegetable when compared to its leaf part. In contrast, vegetables such as F2S4.1-SOR and F2S4-SOL show high HQ values for Cr and Pb, reinforcing their dominance in risk contribution. The significant spatial variation in HQ values underscores the influence of localised contamination sources, such as industrial or agricultural activities, near Farm 2. These findings emphasise the urgent need for targeted mitigation strategies to address Cr and Pb contamination and reduce associated health risks for children. The current results are comparable with findings from Dikotla and Ambushe, (2024), where Cr was the dominant contaminant in vegetables and showed higher levels for children compared to the adults.

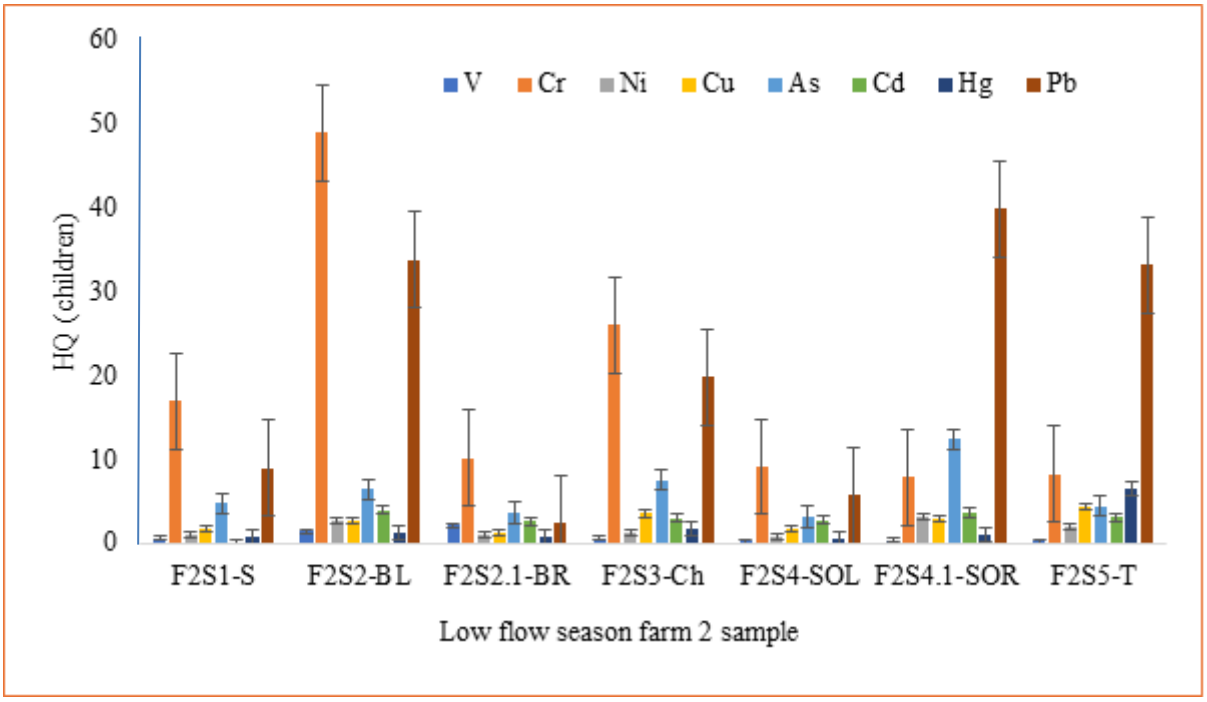

Figure 3.41. The HQ assessment of vegetables obtained from farm 2 for children.

Figure 3.42 represents the HQ results for adults on Farm 3, which present a concerning picture, particularly regarding Cr, As, and Pb, which consistently showed elevated levels across various sampling sites. For instance, the HQ for Cr reaches a striking value of 7.78 for the F3S1-S, indicating significant exposure risks. Arsenic and Pb also display alarmingly high HQ values, with As peaking at 1.97 in F3S2-YS and Pb reaching a critical 11.7 at the same site. These high HQ values suggest that adults in the area are exposed to potentially hazardous levels of these toxic elements, which could lead to severe health implications over time, including respiratory, neurological, and cardiovascular issues.

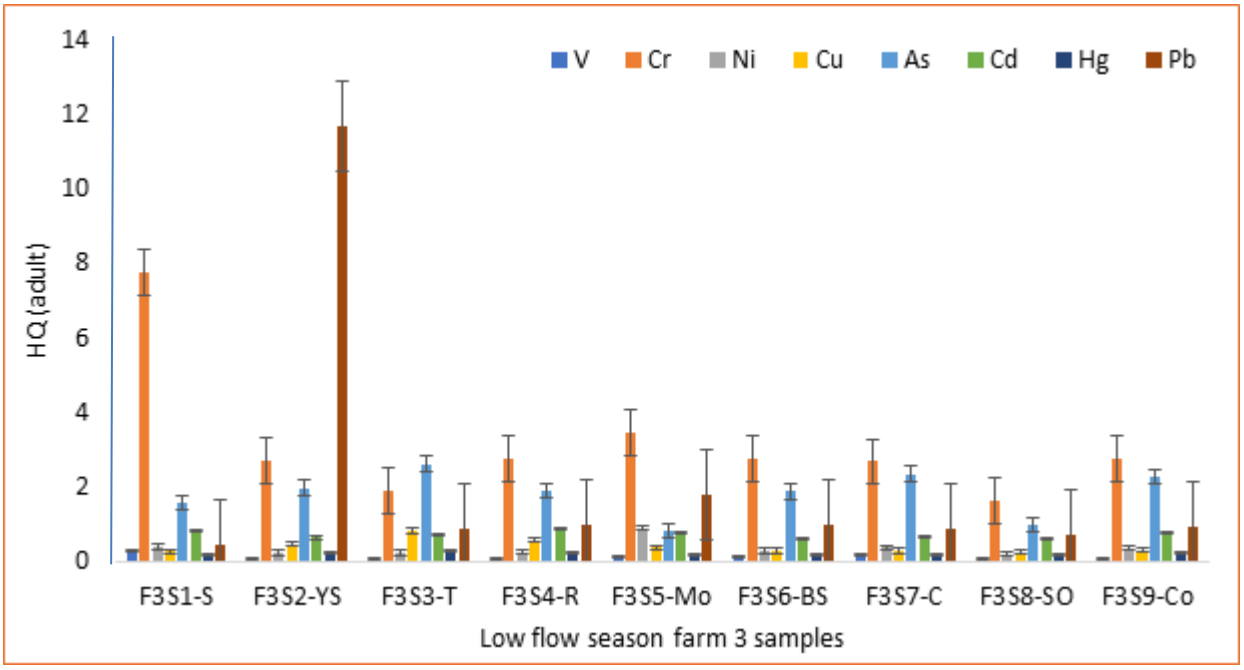

Figure 3.42. The HQ assessment of vegetables obtained from farm 3 for adults.

The elevated levels of HQ for Pb in F3S2-YS, particularly, highlight a potential hotspot of contamination, which might be linked to nearby industrial activities, the use of leaded materials, or historical pollution that persists in the soil. The high HQ for As further intensifies concerns, as it points to possible contamination from pesticides, mining activities, dust-borne from the main road nearby, or natural geochemical processes that introduce As into the environment.

Other elements, such as Ni and Cd, while showing relatively lower HQ values compared to Cr, As, and Pb, still contribute to the overall risk profile. For example, Ni in F3S5-Mo has a HQ value of 0.891, and Cd in F3S3-T has a value of 0.723. These levels, although not as immediately alarming, are still significant, as chronic exposure to even moderate levels of these elements can accumulate over time, leading to long-term health issues. What stands out in all these results is the variability in HQ values across the different sampling sites, suggesting that the contamination is not uniformly distributed but rather concentrated in specific areas and the translocation factor of the vegetable. This patchy distribution of contaminants could be attributed to localized sources such as specific agricultural practices, proximity to industrial zones, or variations in soil composition that affect the mobility and bioavailability of these PTEs.

Given the substantial HQ values observed for multiple toxic elements, there is a clear need for targeted risk mitigation strategies. These should include detailed soil and water testing, public health interventions to reduce exposure, and possibly the introduction of phytoremediation or soil washing techniques in the most affected areas. Furthermore, raising community awareness about the risks associated with these contaminants is crucial to protect both current and future generations from the adverse health effects of prolonged exposure.

Figure 3.43 illustrates the HQ results for children on Farm 3, which reveal a significantly higher risk of exposure to PTEs compared to adults, which is a crucial concern given the vulnerability of children to environmental contaminants (Singh et al. 2018).

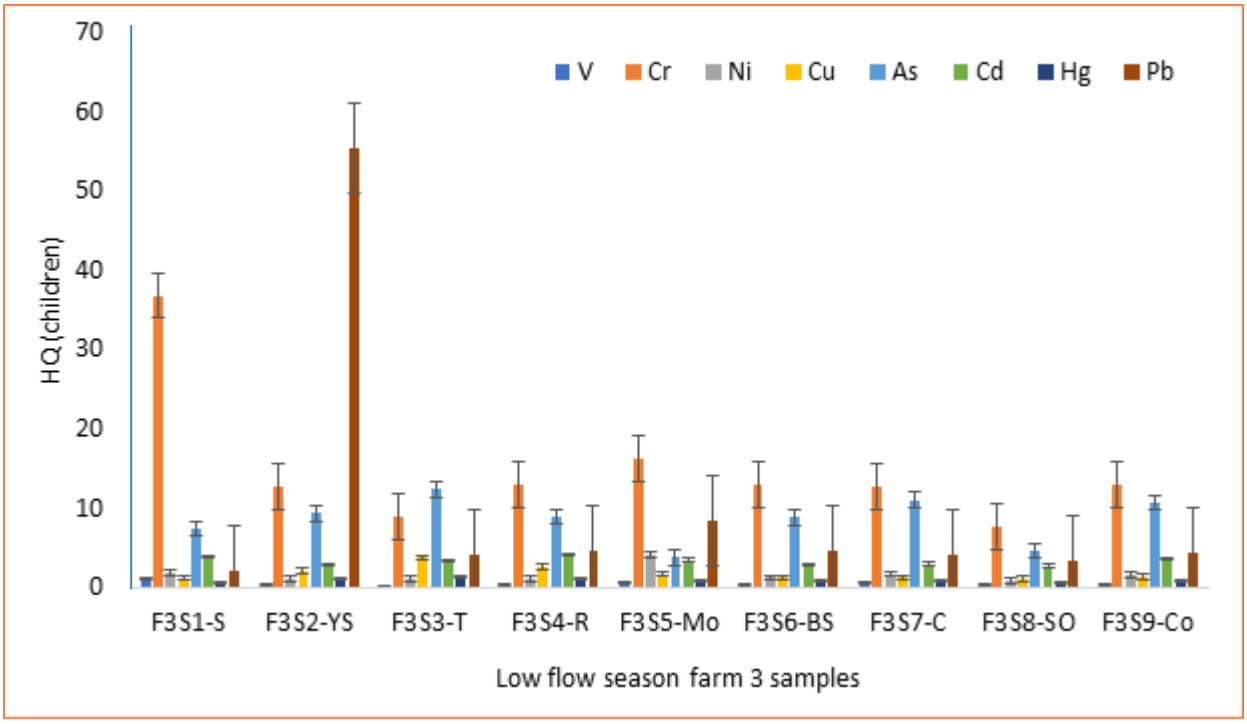

Figure 3.43. The HQ assessment of vegetables obtained from farm 3 for children.

For instance, the HQ for Cr in children reaches extremely high values, particularly at the F3S1-S site (36.8) and F3S5-Mo (16.4). In comparison, the HQ for Cr in adults, although high, is substantially lower (7.78 at F3S1-S and 3.46 at F3S5-Mo) than that of children for 36.8 and 16.4 of F2S1-S and F3S5-Mo, respectively. This suggests that children are at a much higher risk of adverse health effects due to Cr exposure, which can include skin irritation, respiratory issues, and potential carcinogenic effects over prolonged exposure.

Lead showed the most alarming disparity between children and adults. The HQ for Pb in children peaks at an astounding 55.3 in the F3S2-YS, compared to 11.7 in adults at the same site. This indicates a highly elevated risk for children, as Pb exposure is associated with severe developmental and neurological effects, especially in young individuals.

Arsenic also demonstrates higher HQ values for children compared to adults. At F3S3-T, the HQ for children is 12.4, while for adults it is 2.61. This stark difference underscores the greater susceptibility of children to As-related health risks, including potential carcinogenic effects and developmental disorders.

Other elements like Ni and Cd show similar trends, with children's HQ values consistently higher than those for adults across most sampling sites. For example, Ni at F3S5-Mo shows an HQ of 4.22 in children, while in adults it is 0.891. Cadmium at F3S2-YS shows an HQ of 1.23 for children, compared to 0.261 in adults.

These comparisons highlight that children are more at risk from exposure to these PTEs, emphasising the need for targeted interventions to protect them. The higher HQ values in children are likely due to their lower body weight, higher intake rates of food and water relative to body size, and their developing bodies, which make them more susceptible to environmental toxins. This underscores the importance of prioritising children's health in environmental risk assessments and implementing protective measures to reduce their exposure to hazardous substances.

Figure 3.44 presents the HQ values for various PTEs across different sample sites, focusing on adult exposure. Chromium exhibits notably high HQ values across several sites, with F4S8-S recording the highest at 15.7, indicating a significant risk. Similarly, Ni shows elevated HQ at F4S7-Ca with a value of 3.49, suggesting potential health concerns. Arsenic poses a notable risk at F4S3-CT, F4S4-SO, and F4S8-S, with HQ values of 2.66, 2.54, and 4.41, respectively, indicating severe contamination levels that could lead to adverse health effects. Cadmium and Hg also show concerning HQ values, particularly in F4S1-Co and F4S6-Mo, with Cd reaching 2.26 and Hg at 1.52, respectively. Lead, while generally lower than other elements, spikes at F4S3-CT with an HQ of 6.77, indicating a serious health risk. Copper and V show relatively lower HQ values across the sites, with a few exceptions, such as Cu in F4S7-Ca (HQ 3.11) and V in F4S8-S (HQ 0.27). Overall, the results highlight that several sites exhibit HQ values above the threshold of concern (HQ > 1), particularly for Cr, As, Cd, Hg, and Pb, suggesting significant health risks for adults due to exposure to these elements. These findings underscore the need for immediate intervention and remediation strategies to mitigate exposure and reduce potential health impacts on the affected population.

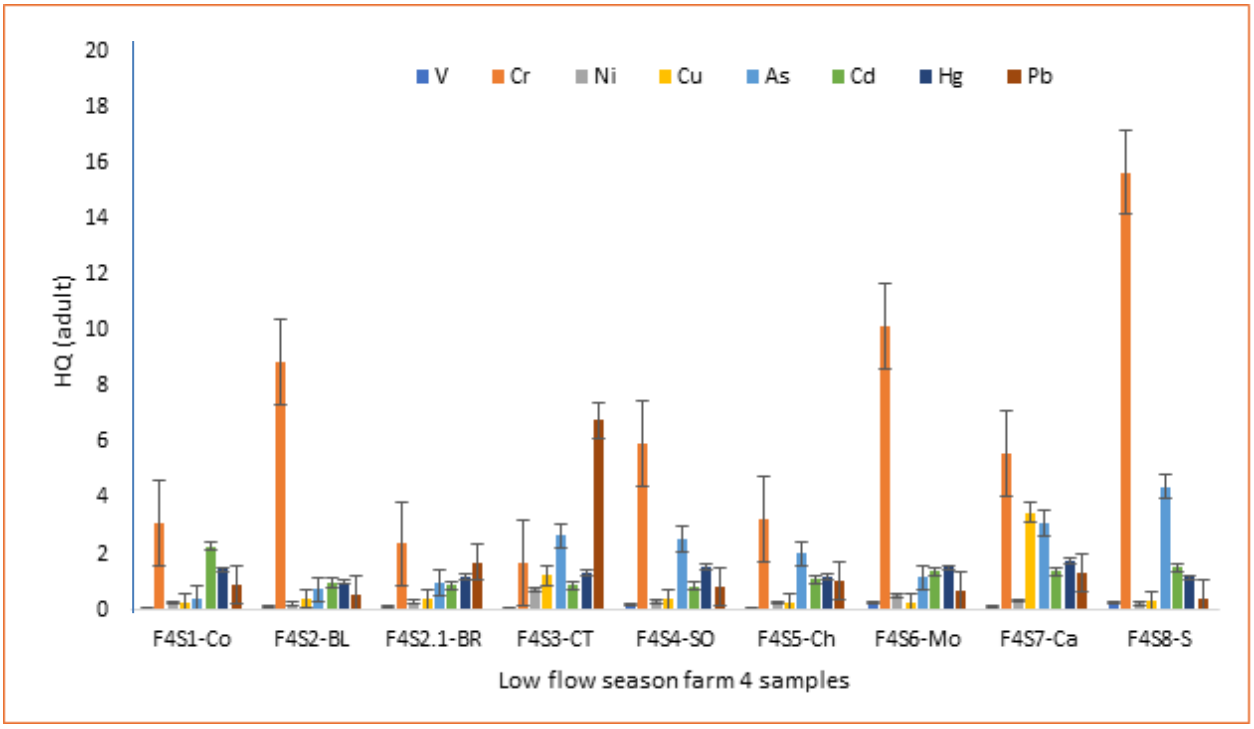

Figure 3.44. The HQ assessment of vegetables obtained from farm 4 for adults.

Figure 3.45 illustrates the HQ values for various PTEs in children across different sampling sites during the low-flow season at Farm 4. Chromium exhibits the most significant concern, with HQ values reaching alarming levels, particularly at sites F4S2-BL and F4S8-S, where Cr HQs exceed 60 and 80, respectively. This indicates a severe health risk to children exposed to Cr at these locations. Arsenic also shows elevated HQ values, with F4S3-CT and F4S8-S standing out, both exceeding an HQ of 20, highlighting a substantial risk.

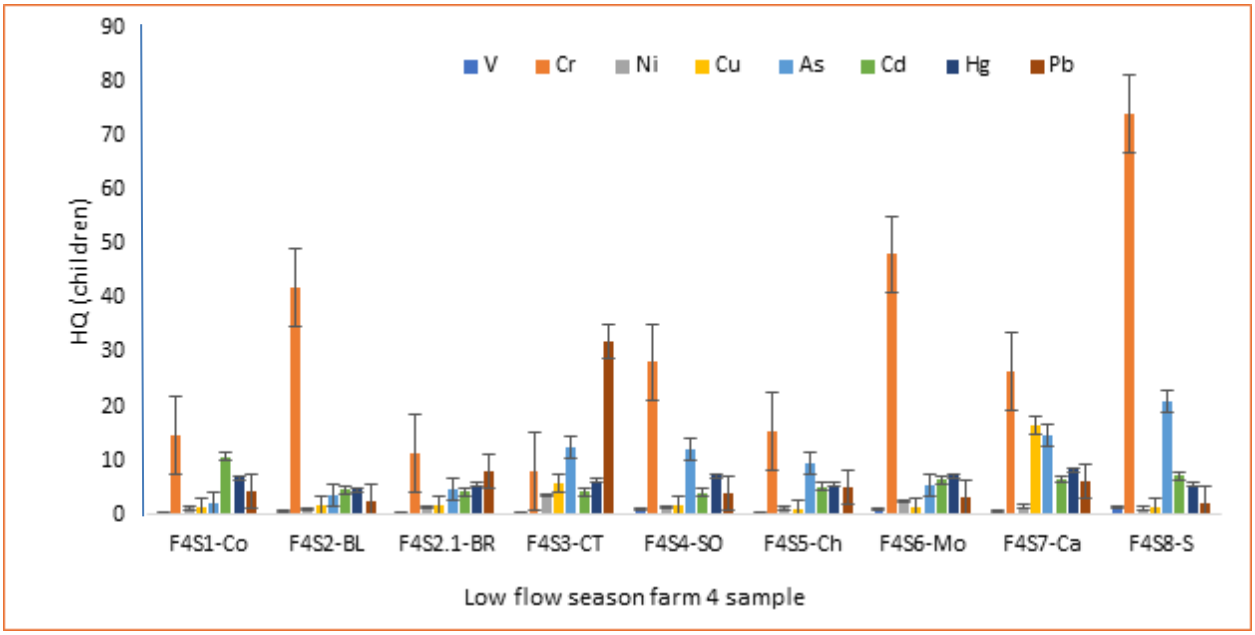

Figure 3.45. The HQ assessment of vegetables obtained from farm 4 for Children.

Nickel and Cu present moderate HQ values across several sites, with Ni showing higher risks at F4S7-Ca and F4S3-CT, while Cu peaks at F4S7-Ca. Lead shows significant HQ values, particularly at F4S3-CT, where the HQ approaches 30, indicating a critical health concern. Mercury and Cd also contribute to the potential health risks, especially at sites like F4S1-Co and F4S6-Mo, where their HQ values are relatively higher than those of adults.

Vanadium exhibits lower HQ values, but they still contribute to the cumulative risk. The overall trend indicates that several sites, especially F4S2-BL, F4S3-CT, F4S6-Mo, and F4S8-S, have multiple PTEs with HQs significantly above the safe threshold for children (HQ > 1). These findings emphasize the urgent need for targeted interventions to reduce exposure and mitigate the health risks posed to children in these areas.

The study conducted by Ametepey et al. (2018) in the Tamale Metropolis, Ghana, revealed elevated HQ values for Cd in carrots, cabbage, onions, and tomatoes. The authors reported HQ and HI values greater than 1 for both adults and children, suggesting significant contamination in the environment that contributes to the accumulation of Cd in vegetables. Similarly, Kumar et al. (2021) carried out a study in the metropolitan city of Lucknow, India, investigating vegetables obtained from street markets to assess human health risks associated with PTEs. In their study, spinach, tomatoes, cabbage, and beetroot were analysed, and the authors reported HQ values greater than 1 for Pb, indicating that lead was the dominant pollutant in the region. Other PTEs, such as Cr, Ni, and Cu, were found to have HQ values below the threshold of 1, indicating a lower health risk. Despite this, the cumulative effects of these elements contributed to higher HI values for both adults and children, indicating a potential risk of long-term exposure.

Figure 3.46 presents the HI values for both adults and children across various vegetable samples collected during the low-flow season. The HI represents the cumulative risk that results from exposure to multiple PTEs and highlights significant disparities between adult and children's populations.

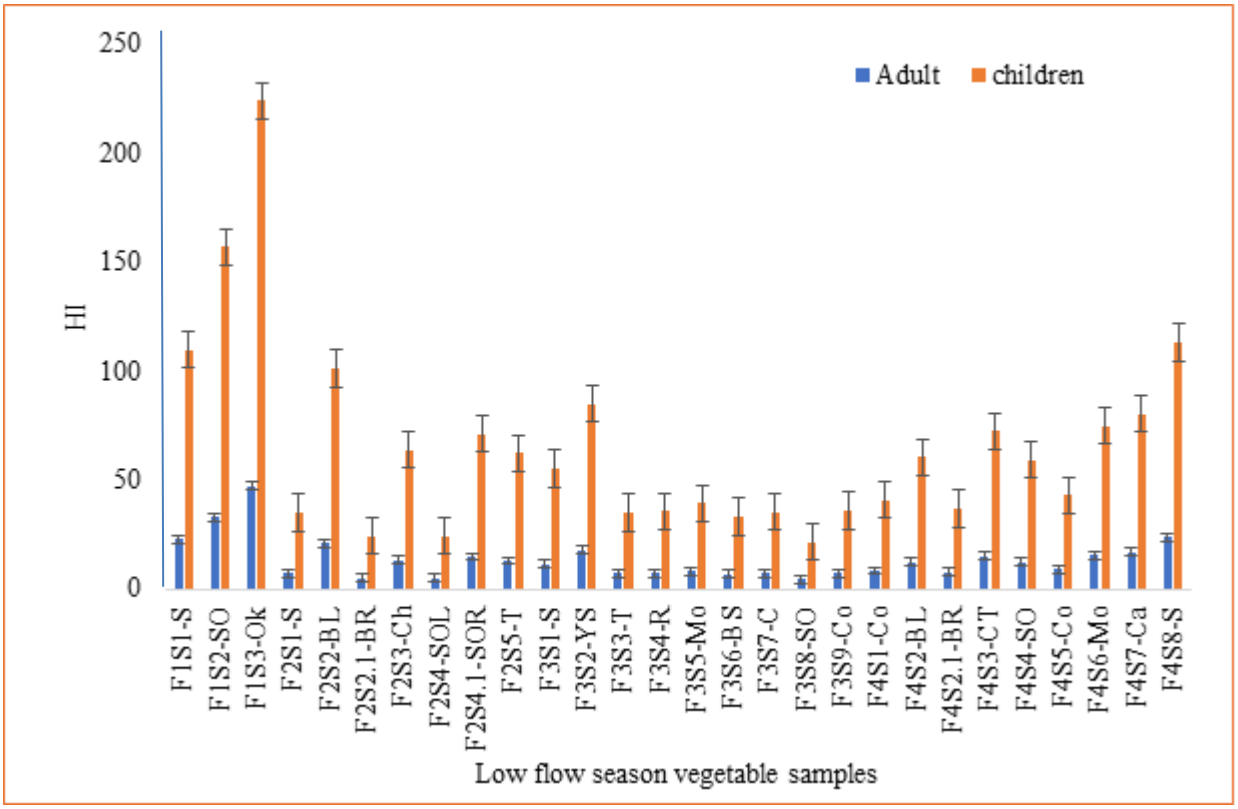

Figure 3.46. The HI assessment of vegetables obtained from farm 1 to 4 for adults and children.

Children consistently exhibit higher HI values compared to adults across all sampling sites, reflecting their increased vulnerability to PTEs exposure. The most alarming results are observed at F13-S-OK, where the HI for children exceeds 200, indicating an extremely high risk that demands immediate attention. Similarly, sites such as F12-SO and F25-S-T also show critically high HI values for children, exceeding 100, further underscoring the severe risk posed to this demographic.

In contrast, adult HI values remain significantly lower across all sites, with the highest recorded value being at F13-S-OK, yet still markedly lower than that of children. This stark difference highlights the disproportionate impact of PTEs exposure on children, making them a priority group for risk mitigation strategies. The impact was also observed from the data reported by Dintsi et al. (2023). Other sites, such as F4S5-SO, F4S8-S, F5S7-Ca, and F2S2-BL, also showed the elevated HI values for children, though not as extreme as the aforementioned sites. However, the consistent pattern of higher risk in children across nearly all sampling sites indicates a widespread issue that must be addressed comprehensively.

Overall, the results indicated that children are at a significantly higher risk from PTEs exposure through vegetable consumption, especially at specific sites like F1S3-OK, F1S2-SO, and F2S5-T. These findings highlight the urgent need for targeted interventions, such as soil and water remediation, public health advisories, and continuous monitoring, to protect vulnerable populations from the adverse health effects associated with these environmental contaminants. The current results are comparable with various studies conducted in Limpopo province (Dikotla and Ambushe, 2024; Dintsi et al. 2023; Moyo and Rapatsa, 2019).

Figure 3.47 presents the HQ values for adults across various vegetable samples from Farms 2, 3, and 4 during the high-flow season, highlighting the potential health risks associated with exposure to multiple PTEs. The data reveals a distinct pattern, with Cr standing out as the most significant contributor to the overall HQ, particularly in specific farm samples. At Farm 2, the sample F2S3-Pk exhibits the highest HQ for Cr, exceeding 20, which indicates a substantial health risk. Other Farm 2 samples, such as F2S1-S and F2S2-BeL, also showed the elevated HQ values for Cr, though they are considerably lower than the content in F2S3-Pk. These findings suggest that Cr contamination is a critical concern in Farm 2 during the high-flow season, requiring immediate attention to mitigate potential health impacts on adults consuming these vegetables.

In Farm 3, the HQ values for Cr are also prominent, particularly in samples F3S3-Co and F3S1-S, where the HQ values are notably higher compared to other PTEs. This trend is consistent across the farm, indicating that Cr is a pervasive contaminant in this area, contributing significantly to the overall risk. Farm 4 continues this pattern, with samples F4S1-Co and F4S2-S showing elevated HQ values for Cr, further underscoring the widespread issue of Cr contamination across these farms. The HQ for other PTEs, such as V, Ni, Cu, As, Cd, Hg, and Pb, remains relatively low across all farms, indicating that Cr is the primary driver of health risks during the high-flow season.

Overall, the results highlight Cr as the most significant concern across Farms 2, 3, and 4 during the high-flow season, with HQ values exceeding safe thresholds in several samples. This underscores the need for targeted interventions, such as soil and water remediation, to address Cr contamination and reduce the associated health risks for adults consuming vegetables from these farms.

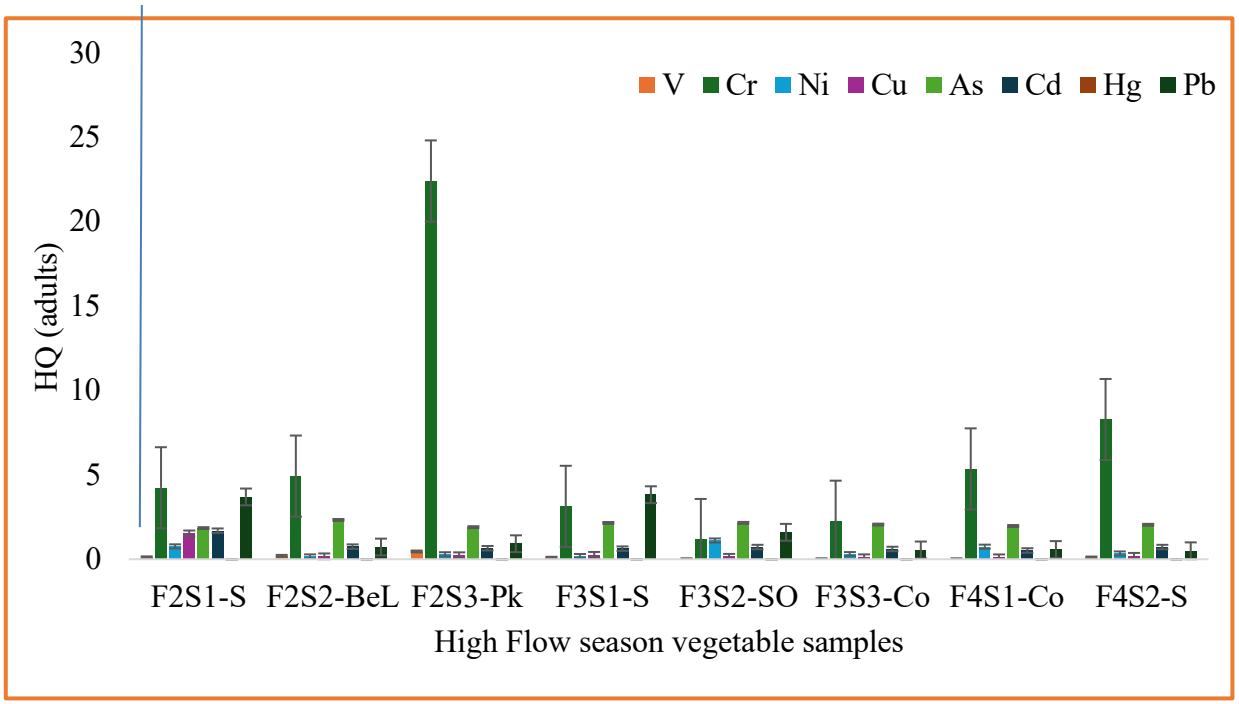

Figure 3.47. The HQ assessment of vegetables obtained from farms 2–4 for adults.

The analysis of HQ values for children during the high-flow season across various farm samples revealed significant health risks associated with exposure to multiple PTEs as shown by Figure 3.48. Notably, Cr exhibits the highest HQ values across several samples, indicating a substantial risk for children. For instance, in the F2S3-Pk sample from Farm 2, the HQ for Cr reaches an alarming value of 106 far exceeding safe thresholds and highlighting a severe health concern. Other Farm 2 samples,

such as F2S1-S and F2S2-BeL, also show elevated Cr HQ values of 20.1 and 23.3, respectively, further emphasizing the widespread Cr contamination in this area during the high-flow season.

In addition to Cr, other PTEs such as Pb and As also contribute significantly to the overall HQ in children. The F3S1-S sample from Farm 3, for instance, shows a high HQ for Pb at 18.1, alongside considerable HQ values for As at 10.2. This pattern suggests that both Pb and As are critical contributors to health risks for children consuming vegetables from this farm. Similarly, the F2S1-S sample from Farm 2 exhibits a high HQ for Pb at 17.5, combined with a notable HQ for As at 8.73, indicating a dual threat from these contaminants.

Farm 4 samples, such as F4S1-Co and F4S2-S, continue this trend, with Cr again emerging as a dominant contaminant, showing HQ values of 25.3 and 39.2, respectively. These findings underscore the pervasive issue of Cr contamination across the farms during the high-flow season. While other elements such as Ni, Cu, Cd, and Hg are also present in the samples, their HQ values are generally lower, suggesting that they pose a relatively lower risk compared to Cr, Pb, and As.

Overall, the results indicated that Cr, Pb, and As are the primary contributors to health risks in children during the high-flow season, with HQ values in several samples exceeding safe levels. This underscores the need for urgent remediation efforts to reduce the presence of these contaminants in the environment and mitigate the associated health risks for children. The current study aligned with the results obtained by Dikotla and Ambushe, (2024) & Dintsi et al. (2023), who reported the elevated HQ for the adult and child population during high flow seasons.

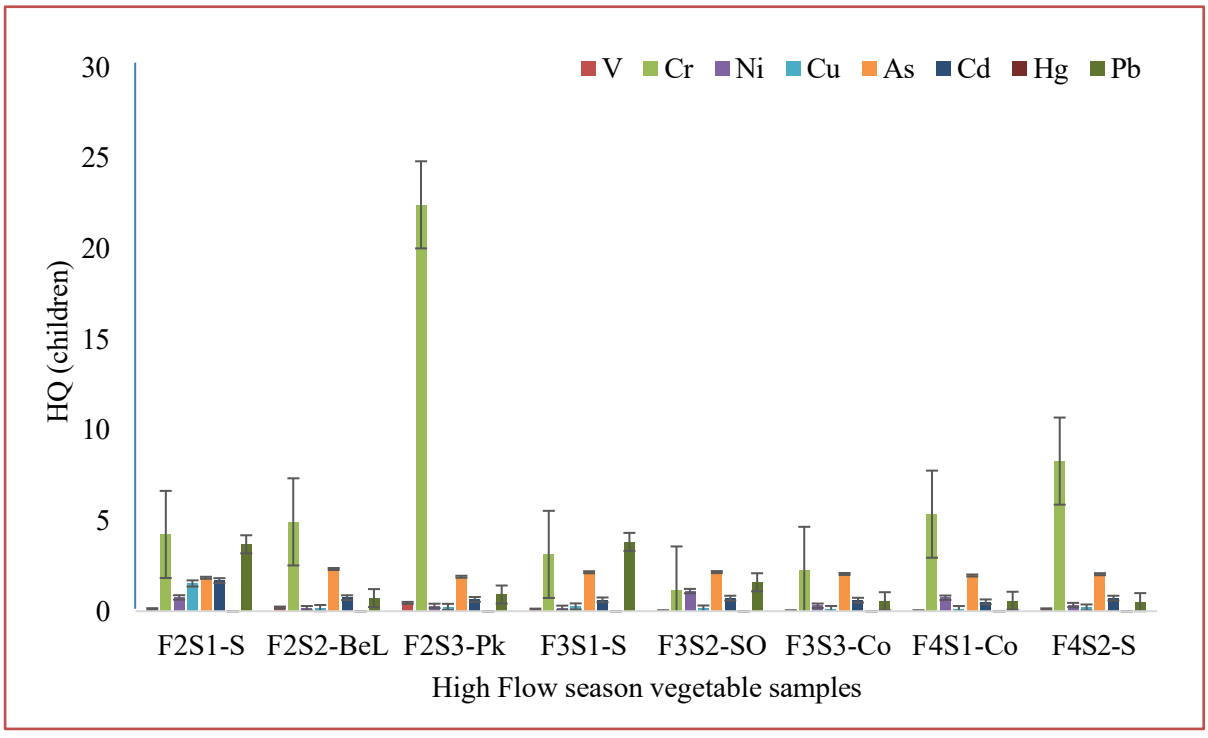

Figure 3.48. The HQ assessment of vegetables obtained from farms 2–4 for children.

Figure 3.49 illustrates that the HI values for both adults and children during the high-flow season demonstrate a notable difference in potential health risks across the various sites, with children consistently facing higher risks compared to adults. The HI values indicate that the cumulative exposure to PTEs is significantly above safe levels, particularly for children, across all the studied locations. At

Farm 2, Site 3 (F2S3-Pk), the highest HI values were recorded, with children showing a striking HI of approximately 127, which is nearly five times higher than the adult HI value for 26.9. This suggests a severe risk of adverse health effects for children in this area, likely due to elevated concentrations of PTEs, which demand urgent attention.

Farm 2, Site 1 (F2S1-S) and Farm 4, Site 2 (F4S2-S**)** also exhibited elevated HI values for children, with values of approximately 65.6 and 57.7, respectively. These figures indicate that children in these areas are at substantial risk, likely due to a combination of various PTEs, as reflected by the high cumulative HI. Adults in these areas, while facing lower risks, still present HI values of 13.9 and 12.2, respectively, indicating that even the adult population is not immune to potential health impacts. Sites such as Farm 3, site 1 (F3S1-S) and Farm 2, site 2 (F2S2-BeL) follow a similar pattern, with children's HI values of approximately 48.6 and 43.9, respectively, highlighting a moderate to high risk in these locations. Adults at these sites also showed elevated HI values, although less pronounced than in children. Lower, yet still concerning, HI values were observed at Farm 3, site 2 (F3S2-SO) and Farm 3, site 3 (F3S3-Co), where children's HI values were about 32.7 and 27.9, respectively. These values indicate that while the risk is comparatively lower than at other sites, the cumulative exposure to PTEs remains a significant health concern for children.

Overall, the data suggests that the health risks associated with exposure to PTEs during the high-flow season are considerably higher for children across all sites, with several locations showing HI values well above safe thresholds. This necessitates targeted interventions to reduce exposure, particularly in the most affected areas, to protect vulnerable populations from long-term health consequences.

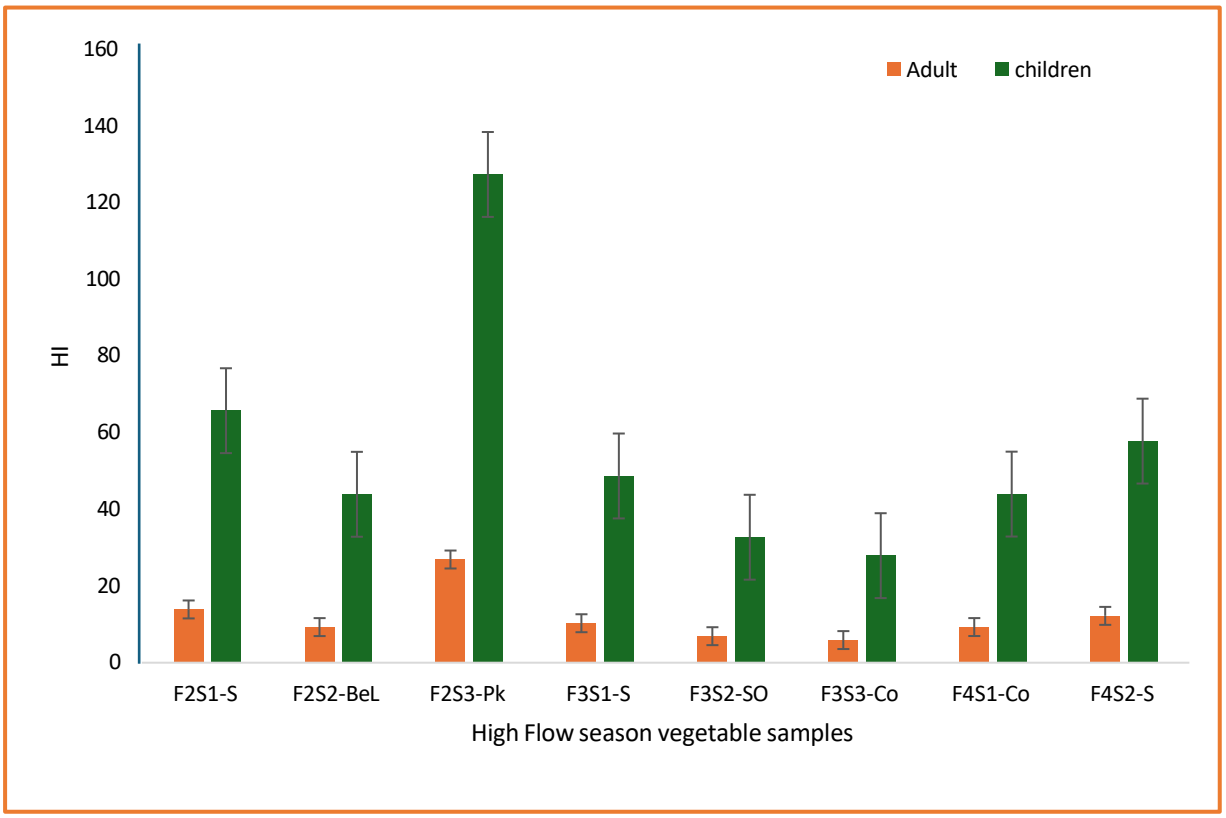

Figure 3.49. The HI assessment of vegetables obtained from farm 2–4 for adults and children.

The current study HQ and HI for children and adults' population showed a significant decrease from low- to high-flow season, but the study by Dintsi et al. (2023) in vegetable samples during high flow showed an increase in HQ and HI during high-flow than low-flow season.

3.15 SPECIATION ANALYSIS METHOD

Retention time identification for each species and evaluation of analytical figures of merit were conducted as reported by Letsoalo et al. (2018) and Letsoalo et al. (2021). The R^2 values greater than 0.999 obtained for calibration curves constructed for different species quantification indicate a high degree of correlation between the concentrations of the species and the peak area (King, 2016). The LODs and LOQs obtained using reagent blanks were comparable to other reported studies, which shows that the method employed is sensitive. The LODs of higher than those observed in this study for Cr(VI) have been reported (Mattusch et al., 2000; Leśniewska et al., 2017). The accuracy of the speciation method was assessed using a spiking-and-recovery procedure due to the lack of SRMs that contain certified concentrations of As and Cr species. The accuracy of the speciation analysis method was confirmed by determining acceptable percentage recoveries, which were in the range from 91.9 to 114% and 85.3 to 113% when spiked with 3 and 20x LOQ concentrations, respectively (US EPA, 2011). The %RSD values of 00603 to 12.4% for the speciation analysis procedure showed high repeatability and reliability of the method (Tiwari & Tiwari, 2010). Analytical figures of merit for the speciation method are presented in Table 3.18.

Table 3.18. LOD, LOQ and percentage recoveries for soil, vegetable spiked at 3× and 20× LOQ

Sample	Analyte	LOD (ng/g)	LOQ (ng/g)	Measured concentration at 3 × LOQ (ng/g)	Measured concentration at 20 × LOQ (ng/g)	Percentage recovery (3 × LOQ) (%)	Percentage recovery (20 × LOQ) (%)
	As(III)	0.161	0.537	26.3 ± 0.90	30.4 ± 3.3	99.2	85.3
	DMA	0.453	1.51	237 ± 22	245 ± 28	103	95.5
	MMA	0.343	1.14	109 ± 9.2	116 ± 3.0	114	101
	As(V)	1.59	5.30	188 ± 8.5	241 ± 18	108	91.6
Soil	Cr(VI)	0.670	2.23	120 ± 7.5	177 ± 16	98.1	110
	As(III)	0.152	0.507	67.7 ± 3.2	64.2 ± 6.1	103	87.8
	DMA	0.0932	0.311	66.2 ± 4.9	66.8 ± 5.6	104	98.0
	MMA	1.35	4.50	55.4 ± 5.3	129 ± 8.3	97.6	104
	As(V)	0.458	1.53	117 ± 10	123 ± 6.9	109	94.1
Vegetable	Cr(VI)	0.598	1.99	1030 ± 74	1130 ± 47	105	113

3.16 SPECIES IDENTIFICATION AND CORRECTION OF POLYATOMIC INTERFERENCES

The retention time is a qualitative analysis parameter and is recorded at the apex of a chromatographic peak (Moldoveanu & David, 2013; Robards & Ryan, 2022). Single analyte standards were used in order to identify the retention time of each analyte, and then a mixture of standards was used to correlate retention time with the identified species in a single analytical run. The resulting chromatogram of the individual species of As and Cr is presented in Figure 3.50. Detection of As and Cr species in environmental samples can be interfered with by the presence of high concentrations of Cl, resulting in polyatomic ion interferences of $Ar^{40}Cl^{35}$ on ^{75}As and $O^{16}Cl^{37}$ on ^{53}Cr. Polyatomic ion interferences were identified overlapping with MMA, As(V), and Cr(VI). Interference at MMA, As(V) and Cr(VI) peaks affected by Cl^- content were corrected daily prior to analysis as recommended by Letsoalo *et al.* (2020) and Low *et al*. (1986). Elimination of these interferences was achieved through an inter-elemental procedure using mathematical correction expressions (Letsoalo *et al*., 2021). In this procedure, a correction factor (CF) for species affected by polyatomic ions interference is determined as the ratio of signal intensity of the interference peak at analyte mass to its signal intensity at the interference-free m/z and is formulated as:

$$CCCC = \frac{sssssssaaaa\ ssssiiiissssssiiii\ oooo\ ssssooiiaaiissii\ ssoossss\ aaii\ aassaaaaiiiiii\ mm/zz}{sssssssaaaa\ ssssiiiissssssiiii\ oooo\ ssssiiiiiiooiiiiiissiiii\ ooiiiiii\ ssooss\ aaii\ ssiiss\ mm/zz} \qquad \textbf{Equation 3}$$

Once the correction factor has been determined, correction of the signals of analytes was carried out using the following equation:

$$IIoorrrrrWWCCttWWCC\ ssssWWCCWWWWss\ rrrrWWrr = HH - (BB \times IICC) \qquad \text{Equation 4}$$

Where A is the measured species area,

B = area of interfering ion (Letsoalo *et al*., 2021).

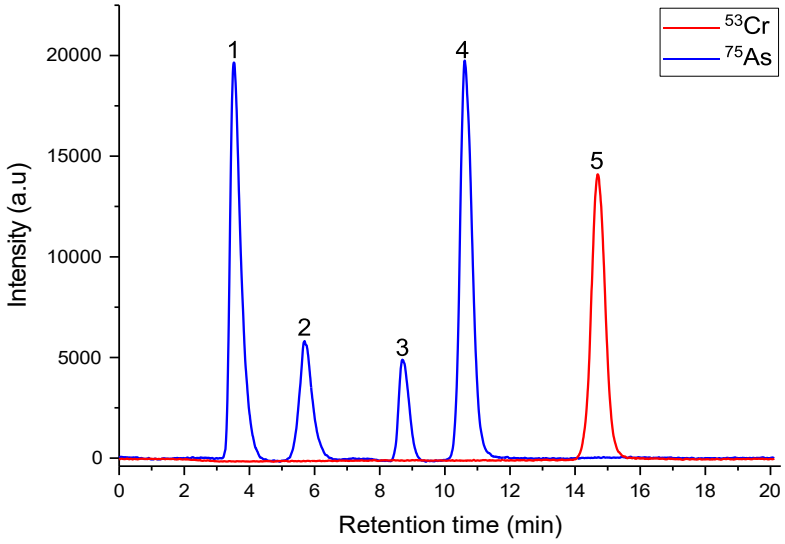

Figure 3.50. Chromatogram showing the separation and retention times of As and Cr species from a 20 µg/L multi-species standard. The peaks and retention times were identified: (1)- As(III)-3.5 min; (2)- DMA-5.7 min; (3)-MMA-8.7-min; (4)-As(V)-10.6 min, and (5)-Cr(VI)-14.7 min.

3.17 SPECIATION ANALYSIS OF As AND Cr IN SOIL SAMPLES

Speciation analysis of As and Cr species in soil samples is presented in Tables 3.19 and 3.20. In the high flow season, the site with high levels of As and Cr species was F1S3 with 3960, 20600, 3110, 4850, 3000 and 30500 ng/g for As(III), DMA, MMA, As(V), Cr(VI) and Cr(III), respectively. The most dominant species among the six was Cr(III). Amongst the As species, DMA displayed a higher average concentration in both seasons of study, which suggests the presence of anaerobic bacteria. The bacteria convert the more toxic species (As(III) and As(V)) into less toxic species such as DMA. This process normally occurs in soil chemically and biologically and is known as As volatilization (Kumar & Gopal, 2015; Kamal & Miah, 2021). The accumulation of DMA and MMA in soil could be attributed to the past use of methylated As compounds and DMA and MMA sodium salts as pesticides (Kamal & Miah, 2021). High concentrations of As(III) in site F1S1 (2010 ng/g) and F2S1 (3960 ng/g) indicate reducing soil environments that favour As(III) presence. The reducing environments promote increased solubility, toxicity and mobility of As(III) than As(V) (Kamal & Miah, 2021). In the low flow season, As(V) dominates sites such as F1S1 (1130 ng/g), F1S2 (2570 ng/g) and F2S2 (3570 ng/g), while it predominates in F1S2 (1190 ng/g in high flow), which shows the soil conditions are aerobic and favours As(V) presence (Moreno-Jiménez *et al*., 2012). The overall trend of species amongst both seasons is observed as MMA < As(III) < As(V) < DMA and As(III) < MMA < DMA < As(V) in the high and low flow seasons, respectively. Unfortunately, no recommended soil quality guidelines are available for As species in soil. The seasonal variation was found to be insignificant as $p > 0.05$ for As(III) ($p=0.342$), DMA ($p=0.691$), MMA ($p=0.906$), and As(V) ($p=0.797$).

During Cr speciation studies, Cr(III) was 100% dominating in the high flow and 75% dominating in the low flow season. Similar observations were noted in South African studies, where Cr(III) was recorded

at higher levels than Cr(VI) in soil (Owolabi *et al*., 2016). Often, high Cr(III) levels are observed in soil sites with microbial organisms that can result in the bio-reduction of Cr(VI) directly. The indirect reduction can also occur in the presence of metabolites from bacteria, which results in Cr immobilisation in soil and thus the high concentrations (Xiao *et al*., 2012). With the proximity of power stations in the Lephalale areas, emissions from coal-fuelled power stations are reported to be major contributors of Cr species to the atmosphere, which ultimately ends up being deposited in the soil of the area. In another study, Cr(VI) in particular was observed to surpass the regional background in air, and these were released through combustion (Venter *et al*., 2016). The soil quality guideline value for Cr(VI) in agricultural land use set by the Ontario Ministry of Environment (OME) is 660 ng/g[54]. In the high flow season, this value was exceeded only in F1S2 and F1S3, while in the low flow season, the value was exceeded in all sites. At a 95% confidence level, the seasonal statistical variation of Cr(VI) ($p=0.387$)and Cr(III) ($p=0.597$) was insignificant as $p > 0.05$.

Table 3.19. Concentrations of As(III), DMA, MMA, As(V), Cr(VI) and Cr(III) recorded in soil during the high flow season.

Soil	As(III) (ng/g)	DMA (ng/g)	MMA (ng/g)	As(V) (ng/g)	Cr(VI) (ng/g)	Cr (III) (ng/g)
F1S1	2010 ± 197	1.79 ± 0.15	<0.343	868 ± 69	235 ± 15	2740 ± 250
F1S2	241 ± 19	348 ± 25	1200 ± 20	1190 ± 100	2120 ± 170	949 ± 77
F1S3	3960 ± 240	20600 ± 530	3110 ± 150	4850 ± 350	3000 ± 170	30500 ± 1800
F1S4	24.9 ± 1.3	226 ± 20	92.0 ± 8.4	158 ± 0.30	116 ± 10	385 ± 33
F2S1	359 ± 22	<0.453	71.4 ± 0.13	<1.59	236 ± 22	284 ± 26
F2S2	1.51 ± 0.088	43.4 ± 0.62	0.471 ± 0.053	<1.59	11.2 ± 0.99	34.1 ± 3.0

Table 3.20 Concentrations of As(III), DMA, MMA, As(V), Cr(VI) and Cr(III) recorded in soil during the low flow season.

Soil	As(III) (ng/g)	DMA (ng/g)	MMA (ng/g)	As(V) (ng/g)	Cr(VI) (ng/g)	Cr (III) (ng/g)
F1S1	373 ± 16	860 ± 18	438 ± 12	1130 ± 43	2260 ± 47	635 ± 13
F1S2	452 ± 46	2560 ± 220	1070 ± 59	2570 ± 190	2200 ± 73	4540 ± 14
F2S1	<0.161	6550 ± 360	1160 ± 65	1330 ± 160	2890 ± 120	6150 ± 250
F2S2	1600 ± 71	2490 ± 150	1390 ± 140	3570 ± 120	2370 ± 59	6770 ± 170

3.18 SPECIATION ANALYSIS OF AS AND CR IN VEGETABLES

Vegetable sample analysis was done in triplicate and summarised in Tables 3.21 and 3.22 for the high and low flow seasons, respectively. The recorded concentrations in the high flow season ranged from 1.55 to 189 ng/g, 40.1 to 153 ng/g, 9.38 to 292 ng/g, 0.91 to 262 ng/g for As(III), DMA, MMA and As(V), respectively. In the low flow season, concentration ranged from 7.03 to 52.9 ng/g, 0.338 to 30.3 ng/g, 2.48 to 15.7 ng/g and 0.72 to 27.8 ng/g for As(III), DMA, MMA and As(V), respectively. These concentration ranges are lower than those observed in the high-flow season. The observed concentrations are higher than those obtained in other studies (Laizu, 2008). Vegetables use various mechanisms to uptake As. These include the absorption of As(V) from soil to plant *via* the high-affinity PO_4^{3-} transporter through the phosphate transport pathway. The other mechanisms involve the absorption of As(III), DMA and MMA through the aquaporin channels, which is proposed to be another pathway of absorption (Kamal & Miah, 2021). Overall, in this study, the most dominating species of As was As(III), followed by As(V), while DMA and MMA were the least dominating. This raises quite a concern as it is known that As(III) and As(V) are classified as carcinogens in humans, and these species account for 60% and 78% of As species, respectively (Signes-Pastor *et al*., 2008). Unfortunately, MPLs of As species in vegetables have not yet been established (EFSA, 2009). Statistical analysis revealed significant seasonal variations for DMA (p=0284), MMA (p=0.0322), and As(V) (p=0.0347), while insignificant variation was observed in As(III) (p=0.0789).

Table 3.21. Concentrations of As(III), DMA, MMA, As(V), Cr(VI), and Cr(III) recorded during the high flow season in vegetable samples.

Vegetable	As(III) (ng/g)	DMA (ng/g)	MMA (ng/g)	As(V) (ng/g)	Cr(VI) (ng/g)	Cr (III) (ng/g)
F1S1-S	63.0 ± 5.8	62.0 ± 0.52	34.3 ± 0.19	99.8 ± 6.7	963 ± 57	15000 ± 840
F1S2-C	25.6 ± 0.65	40.1 ± 3.1	35.3 ± 0.73	8.97 ± 0.51	722 ± 62	3820 ± 330
F1S2-P	67.5 ± 6.5	<0.0932	34.3 ± 0.87	92.3 ± 4.1	602 ± 19	7780 ± 250
F1S2-S	49.1 ± 2.5	<0.0932	61.3 ± 6.6	262 ± 6.7	1090 ± 55	10200 ± 520
F1S3-C	189 ± 4.3	131 ± 6.8	292 ± 3.6	48.9 ± 4.2	731 ± 24	1850 ± 60
F1S3-S	160 ± 11	<0.0932	70.7 ± 8.7	95.7 ± 4.5	764 ± 40	5930 ± 310
F1S4-T	100 ± 1.4	119 ± 6.1	107 ± 3.5	1.05 ± 0.090	956 ± 40	17400 ± 740
F2S1-C	16.1 ± 1.5	53.4 ± 3.1	9.48 ± 0.36	<0.458	1060 ± 87	1960 ± 120
F2S1-S	502 ± 31	<0.0932	<1.35	81.3 ± 3.5	1180 ± 97	9220 ± 480
F2S2-C	1.55 ± 0.15	<0.0932	31.7 ± 0.24	0.91 ± 0.070	594 ± 18	1850 ± 55
F2S2-S	54.7 ± 1.2	153 ± 0.095	27.7 ± 1.8	12.1 ± 0.91	962 ± 88	11100 ± 1000

The concentration ranges of 594 to 1180 ng/g (Cr(VI)) and 1850 to 17400 ng/g (Cr(III)) were recorded in the high-flow season, whereas ranges of 197 to 687 ng/g (Cr(VI)) and 374 to 3540 ng/g (Cr(III)) were recorded during the low flow season in vegetables. Higher Cr concentrations are observed with the less toxic Cr(III), and Cr(VI) only accounts for 10% and 27% overall during both sampling seasons, which is still substantially high in vegetables. It is suggested that high Cr(III) observed is due to its solubility, making it highly mobile during its absorption by the vegetables (Gezahegn *et al*., 2021). Although Cr(III) is a crucial nutrient required for normal energy metabolism, high levels of it in children can lead to long-term adverse health effects (Wilbur *et al*., 2012). As with As, MPLs of Cr species in vegetables have not yet been set (Benford *et al*., 2014). Statistical variation was seasonally significant for Cr(III) as $p < 0.05$, whereas for Cr(VI), the variation was not significant as $p > 0.05$ at 95% confidence level.

Table 3.22. Concentrations of As(III), DMA, MMA, As(V), Cr(VI), and Cr(III) recorded during the low flow season in vegetable samples.

Vegetables	As(III) (ng/g)	DMA (ng/g)	MMA (ng/g)	As(V) (ng/g)	Cr(VI) (ng/g)	Cr (III) (ng/g)
F1S1-C	41.8 ± 2.1	0.338 ± 0.032	<1.35	0.870 ± 0.087	197 ± 13	1690 ± 110
F1S1-M	52.9 ± 2.6	6.17 ± 0.57	<1.35	27.8 ± 0.99	687 ± 8.7	2590 ± 33
F1S1-O	34.0 ± 1.5	<0.0932	15.7 ± 0.36	19.9 ± 1.1	603 ± 23	1550 ± 58
F1S1-S	7.83 ± 0.62	7.47 ± 0.55	2.48 ± 0.096	0.720 ± 0.045	668 ± 22	652 ± 22
F1S2-C	28.1 ± 2.7	6.54 ± 0.097	5.42 ± 0.075	4.28 ± 0.071	566 ± 38	1790 ± 100
F1S2-M	37.8 ± 1.6	30.3 ± 2.9	3.66 ± 0.23	6.86 ± 0.40	608 ± 18	3540 ± 110
F2S1-C	31.5 ± 1.7	1.38 ± 0.091	4.89 ± 0.24	1.45 ± 0.12	517 ± 9.3	483 ± 8.6
F2S1-S	8.60 ± 0.30	3.85 ± 0.19	3.74 ± 0.34	2.40 ± 0.062	585 ± 8.7	1240 ± 18
F2S2-C	7.03 ± 0.44	<0.0932	6.97 ± 0.00042	2.20 ± 0.13	646 ± 31	374 ± 18
F2S2-O	13.8 ± 1.0	<0.0932	<1.35	3.29 ± 0.20	500 ± 28	1750 ± 98
F2S2-S	28.6 ± 0.86	1.09 ± 0.054	3.55 ± 0.20	5.30 ± 0.31	579 ± 8.7	931 ± 51

3.19 CARCINOGENIC EFFECTS BASED ON As(III), As(V) AND Cr(VI)

Speciation analysis is conducted to determine the toxicity/ carcinogenicity because the total concentration yielded insufficient information for health risk assessments. This is due to certain species of PTEs being more toxic than others, which cannot be accurately determined from total concentration studies (Tchounwou *et al*., 2012). Therefore, evaluation of carcinogenic effects was based on results obtained from speciation studies of As(III), As(V) and Cr(VI). Consumption of a vegetable leads to

carcinogenic risks if the threshold ILCR is greater than 10^{-4}. The acceptable ICLR ranged from 10^{-6} to 10^{-4}, and an ICLR value less than 10^{-6} denotes that cancer risks are negligible. The obtained results are presented in Tables 3.23 and 3.24.

Table 3.23. The ILCR data obtained from the analysis of As(III), As(V) and Cr(VI) during the high flow season.

	As(III)		As(V)		Cr(VI)	
	Adults	Children	Adults	Children	Adults	Children
Vegetable	ILCR					
F1S1-S	1.59×10^{-4}	7.53×10^{-4}	2.52×10^{-4}	1.19×10^{-3}	2.43×10^{-3}	1.15×10^{-2}
F1S2-C	6.48×10^{-5}	3.06×10^{-4}	2.27×10^{-5}	1.07×10^{-4}	1.83×10^{-3}	8.64×10^{-3}
F1S2-P	1.71×10^{-4}	8.07×10^{-4}	2.33×10^{-4}	1.10×10^{-3}	1.52×10^{-3}	7.20×10^{-3}
F1S2-S	1.24×10^{-4}	5.87×10^{-4}	6.61×10^{-4}	3.13×10^{-3}	2.75×10^{-3}	1.30×10^{-2}
F1S3-C	4.78×10^{-4}	2.26×10^{-3}	1.24×10^{-4}	5.84×10^{-4}	1.85×10^{-3}	8.75×10^{-3}
F1S3-S	4.04×10^{-4}	1.91×10^{-3}	2.42×10^{-4}	1.14×10^{-3}	1.93×10^{-3}	9.14×10^{-3}
F1S4-T	2.53×10^{-4}	1.20×10^{-3}	2.65×10^{-6}	1.25×10^{-5}	2.42×10^{-3}	1.14×10^{-2}
F2S1-C	4.07×10^{-5}	1.93×10^{-4}	N/A*	N/A*	2.67×10^{-3}	1.26×10^{-2}
F2S1-S	1.27×10^{-3}	6.01×10^{-3}	2.05×10^{-4}	9.72×10^{-4}	2.97×10^{-3}	1.41×10^{-2}
F2S2-C	3.92×10^{-6}	1.85×10^{-5}	2.31×10^{-6}	1.09×10^{-5}	1.50×10^{-3}	7.11×10^{-2}
F2S2-S	1.38×10^{-4}	6.54×10^{-4}	3.07×10^{-5}	1.45×10^{-4}	2.43×10^{-3}	1.15×10^{-2}

In the high-flow season, it was observed that most of the vegetable samples surpassed the recommended threshold risk limit of 1×10^{-4}. This was not the case for F1S2 C (adults: As(III) & As(V)), F1S4 T (adults and children: As(V)), F2S2-C (adults and children: (As(III) and As(V)) and F2S2 (adults: As(V)) as the observed cancer risk value was below the limit indicating that these individual species would have lower chances of cancer risks. Amongst the three species, Cr(VI) displayed a higher cancer

risk in the vegetables. The overall cancer risk associated with consuming these vegetables indicates that all these vegetables have a high chance of cancer risk. In adults, the overall cancer risk ranged from 1.91×10^{-3} to 3.54×10^{-3} in farm 1, whereas it ranged from 1.51×10^{-3} to 4.45×10^{-3} in farm 2. This means that an excess of 191 to 354 cancer cases per 100000 adult exposures would occur in farm 1, and 151 to 445 cancer cases per 100000 adult exposures would occur. In children, the 167 cancer cases and 211 cancer cases per 10000 children exposure would occur if the vegetable with the highest ILCR (F1S2-S and F2S1-S) was consumed from farm 1 and farm 2.

Table 3.24. The ILCR data obtained from the analysis of As(III), As(V) and Cr(VI) during the low flow season.

	As(III)		As(V)		Cr(VI)	
	Adults	Children	Adults	Children	Adults	Children
Vegetables	ILCR					
F1S1-C	1.06×10^{-4}	5.00×10^{-4}	2.20×10^{-6}	1.04×10^{-5}	4.98×10^{-4}	7.47×10^{-4}
F1S1-M	1.34×10^{-4}	6.33×10^{-4}	7.03×10^{-5}	3.33×10^{-4}	1.74×10^{-3}	2.61×10^{-3}
F1S1-O	8.61×10^{-5}	4.07×10^{-4}	5.04×10^{-5}	2.38×10^{-4}	1.52×10^{-3}	2.29×10^{-3}
F1S1-S	1.98×10^{-5}	9.37×10^{-5}	1.82×10^{-6}	8.61×10^{-6}	1.69×10^{-3}	2.53×10^{-3}
F1S2-C	7.09×10^{-5}	3.36×10^{-4}	1.08×10^{-5}	5.12×10^{-5}	1.43×10^{-3}	2.15×10^{-3}
F1S2-M	9.56×10^{-5}	4.52×10^{-4}	1.74×10^{-5}	8.21×10^{-5}	1.54×10^{-3}	2.31×10^{-3}
F2S1-C	7.96×10^{-5}	3.77×10^{-4}	3.67×10^{-6}	1.74×10^{-5}	1.31×10^{-3}	1.96×10^{-3}
F2S1-S	2.18×10^{-5}	1.03×10^{-4}	6.07×10^{-6}	2.87×10^{-5}	1.48×10^{-3}	2.22×10^{-3}
F2S2-C	1.78×10^{-5}	8.40×10^{-5}	5.57×10^{-6}	2.64×10^{-5}	1.63×10^{-3}	2.45×10^{-3}
F2S2-O	3.49×10^{-5}	1.65×10^{-4}	8.32×10^{-6}	3.94×10^{-5}	1.26×10^{-3}	1.90×10^{-3}
F2S2-S	7.22×10^{-5}	3.42×10^{-4}	1.34×10^{-5}	6.35×10^{-5}	4.88×10^{-4}	2.44×10^{-4}

In the low-flow season, a decrease in the cancer risk was observed for adults, particularly with As(III) and As(V), as most samples had a cancer risk less than the threshold. Only F1S1-C and F1S1-M displayed a cancer risk exceeding the As(III) species threshold. Another decrease was observed in children consuming most vegetables containing As(V) species. Regarding As(III), a cancer risk below the threshold was recorded for F1S1-S and F2S2-C. Higher probabilities of cancer risks were observed

in adults and children consuming vegetable samples containing Cr(VI), which surpassed the recommended ILCR threshold. The risk of developing cancer trend upon consumption of the vegetable displayed: F2S2-S < F1S1-C < F2S2-O < F2S1-C < F2S1-S < F1S2-C < F1S2-M < F2S2-C < F1S1-O < F1S1-S < F1S1-M. Overall, F1S1-C recorded a high cancer risk of 97 cases per 50000 adults exposed and 357 cancer cases per 100000 children in farm 1. In farm 2, the 83 cases per 50000 adults exposed and 8 cancer cases per 50000 children exposed. Overall, all the vegetables, when consumed, lead to higher cancer cases observed, with the cancer risk in children being higher than that observed in adults. Amongst the two sampling seasons, more cancer risks were observed in the high-flow season than in the low-flow season. From the above data, consumption of these vegetables will result in greater cancer risks in children than in adults and is also observed in similar studies such as that of Bello *et al*. (2019) & Zhang *et al*. (2018). The Cr(VI) is the most dominant carcinogen, and its exposure and As species to the environment should be controlled to save the population from exposure and associated health risks (Sultana *et al*., 2017).

3.20 ION IMPRINTED POLYMERS BASED SENSORS METHOD

3.20.1 Material characterisation of graphenes and polymers

All synthesised materials were characterised and analysed by various analytical and spectroscopic techniques, including ICP-OES, ICP-MS, FTIR spectroscopy, PXRD, BET, SEM-EDS, TEM and Raman spectroscopy.

3.20.1.1 FTIR spectroscopy analysis

The FTIR spectroscopy was employed to analyse the surface properties of polymers and graphene to study surface modifications and confirm the formation of desired products. As seen from Figure 3.51a**, t**here are oxygen-containing functional groups such as O-H stretch (~3400 cm^{-1}) from adsorbed water (Mnyipika et al., 2021), C-O-C stretch (~1200-1300 cm^{-1}) of epoxy, C-O stretch (~1050-1100 cm^{-1}) related to alkoxy, carbonyl C=O stretch peak at ~1640 cm^{-1} are observed (Li, Xu, Chen, et al., 2024). These are to be more visible in GO due to oxidation and slightly reduced in rGO, indicating partial removal during the reduction process and restoration of the graphene lattice, as shown in the PXRD. All three spectra show the presence of a C=C stretch peak at **~**1493 cm^{-1} with varying intensities due to the aromatic sp^2 carbon framework. In GO, this peak is slightly diminished due to oxidation disrupting the conjugated structure, but it becomes more prominent in rGO as the sp^2 domains are restored during reduction (Eigler & Dimiev, 2016). The spectra for polymers (Figure 3.51b) show common peaks for the polymeric backbone, such as the O-H stretch (~3400 cm^{-1}), C-H stretch (~3000 cm^{-1}), C=O stretch (~1720 cm^{-1}), and C-O-C stretch (~1200-1300 cm^{-1}). As a reference material with no imprinting or ion complexation, NIP is similar in backbone (Kong et al., 2018) to IIP but lacks peaks associated with Cd(II) interactions (e.g., C=N at ~1400-1500 cm^{-1} and Cd-O (~950 cm^{-1}) (Hu et al., 2021). The

unleached Cd-IP shows peaks for Cd-O (~950 cm^{-1}) and stronger C=N (~1400-1500 cm^{-1}), confirming the presence of Cd(II) ions.

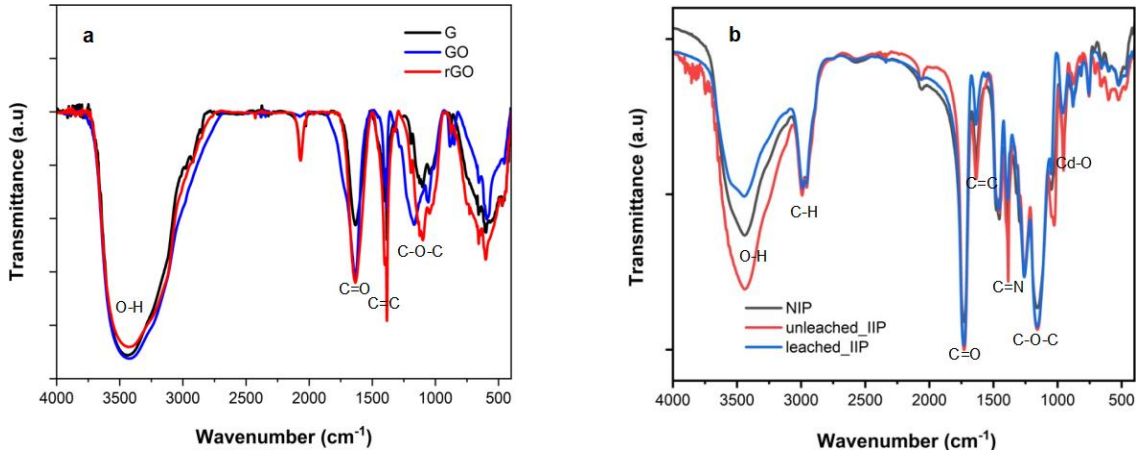

Figure 3.51. FTIR spectra of (a) G, GO and rGO, (b) imprinted and non-imprinted polymers.

Even though the leached Cd-IP retains slight traces of Cd(II)-related interactions, it exhibits reduced intensity for these peaks, indicating successful removal of Cd(II) ions during leaching. Thus, the FTIR spectra demonstrate how functional group changes correspond to chemical transformations, which are crucial for tailoring these materials' properties for sensor applications.

3.20.1.2 Raman Spectroscopy

Raman spectroscopy is essential for analysing carbon-based materials like G, GO and rGO. Figure 3.52a and b present spectra corresponding to these materials, with notable peaks labelled as D (~1350 cm^{-1}), G (~1580 cm^{-1}), and 2D (~2700 cm^{-1}). There is a sharp G-band and intense 2D-band seen in G to indicate a highly ordered graphitic structure with minimal defects, correlating to the results reported in the literature (Sivakumar et al., 2024). The D-band in G is weak or absent, confirming the absence of significant lattice defects. In GO, the D-band emerges strongly due to defects introduced by the oxidation process, such as oxygen-containing functional groups (e.g., hydroxyl and epoxy) (Haque & Wong, 2017). The G-band of GO broadens slightly to reflect a partial disruption of the sp^2 network, while the weakening of the 2D-band shows a loss of graphitic stacking. A higher D-band intensity is observed in rGO than in GO. This indicates increased defects during the reduction process, such as partial restoration of the sp^2 structure (Eigler & Dimiev, 2016) and remaining disordered regions, as seen from FTIR spectroscopy.

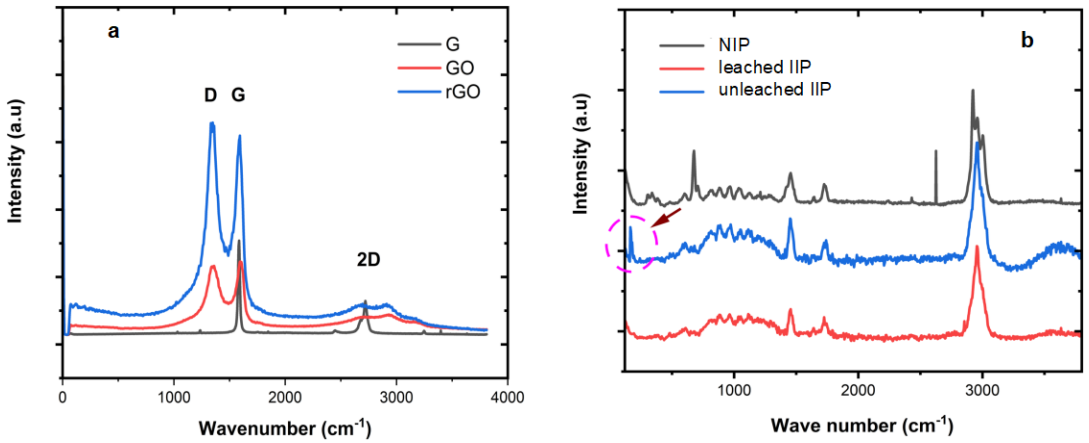

Figure 3.52. Raman spectra of (a) G, GO, rGO, (b) imprinted and non-imprinted polymers.

Structural rearrangement by removal of some oxygen-containing functional groups is seen as a slight shift in the G-band of rGO. Compared to G, the 2D band in rGO is b**r**oader**,** reflecting incomplete restoration of graphitic stacking. Increased I_D/I_G ratios from 0.95 in GO to 1.07 in rGO (higher than those reported elsewhere (Bhardiya et al., 2021; Sim et al., 2022) but lower than reported by Kim et al. (Kim et al., 2023)) and broadened 2D-band show that the reduction process leaves significant defects and disorder. The Cd-O band (~200 cm^{-1}) present in the unleached Cd-IP and absent in the NIP and leached IP confirms a successful incorporation of Cd(II) into the matrix polymer. Thus, these results are consistent with FTIR spectra and the expected changes in properties of G, GO and rGO during functionalisation and synthesis.

3.20.1.3 Powder XRD analysis

The PXRD patterns reveal distinct structural changes during the transformation from G to GO and rGO (Figure 3.53a). The pristine G exhibits a sharp, intense peak at ~26.6° (002) (Hassanpoor & Rouhi, 2021), indicating a highly ordered crystalline structure with regular interlayer spacing (0.172 nm). Additional peaks at higher angles of 004 and 006 planes confirm its well-defined crystalline nature. Upon oxidation to GO, the characteristic G peak shifts to a lower angle (~9.05°), demonstrating significant expansion of the interlayer spacing (0.488 nm) due to the intercalation of oxygen-containing functional groups (Hu et al., 2021). This peak's broader and less intense nature suggests reduced crystallinity and a more disordered structure.

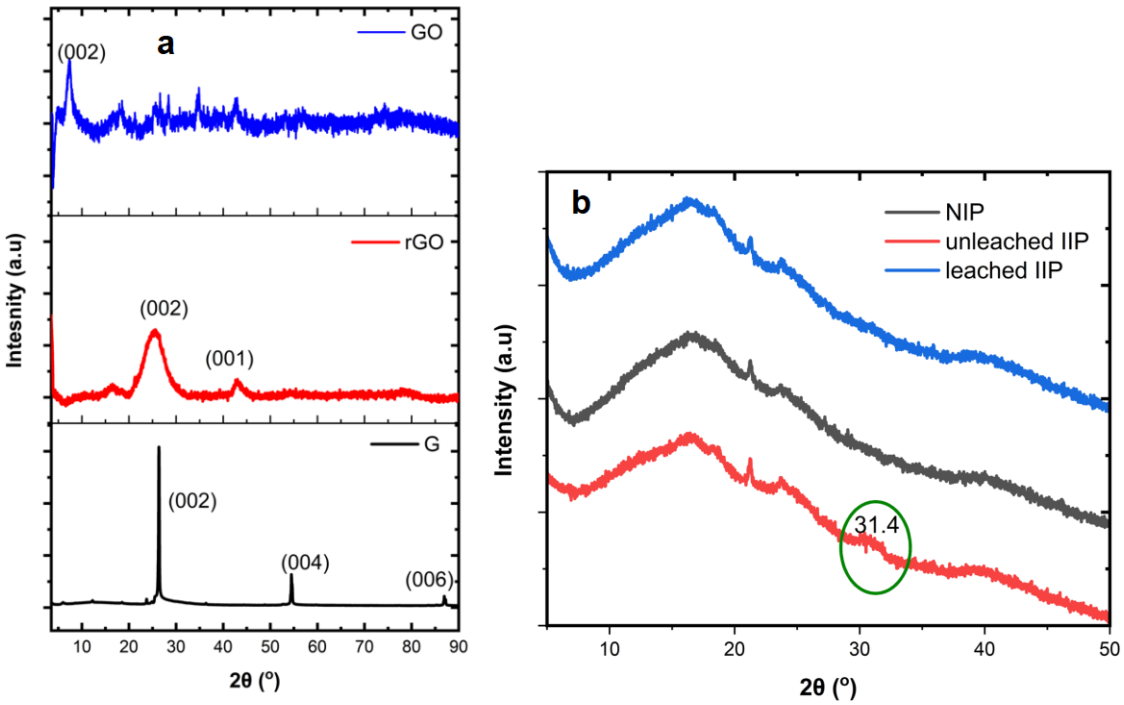

Figure 3.53. PXRD spectra of (a) G, GO and rGO, (b) imprinted and non-imprinted polymers.

The rGO pattern shows a broad, low-intensity peak at ~24.6° (002), positioned between the GO and G peaks (Viprya et al., 2023). This agrees with FTIR and Raman spectroscopy results, indicating partial yet almost complete restoration of the graphitic structure and interlayer spacing (0.1857 nm) during reduction, though the broadness of the peak reveals that the material retains some disorder and does not fully recover the original crystalline organisation of G. The above outcome agrees with the published literature (Bhardiya et al., 2021; Hassanpoor & Rouhi, 2021; Hu et al., 2021; Letsoalo et al., 2021; Mnyipika et al., 2021). A weak turbostratic peak ~42.6° (011) confirms the incomplete reduction process in rGO with better electrical properties (Viprya et al., 2023) as seen from the FTIR spectra. The leached and unleached IIPs and NIP (Figure 3.53b) differ from the presence and absence of the Cd peak appearing at ~31.4° (Letsoalo et al., 2021).

3.20.1.4 Brunauer-Emmett−Teller analysis

The BET isotherms of unleached and leached Cd(II) imprinted polymers (IPs) exhibit Type IV isotherms with H3 hysteresis loops, characteristic of mesoporous materials (Alberoni et al., 2021), as shown in Figure 3.54. The unleached polymer demonstrated a higher nitrogen adsorption capacity (~500 cm^3/g STP) and larger pore size (17 nm) compared to the leached polymer (~350 cm^3/g STP, 14 nm), indicating a higher total pore volume and more complex pore network.

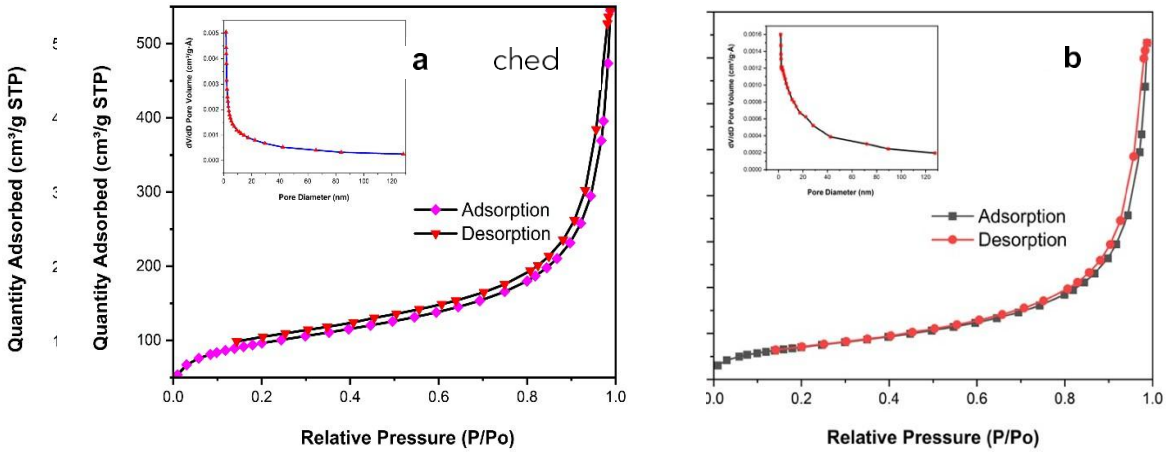

Figure 3.54. BET isotherms of (a) unleashed and (b) leached imprinted polymers.

Upon leaching, the BET surface area increased from 130 m²/g to 329 m²/g, significantly higher than the 79.3 and 106 m²/g reported by Letsoalo et al (Letsoalo et al., 2021) and a 270.4 m²/g (Fattahi et al., 2021) but less than the 546.3 m^2/g from Cao et al (Cao et al., 2021) due to their material's smaller pore size (2.07 nm). The pore size distribution became more uniform, reflecting structural changes due to template ion removal (Kong et al., 2018). Both polymers displayed steep adsorption at high relative pressures (P/Po > 0.9), suggesting macropores or interparticle voids, with minor micropore contributions at low pressures (P/Po < 0.1) (Cheng et al., 2017). These transformations highlight the critical role of the leaching process in modifying porosity and enhancing the polymer's ion recognition and binding capabilities.

3.20.1.5 SEM-EDS analysis

The SEM and EDS analyses provide comprehensive insights into the elemental composition and morphological characteristics of the IIPs before and after the leaching process. The EDS spectrum (Figure 3.55a) of the unleached polymer shows a prominent peak corresponding to Cd, which disappeared after leaching (Figure 3.55b), confirming a successful removal of the template Cd(II) ions (Wang et al., 2020) during the leaching process, creating specific recognition cavities in the polymer matrix. These results support the ICP-MS analyses where <0.08 μg/L of Cd was detected in the solution after seven cycles of 24 h leaching. The SEM micrographs reveal distinct morphological differences between the three polymer variants. The NIP (Figure 3.55c) displays a relatively smooth, layered structure with some surface irregularities (Li, Xu, Li, et al., 2024) in contrast to the leached Cd-IP (Figure 3.55e**),** which exhibits a more rough morphology with an uneven geometric surface, suggesting the formation of specific binding cavities after template removal (Xiao et al., 2021).

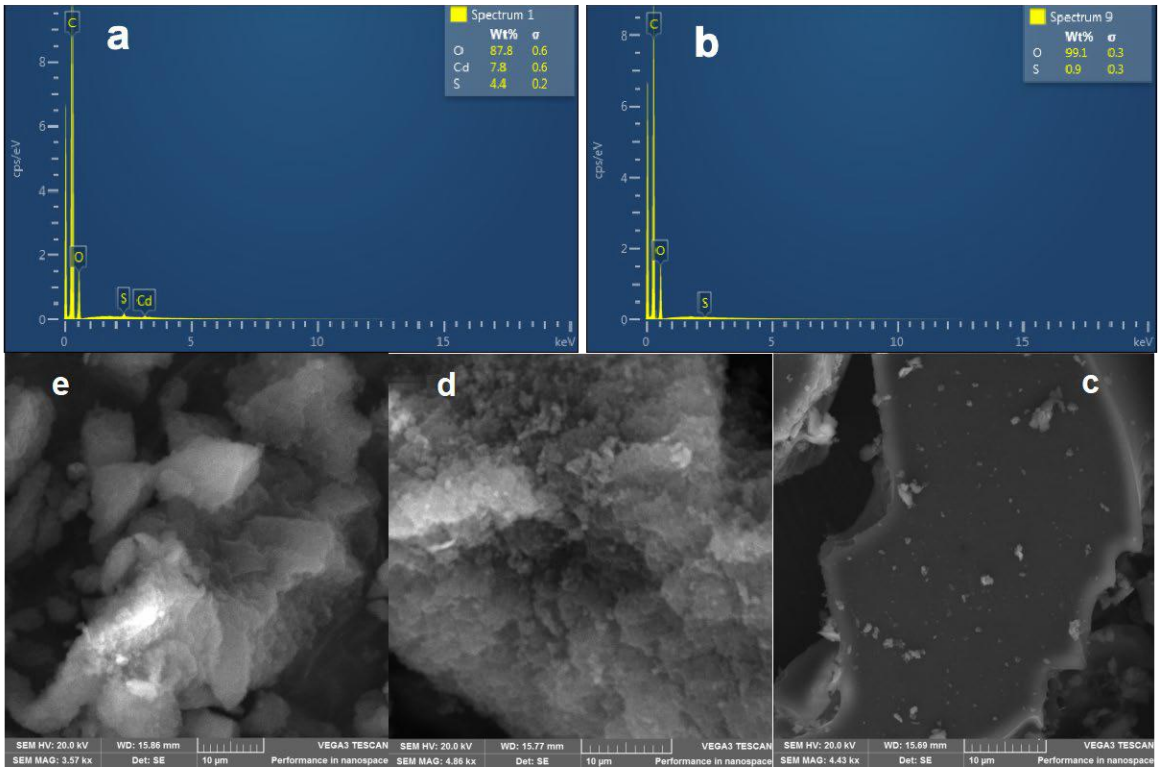

Figure 3.55. EDS spectra (a) before and (b) after leaching and SEM images of (c) NIP, (d) unleached IIP, and (e) leached IIP.

The unleached Cd-IP (Figure 3.55d) shows a more aggregated, even surface texture with visible particle clusters and a few cavities (Letsoalo et al., 2021), likely due to the presence of coordinated Cd(II) ions within the polymer matrix. These complementary analyses demonstrate a successful removal of template ions (Du et al., 2024), creating a material with specific recognition sites for Cd(II) detection, supporting the intended design of the sensor material.

3.20.1.6 Chemo-resistive sensor performance

The IIP-rGO sensor combines the molecular selectivity of IIPs with the electrical conductivity of rGO to detect target metal ions. The imprinted cavities in the IIP are highly selective and designed to complement the size, coordination geometry, and functional groups (Ding et al., 2023) of target ions (e.g. Cd(II)). These ions interact with the rGO upon binding, inducing changes in the composite's electrical properties, such as resistance or conductivity, due to charge transfer or surface modification effects (Yu et al., 2022). The resulting relative resistance change ($\Delta R/R_0$) correlates with the metal ion concentration, enabling quantitative analysis. This transduction of metal-ion binding into electrical signals makes the sensor highly effective for precise detection and calibration in various applications (Abdul Halim et al., 2024).

3.20.1.7 The rGO: IIP ratio optimisation

Figure 3.56 illustrates the $\Delta R/R_0$ responses for various sensor configurations exposed to Cd(II) concentrations ranging from 5 µg/L to 10000 µg/L. All sensors show significant responses to increasing analyte concentrations, stabilising over time, which indicates reliable signal saturation.

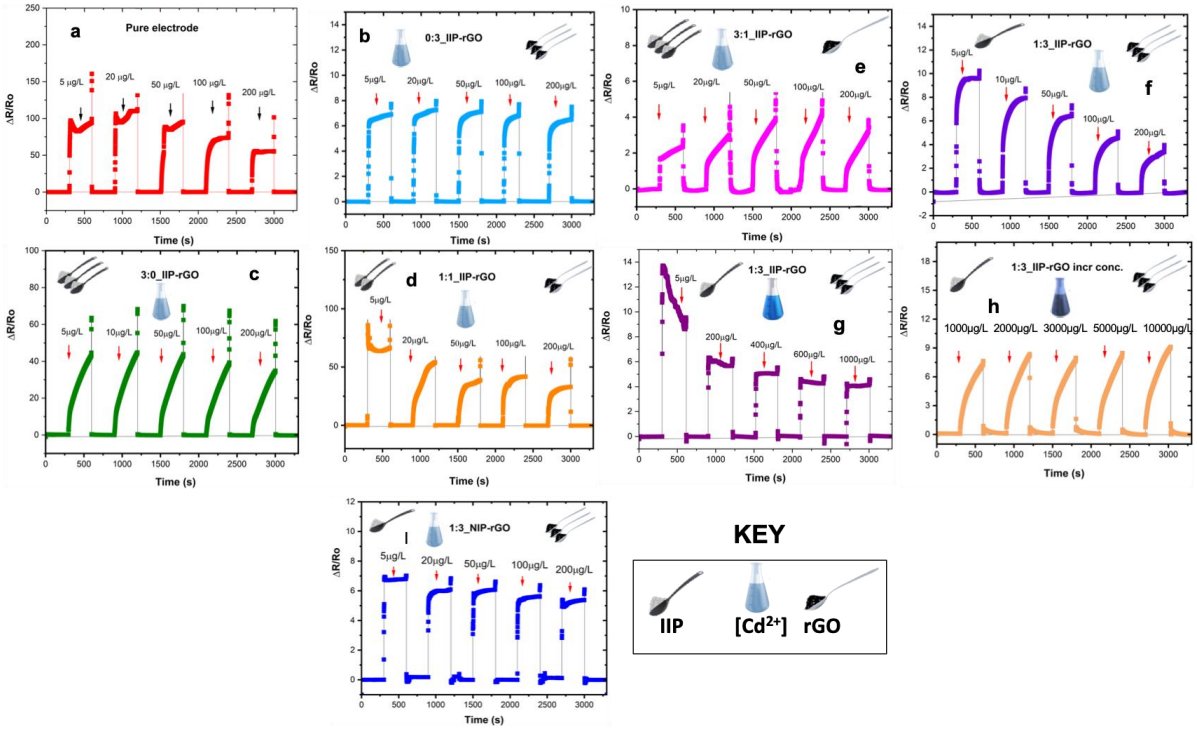

Figure 3.56. Optimisation of sensor response for pure electrode, NIP and other IIP-rGO ratios used to make sensors.

The pure electrode demonstrates a high resistance change due to the absence of rGO and IIP, but its lack of selectivity and stability limits practical use. Even though the 0:3 IIP:rGO sensor shows limited sensitivity, adding rGO improves conductivity and reduces resistance variation, with higher rGO content enhancing sensor performance. The 3:0 IIP:rGO sensor offers better resolution due to IIP's molecular recognition but lacks rGO's conductivity benefits. The 1:1 IIP:rGO ratio shows balanced sensitivity, stability, and linearity (Zhang et al., 2023), leveraging rGO's conductivity and IIP's recognition capability, making it suitable for scalable applications. Further optimisation led to the 1:3 IIP:rGO sensor, which combines high sensitivity, selectivity, and dynamic range. The sensor maintains linearity for concentrations up to 600 µg/L but becomes less effective at extremely high concentrations. At 1000–10000 µg/L, the response broadens but sacrifices sensitivity. The NIP sensor confirms the specificity of imprinted sensors, showing consistently low responses and validating the role of analyte-specific binding in imprinted configurations. Hence, the 1:3 IIP:rGO sensor is the most versatile configuration, balancing sensitivity, stability, and dynamic range, making it ideal for real-world applications (Zhang et al., 2024).

3.20.1.8 Effect of solution pH

Figure 3.57 shows a comparative analysis of IIP and NIP sensor responses across pH levels, highlighting key interactions between Cd(II) ions and the sensing materials. The IIP sensor performs optimally (lowest ΔR/Ro) in acidic and neutral conditions (pH 2-4 and 7 (Huang et al., 2021)), with the best response at pH 2, aligning with Cd's solution chemistry, where free Cd(II) ions dominate and readily bind to imprinted recognition sites. Sensor performance declines at higher pH (pH 8–11) due to the formation of insoluble hydroxide complexes ($Cd(OH)^{+}$ and $Cd(OH)_2$), which reduce binding efficiency. At pH ≥12, the solubility of Cd complexes like $Cd(OH)_4^{2-}$ improves, slightly altering sensor response. Hence, pH 7 (Bhardiya et al., 2021; Hu et al., 2021; Zhang et al., 2024) was chosen as optimum since most water sources are around neutral pH. Conversely, the NIP sensor exhibits higher and less stable ΔR/Ro values, reflecting non-specific, inefficient interactions with Cd(II) species due to the absence of imprinted sites. Instability in the mid-pH range (pH 6–8) further supports random binding.

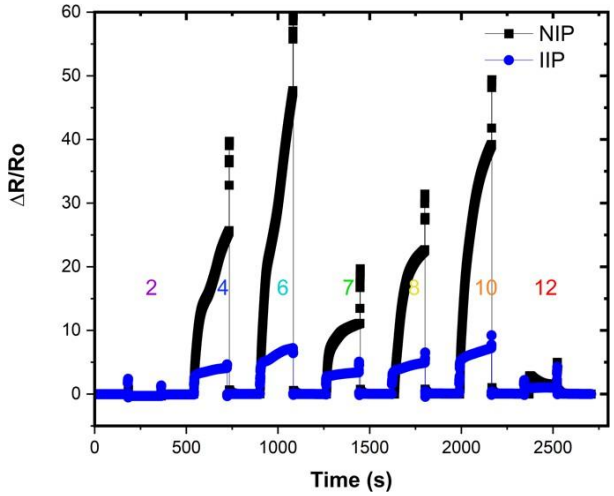

Figure 3.57. Effect of pH (2-12) on the sensor electrode for Cd-IP and NIP.

This analysis confirms the effectiveness of molecular imprinting, with the IIP sensor being most suitable for slightly acidic to neutral conditions for specific Cd(II) recognition.

3.20.1.9 Selectivity, repeatability, reproducibility, and stability

i) Repeatability study

The sensor response was tested in a 20 µg/L standard solution seven times to ensure consistent readings. The sensor demonstrates excellent reproducibility across seven replicate measurements, with consistent cycles showing a stable baseline, rapid analyte response (ΔR/Ro ≈ 7), and effective baseline recovery upon rinsing (Figure 3.58) with a remarkably low percentage relative standard deviation (%RSD) of 1.83% and standard deviation (σ) = 0.134) almost similar to Bhardiya's 1.2 % (Bhardiya et al., 2021).

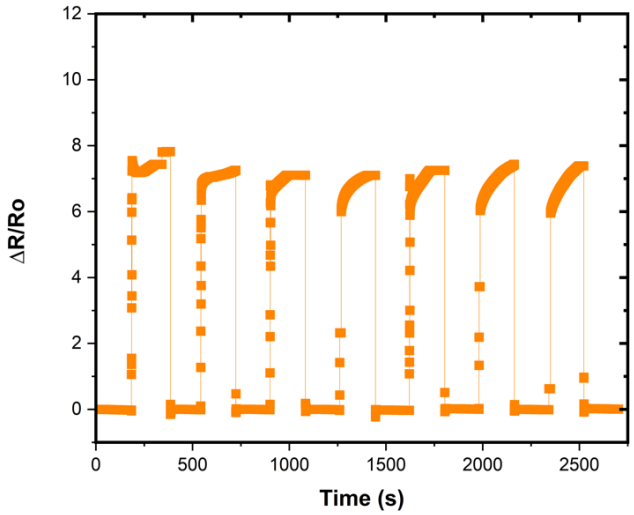

Figure 3.58. Repeatability studies of the Cd-IP sensor. (n=7).

The %RSD is less than that reported before in Cd(II)-IP sensor work (Costa et al., 2023; Mnyipika et al., 2021; Wang et al., 2020), confirming high precision and repeatability, as values below 5% are considered acceptable for analytical methods (Mishalanie et al., 2016). The consistent return to baseline indicates effective surface regeneration, while uniform response magnitudes reflect stable binding site accessibility and electronic performance. Thus, rapid response times and maintained kinetic properties across replicates highlight the sensor's reliability for repeated measurements, making it suitable for real-world analytical applications.

ii) Reproducibility study

The fabricated sensors exhibit excellent reproducibility (Figure 3.59), highlighting the robustness and reliability of the sensor fabrication protocol. A σ of 0.036 across six responses and a low %RSD of 2.02% demonstrate superior sensor-to-sensor consistency, surpassing the typical acceptance threshold for analytical methods (%RSD < 5%) (Mishalanie et al., 2016). These results align with similar work (Mnyipika et al., 2021; Wang et al., 2020; Wang et al., 2023; Zhang et al., 2024; Zhang et al., 2023), validating the fabrication process's precision and confirming the sensing mechanism's stability across multiple sensors. All sensors displayed consistent baseline stability ($\Delta R/R_0 \approx 0$) and comparable response magnitudes upon analyte introduction, with uniform plateau regions indicating similar binding kinetics and capacities.

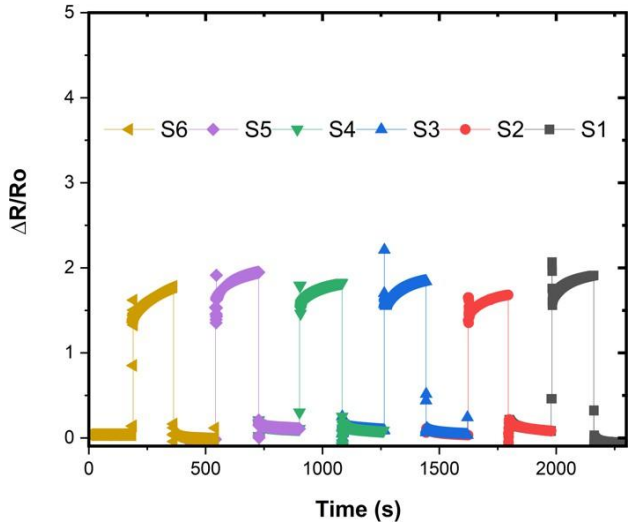

Figure 3.59. Reproducibility studies of the Cd-IP sensors (S = sensor).

Minor variations in response profiles, likely due to slight differences in electrode surface morphology or molecular imprinting efficiency during fabrication (Fafa & Zazoua, 2024), were negligible and did not significantly affect overall performance, as evidenced by the low RSD. These findings confirm the reliability of the fabrication protocol in producing high-quality, reproducible sensors.

iii) Selectivity study

The sensor's selectivity towards Cd(II) was evaluated against potential interfering metal ions (Hg(II), Pb(II), Ni(II), Mn(II), Cu(II), Zn(II), Mg(II), Ca(II), and their mixture) at 20 µg/L concentrations as shown in Figure 3.60.

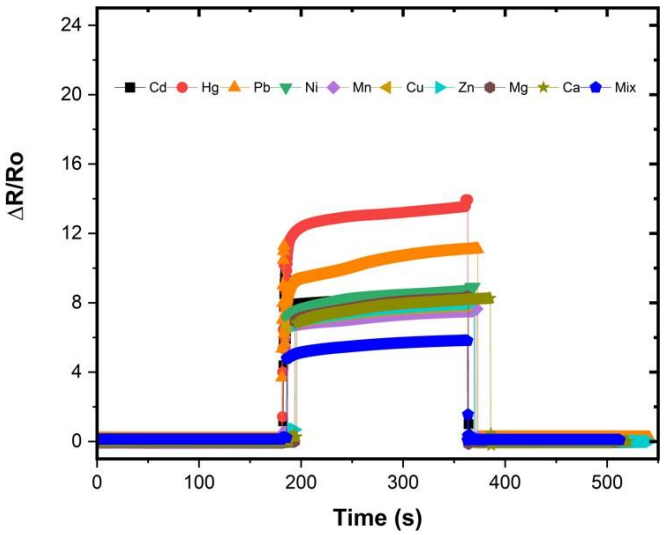

Figure 3.60. Selectivity studies of the Cd-IP sensors towards various cations.

Hg(II) exhibited the highest interference (+9.8% offset), likely due to its comparable ionic radius and electronic configuration to Cd(II) (Fafa & Zazoua, 2024). While Pb(II) showed moderate interference,

other ions, including Zn(II), Mg(II), and Ni(II), demonstrated minimal impact (-2.4%, -1.2%, and +0.1%, respectively), indicating robust selectivity (Hu et al., 2021; Wang et al., 2020). The mixed-ion solution yielded a -7.3% offset, suggesting competitive binding effects. Although the sensor displayed excellent selectivity against most interferents, careful consideration is required for samples containing Hg(II) and Pb(II) (Fafa & Zazoua, 2024). Future work should focus on enhanced leaching strategies to improve template removal and cavity specificity.

iv) Stability study

The long-term stability of the sensor was assessed over 60 days under controlled conditions, with $\Delta R/R_0$ values recorded at 0, 30, and 60 days showing plateau responses of 9.5, 9.8, and 10.2, respectively (Figure 3.61). Statistical analysis yielded a mean response of 9.8 ± 0.35 $\Delta R/R_0$ and an %RSD of 3.57% related to most sensor studies on Cd (Bhardiya et al., 2021; Choudhari et al., 2023; Fafa & Zazoua, 2024; Hassanpoor & Rouhi, 2021; Hu et al., 2021; Huang et al., 2021; Li, Xu, Li, et al., 2024; Wang et al., 2023; Zhang et al., 2024; Zhang et al., 2023), indicating reasonable stability but with a discernible trend of increasing resistance drift over time. The drift was observed likely due to material ageing, structural reorganisation, or environmental interactions affecting binding site functionality. Despite this drift, the sensor maintained its characteristic response profile, suggesting preserved functionality but reduced sensitivity at 60 days.

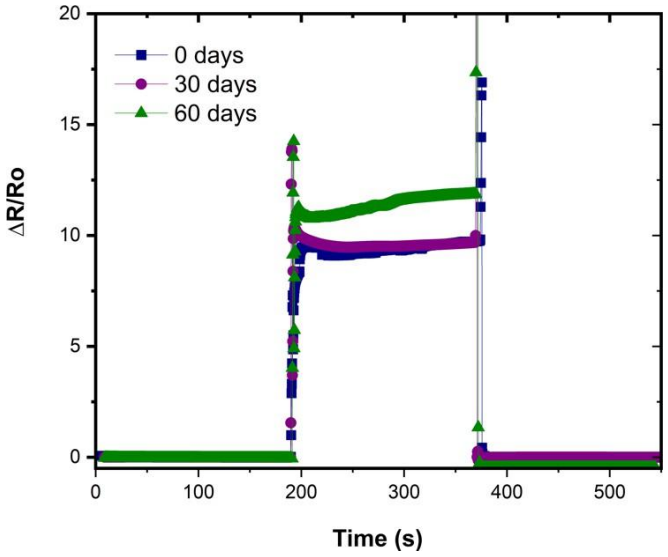

Figure 3.61. Stability studies of the Cd-IP sensors over a 60-day period.

These findings highlight the need for recalibration or drift compensation strategies for long-term use, along with optimisation efforts such as improved storage conditions, surface protection measures, and standardisation protocols to enhance durability and reliability.

v) Analytical figures of merit and real water sample application

Analytical figures of merit, sensitivity, LOD, and coefficient of determination (R^2) were evaluated at optimum sensor conditions using 50 mL of 5 –200 µg/L standard solutions of Cd(II) and a blank. The Cd-IP analytical curve linearised to the equation: $y = 12.732 - 1.765\ln x$ was obtained in a dynamic linear range of 5 –600 µg/L with a R^2 value of 0.9965 compared to 0.8551 of the NIP electrode Figure 3.62.

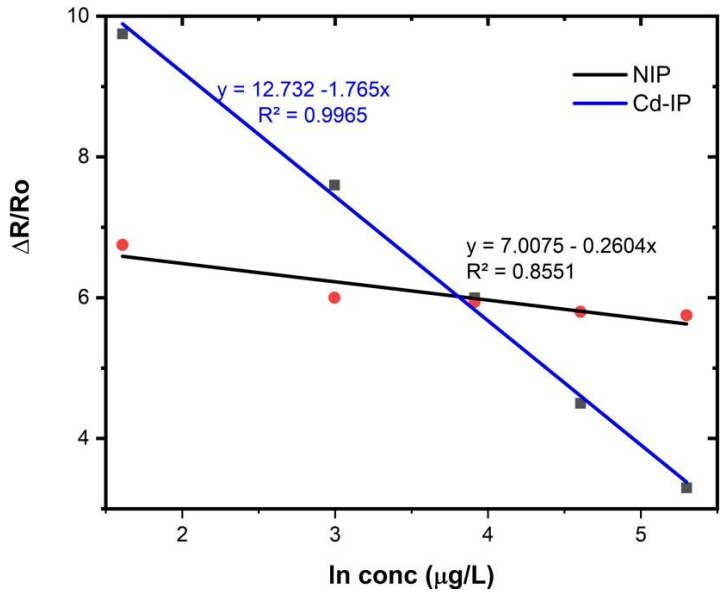

Figure 3.62. Linearised forms of NIP vs IIP calibration plots.

The sensitivity of the sensor (slope of the curve) and LOD were determined at 1.765 µg/L and 0.704 µg/L, ($LOD = \frac{3.3\sigma_{blank}}{S}, s = \text{slope of the curve}$), which is lower than the WHO and SANS's 3 µg/L limit (SANS, 2022; WHO, 2022). A comparison of this work's sensor analytical performance to other similar sensors of Cd(II) reported in the literature is outlined in Table 3.25. The developed Cd-IIP-rGO sensor in this work demonstrates balanced performance metrics, showing improved LOD (0.7 µg/L) compared to similar Cd sensor designs while maintaining a practical linear range. Although some sensors in the literature show superior individual metrics, the combination of detection limit and working range positions this sensor as a viable option for practical applications, outperforming several established electrode designs regarding detection capabilities.

The percentage recoveries (%R) (Table 3.26) for Cd(II) detection in four water samples analysed using the 1:3 Cd-IP-rGO sensor ranged from 91.6% to 105% (Costa et al., 2023; Fafa & Zazoua, 2024; Li, Xu, Li, et al., 2024; Wang et al., 2023; Zhang et al., 2024), indicating acceptable accuracy for ultra-trace level detection.

Table 3.25. Comparison of the prepared sensor with other Cd(II) modified electrodes.

Electrode	Linear range (µg/L)	LOD (µg/L)	Reference
IIPpy/rGO/GCE	1 - 100	0.26	(Xiao et al., 2021)
IIPoPD/rGO/GCE	1-50	0.13	(Xiao et al., 2021)
IIP-PEDOT/SPPtE	0.5 - 75	0.07	(Fafa & Zazoua, 2024)
IIP/rGO-FET	2 - 200	0.83	(Hu et al., 2021)
RGO/MnO_2/Nafion/GCE	4 - 150	1.12	(Hassanpoor & Rouhi, 2021)
SnO_2@BCG/GCE	1 – 400	0.1	(Bhardiya et al., 2021)
rGO@TiO_2/GCE	0.01–10 µM	12 nM	(Zhang et al., 2024)
PoPD-IIP/3DPrGO/GCE	1 - 100	0.11	(Wang et al., 2023)
MnO_2@RGO/GCE/DPV	0.0 5 –700	0.0151	(Mnyipika et al., 2021)
Cd-IIP-rGO	5 - 200	1.77	(Letsoalo et al., 2021)
CS/rGO-IIP/GCE	1 - 160	0.2	(Li, Xu, Li, et al., 2024)
rGO@TiO_2/GCE	1 – 1000 nM	1.33 nM	(Zhang et al., 2023)
PoPD/ERGO/GCE	1 – 50	0.13	(Wang et al., 2020)
Cd-IP-rGO	5 - 200	0.7	This work

Table 3.26. Real water samples spike recoveries for the Cd-IP sensor.

Sample	Added Conc (µg/L)	Detected Conc (µg/L)	%R
Driekop BW 6	0.9	0.945	105
Driekop BW 5	0.9	0.918	102
Steelpoort RW 3	0.9	0.8829	98.1
Steelpoort RW 2	0.9	0.8244	91.6

BW = borehole water, RW = river water, %R = percentage recovery

Samples from Driekop BW showed higher percentage recoveries compared to Steelpoort RW. The variation in percentage recoveries may result from matrix effects or slight inconsistencies in sensor performance across different water chemistries. However, all percentage recoveries fall within an acceptable range for environmental monitoring (typically 80–120%) (Mishalanie et al., 2016), demonstrating the sensor's reliability for detecting Cd(II) in diverse water sources.

3.21 REMOVAL OF METAL IONS IN WATER

3.21.1 Effect of pH on the removal of metal ions

The pH level plays a pivotal role in influencing various aspects, including the solubility of metal ions, the ionization extent of adsorbates during adsorption, and the presence of rival ions competing for active sites on the bio-sorbent. To ascertain the optimal pH for treating water contaminated with Ni(II) and Cd(II), a batch study was conducted, ranging from pH 3 to 8 and the results are shown in Figure 3.63.

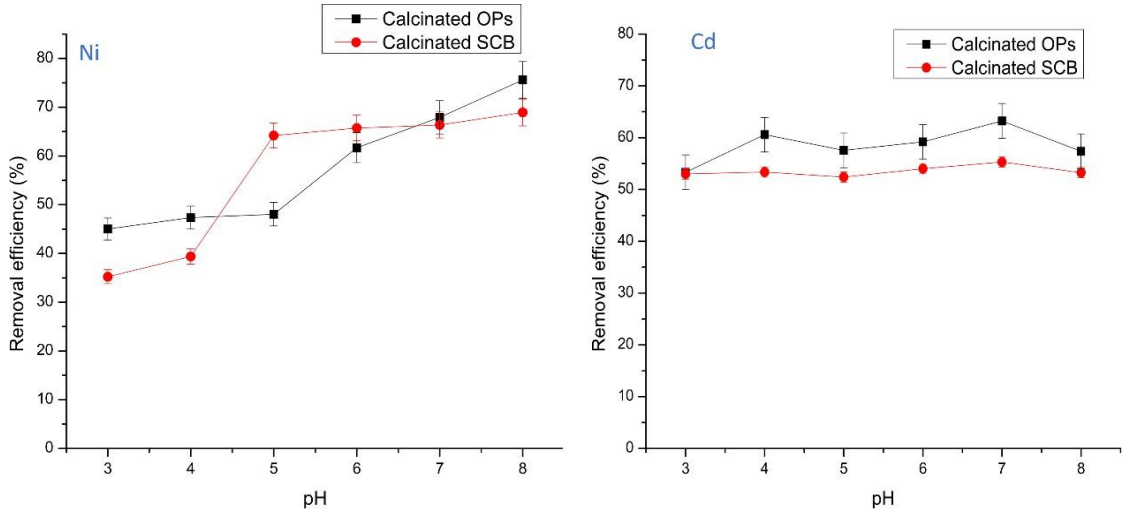

Figure 3.63. The effect of pH on percentage removal of Ni(II) and Cd(II).

In Figure 3.63, calcined SCB showed similar effectiveness to calcined OPs in removing Ni(II) and Cd(II) with the optimum pH being 8 for Ni(II) and 7 for Cd(II), regarding the percentage removal. A precipitate was noticed for both metal ions beyond pH 8, so optimization studies were conducted up to pH 8. This similarity is attributed to introducing oxygen-rich functional groups that act as attachment points for positively charged metal ions, leading to increased adsorption as pH levels rise. At lower pH values, adsorption was limited, and metal ion removal was inhibited, possibly because of the competition between hydrogen and metal ions on the sorption site. When the concentration of hydronium ions in the solution is high (at lower pH), these ions seem restricted due to the repulsive forces (Gupta and Kumar, 2019). These findings highlight the effectiveness of the calcined bio-sorbents to remediate water contaminated by Ni(II) and Cd(II).

3.21.2 Effect of contact period on the removal of Ni(II) and Cd(II) by calcinated OPs and SCB

Contact time affects the efficiency and the equilibrium process. This is because the extended contact period means there is more time for metal ions to interact with the surface of the bio-sorbents. However, a longer contact time also means the process takes longer and can be costly (Khaskheli et al., 2011). Therefore, the contact period is a crucial parameter affecting the sorption of metal ions for practical applications, as illustrated in Figure 3.64.

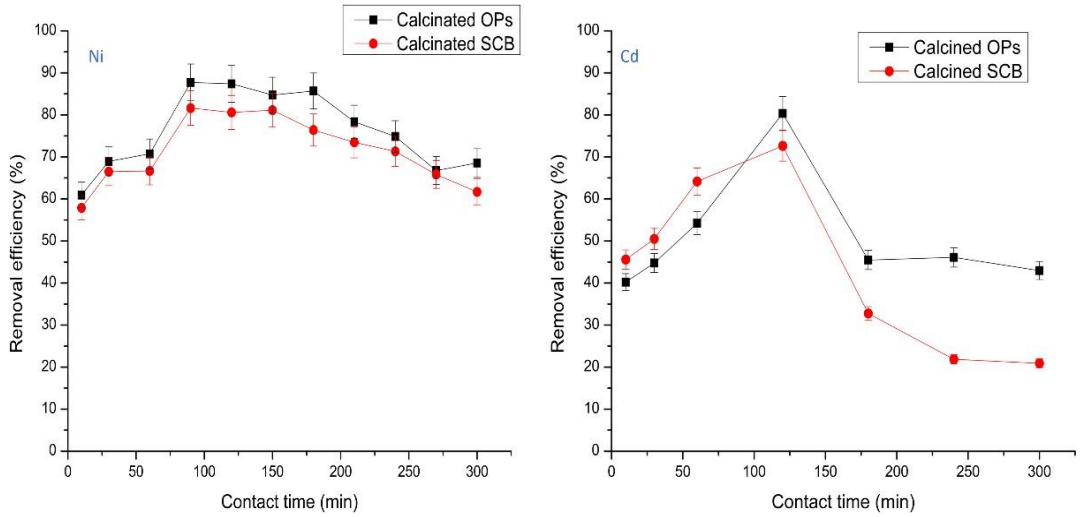

Figure 3.64. The effect of contact time on percentage removal of Ni(II) and Cd(II).

Adsorption exhibited enhancement from the 10th to the 30th min, with a slight further increase from the 30th to the 60th min. The most significant adsorption rate occurred between the 60th and 90th min, followed by a gradual decline beyond this timeframe. Equilibrium was reached after 270 min, attributed to the initial abundance of vacant sites for bio-sorption that diminished over time due to surface site depletion and repulsive forces between solute molecules and the bulk phase. The optimal contact time for Ni(II) remediation in water was found to be 90 min.

For Cd(II), the RE increased from 10 to 120 min, then started decreasing after 120 min due to saturation. The continued rise in contact time led to desorption of metal ions from the calcined bio-sorbents. Consequently, 120 min was identified as the maximum contact time for remediating wastewater contaminated by Cd(II). In conclusion, knowledge of the delicate adsorption patterns and ideal contact times for the remediation of Cd(II) and Ni(II) is essential for the effective planning and execution of water purification procedures.

3.21.3 Effect of adsorbent dosage on adsorption of metal ions

The bio-sorbent dosage plays a crucial role in adsorption, impacting both the economic viability of the technology and its effectiveness. To illustrate, a more significant amount of adsorbent used typically results in a more effective removal of metal ions. Nevertheless, this also drives up the overall expenses associated with the technology, as shown in Figure 3.65.

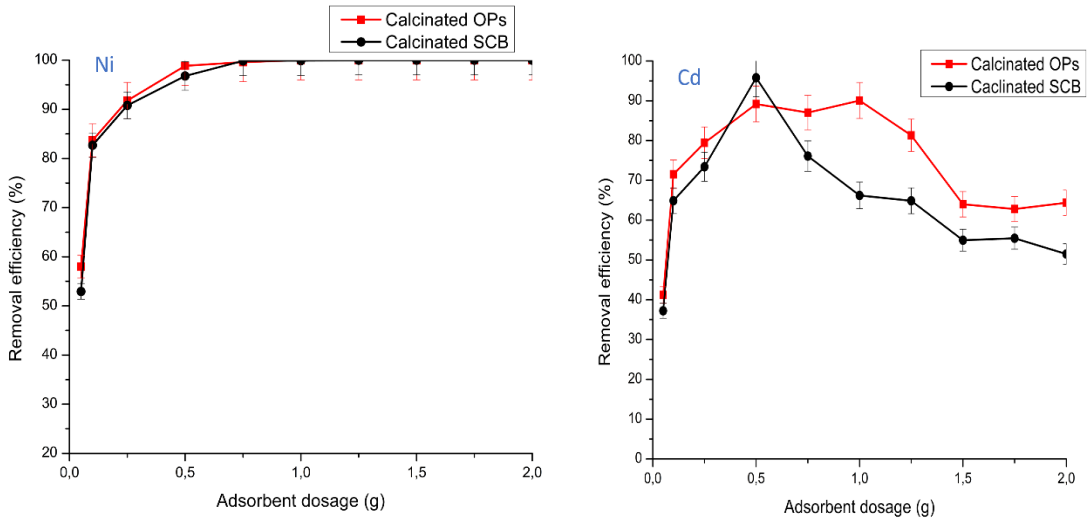

Figure 3.65. The effect of adsorbent dosage on percentage removal of Ni(II) and Cd(II).

The results showed that the percentage removal also increases as the dosage increases. This can be caused by increased availability of active sites on the bio-sorbents resulting from increasing the bio-sorbent amount used. Further increase in adsorbent dosage had no significant increase in metal removal efficiency. This is ascribed to the fact that higher adsorbent dosage provides more active sites that may remain unused during the ion reaction (Ezeonuegbu et al., 2021). This also highlights the efficiency of the calcined bio-sorbents in removing these metal ions from simulated aqueous solutions.

3.21.4 Effect of initial ion concentration on adsorption

The initial metal ion concentration is an essential parameter in adsorption because it affects the equilibrium and kinetics. For example, the process quickly reaches equilibrium when the initial metal ions concentration is high. This is due to the high metal ions available to interact with the surface sites of the bio-sorbents and the greater rate of diffusion of metal ions (Mahmudiono et al., 2022), as shown in Figure 3.66.

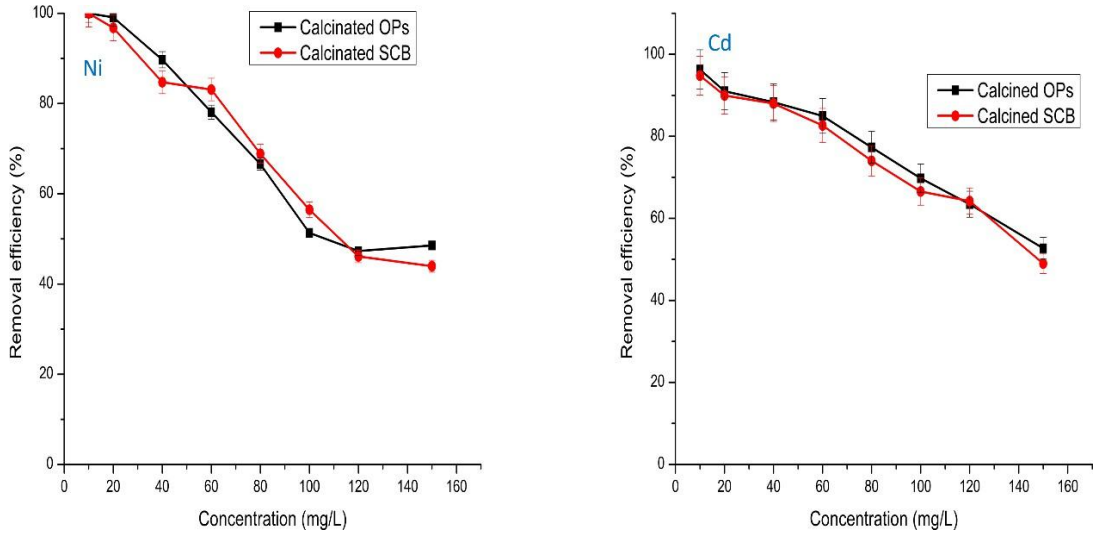

Figure 3.66. The effect of initial metal ion concentration on percentage removal of Ni(II) and Cd(II).

The percentage removal decreased with the increase in metal concentration, as observed in Figure 3.66. This could be explained by the fact that at lower concentrations, there is a higher proportion of active sites in comparison to the metal ion concentrations. As a result, Ni(II) and Cd(II) readily adhere to the surface of the calcinated bio-sorbents, leading to the observed removal efficiency. The decline in metal ion removal efficiency at higher concentrations could be attributed to all adsorbents having a finite number of active sites, which can become saturated beyond a certain concentration threshold (Yin et al., 2023). Similar adsorption patterns were reported by Yue *et al.* (2016) on the utilisation of infused tea leaves for the removal of metal ions, namely, Fe(II), Pb(II), and Cd(II).

3.21.5 Effect of solution temperature on the adsorption of metal ions

The solution temperature is an essential parameter of the adsorption process because it affects the thermodynamics and adsorption rate. For instance, higher temperature can increase the adsorption process by increasing the degree of randomness of the process, thereby increasing the rate of adsorption by increasing the number of collisions between the metal ions and the surface of the bio-sorbents (Selmi et al., 2020). The effect of solution temperature on percentage removal of metal ions is shown in Figure 3.67.

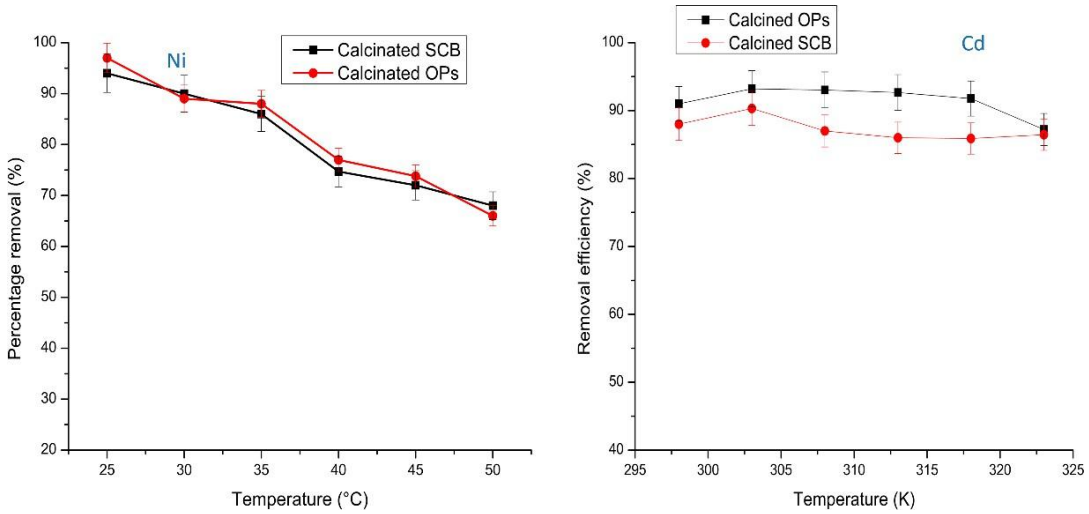

Figure 3.67. The effect of solution temperature on percentage removal of Ni(II) and Cd(II).

The findings indicate that as the temperature rises, adsorption decreases, and this is presumably attributed to various factors. One key factor is the diminished electrostatic forces between the active sites on the bio-sorbents and the metal ions at elevated temperatures. This phenomenon weakens the interaction between the metal ions and the active sites. The decline in the RE of Ni(II) primarily results from reduced surface activity, implying that the adsorption of Ni(II) by activated SCB and OPs is an exothermic process. This means that this process releases energy in heat, indicating that the metal ions are more stable on the adsorbent's surface than when they are free in the solution (Al-Ghouti and Al-Absi, 2020). These findings also highlight a crucial insight regarding the developed technique, as they demonstrate that the utilization of activated SCB and OPs for adsorption doesn't necessitate an external energy input. This enhances the cost-efficiency and sustainability of the adsorption process, which is a highly favourable aspect in the design of adsorption systems.

3.22 CHARACTERIZATION STUDIES OF BIO-SORBENTS

Characterization of bio-sorbents was performed, and the results are presented in subsequent sections.

3.22.1 Characterization of bio-sorbents by Zeta potential

Figure 3.68 shows the zeta potential of the pure and calcinated OPs and SCB.

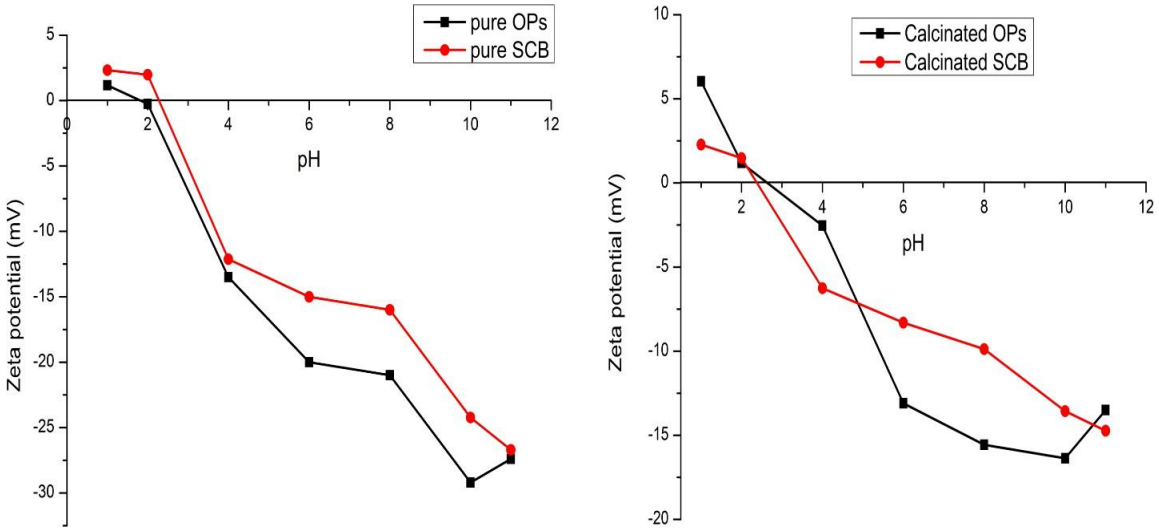

Figure 3.68. Zeta potential of the pure and calcinated bio-sorbents.

Zeta potential analysis was conducted to determine the surface charge of biochar and compare it to the surface charge of pure SCB and OPs. Zeta potential analysis was also employed to identify the point of zero charge (PZC), which is the pH at which the surfaces of these materials carry no net charge. The findings revealed that the PZC for OPs biochar was measured at 2.4, while for SCB biochar, it was 2.2. Beyond this pH threshold, the surface charge became negative, and these conditions are conducive to electrostatic interactions with cations (specifically, Ni(II) and Cd(II)), signifying an imminent adsorption process at any pH above the PZC. This adsorption results from attractive forces between the biochar's surface and metal ions. At pH levels below the PZC, the zeta potential was positive for both bio-sorbents, indicating the presence of repulsive forces within that pH range.

3.22.2 Characterization of bio-sorbents by FTIR spectroscopy

Fourier transform infrared spectroscopy analysis was conducted on pure and calcinated adsorbent materials to gain a deeper insight into the various functional groups within these materials. Figure 3.69 displays the FTIR spectra of the bio-sorbents before and after calcination, as well as after adsorption of metal ions by calcinated bio-sorbents.

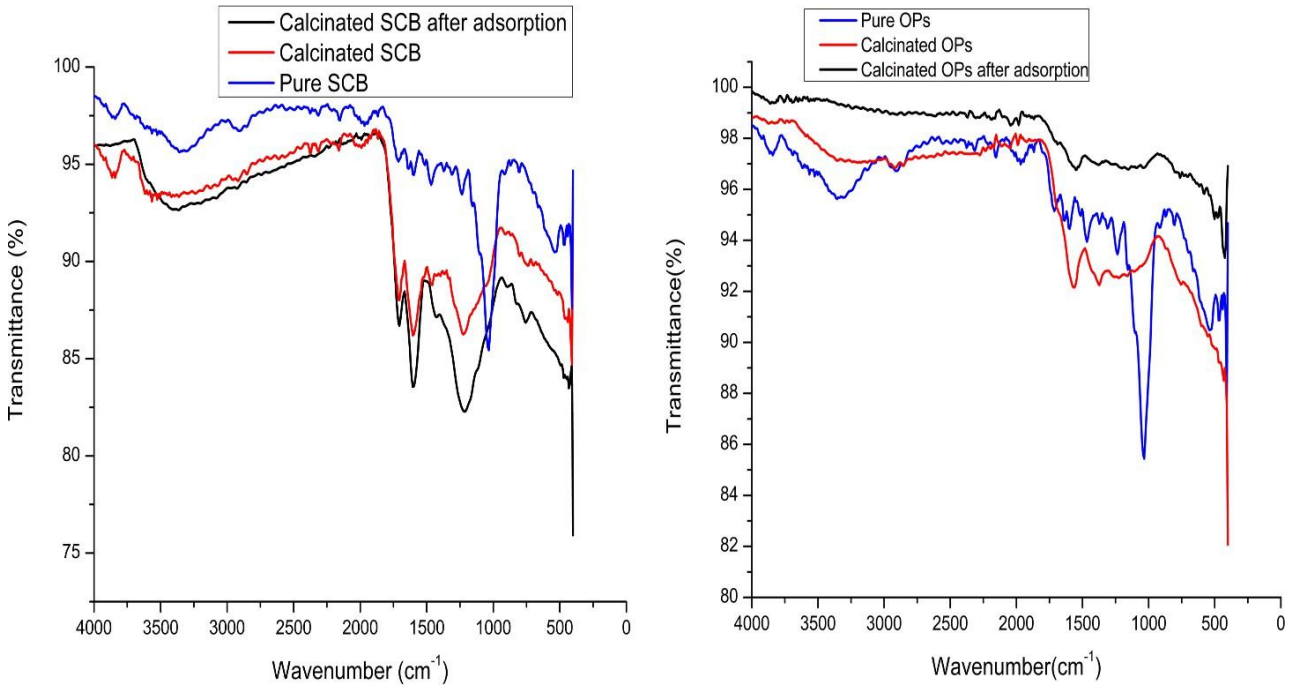

Figure 3.69. FTIR spectra of the pure bio-sorbents, calcinated bio-sorbents, and after-adsorption of Ni(II).

Similar peaks are generally observable in all materials, but those originating from the pure bio-sorbents exhibit higher intensity than those from the calcinated bio-sorbents. An exception to this trend is the peak at 3300 cm^{-1}, which is readily detectable in pure SCB, a material that has not undergone calcination. In contrast, this peak vanishes in the case of calcinated SCB. This peak is attributed to the stretching vibrations of –OH, indicating the presence of water and hemicellulose, specifically in the biomass. The reduction in peak intensity in the calcinated materials is linked to the degradation of fibers during thermal treatments, leading to the breaking of chemical bonds and the disintegration of species. The peak observed around 3400 cm^{-1} indicates the presence of a hydroxyl group. The peak appearing around 2900 cm^{-1} can be assigned to the C-H stretching vibration. The peaks at 1400 cm^{-1} indicate the C-O groups that come from the presence of carboxylic groups in the biomass (Mahrous et al., 2022).

3.22.3 Characterization of bio-sorbents by SEM–EDS

The pure SCB and OPs were analysed by SEM-EDS to study their structural morphology and chemical composition. The SEM-EDS of pure OPs and SCB results are shown in Figure 3.70 and the SEM-EDS of calcinated OPs and SCB results are shown in Figure 3.71.

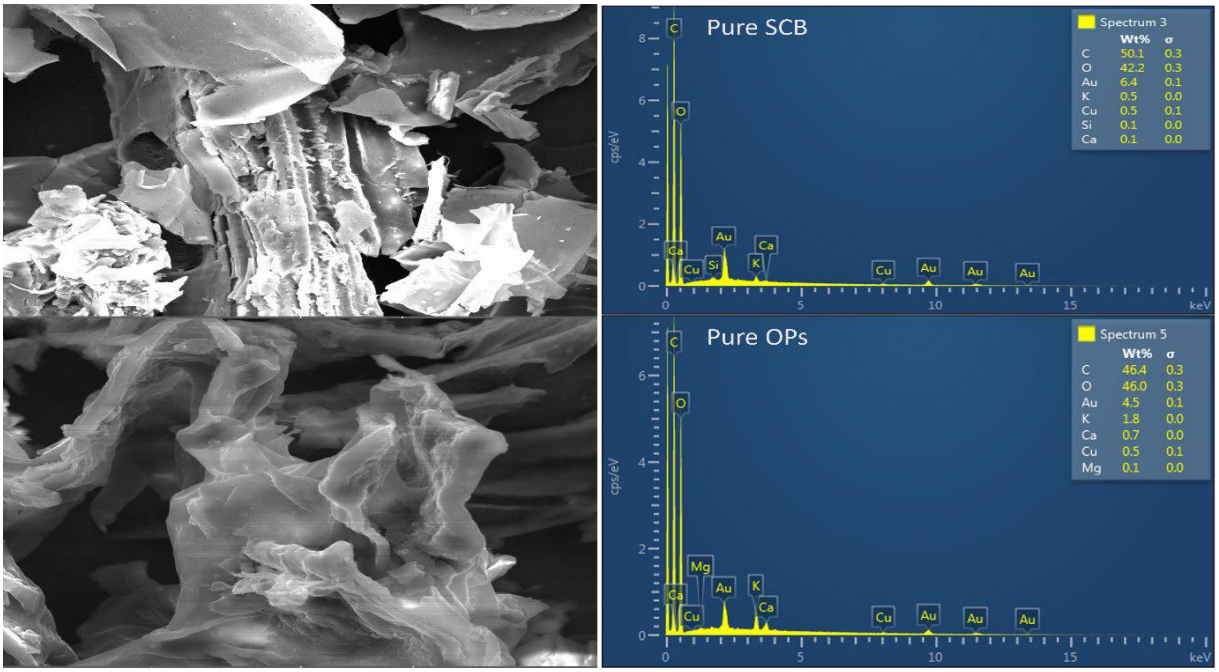

Figure 3.70 SEM-EDS of pure OPs and pure SCB.

The outcomes demonstrate a variety of pore sizes and shapes in both bio-sorbents. These images illustrate that the prepared SCB and OPs powders exhibit an irregular structure. This irregularity can enhance the ability of the bio-sorbents to capture Ni ions at various locations on the sorbent material.

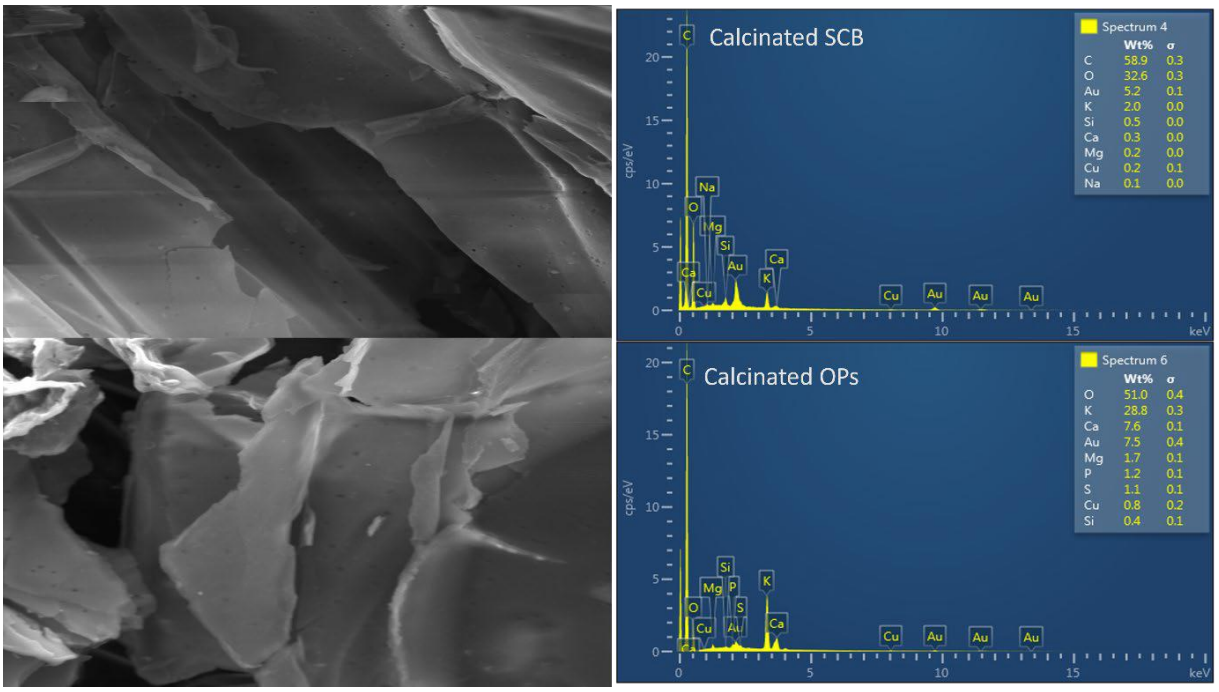

Figure 3.71. SEM-EDS of calcinated OPs and calcinated SCB.

These findings indicate that calcinated organic materials possess a substantial oxygen content of 25%, while the rest comprises carbon (75%). Before SEM-EDS analysis, the samples underwent Au coating, elucidating the elevated Au composition evident in the EDS results. This also means that activated carbon made from OPs has a high percentage of carbon. The uneven composition of the organic materials' biochar, characterized by lengthy and slender fibres. The biochar's surface is sleek and features a variety of pores with varying sizes and shapes. The exterior surface displays numerous

grains and an assorted structural configuration. The presence of a porous structure is a crucial characteristic of the biochar, enabling it to adsorb metal ions, as explained by Yan et al. (2022).

The SEM micrographs were carried out after subjecting SCB to thermal treatment to explore any changes in its structure or the effects of pyrolysis on the morphological features of SCB. The micrographs demonstrate that pyrolyzed SCB possesses a highly porous and uniform structure. This enhanced porosity in SCB plays a significant role in adsorption, as it increases the biochar's capacity to retain water and provides additional sites for the sorption of metal ions, as reported in literature (Raul et al., 2021). The EDS analysis also reveals a substantial presence of carbon and oxygen. This indicates that the surface polarity (oxygen molecules have a partially negative charge) of SCB is enhanced following pyrolysis, thereby increasing its capacity to capture metal ions. Simultaneously, the elevated carbon content and the significant porosity provide additional binding sites for adsorption.

A considerable number of active sites are present, as indicated by the elevated oxygen composition. These results are consistent with the FTIR data, which show multiple functional groups that carry oxygen. It is clear that OPs have more oxygen in them than SCB when comparing the pure bio-sorbents. This difference results from OPs containing pectin, which is made up of chain molecules high in oxygen atoms and adds to their structural makeup (Karim *et al.*, 2023). Because of the higher oxygen content in OPs, more surface sites are available for the adsorption of metal ions. The substantial oxygen content renders these bio-sorbents highly effective in removing water contaminants like Ni(II) and Cd(II).

3.22.4 Characterisation of bio-sorbents by SEM-EDS after adsorption

The SEM was used to investigate the interaction of Ni with the calcinated bio-sorbents, and the results are demonstrated in Figure 3.72.

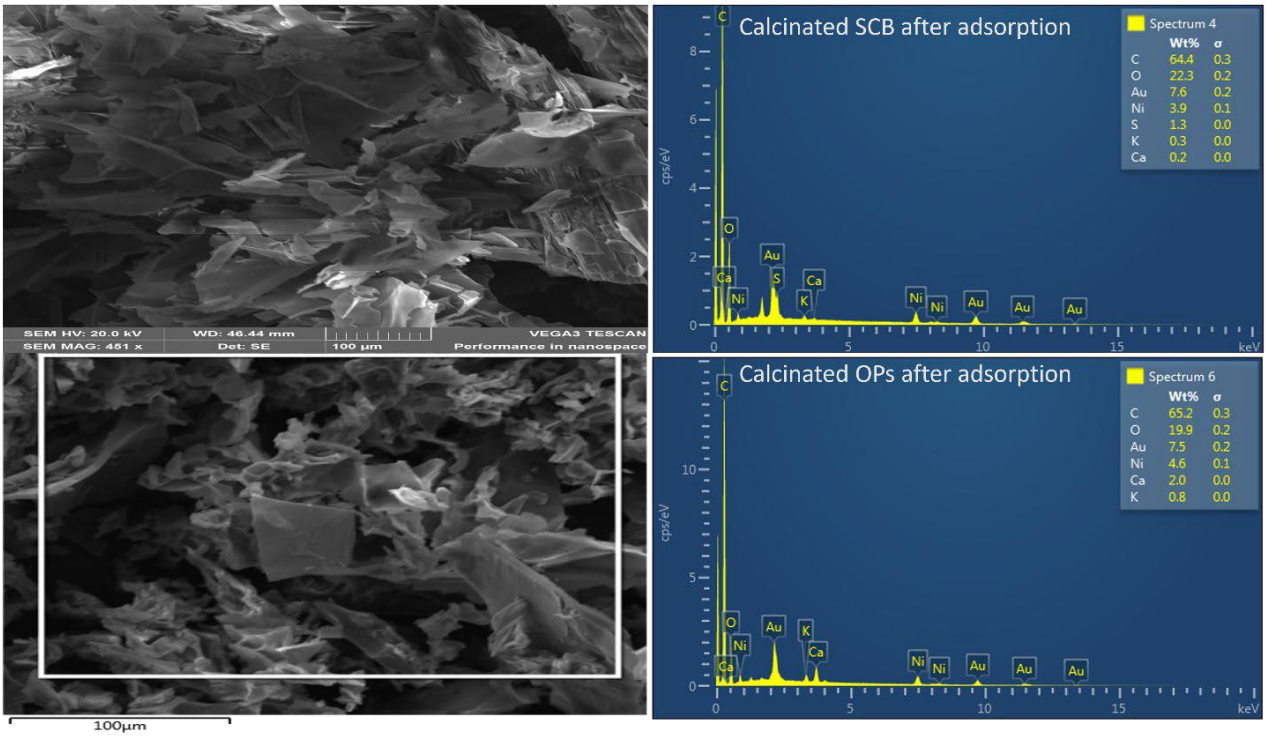

Figure 3.72. SEM-EDS of calcinated OPs and calcinated SCB after adsorption of Ni(II).

Before adsorption, the SEM images of pure SCB revealed a porous structure with irregular shapes. Subsequent to biosorption, the SEM images displayed pores filled with Ni(II) on the surface of the bio-

sorbents. These images exhibited bulky, shiny particles and extended layers loaded with metal ions, which were not present in the pure bio-sorbents. The EDS analysis confirmed the presence of adsorbed metal ions, specifically Ni(II). The compositional percentages of calcinated SCB after adsorption were found to be 64.4% C, 22.3% O, and 3.9% Ni, providing further evidence of Ni being adsorbed onto the surface of the calcinated SCB. After adsorption, the elements detected on calcinated OPs were C, O, and Ni, with the following composition percentages: 65.2% C, 19.9% O, and 4.6% Ni. The data further substantiates the successful adsorption of Ni(II) onto the surface of calcinated OPs.

3.22.5 Characterisation of bio-sorbents by PXRD

Powder X-ray diffraction analysis was performed to determine the crystallinity of pure and calcinated bio-sorbents. The results are shown in Figure 3.73.

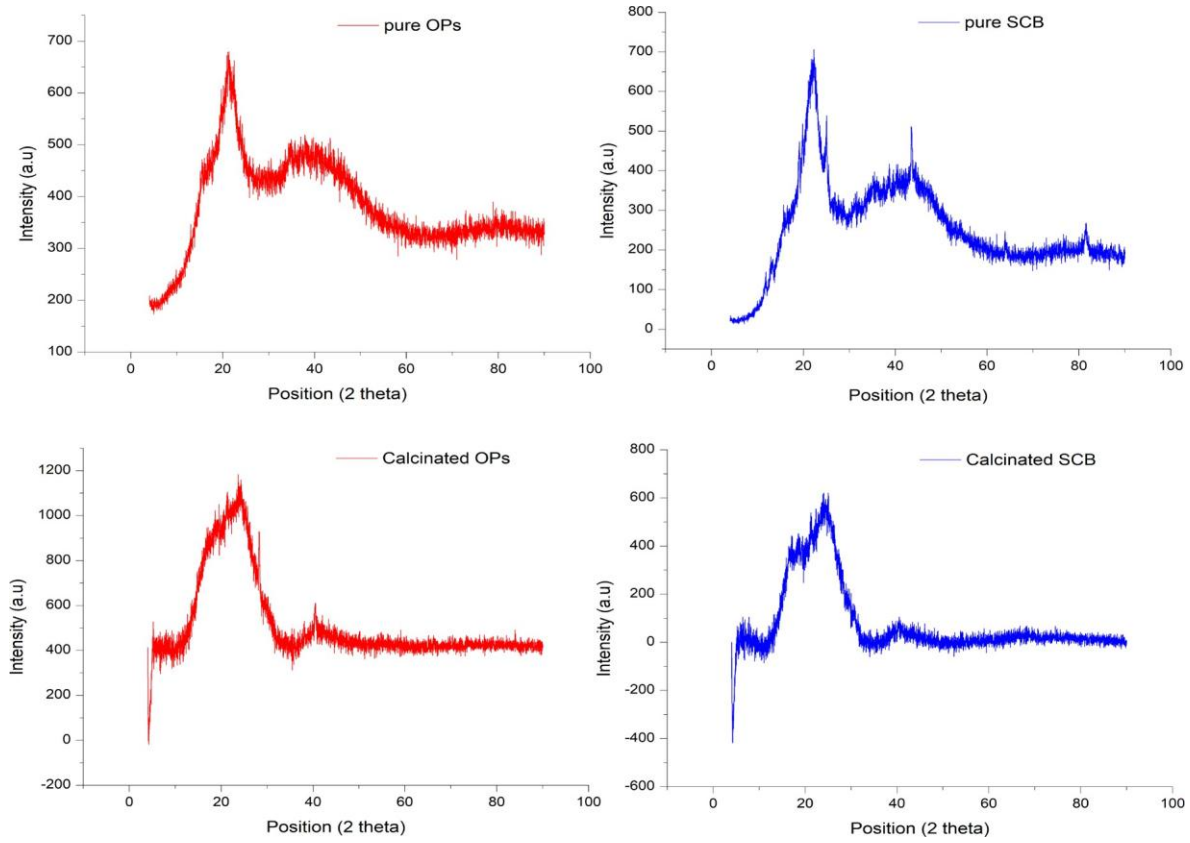

Figure 3.73. PXRD diffractograms of the pure and calcinated bio-sorbents.

A broad peak is observed in the range of 2θ=18˚ to 28˚, indicating a high level of amorphousness in the material, which is advantageous for porous materials. These peaks are evident in both the pure and calcinated bio-sorbents. As previously discussed, these bio-sorbents comprise cellulose, hemicellulose, lignin, and pectin. The cellulose peak could be attributed to the peaks around 20˚ and 45˚. The non-crystalline structure of these bio-sorbents results from the interaction between hydrogen bonding and weak van der Waals forces between adjacent molecules. Johar et al. (2012) reported that the other components of these bio-sorbents, namely hemicellulose, lignin, and pectin, exhibit amorphous characteristics by their nature. It is also worth noting that both the bio-sorbents and their calcinated forms display similar diffraction patterns, indicating that calcination does not alter the amorphousness of these materials. This also means that the components of these bio-sorbents do not decompose before the pyrolysis temperature used.

3.22.6 Characterisation of bio-sorbents by TGA

The International Confederation for Thermal Analysis and Calorimetry (ICTAC) describes TGA as a set of methods that observe alterations in a sample's physical or chemical characteristics over time under the influence of a temperature regimen. The thermal decomposition process is influenced by the organic and inorganic composition of biomass (Yaradoddi et al., 2021). It measures and documents sample mass and temperature changes. The temperature regimen can involve heating, cooling, maintaining isothermal conditions, or a mix of these (Saadatkhah et al., 2020). The accompanying figure (Figure 3.74) illustrates the TGA of both the untreated and calcined bio-sorbents.

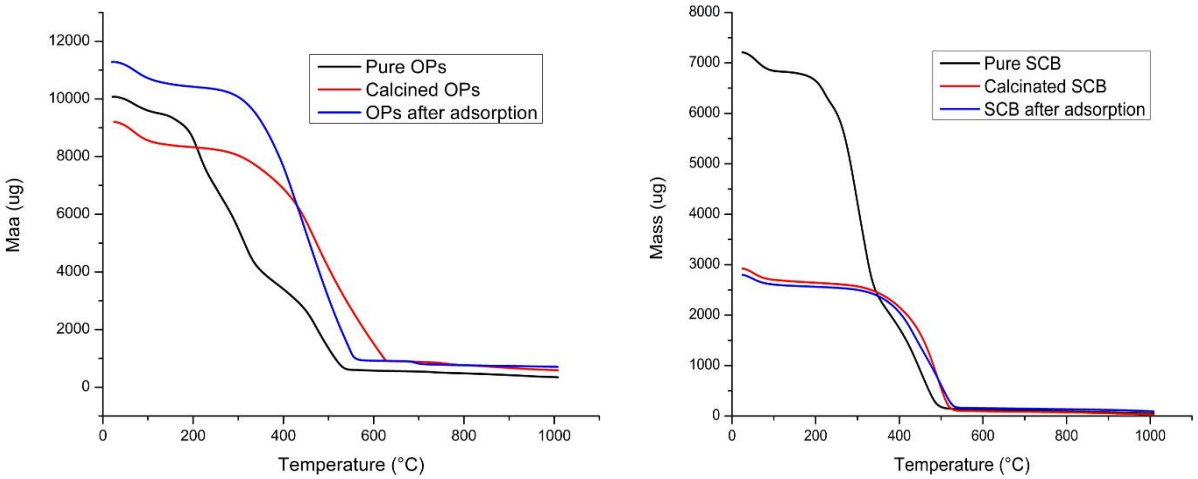

Figure 3.74. TGA of the pure bio-sorbents, calcinated bio-sorbents, and after-adsorption of Ni(II).

The mass loss curves obtained from TGA measurements can be understood to represent the distinct degradation of the three primary organic components in woody biomass: cellulose, hemicellulose, and lignin. The TGA curves in Figure 3.27 demonstrate the different weight loss events as the temperature increases. The first weight loss event occurred between room temperature and 200 °C, and this is the mass loss of volatile components, particularly water and other light molecules (Yaradoddi et al., 2021). The loss of cellulose and hemicellulose follows this, which is well supported by Varma and Mondal (2016), who stated that the loss of cellulose and hemicellulose occurs between 200 and 350 °C. The last degradation pattern is attributed to the loss of lignin and pectin (Kamsonlian *et al.*, 2011).

The main differences between the pure and calcinated bio-sorbents are that the pure bio-sorbents showed the loss of moisture and volatile components at lower temperatures. In contrast, pyrolyzed bio-sorbents showed a reduced weight loss because pyrolysis involves heating the pure bio-sorbents at high temperatures, leading to a significant reduction in weight. This is evident in Figure 3.27 with the alteration of peaks observed because pyrolysis can shift or change the peaks. As the temperature increases, the pure bio-sorbents showed a pattern of degradation of their components, such as carbohydrates, cellulose, and hemicellulose, while the calcinated bio-sorbents showed no specific pattern. This indicates that pyrolysis breaks down the complex organic structures of OPs and SCB into simple compounds, forming char.

3.23 REMOVAL OF Pb(II) IONS FROM AQUEOUS SOLUTIONS USING NATURAL AND HDTMA-MODIFIED BENTONITE AND KAOLIN CLAYS

3.23.1 SEM characterisation

Scanning electron microscopic images of the modified and unmodified clays are depicted in Figure 3.75. Bentonite (a) displays sponge-like structures which are separated by distinct void spaces; however, upon modification with HDTMA, there is aggregation on the surface of the clay structure. The void spaces between the clay particles on bentonite also diminish after modification. The modification of bentonite by HDTMA changes the morphology greatly, and similar observations were reported in other studies (Dinh et al., 2022; Ltifi et al., 2018). The SEM images of kaolin (c) show an agglomerated flake-like structure with void spaces also appearing between the particles, the surface morphology of kaolin upon modification does not change drastically, except the void spaces diminish and there is more particle agglomeration observed. A study by Prabawa et al. (2020), also reported no significant changes in the morphology of kaolin upon modification with urea, however, the study reported a slight increase in the distance between the kaolin particles upon modification, which is opposite to what was observed in the current study.

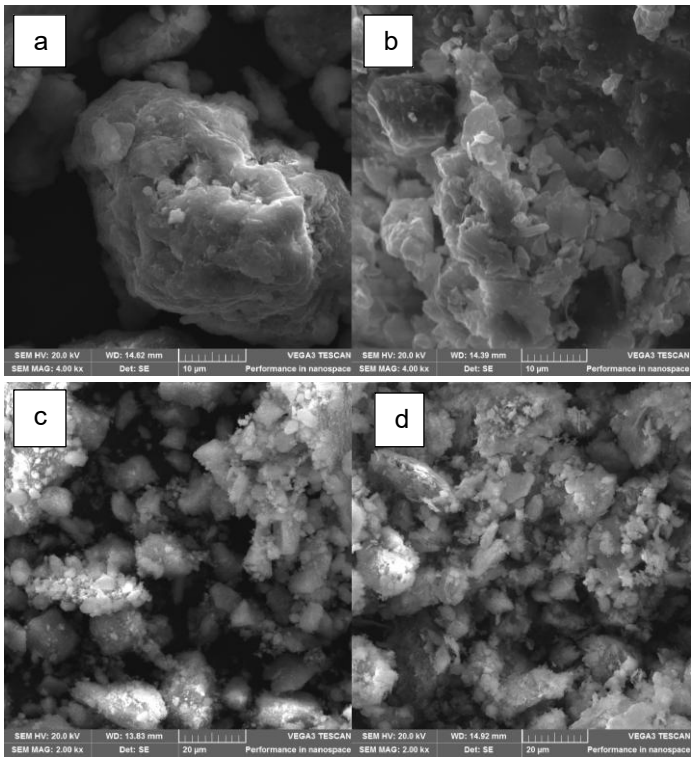

Figure 3.75. SEM images of (a) bentonite (b) organobentonite (c) kaolin and (d) organokaolin.

3.23.2 Characterisation using BET, PXRD and Zetasizer

Summary of the BET, PXRD and Zetasizer characterization results of the four adsorbents are shown in Table 3.27.

The BET specific surface area results indicate that the modification of bentonite and kaolin by HDTMA reduced the specific surface area by almost 50% and 12%, respectively. The average pore sizes and pore volumes also decreased upon modification. A study by Andrunik and Bajda (2019) also reported a decrease in pore volume and specific surface area of bentonite clay upon modification with a cationic surfactant. The decrease in pore size, pore volume and specific surface area can be explained by the change in surface properties of the clays upon incorporating HDTMA. The addition of HDTMA into the interlayer space causes an expansion of the interlayers. The d_{001} space for bentonite increased from 17.6 to 17.9 Å, while that of kaolin increased from 3.59 to 3.68 Å upon modification. This behaviour

leads to an increase in the packing density of the organoclays, as a result, the pores get blocked, leading to a decrease in pore size, pore volume and BET specific surface area (Choi et al., 2023; Schmidt et al., 2020).

Table 3.27 Summary of BET, PXRD and Zetasizer results.

Parameters	Adsorbent			
	Bentonite	Organobentonite	Kaolin	Organokaolin
BET specific surface area (m^2/g)	38.7	19.4	9.51	8.37
Pore size (Å)	190.9	123.9	957.6	95.12
Pore volume (cm^3/g)	0.185	0.0191	0.228	0.0251
Point of zero charge (pHpzc)	None	7.6	2.5	11.1
d_{001}-space (A)	17.6	17.9	3.59	3.68

3.23.3 Characterisation using FTIR spectroscopy and TGA

To confirm the successful incorporation of HDTMA into the clays, further characterization of the modified clay samples was conducted by means of FTIR spectroscopy and TGA analysis. The results of the analysis are recorded in **Figure 3.76**. The FTIR spectra and TGA thermograms of the unmodified kaolin and bentonite clays used in this study are discussed in previous work (Kgabi and Ambushe, 2023). The successful intercalation of HDTMA into the clays' structures has been confirmed in other studies by the appearance of CH_2 and CH_3 group peaks in the region around 2930 and 2870 cm^{-1}, respectively (Dinh et al., 2022; Ltifi et al., 2018). This study also confirmed the successful modification of the clays by HDTMA through these characteristic peak intensities. The sharp CH_2 and CH_3 vibrations observed at 2933 and 2864 cm^{-1} confirm the intercalation of HDTMA onto the clays. The spectra of bentonite, kaolin and organobentonite also show the presence of -OH stretching bands at 3618 – 3684 cm^{-1}. The bands at 995 – 1003 cm^{-1} are assigned to the Si-O stretching vibrations (Kgabi and Ambushe, 2023; Morekhure-Mphahlele et al., 2017). The band at 1472 cm^{-1} is attributed to the N-C stretching of HDTMA (Castro-Castro et al., 2020), further confirming the successful modification.

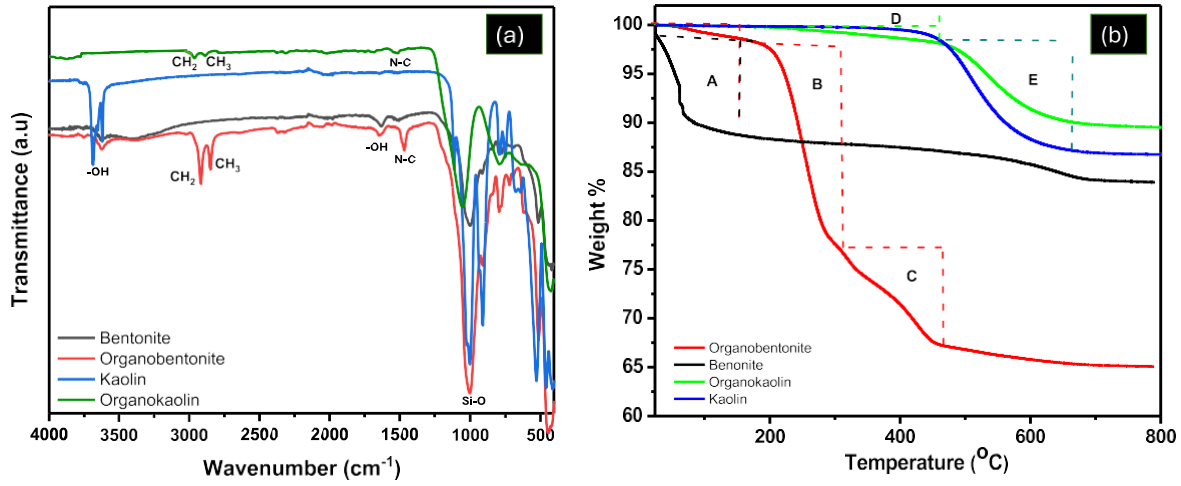

Figure 3.76. (a) FTIR spectra and (b) TGA curves of the natural and modified kaolin and bentonite clays.

To further reconfirm this intercalation of HDTMA into the structures of the clays, the clays were subjected to thermal treatment using TGA set to a temperature range of 25 - 800 °C for 90 minutes. The TGA curve of organobentonite shows three stages of mass loss. The first stage (A) at 90 -200 °C shows a mass loss of 2.8% which is attributed to dehydration of physically adsorbed water molecules and those intercalated in the interlayers. This mass loss is lower than that of unmodified bentonite (12.23%) and confirms the modified bentonite is less hydrophilic (Bousba et al., 2018). The second stage (B) occurs between 200 – 300 °C shows a mass loss of 19.2% which is due to the decomposition of HDTMA on the surface of bentonite (Sternik et al., 2017). The mass loss of 9.7% occurring at the third stage (C) between 300 – 450 °C is due to the decomposition of HDTMA in the interlayer spaces of the clay (Bousba et al., 2018; Sternik et al., 2017).

The TGA curve of organokaolin shows two stages of mass loss, the first stage (D) at temperatures between 220 - 450 °C is likely due to the decomposition of both the HDTMA on the surface and the interlayers of the clay. This mass loss is very minimal compared to that of organobentonite, this is because kaolin has less CEC, as such less HDTMA was used to modify the clay. The second stage of mass loss (E) at 450 - 650 °C is due to dehydroxylation (Kgabi and Ambushe, 2023). The mass loss due to dehydroxylation is less in organokaolin (7.11%) compared to kaolin (13.37%). The annealing of the kaolin prior to modification with HDTMA dehydrolyzes it (Wahyuni et al., 2018), as such organokaolin has fewer OH groups in its interlayers resulting in less dihydroxylation (Wahyuni et al., 2018). Both the FTIR spectra and TGA results confirm the successful intercalation of HDTMA onto bentonite and kaolin clays.

3.24 FACTORS AFFECTING THE PB(II) UPTAKE

3.24.1 Effect of pH

The effect of solution pH on the removal of Pb(II) using bentonite and HDTMA-bentonite was studied by adsorbing 10 mg/L of Pb(II) solution in 100 mL at pH range of 1 to 6. The mass of clay used was 300 mg, and the solution was agitated at 300 rpm for 2 hours. Figure 3.77a shows the results of the study. The pH plays an important role in the removal of Pb(II) due to its impact on the formation of different forms of Pb(II) compounds, such as $Pb(OH)^{+}$ or $Pb(OH)_2$ precipitates (Cruz-Lopes et al., 2021). As depicted in Figure 3.77a, the effectiveness of the adsorption of Pb(II) onto all four adsorbents increased as the pH was raised from 1 to 6. Above the pH of 6, Pb(II) ions precipitated out of solution; hence, pH 6 was chosen as the ideal pH for this study. The precipitation of Pb(II) ions from solution at pHs above 6 was also reported in other studies [54]. Bentonite exhibits a negatively charged surface throughout all pH ranges, as determined by the zeta potential studies. This allows it to remove Pb(II) ions at most pH ranges. The adsorption phenomenon of bentonite and kaolin can be well explained by ion exchange mechanism (Obsa et al., 2024; Dinh et al., 2022). However, the maximum removal of Pb(II) cations at pH of 6 by the two organoclays indicates that the main mechanism of removal is not ion exchange since the point of zero charge (pH_{PZC}) is at pH 7.8 and 10.2 for organobentonite and organokaolin, respectively. This finding suggests the removal of Pb(II) ions by the organoclays is likely to be due to the formation of inner-sphere complexes, as reported in a similar study (Dinh et al., 2022). The modification of bentonite and kaolin reduces hydophilicity of the clay's structures, which allows for the Pb(II) ions to form inner-sphere complexes with the silanol and aluminol groups on the surface of the organoclays (Strawn, 2021).

3.24.2 Effect of Pb(II) concentration

To investigate the maximum Pb(II) concentration removal by the adsorbents, the initial metal ion concentration was varied from 5 to 100 mg/L. The experiments were performed at a pH of 6. Figure 3.77b shows the impact of initial Pb(II) concentrations on the adsorption efficiency of the adsorbents. The results clearly show that the removal efficiency decreases with an increase in initial concentration for all adsorbents. This can be attributed to adsorption site saturation (Dinh et al., 2022). As the concentration of Pb(II) ions in the solution increases, the available adsorption sites on the clay start to get saturated. At higher concentrations, more and more of these sites become saturated with Pb(II) ions, leading to reduced capacity for further adsorption (Tadesse, 2022; Hussain et al., 2021). The maximum adsorption concentration for bentonite and organobentonite was 30 mg/L, while for kaolin and organokaolin, it was 10 mg/L. As expected from the elemental composition of the clays, natural kaolin showed a lower Pb(II) removal compared to natural bentonite due to its having low CEC and specific surface area.

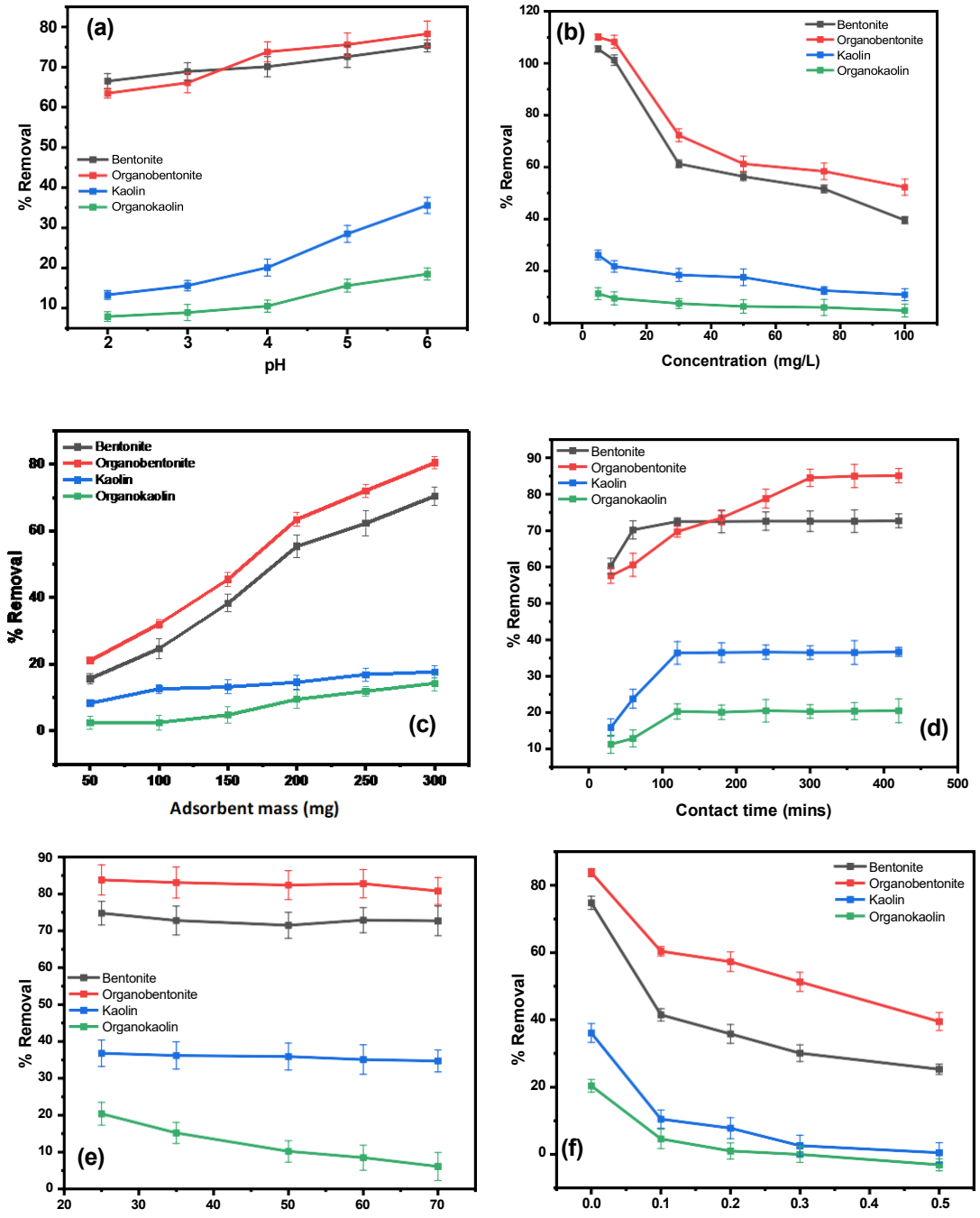

Figure 3.77. The effects of (a) pH, (b) initial Pb(II) concentration, (c) adsorbent mass, (d) contact time, (e) temperature and (f) KCl ionic strength (KCl concentration) on the removal of Pb(II) from solution.

The presence of cations such as Na^+, K^+ and Ca^{2+} allows for bentonite's better ion-exchange capacity (Kumari et al., 2021). Modified kaolin showed a lower Pb(II) removal compared to the natural kaolin, which can be attributed to the increased hydrophobicity of the clay. Because kaolin has a low CEC, the incorporation of HDTMA into its structure renders it almost completely hydrophobic, making it difficult to adsorb the Pb(II) ions in solution.

3.24.3 The effect of adsorbent mass

The effect of adsorbent mass on the removal of Pb(II) was studied through adsorbing 10 mg/L of Pb(II) solutions using kaolin and organokaolin, as well as 30 mg/L of Pb(II) solutions using bentonite and organobentonite at pH of 6 for 2 hours. The mass of the adsorbents was varied between 50 mg and 300 mg. Figure 3.77c shows the results of the study. As expected, the percentage removal of Pb(II) ions from solution increased with an increase in the adsorbent mass. This is because the addition of

more adsorbent implies an increase in the available adsorbent sites for adsorption to take place (Abbou et al., 2021). An increase in the specific surface area allows more opportunities for Pb(II) ions to interact with the surface of the clay with less competition. For bentonite and organobentonite, the mass of 200 mg was sufficient to remove 55% and 65% of the 30 mg/L Pb(II) ions. Although the percentage removal for kaolin and bentonite increased with an increase in the adsorbent dosage, beyond 200 mg/L, there was little change in percentage removal; thus, 200 mg was chosen as the ideal amount of adsorbent for this study.

3.24.4 The effect of contact time

To study the effect of contact time, solutions of 10 mg/L of Pb(II) were treated with kaolin and organokaolin, while 30 mg/L solutions were treated with bentonite and organobentonite using 200 mg of adsorbent at pH 6. The contact time was varied from 30 to 400 minutes. The results from Figure 3.77d indicated that adsorption efficiency increased with contact time until equilibrium: 180 minutes for bentonite, 120 minutes for kaolin and organokaolin, and 300 minutes for organobentonite. Within the first 30 minutes, over 50% of Pb(II) was adsorbed by bentonite and organobentonite, compared to approximately 15% and 10% by kaolin and organokaolin, respectively. The removal capacity increased steadily until equilibrium. Organobentonite's Pb(II) removal gradually increased until equilibrium at 300 minutes. The modification with the surfactant facilitates inner-sphere complex formation [59]. This formation of inner-sphere complexes, while increasing the removal efficiency, also prolonged the time to reach equilibrium due to complex interactions (Dinh et al., 2022; Zhu et al., 2015). The highest percentage removals were 20.1% for organokaolin, 36.4% for kaolin, 72.7% for bentonite, and 82.5% for organobentonite.

3.24.5 The effect of temperature

The effect of temperature on the removal of Pb(II) was studied through adsorbing 10 mg/L of Pb(II) solutions using kaolin and organokaolin, as well as 30 mg/L of Pb(II) solutions using bentonite and organobentonite at a pH of 6, using 200 mg of the adsorbent at the equilibrium contact times reported in section 3.24.4. The temperature was varied between room temperature (23 - 25 °C) and 70 °C. The findings are shown in Figure 3.77e. The results show that Pb(II) removal efficiency by the four adsorbents decreased with an increase in temperature, indicating an exothermic nature of the adsorption. The decrease in the percentage removal could be attributed to the weakening of the attraction between the Pb(II) ions and the clay material (Ergüvenerler et al., 2020; Singh and Bhateria, 2020). This results in a decrease in the sorption of the ions. At high temperatures, the boundary layer's thickness is decreased because of the increased tendency of the Pb(II) ions to desorb from the surface of the adsorbent back into the solution, which results in a decreased adsorption as the temperature is increased (Singh and Bhateria, 2020). Thus, room temperature was chosen as the best temperature for this study. The final concentrations of Pb(II) in solution after treatment were reduced from 10 mg/L to 7.96 mg/L using organokaolin and to 6.33 mg/L using kaolin. For bentonite and organobentonite, the remaining Pb(II) ions in solution were reduced from 30 mg/L to 8.12 mg/L and 5.25 mg/L, respectively.

3.24.6 The effect of ionic strength (KCl concentration)

The effect of ionic strength on the adsorption of Pb(II) ions onto the various adsorbents was studied by varying KCl concentration. The results shown in **Figure 3.77f** demonstrated that the removal efficiency of Pb(II) decreased with increasing KCl concentration. Specifically, organobentonite's adsorption dropped from 83% to 41%, while bentonite, kaolin, and organokaolin showed reductions from 78.2%, 37.4%, and 20.8% to 21.1%, 3.7%, and 0.1%, respectively. The electrostatic attraction between the K^+ cations and the permanent negative charge on the clay's surface can result in the formation of outer-sphere complexes at the planar sites. Inner-sphere complexes can also be formed between the K^+ cations and the Al-O- and Si–O–groups in the clays' structure (Dinh et al., 2022). Thus, this leads to fewer adsorption sites being available for the uptake of the Pb(II) ions, resulting in a lower percentage removal of Pb(II) by the adsorbents. Similar findings were reported elsewhere (Hu et al., 2014), where the presence of Na^+ in solution resulted in a decrease in the adsorption of Cd(II) ions.

3.25 REAL WATER TREATMENT AND REUSABILITY STUDIES

The application of the clay adsorbents to real water samples is of crucial importance for industrial applications. Figure 3.78 shows the treatment of borehole water samples using the four adsorbents. The removal percentages for Pb(II) ions in solution were 72.3% for bentonite, 77.8% for organobentonite, 21.9% for kaolin and 5.4% for organokaolin. Due to the loss of the clay sample with each regeneration cycle, 1.0 g mass was used as the initial mass for this study. Considering the initial mass used in this experiment was 1.0 g, compared to the mass of 200 mg used for the simulated solutions, it is evident that the percentage removal for Pb(II) in borehole water samples is lower compared to that of simulated solutions. This can be attributed to the presence of other competing ions in solution. The real water sample contains trace amounts of other PTEs such as Cd, Cr, As and others, which all compete for the active sites on the adsorbents.

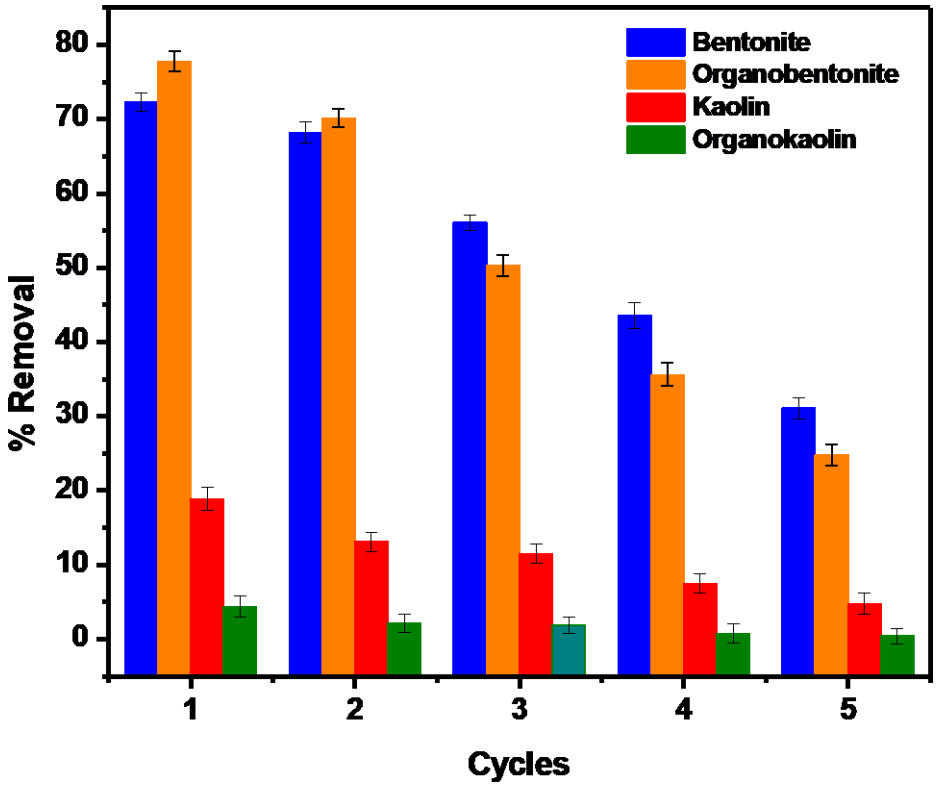

Figure 3.78. Reusability cycles of the four adsorbents on Pb(II) uptake.

The reusability of adsorbents is another important factor in determining the economic feasibility of the adsorbents in terms of production costs. Therefore, investigating the reusability of adsorbent materials is essential. The spent adsorbents were regenerated using 0.01 M HCl as a desorbing agent (Mudzielwana, 2019). Figure 3.78 shows that the removal efficiency of the adsorbents decreased with each of the four regeneration cycles. For the first two cycles, organobentonite removed more Pb(II) ions from solution compared to the natural bentonite, however, from cycle 3 the performance of organobentonite decreased sharply and the regenerated natural bentonite showed greater efficiency than that of organobentonite. The regeneration of organobentonite with HCl may lead to the destruction of the surfactant, and therefore changing the chemistry of the clay. This results in decreased performance of the clay with each regeneration cycle (Momina et al., 2018). The decrease in Pb(II) percentage removal with each cycle may also be due to incomplete Pb(II) ions removal from previous cycles, which reduce the available active sites for the adsorption of more Pb(II) ions (Mudzielwana, 2019). The successful regeneration of the adsorbents for up to four cycles indicate their potential as a stable and re-usable adsorbent for Pb(II) removal from real water samples.

3.26 WORKSHOP ON COMMUNITY ENGAGEMENT

This section focuses on community engagement workshop, which outlines the workshop activities, the targeted communities, and findings of the research that were presented in the workshop.
The workshop was held on 3rd and 4th of October 2024 in Polokwane, Limpopo province. The workshop involved participation of project leaders and team members of other currently running and recently completed projects that focused on water quality of water bodies in Limpopo province. These projects include:

1. Investigation of Potentially Toxic Elements in Selected Water Bodies in Limpopo Province: Transport, Fate and Risk Assessment, and Detection and Remediation Method Development – In progress (Project leader: Prof AA Ambushe (University of Johannesburg))
2. A Combination of Rapid Direct Analysis and Machine Learning Assisted Suspect Screening of Emerging Pollutants and their Contribution to Antimicrobial Resistance – In progress (Project leader: Dr Nuapia (University of Limpopo))
3. Development and Testing of Zr^{4+}/Ag^{+} Metal Oxide Modified Zeolite-Cellulose Membrane for Fluoride and Pathogen Removal from Groundwater-Completed (Project leader: Dr Mudzielwana (University of Venda))

The project leaders of the aforementioned projects met via Microsoft Teams on 17 July 2024. The meeting was chaired by Dr Eunice Ubomba-Jaswa (Research Manager: Water Resources Quality & Management), and the project leaders agreed to run the workshop on 3 and 4 October 2024 in Polokwane, Limpopo province. The stakeholders from different sectors and communities were invited to participate in this workshop. These include water treatment professionals from municipalities and communities in the study areas in Limpopo province. Project leaders and team members of the above three projects participated and presented the findings of their research.

The presentations from this project entailed the status of water quality of selected rivers as well as borehole water in study areas, with special focus on levels of potentially toxic elements and their species. The human health risk assessment associated with water and vegetables was presented in this workshop. The treatment methods developed using agricultural by-products were presented in this workshop. This project included fabrication of ion-imprinted polymer-based sensors for the detection of toxic elemental species such as Pb, Cd and Hg in water. The developments in sensor fabrication and their application will also be presented in the workshop.

The Community Engagement Workshop on Water Quality was held from 3 to 4 October 2024 in Polokwane, Limpopo Province. The workshop focused on the knowledge dissemination of outputs from the Water Research Commission (WRC) funded projects. (Research Manager: Water Resources Quality & Management) and Ms Penny Jaca from the WRC attended the workshop. Dr Eunice Ubomba-Jaswa delivered opening remarks. Prof AA Ambushe presented an oral presentation entitled: “Identifying the Complex Drivers of Water Quality Deterioration in Limpopo Province and Strategies to Improve and Remediate Water in South Africa”. Prof MA Mamo also attended the workshop and presented an oral presentation entitled: “A novel chemo-resistive sensor for sensitive detection of Pb(II) ions using interdigital gold electrode fabricated with reduced graphene oxide-based ion-imprinted polymer”. Both Prof AA Ambushe and Prof MA Mamo chaired presentation sessions and discussions with invited stakeholders. Seven postgraduate students (Sifelani Dube, Vincent Masilela, Ntsieni Molaudzi, Pertunia Dikotla, Tsakane Maluleke, Samuel Makobe and Lutendo Mashavha) from Prof Ambushe’s research group attended the workshop and presented their research findings as oral presentations and all performed very well. Dr Nuapia from the University of Limpopo presented via Teams presented an oral presentation. Dr Mudzielwana from the University of Venda and his team presented three oral presentations. Dr Mudzielwana also chaired a session. Prof Ambushe’s collaborators from the University of Limpopo (Prof Magadzu and Dr Macevele) attended the workshop.

Prof Magadzu chaired a session and Dr Macevele delivered an oral presentation. Each workshop session was followed by questions, comments and discussion, which gave opportunities to stakeholders to participate in the discussion. The workshop offered an opportunity for invited stakeholders to understand the findings of the research work on the water quality of rivers in Limpopo Province and possible solutions from these projects that might have a direct application to the problems of the communities residing in the vicinity of polluted water bodies. The workshop also served as a platform for stakeholders to express their research needs regarding water quality in the province to the WRC and the Universities of Johannesburg, Limpopo and Venda, which should enable better alignment between research output and stakeholder needs.

CHAPTER 4: CONCLUSIONS AND RECOMMENDATIONS

The methods employed in this study yielded accurate results for quantification of As, Cd, Cr, Cu, Pb, Ni, Hg, and V in water, sediment, soil, and vegetable samples with quantitative percentage recoveries, which ranged from 75.5 to 115%. It was observed that the total concentrations of As, Cd, Cr, Cu, Pb, Hg, Ni, and V in water were below the MPLs stipulated by the WHO, SANS and DWAF during both low and high flow seasons. As a result, the water from Mokolo River was found to be safe for drinking and irrigation purposes with respect to the measured PTEs (As, Cd, Cr, Cu, Pb, Hg, Ni, and V). The total concentrations of Cd, Pb, and Hg in sediment in both seasons surpassed the PEL values recommended by Canadian sediment quality guidelines in some sites, suggesting that adverse biological effects will occur frequently on the aquatic species and food chain with respect to these analytes. This threatens the aquatic species available and was likely linked to untreated industrial effluents and sewage discharge into the river. The total concentrations of Cd, Cr, and Cu surpassed the soil quality guidelines stipulated by the CCME, posing a serious threat to the food chain, and this was linked to the use of fertilizers, which presumably contain the PTEs at the farms to improve the fertility of the soil. The total concentrations of Cd, Cr, Hg, Ni, and V surpassed the MPLs stipulated by WHO/FAO during the low-flow season, whereas Cd, Cr, Cu, Pb, Ni, and V exceeded during the high-flow season. Increased concentration of As, Cd, Cr, Cu, Pb, Hg, Ni, and V were observed in water, sediment, soil, and vegetables during the high-flow season than during the low-flow season. Thus, this variation is due to higher water levels in seasons of higher precipitation or rainfall, whereby PTEs are carried out by rain from the environment into the water bodies. The non-carcinogenic health risk assessment revealed that the THQ values of PTEs owing to consumption of vegetables from the farms in the vicinity of Mokolo River were greater than 1 for As, Cd, Cr, Cu, Ni, and Pb with respect to the adult population. Additionally, it was discovered that due to consumption of these vegetables, the THQ values of PTEs for the child population were greater than 1 for As, Cd, Cr, Cu, Pb, Ni, and Hg. Due to the consumption of each vegetable, the total non-carcinogenic effect of PTEs as calculated by the HI was greater than 1 for both the adult and child population. This suggests that there are possible health risks threatening the health of the Lephalale adult and child population consuming these contaminated vegetables. This study revealed that non-carcinogenic health risks associated with vegetable consumption would be far greater in children than in adults with THQs, suggesting that serious chronic risks could be observed. The carcinogenic risk assessment indicated that the probability of higher cancer risks associated with vegetable consumption was 4.73 times higher in children than in adults. When the assessment was based on the toxic As and Cr species, Cr(VI) had the highest cancer risk. In general, it was concluded that the consumption of contaminated vegetables could result in high cancer risks for both adults and children.

This study also investigated the presence and distribution of selected PTEs in water, soil, sediment, and vegetable samples from the Sekhukhune District, focusing on seasonal variations and associated health risks. The findings revealed that Cr and V were the dominant contaminants in both river and borehole water samples, particularly during the low-flow season. These elevated concentrations are likely linked to industrial activities, such as mining and smelting, as well as the proximity to roads and human settlements. In addition to water contamination, the study highlighted the significant accumulation of PTEs in soils and vegetables irrigated with borehole water. High concentrations of Cr,

V, Pb, and As were detected in soils, particularly in farms located near industrial and road areas. Vegetables such as cabbage and spinach showed elevated levels of Cu and Cr, raising concerns about the transfer of contaminants from soil to edible plants, which poses a potential risk to human health through dietary intake. Overall, the study revealed that industrial activities, particularly mining and smelting, could be major contributors to PTEs contamination in the region. The findings indicate the need for regular monitoring of water, soil, and vegetable quality to mitigate health risks and ensure the sustainability of agricultural practices. The human health risk assessment of this study revealed significant health risks associated with the ingestion of PTEs through contaminated water and vegetables in the Sekhukhune District. The evaluation, based on HQ and HI metrics, highlighted risks to both adults and children, with children being more vulnerable during both low and high-flow seasons.

This study also presented a highly effective approach for fabricating a Cd(II) sensor based on rGO and IIPs. Through systematic optimisation, the sensor demonstrated an excellent sensitivity of 1.765 µg/L, selectivity, and stability, particularly with the 1:3 (IIP:rGO ratio), which emerged as the most suitable configuration for practical applications. The results confirmed a LOD of 0.704 µg/L in a dynamic linear range of 5 - 600 µg/L Cd(II) solution, which revealed the robustness of the sensor's molecular recognition sites and its ability to maintain consistent performance over multiple measurement cycles and extended storage periods. While some drift was observed over a sixty-day period, the response profiles retained their characteristic patterns, indicating that the sensor's fundamental sensing mechanism remained intact. Percentage recoveries of 91.6% to 105% from real water sample analysis emphasise the potential of the rGO-IIP-based sensor for real-world applications in environmental monitoring and other analytical fields. Future work should focus on enhancing long-term stability and selectivity through improved fabrication techniques and storage conditions.

This study successfully assessed and compared the efficacy of calcined OPs and SCB for removing Ni(II) and Cd(II), both individually and in combined form, from simulated aqueous solution and real wastewater samples (AMD). Investigation of Ni(II) and Cd(II) bio-sorption included examining the impacts of pH, contact time, bio-sorbent dosage, initial metal ion concentration, and solution temperature. The results revealed that calcined OPs achieved over 99% removal of 20 mg/L Ni(II) within 60-90 minutes, while calcined SCB reached over 97% removal within 120 minutes. The OPs: SCB composite, in a 5:5 ratio, removed over 92% of Ni(II) under optimal conditions. Calcined OPs could remove over 98% of 20 mg/L Cd(II) at an optimum contact time of 120 minutes, and calcined SCB could remove over 96% at the same optimum contact time. The OPs:SCB composite were able to remove over 92% of Cd(II) at a 5:5 ratio at an optimum contact time of 60 minutes.

In this study, organokaolin and organobentonite were successfully synthesized using HDTMA as the modifier, and the adsorbents' efficiency in removing Pb(II) from aqueous solutions was investigated. Organobentonite showed a higher Pb(II) adsorption capacity (18.75 mg/g) compared to the natural bentonite (14.71 mg/g) , while the opposite effect was observed for kaolin (4.19 mg/g) and organokaolin (2.26 mg/g). The most favorable conditions for Pb(II) removal were pH = 6, room temperature (23 - 25 °C) and adsorbent mass of 200 mg. The ideal contact time for adsorption by organokaolin, kaolin and bentonite were 120 minutes, while for organobentonite it was 300 minutes. This time increase in organobentonite-Pb(II) adsorption is due to the formation of new chemical bonds. The results of the removal of Pb(II) using kaolin and organokaolin were unsatisfactory due to the low adsorption capacities determined. The combination of bentonite and HDTMA did, however, demonstrate the synergetic advantage towards Pb(II) adsorption. The reusability study also revealed that the spent adsorbents can be reused to achieve good Pb(II) percentage removal for up to four cycles. Overall, the results of this study showed that organobentonite and bentonite can serve as promising materials for the removal of Pb(II) ions from water/wastewater in South Africa and other countries. However, modifying bentonite with HDTMA increases the costs of the adsorbent material. The unmodified natural bentonite yielded about 79% of the capacity of removal of Pb(II) by organobentonite. Furthermore, to achieve the best removal of Pb(II) by organobentonite, it required 300 minutes compared to the contact time of 120 minutes, which needed by bentonite to achieve the highest removal of Pb(II). Thus, taking into

consideration costs incurred by modification and the longer time required to achieve the best removal of Pb(II) using organobentonite as an adsorbent material, we recommend the use of natural bentonite, which yielded quantitative removal of Pb(II) from water. This study is not only limited to Pb but can also be extended to treating other PTEs such as Cr, As, Cd and others from aqueous solutions.

REFERENCES

Abdul Halim, A., Sulaiman, S. S., Nordin, A. N., & Bajunaid Hariz, H. (2024). Systematic review study on application of Ion Imprinted Polymer (IIP) in heavy metals detection. International Journal of Environmental Analytical Chemistry, 104(16), 4470-4494. https://doi.org/10.1080/03067319.2022.2106426

Abbou, B.; Lebkiri, I.; Ouaddari, H.; Kadiri, L.; Ouass, A.; Habsaoui, A.; Lebkiri, A.; Rifi, E.H. Removal of Cd(II), Cu(II), and Pb(II) by Adsorption onto Natural Clay: A Kinetic and Thermodynamic Study. *Turk J Chem* **2021**, *45*, 362, doi:10.3906/KIM-2004-82.

Addo-Bediako, A., 2020. Assessment of heavy metal pollution in the Blyde and Steelpoort Rivers of the Olifants river system, South Africa. Pol J Environ Stud 29, 3023–3029. https://doi.org/10.15244/pjoes/112621

Addo-Bediako, A., Matlou, K., Makushu, E., 2018. Heavy metal concentrations in water and sediment of the Steelpoort River, Olifants River System, South Africa. Afr J Aquat Sci. https://doi.org/10.2989/16085914.2018.1524745

Adhikari, Sutapa, Marcelo-Silva, J., Beukes, J.P., van Zyl, P.G., Coetsee, Y., Boneschans, R.B., Siebert, S.J., 2022a. Total and hexavalent chromium and other potentially toxic element contamination of useful plant leaves in a polluted mining-smelting region of South Africa and health risks. Environmental Advances 100260. https://doi.org/10.1016/j.envadv.2022.100260

Adhikari, S, Marcelo-Silva, J., Beukes, J.P., van Zyl, P.G., Coetsee, Y., Boneschans, R.B., Siebert, S.J., 2022b. Contamination of useful plant leaves with chromium and other potentially toxic elements and associated health risks in a polluted mining-smelting region of South Africa. Environmental Advances 9, 1–11. https://doi.org/10.1016/J.ENVADV.2022.100301

Adhikari, Sutapa, Marcelo-Silva, J., Beukes, J.P., van Zyl, P.G., Coetsee, Y., Boneschans, R.B., Siebert, S.J., 2022c. Total and hexavalent chromium and other potentially toxic element contamination of useful plant leaves in a polluted mining-smelting region of South Africa and health risks. Environmental Advances. https://doi.org/10.1016/j.envadv.2022.100260

Adhikari, S., Marcelo-Silva, J., Rajakaruna, N., Siebert, S.J., 2022. Influence of land use and topography on distribution and bioaccumulation of potentially toxic metals in soil and plant leaves: A case study from Sekhukhuneland, South Africa. Science of The Total Environment 806, 150659. https://doi.org/10.1016/j.scitotenv.2021.150659

Al-Ghouti, M.A., Al-Absi, R.S. (2020). Mechanistic understanding of the adsorption and thermodynamic aspects of cationic methylene blue dye onto cellulosic olive stones biomass from wastewater. Scientific Reports, 10(1), 1–18. https://doi.org/10.1038/s41598-020-72996-3.

Alberoni, C., Barroso-Martín, I., Infantes-Molina, A., Rodríguez-Castellón, E., Talon, A., Zhao, H., You, S., Vomiero, A., & Moretti, E. (2021). Ceria doping boosts methylene blue photodegradation in titania nanostructures. Materials Chemistry Frontiers, 5(11), 4138-4152. https://doi.org/10.1039/d1qm00068c

Ali, H., Khan, E. and Ilahi, I. (2019) 'Environmental Chemistry and Ecotoxicology of Hazardous Heavy Metals : Environmental Persistence , Toxicity , and Bioaccumulation', *Journal of Chemistry*, 2019, pp. 1–14. Available at: https://doi.org/10.1155/2019/6730305%0AReview.

Alkhatib, M. *et al.* (2022) 'Heavy Metals Concentrations in Leafy Vegetables in Palestine , Case Study : Jenin and Bethlehem Districts', *Journal of Environmental Protection*, 13, pp. 97–111. doi: 10.4236/jep.2022.131006.

Alloway, B. J. (2013). Sources of heavy metals and metalloids in soils, Heavy metals in soils: Trace metal and metalloids in soils and Bioavailability. springer, Dordrecht, Netherlands, 1-50.

Alam, S. N., S., Sharma, N. & Kumar, L. (2017). Synthesis of Graphene Oxide (GO) by Modified Hummers Method and Its Thermal Reduction to Obtain Reduced Graphene Oxide (rGO). Graphene, 6, 1–18.

Alsafran, M., Usman, K., Rizwan, M., Ahmed, T. & Al Jabri, H. The Carcinogenic and Non-Carcinogenic Health Risks of Metal(oid)s Bioaccumulation in Leafy Vegetables: A Consumption Advisory. *Front. Environ. Sci.* **9**, 380 (2021).

Ametepey, S.T., Cobbina, S.J., Akpabey, F.J., Duwiejuah, A.B., Abuntori, Z.N., 2018. Health risk assessment and heavy metal contamination levels in vegetables from tamale metropolis, Ghana. Int J Food Contam 5, 1–8. https://doi.org/10.1186/s40550-018-0067-0

Amwele, H.R., Motsei, L., Kalumbu, G., Kgabi, N., Raymond, L.N., Victor, M.T., 2017. Investigation of possible human exposure to metals concentration in vegetables. J Toxicol Environ Health Sci 9, 66–72. https://doi.org/10.5897/jtehs2016.0375

Andrunik, M.; Bajda, T. Modification of Bentonite with Cationic and Nonionic Surfactants: Structural and Textural Features. *Materials* **2019**, *12*, doi:10.3390/MA12223772.

Amwele, H. R., Motsei, L., Kalumbu, G., Kgabi, N., Limen Njinga, R. and Tshivhase, V. M. (2017). Investigation of possible human exposure to metals concentration in vegetables. J. Toxicol. Environ. Heal. Sci., 9, 66–72.

Antoniadis, V., Golia, E.E., Liu, Y.-T., Wang, S.-L., Shaheen, S.M., Rinklebe, J. (2019). Soil and maize contamination by trace elements and associated health risk assessment in the industrial area of Volos, Greece. Environment international, 124, 79-88.

Anwar, S., Nawaz, M. F., Gul, S., Rizwan, M., Ali, S., and Kareem, A. (2016). Uptake and Distribution of Minerals and Heavy Metals in Commonly Grown Leafy Vegetable Species Irrigated with Sewage Water. Environ. Monit. Assess. 188 (9), 541. doi:10.1007/s10661-016-5560-4

Aralu, C.C., Okoye, P.A.C., Abugu, H.O., Ochiagha, K.E., Egbueri, J.C., 2024. Evaluating the seasonal variations of risks associated with potentially toxic elements in underground water sources near a dumpsite in Awka, Nigeria. Journal of Hazardous Materials Advances 15, 1–12. https://doi.org/10.1016/j.hazadv.2024.100440

Aschale, M., Sileshi, Y. and Kelly-quinn, M. (2019) 'Health risk assessment of potentially toxic elements via consumption of vegetables irrigated with polluted river water in Addis', *Environmental Systems Research*, 8(29), pp. 1–13. doi: 10.1186/s40068-019-0157-x.

Atangana, E., Oberholster, P.J., 2021. Using heavy metal pollution indices to assess water quality of surface and groundwater on catchment levels in South Africa. Journal of African Earth Sciences 182, 1–12. https://doi.org/10.1016/j.jafrearsci.2021.104254

Baig, U., Rao, R.A.K., Khan, A.A., Sanagi, M.M. and Gondal, M. A. (2015). Removal of carcinogenic hexavalent chromium from aqueous solutions using newly synthesized and characterized polypyrrole–titanium (IV) phosphate nanocomposite. Chem. Eng. J., 280, 494–504.

Bajpai, M. and Katoch, S. (2017). Treatment of first-flush rainwater by natural low-cost adsorbents using multimedia filter technology, Engineering Sciences International Research Journal, 5, pp.58-62.

Bello, S., Nasiru, R., Garba, N. N. & Adeyemo, D. J. Carcinogenic and non-carcinogenic health risk assessment of heavy metals exposure from Shanono and Bagwai artisanal gold mines, Kano state, Nigeria. *Sci. African* **6**, e00197 (2019).

Belew, A.A., Besha, A.T., Belete, A.A., 2024. Determination of heavy metals and health risk assessment in drinking water in Jigjiga City, Ethiopia. Discover Environment 2, 1–21. https://doi.org/10.1007/s44274-024-00071-z

Benford, D., Ceccatelli, S., Cottrill, B., DiNovi, M., Dogliotti, E., Edler, L., Farmer, P., Fürst, P.,

Hoogenboom, L., Katrine Knutsen, H., Lundebye, A.-K., Metzler, M., Stefano Nebbia, C., Rietjens, I., *et al.* Scientific Opinion on the risks to public health related to the presence of chromium in food and drinking water. *EFSA J.* **12**, 3595 (2014).

Beronius, A. & Vandenberg, L. N. Using systematic reviews for hazard and risk assessment of endocrine disrupting chemicals. Rev. Endocr. Metab. Disord. 16, 273–287 (2015).

Bhardiya, S. R., Asati, A., Sheshma, H., Rai, A., Rai, V. K., & Singh, M. (2021). A novel bioconjugated reduced graphene oxide-based nanocomposite for sensitive electrochemical detection of cadmium in water. Sensors and Actuators B: Chemical, 328, 129019. https://doi.org/https://doi.org/10.1016/j.snb.2020.129019

Bhuyan, M.S., Bakar, M.A., 2017. Seasonal variation of heavy metals in water and sediments in the Halda River, Chittagong, Bangladesh. Environmental Science and Pollution Research 24, 27587–27600. https://doi.org/10.1007/s11356-017-0204-y

Bousba, S.; Bougdah, N.; Messikh, N.; Magri, P. Adsorption Removal of Humic Acid from Water Using a Modified Algerian Bentonite. *Physical Chemistry Research* **2018**, *6*, 613–625, doi:10.22036/PCR.2018.129154.1482.

Branger, C., Meouche, W. and Margaillan, A. (2013). Recent advances on ion-imprinted polymers. React. Funct. Polym. 73, 859–875.

Birch, G.F., Wang, X., Liu, E., Laidlaw, M., 2023. Similarity in human health risk assessment using models of soil-blood lead levels (IEUBK) and non-carcinogenic condition (US EPA 2002). Science of the Total Environment 898, 1–8. https://doi.org/10.1016/j.scitotenv.2023.165512

Brunauer, S., Emmett, P. H. & Teller, E. (1938). Adsorption of Gases in Multimolecular Layers. J Am Chem Soc, 60, 309–319.

Bvenura, C. and Afolayan, A. J. (2012) 'Heavy metal contamination of vegetables cultivated in home gardens in the Eastern Cape', *South African Journal of Science*, 108(9/10), pp. 1–6.

Cai, X. *et al.* (2014). Novel Pb2+ ion imprinted polymers based on ionic interaction via synergy of dual functional monomers for selective solid-phase extraction of Pb2+ in water samples. ACS Appl Mater Interfaces, 6, 305–313.

Cao, H., Yang, P., Ye, T., Yuan, M., Yu, J., Wu, X., Yin, F., Li, Y., & Xu, F. (2021). Recognizing adsorption of Cd(Ⅱ) by a novel core-shell mesoporous ion-imprinted polymer: Characterization, binding mechanism and practical application. Chemosphere, 278, 130369. https://doi.org/https://doi.org/10.1016/j.chemosphere.2021.130369

Carbon Waters. (2020). How to differentiate Graphene: Production processes. *Graphene* https://www.carbon-waters.com/how-to-differentiate-graphene/

Caruso, J.A., Montes-Bayon, M. (2003). Elemental speciation studies—new directions for trace metal analysis, Ecotoxicology and Environmental Safety, 56, 148 – 163.

Castro-Castro, J.D.; Macías-Quiroga, I.F.; Giraldo-Gómez, G.I.; Sanabria-González, N.R. Adsorption of Cr(VI) in Aqueous Solution Using a Surfactant-Modified Bentonite. *Scientific World Journal* **2020**, *2020*, doi:10.1155/2020/3628163.

Caussy, D., Gochfeld, M., Gurzau, E., Neagu, C., Ruedel, H. (2003). Lessons from case studies of metals: investigating exposure, bioavailability, and risk, Ecotoxicology and Environmental Safety, 56, 45-51.

Chakraborty, P., Jayachandran, S., Babu, P.V.R., Karri, S., Tyadi, P., Yao, K.M., Sharma, B.M. (2012). Intra-annual variations of arsenic totals and species in tropical estuary surface sediments. Chem. Geol. 322–323, 172–180.

Chanra, J.; Budianto, E.; Soegijono, B. Surface Modification of Montmorillonite by the Use of Organic Cations via Conventional Ion Exchange Method. *IOP Conf Ser Mater Sci Eng* **2019**, *509*, doi:10.1088/1757-899X/509/1/012057.

Chen, K., Zhang, T., Chen, X., He, Y. & Liang, X. (2018). Model construction of micro-pores in shale: A case study of Silurian Longmaxi Formation shale in Dianqianbei area, SW China. Petroleum Exploration and Development, 45, 412–421.

Chen, M.L., Ma, L.Y., Chen, X.W. (2014). New procedures for arsenic speciation: A review, Talanta, 125, 78-85.

Cheng, S., Zhang, L., Xia, H., & Peng, J. (2017). Characterization and adsorption properties of La and Fe modified activated carbon for dye wastewater treatment. Green Processing and Synthesis, 6(5), 487-498. https://doi.org/10.1515/gps-2016-0120

Choi, N.; Son, Y.; Kim, T.H.; Park, Y.; Hwang, Y. Adsorption Behaviors of Modified Clays Prepared with Structurally Different Surfactants for Anionic Dyes Removal. *Environmental Engineering Research* **2023**, *28*, doi:10.4491/EER.2022.076.

Choudhari, U., Ramgir, N., Late, D., Jagtap, S., Debnath, A. K., & Muthe, K. P. (2023). Selective detection of Cd (II) and Cr (VI) ions using rGO functionalized metal doped SnO2 nanocomposites. Microchemical Journal, 190, 108728. https://doi.org/https://doi.org/10.1016/j.microc.2023.108728

Codex alimentarius commission joint FAO/WHO, 2002. AGENDA ITEM 4 CX/AF 02/5 May 2002 JOINT FAO/WHO FOOD STANDARDS PROGRAMME AD HOC INTERGOVERNMENTAL CODEX TASK FORCE ON ANIMAL FEEDING Third Session INFORMATION PAPER ON ESTABLISHMENT OF CODEX MAXIMUM LEVELS AND RESIDUES LIMITS FOR FEEDINGSTUFFS AND FOODS Prepared by the Secretariat of the Codex Alimentarius Commision BACKGROUND. Denmark.

Constantine, M., Musingafi, C. and Tom, T. (2014). Fresh water sources pollution: A human related threat to fresh water security in South Africa, Journal of Public policy and Governance. Available at: http://www.rassweb.com72 (Accessed: 22 April 2021).

Costa, M., Di Masi, S., Garcia-Cruz, A., Piletsky, S. A., & Malitesta, C. (2023). Disposable electrochemical sensor based on ion imprinted polymeric receptor for Cd(II) ion monitoring in waters. Sensors and Actuators B: Chemical, 383, 133559. https://doi.org/10.1016/j.snb.2023.133559

Cruz-Lopes, L.P.; Macena, M.; Esteves, B.; Guiné, R.P.F. Ideal PH for the Adsorption of Metal Ions Cr6+, Ni2+, Pb2+in Aqueous Solution with Different Adsorbent Materials. *Open Agric* **2021**, *6*, 115–123, doi:10.1515/OPAG-2021-0225/MACHINEREADABLECITATION/RIS.

Cui, L., Wu, J. and Ju, H. (2015). Electrochemical sensing of heavy metal ions with inorganic, organic and bio-materials. Biosens. Bioelectron. 63, 276–286.

Cui, W., Meng, Q., Feng, Q., Zhou, L., Cui, Y. & Li, W. Occurrence and release of cadmium, chromium, and lead from stone coal combustion. *Int. J. Coal Sci. Technol.* **6**, 586–594 (2019).

Dadar, M., Adel, M., Nasrollahzadeh Saravi, H. & Fakhri, Y. (2017). Trace element concentration and its risk assessment in common kilka (Clupeonella cultriventris caspia Bordin, 1904) from southern basin of Caspian Sea. Toxin Rev. 36, 222–227.

Datry, T., Malard, F., Gibert, J., 2004. Dynamics of solutes and dissolved oxygen in shallow urban groundwater below a stormwater infiltration basin. Science of the Total Environment 329, 215–229. https://doi.org/10.1016/j.scitotenv.2004.02.022

De Leon, C.A.P., Montes-Bayon, M., Caruso, J.A. (2002). Elemental speciation by chromatographic separation with inductively coupled plasma mass spectrometry detection, Journal of Chromatography A, 974, 1 – 21.

Department of Cooperative governance and traditional affairs, 2019. PROFILE: SEKHUKHUNE DISTRICT.

Dikotla, P., Ambushe, A.A., 2024. INVESTIGATION OF TRANSPORT AND FATE OF SELECTED TOXIC METALS IN. Johannesburg.

Ding, C., Deng, Y., Merchant, A., Su, J., Zeng, G., Long, X., Zhong, M.-E., Yang, L., Gong, D., Bai, L., Zhou, X., & Liu, X. (2023). Insights into Surface Ion-imprinted Materials for Heavy Metal Ion Treatment: Challenges and Opportunities. Separation & Purification Reviews, 52(2), 123-134. https://doi.org/10.1080/15422119.2022.2044352

Dinh, V.P.; Nguyen, P.T.; Tran, M.C.; Luu, A.T.; Hung, N.Q.; Luu, T.T.; Kiet, H.A.T.; Mai, X.T.; Luong, T.B.; Nguyen, T.L.; et al. HTDMA-Modified Bentonite Clay for Effective Removal of Pb(II) from Aqueous Solution. *Chemosphere* **2022**, *286*, doi:10.1016/j.chemosphere.2021.131766.

Dintsi, B.S., Letsoalo, M.R., Ambushe, A.A., 2023. Bioaccumulation and Human Health Risk Assessment of Arsenic and Chromium Species in Water–Soil–Vegetables System in Lephalale, Limpopo Province, South Africa. Minerals 13, 1–27. https://doi.org/10.3390/min13070930

Dokou, Z., Karagiorgi, V., Karatzas, G.P., Nikolaidis, N.P., Kalogerakis, N. (2016). Large scale groundwater flow and hexavalent chromium transport modeling under current and future climatic conditions: the case of Asopos River Basin, Environ Sci Pollut Res, 23: 5307–5321.

Duan, B., Zhang, W., Zheng, H., Wu, C., Zhang, Q. & Bu, Y. Comparison of Health Risk Assessments of Heavy Metals and As in Sewage Sludge from Wastewater Treatment Plants (WWTPs) for Adults and Children in the Urban District of Taiyuan, China. *Int. J. Environ. Res. Public Health* **14**, 1194 (2017).

Du, Y., Gao, B., Zhou, H., Ju, X., Hao, H., Yin, S., 2013. Health Risk Assessment of Heavy Metals in Road Dusts in Urban Parks of Beijing, China. Procedia Environ Sci 18, 299–309. https://doi.org/10.1016/j.proenv.2013.04.039

DWAF, 1996. Department of Water Affairs and Forestry WATER QUALITY GUIDELINES DOMESTIC USE, second edition. ed. Department of water affairs and forestry, Pretoria.

DWAF (1996) *WATER QUALITY GUIDELINES DOMESTIC*. 2nd edn. Pretoria: Department of Water Affairs and Forestry.

Edokpayi, Joshua Nosa, Enitan, A.M., Mutileni, N., Odiyo, J.O., 2018. Evaluation of water quality and human risk assessment due to heavy metals in groundwater around Muledane area of Vhembe District, Limpopo Province, South Africa. Chem Cent J 12, 1–16. https://doi.org/10.1186/s13065-017-0369-y

EFSA, E. Scientific Opinion on Arsenic in Food. *Sci. Opin. Arsen. Food EFSA J.* **7**, 1351–1355 (2009).

Envirotech Online. (2019). Analytical challenges in mercury determination. *Environmental Laboratory* https://www.envirotech-online.com/news/environmental-laboratory/7/milestone-srl/analytical-challenges-in-mercury-determination/48872.

Eigler, S., & Dimiev, A. M. (2016). Functionalization and Reduction of Graphene Oxide. In A. M. Dimiev & S. Eigler (Eds.), Graphene Oxide: Fundamentals and Applications (pp. 175-229). John Wiley & Sons, Ltd. https://doi.org/10.1002/9781119069447.ch6

Ergüvenerler, F.; Targan, Ş.; Tirtom, V.N. Removal of Lead from Aqueous Solutions by Low Cost and Waste Biosorbents (Lemon, Bean and Artichoke Shells). *Water Science and Technology* **2020**, *81*, 159–169, doi:10.2166/WST.2020.093.

Esfandiar, N., Nasernejad, B. and Ebadi, T. (2014). Removal of Mn (II) from groundwater by sugarcane bagasse and activated carbon (a comparative study): Application of response surface methodology (RSM). Journal of industrial and engineering chemistry, 20(5), pp.3726-3736.

Ezeonuegbu, B.A., Machido, D.A., Whong Clement, M.Z., Japhet Wisdom, S., Alsharif, K.F., Yaro, C.A., Batiha, G.E.-S. (2021). Agricultural Waste of Sugarcane Bagasse as Efficient Adsorbent for Lead and Nickel Removal from untreated Wastewater: Biosorption, Equilibrium Isotherms, Kinetics and Desorption studies. Biotechnology Reports, 30, e00614. doi:https://doi.org/10.1016/j.btre.2021.e00614.

Fafa, S., & Zazoua, A. (2024). A new electrochemical sensor based on a screen-printed electrode modified with an ion-imprinted PEDOT for the detection and the quantification of Cd(II). Microchemical Journal, 204, 110977. https://doi.org/10.1016/j.microc.2024.110977

Fakhri, Y., Mousavi Khaneghah, A., Hadiani, M. R., Keramati, H., Hosseini Pouya, R., Moradi, B. and da Silva, B. S. (2017). Non-carcinogenic risk assessment induced by heavy metals content of the bottled water in Iran. Toxin Rev. 36, 313–321.

Farivar, F., Yap, P. L., Karunagaran, R. U. & Losic, D. (2021). Thermogravimetric Analysis (TGA) of Graphene Materials: Effect of Particle Size of Graphene, Graphene Oxide and Graphite on Thermal Parameters. C — Journal of Carbon Research, 7, 41.

Fattahi, M., Ezzatzadeh, E., Jalilian, R., & Taheri, A. (2021). Micro solid phase extraction of cadmium and lead on a new ion-imprinted hierarchical mesoporous polymer via dual-template method in river water and fish muscles: Optimization by experimental design. Journal of Hazardous Materials, 403, 123716. https://doi.org/https://doi.org/10.1016/j.jhazmat.2020.123716

Fernando Reboredo, Manuela Simões, Celeste Jorge, Malva Mancuso, Jorge Martinez, Mauro Guerra, José C. Ramalho, Maria Fernanda Pessoa and Fernando Lidon, (2019). Environmental Science and Pollution Research, 26: 2512–2522.

Fu, S. *et al.* (2021). Accurate characterization of full pore size distribution of tight sandstones by low-temperature nitrogen gas adsorption and high-pressure mercury intrusion combination method. Energy Sci Eng, 9, 80–100.

Gebeyehu, H. R. and Bayissa, L. D. (2020) 'Levels of heavy metals in soil and vegetables and associated health risks in Mojo area ', *PLoS ONE*, 15(1), pp. 1–22.

Genchi, G. *et al.* (2020) 'Nickel : Human Health and Environmental Toxicology', *International Journal of Environmental Research and Public Health*, 17(679), pp. 1–21.

Gentry, R., Franzen, A., Van Landingham, C., Greene, T. and Plotzke, K. (2017). A global human health risk assessment for octamethylcyclotetrasiloxane (D4). Toxicol. Lett. 279, 23–41.

Gezahegn, A. M., Feyessa, F. F., Tekeste, E. A. & Beyene, E. M. Chromium Laden Soil, Water, and Vegetables nearby Tanning Industries: Speciation and Spatial Distribution. *J. Chem.* **2021**, (2021).

Gitari, W.M., Ngulube, T., Masindi, V., Gumbo, J.R. (2015). Defluoridation of groundwater using Fe^{3+}-modified bentonite clay: optimization of adsorption conditions, Desalination and Water Treatment, 53(6), 1578-1590.

Gupta, N., Yadav, K.K., Kumar, V., Kumar, S., Chadd, R.P., Kumar, A., 2019. Trace elements in soil-vegetables interface: Translocation, bioaccumulation, toxicity and amelioration - A review. Science of the Total Environment 651, 2927–2942. https://doi.org/10.1016/j.scitotenv.2018.10.047

Gupta, S., Kumar, A. (2019). Removal of nickel(II) from aqueous solution by biosorption on A. barbadensis Miller waste leaves powder. Applied Water Science, 9(4), 1–11. https://doi.org/10.1007/s13201-019-0973-1.

Haider, F.U., Liqun, C., Coulter, J.A., Cheema, S.A., Wu, J., Zhang, R., Wenjun, M., Farooq, M., 2021. Cadmium toxicity in plants: Impacts and remediation strategies. Ecotoxicol Environ Saf 211, 1–22. https://doi.org/10.1016/j.ecoenv.2020.111887

Haque, M. M., & Wong, D. K. Y. (2017). Improved dye entrapment–liberation performance at electrochemically synthesised polypyrrole–reduced graphene oxide nanocomposite films. Journal of Applied Electrochemistry, 47(7), 777-788. https://doi.org/10.1007/s10800-017-1079-9

Hassanpoor, S., & Rouhi, N. (2021). Electrochemical sensor for determination of trace amounts of cadmium (II) in environmental water samples based on MnO2/RGO nanocomposite. International Journal of Environmental Analytical Chemistry, 101(4), 513-532. https://doi.org/10.1080/03067319.2019.1669582

Heravizadeh, O. R., Khadem, M., Nabizadeh, R. & Shahtaheri, S. J. (2019). Synthesis of molecularly imprinted nanoparticles for selective exposure assessment of permethrin: Optimization by response surface methodology. J Environ Health Sci Eng, 17, 393–406.

Hoaghia, M.-A., Cadar, O., Moisa, C., Roman, C., Kovacs, E. (2022). Heavy metals and health risk assessment in vegetables grown in the vicinity of a former non-metallic facility located in Romania, Environmental Science and Pollution Research, 29, 40079–40093.

Hu, J., Sedki, M., Shen, Y., Mulchandani, A., & Gao, G. (2021). Chemiresistor sensor based on ion-imprinted polymer (IIP)-functionalized rGO for Cd(II) ions in water. Sensors and Actuators B: Chemical, 346, 130474. https://doi.org/10.1016/j.snb.2021.130474

Hu, X. jiang; Liu, Y. guo; Zeng, G. ming; You, S. hong; Wang, H.; Hu, X.; Guo, Y. ming; Tan, X. fei; Guo, F. ying Effects of Background Electrolytes and Ionic Strength on Enrichment of Cd(II) Ions with Magnetic Graphene Oxide-Supported Sulfanilic Acid. *J Colloid Interface Sci* **2014**, *435*, 138–144, doi:10.1016/J.JCIS.2014.08.054.

Huang, W., Liu, Y., Wang, N., Song, G., Yin, X., Zhang, L., Ni, X., & Xu, W. (2021). A Sensitive Electrochemical Sensor Based on Ion Imprinted Polymers with Gold Nanoparticles for High Selective Detecting Cd (II) Ions in Real Samples. Journal of Inorganic and Organometallic Polymers and Materials, 31(5), 2043-2053. https://doi.org/10.1007/s10904-021-01892-8

Hussain, S.T.; Khaleefa Ali, S.A. Removal of Heavy Metal by Ion Exchange Using Bentonite Clay. *Journal of Ecological Engineering* **2021**, *22*, 104–111, doi:10.12911/22998993/128865.

International Agency Research on Cancer (IARC). (2004). Some drinking-water disinfectants and contaminants, including arsenic, IARC Monographs on the evaluation of carcinogenic risks to humans, http://monographs.iarc.fr/ENG/Monographs/vol84/mono84.pdf, (Accessed on 18/04/2018).

Islam, S. *et al.* (2015) 'Alteration of Water Pollution Level with the Seasonal Changes in Mean Daily Discharge in Three Main Rivers around Dhaka City, Bangladesh', *Environments*, 2, pp. 280–294. doi: 10.3390/environments2030280.

Jagtap, R., Maher, W. (2015). Measurement of mercury species in sediments and soils by HPLC–ICPMS. Microchemical Journal, 121, 65–98.

Johar, N., Ahmad, I. and Dufresne, A. (2012) "Extraction, preparation, and characterization of cellulose fibers and nanocrystals from rice husk," Industrial Crops and Products, 37(1), 93–99. https://doi.org/10.1016/j.indcrop.2011.12.016.

Kamal, M. Z. U. & Miah, M. Y. Arsenic Speciation Techniques in Soil Water and Plant: An Overview. *Arsen. Monit. Remov. Remediat.* (2021) doi:10.5772/INTECHOPEN.99273.

Kamil, A. F., Abdullah, H. I., Rheima, A. M. & Khamis, W. M. (2021). Modification of hummers presses for synthesis graphene oxide nano-sheets and graphene oxide /Ag nanocomposites. Journal of Ovonic Research, 17, 253–259.

Kamsonlian, S., Suresh, S. and Chand, S. (2011). (2011) "Characterization of Banana and Orange Peels : Biosorption Mechanism," International Journal of Science Technology & Management, 2(4), 1–7.

Karim, A., Raji, Z., Karam, A. and Seddik Khalloufi (2023). Valorization of Fibrous Plant-Based Food Waste as Biosorbents for Remediation of Heavy Metals from Wastewater—A Review. Molecules, 28(10), pp.4205–4205. doi:https://doi.org/10.3390/molecules28104205.

Kaviyarasu, K., Manikandan, E., Paulraj, P., Mohamed, S. B. & Kennedy, J. (2014). One dimensional well-aligned CdO nanocrystal by solvothermal method. J Alloys Compd, 593, 67–70.

Kgabi, D.P.; Ambushe, A.A. Characterization of South African Bentonite and Kaolin Clays. *Sustainability* **2023**, *15*, 12679, doi:10.3390/SU151712679.

Kgabi, D.P., Ambushe, A.A. (2021). Speciation and bioavailability of mercury in sediments from Mokolo River, Limpopo Province, South Africa, Journal of Environmental Science and Health, Part A, https://doi.org/10.1080/10934529.2021.1949918

Kgaphola, M.J., Ramoelo, A., Odindi, J., Mwenge Kahinda, J.M., Seetal, A.R., Musvoto, C., 2023. Impact of land use and land cover change on land degradation in rural semi-arid South Africa: case of the Greater Sekhukhune District Municipality. Environ Monit Assess 195, 1–21. https://doi.org/10.1007/s10661-023-11104-0

Khairiah, J., Lim, K. H., Ahmad-Mahir R. and Ismail, B.S. (2006). Heavy metals from agricultural soils from Cameron Highlands, Pahang and Cheras, Kuala Lumpur, Malaysia. Bulletin of Environmental Contamination Toxicology 77:608–615.

Khan, M.A., Khan, S., Khan, A., Alam, M., 2017. Soil contamination with cadmium, consequences and remediation using organic amendments. Science of the Total Environment 601–602, 1591–1605. https://doi.org/10.1016/j.scitotenv.2017.06.030

Khaskheli, M.I., Memon, S.Q., Siyal, A.N., Khuhawar, M.Y. (2011). Use of Orange Peel Waste for Arsenic Remediation of Drinking Water. Waste and Biomass Valorization, 2(4), 423–433. doi:https://doi.org/10.1007/s12649-011-9081-7.

Kibechu, R. W., Mamo, M. A., Msagati, T. A. M., Sampath, S. & Mamba, B. B. (2014). Synthesis and application of reduced graphene oxide and molecularly imprinted polymers composite in chemo sensor for trichloroacetic acid detection in aqueous solution. Phys. Chem. Earth**,** 76–78, 49–53.

Kien, C.N., Noi, N. V., Son, L.T., Ngoc, H.M., Tanaka, S., Nishina, T., IWasaki, K., 2010. Heavy metal contamination of agricultural soils around a chromite mine in Vietnam. Soil Sci Plant Nutr 56, 344–356. https://doi.org/10.1111/j.1747-0765.2010.00451.x

Kim, M.-S., Lee, H.-Y., & Choi, S.-W. (2023). Research on Physicochemical Properties of Graphene Oxide (GO) and Reduced Graphene Oxide (R-GO). Composites Research, 36(3), 167-172. https://doi.org/10.7234/composres.2023.36.3.167

King, M. Correlation and regression. in *Fisheries Biology, Assessment and Management* 391–440 (John Wiley & Sons, Ltd, 2016). doi:10.1007/978-3-319-43561-9_9.

Kiss, T., Enyedy, É. A. and Jakusch, T. (2017). Development of the application of speciation in chemistry, Coordination Chemistry Reviews, 352, 401–423. doi: 10.1016/j.ccr.2016.12.016.

Kong, D., Qiao, N., Wang, N., Wang, Z., Wang, Q., Zhou, Z., & Ren, Z. (2018). Facile preparation of a nano-imprinted polymer on magnetite nanoparticles for the rapid separation of lead ions from aqueous solution. Physical Chemistry Chemical Physics, 20(18), 12870-12878. https://doi.org/10.1039/c8cp01163j

Kumar, A., Jigyasu, D.K., Kumar, A., Subrahmanyam, G., Mondal, R., Shabnam, A.A., Cabral-Pinto, M.M.S., Malyan, S.K., Chaturvedi, A.K., Gupta, D.K., Fagodiya, R.K., Khan, S.A., Bhatia, A., 2021. Nickel in terrestrial biota: Comprehensive review on contamination, toxicity, tolerance and its remediation approaches. Chemosphere. https://doi.org/10.1016/j.chemosphere.2021.129996

Kumar, P., Kumar, S., Singh, R.P., 2021. High Contamination of Toxic Heavy Metals in Vegetables and Their Associated Health Risk Assessment from Different Vegetable markets of the Metropolitan City, Lucknow, India. Int J Environ Res 15, 837–847. https://doi.org/10.1007/s41742-021-00345-x

Kumar, A.R., Riyazuddin, P. (2010). Preservation of inorganic arsenic species in environmental water samples for reliable speciation analysis, Trends in analytical chemistry, 29, 1212 – 1222.

Kumar, B. L. & Gopal, D. V. R. S. Effective role of indigenous microorganisms for sustainable environment. *3 Biotech* **5**, 867–876 (2015).

Kumari, N.; Mohan, C.; Kumari, N.; Mohan, C. Basics of Clay Minerals and Their Characteristic Properties. *Clay and Clay Minerals* **2021**, doi:10.5772/INTECHOPEN.97672.

Kusumkar, V. V., Galamboš, M., Viglašová, E., Daňo, M. & Šmelková, J. (2021). Ion-imprinted polymers: synthesis, characterization, and adsorption of radionuclides. Mater. 14, 1083.

Kwikima, M. M., Mateso, S. & Chebude, Y. (2021). Potentials of agricultural wastes as the ultimate alternative adsorbent for cadmium removal from wastewater. A review. Sci. African, 13, e00934.

Laizu, J. Speciation of arsenic in vegetables and their correlation with inorganic phosphate level. *Bangladesh J. Pharmacol.* **2**, 88–94 (2008).

Lasheen, M.R., Ammar, N.S. and Ibrahim, H.S. (2012). Adsorption/desorption of Cd (II), Cu (II) and Pb (II) using chemically modified orange peel: Equilibrium and kinetic studies. Solid State Sciences, 14(2), pp.202-210.

Leśniewska, B., Gontarska, M. & Godlewska-Żyłkiewicz, B. Selective Separation of Chromium Species from Soils by Single-Step Extraction Methods: a Critical Appraisal. *Water. Air. Soil Pollut.* **228**, 1–14 (2017).

Letsoalo, M.R., Godeto, T.W., Magadzu, T., Ambushe, A.A. (2018). Quantitative speciation of arsenic in water and sediment samples from Mokolo River in Limpopo Province, South Africa, Analytical Letters, Anal. Lett. 51, 2761–2775.

Letsoalo, M. R., Mamo, M. A. & Ambushe, A. A. (2021a). Simultaneous quantitative speciation of selected toxic elements in water using high-performance liquid chromatography coupled to inductively coupled plasma-mass spectrometry (HPLC-ICP-MS). *Phys. Chem. Earth* 103011.

Letsoalo, M. R., Mamo, M. A. & Ambushe, A. A. (2021b). Synchronous extraction and quantitative speciation of arsenic and chromium in sediments by high-performance liquid chromatography–inductively coupled plasma–mass spectrometry (HPLC-ICP-MS). *Anal. Lett.* 54, 1943–1967.

Letsoalo, M. R., Ambushe, A. A. & Mamo, M. A. (2021). Novel Chemoresistive Sensor for Sensitive Detection of Pb^{2+} Ions Using an Interdigital Gold Electrode Fabricated with a Reduced Graphene Oxide-Based Ion-Imprinted Polymer. ACS Omega, 6, 31528–31538.

Li, W., Xu, S., Chen, Y., Wang, Z., Cao, M., & Liu, Y. (2024). Super-efficient and stable detection of toxic heavy metal by polyethylenimine-modified graphene electrode sensor. Journal of Materials Science: Materials in Electronics, 35(16), 1065. https://doi.org/10.1007/s10854-024-12838-4

Li, W., Xu, S., Li, Z., Liu, L., Wang, Z., & Dai, X. (2024). Highly sensitive electrochemical Cd(II) detector based on ion-imprinted modified glassy carbon electrode. New Journal of Chemistry. https://doi.org/10.1039/d4nj04806g

Li, Z., Ma, Z., van der Kuijp, T. J., Yuan, Z. and Huang, L. (2014). A review of soil heavy metal pollution from mines in China: Pollution and health risk assessment. Sci. Total Environ. 468–469, 843–853.

Liu, P., Wu, Z., Ge, X. & Yang, X. (2019). Hydrothermal synthesis and microwave-assisted activation of starch-derived carbons as an effective adsorbent for naphthalene removal. RSC Adv, 9, 11696–11706.

Luo, X. *et al.* (2020) 'Potentially toxic elements (PTEs) in crops, soil, and water near Xiangtan manganese mine, China: potential risk to health in the foodchain', *Environmental Geochemistry and Health*, 42(7), pp. 1965–1976. doi: 10.1007/s10653-019-00454-9.

Mahmudiono, T. Bokov, D., Widjaja, G., Konstantinov, I.S., Setiyawan, K., Abdelbasset, W.K., Majdi, H.Sh., Kadhim, M.M., Kareem, H.A., Bansal, K. (2022). Removal of heavy metals using food industry waste as a cheap adsorbent. Food Science and Technology, 42, 1-6. doi:https://doi.org/10.1590/fst.111721.

Makgoale, M.M., Addo-Bediako, A., Ayisi, K.K., 2022. DISTRIBUTION PATTERN OF MACROINVERTEBRATE FUNCTIONAL FEEDING GROUPS IN THE STEELPOORT RIVER, SOUTH AFRICA. Appl Ecol Environ Res 20, 189–206. https://doi.org/10.15666/aeer/2001_189206

Mallongi, A., Rauf, A.U., Daud, A., Hatta, M., Al-Madhoun, W., Amiruddin, R., Stang, S., Wahyu, A., Astuti, R.D.P., 2022. Health risk assessment of potentially toxic elements in Maros karst groundwater: a Monte Carlo simulation approach. Geomatics, Natural Hazards, and Risk 13, 338–363. https://doi.org/10.1080/19475705.2022.2027528

Martínez, J., Mendoza, R., de la Torre, M.J., Hidalgo, M.C., 2024. Potentially Toxic Elements (PTEs) Dispersion in Alluvial Deposits from Abandoned Mining Sites. Minerals 14. https://doi.org/10.3390/min14040340

McConnell, J.R., Wilson, A.I., Stohl, A., Arienzo, M.M., Chellman, N.J., Eckhardt, S., Thompson, E.M., Pollard, A.M., Steffensen, J.P., 2018. Lead pollution recorded in Greenland ice indicates European emissions tracked plagues, wars, and imperial expansion during antiquity. Proc Natl Acad Sci U S A 115, 5726–5731. https://doi.org/10.1073/pnas.1721818115

Mohajane, C., Manjoro, M., 2022. Sediment-associated heavy metal contamination and potential ecological risk along an urban river in South Africa. Heliyon 8, 1–9. https://doi.org/10.1016/j.heliyon.2022.e12499

Mohamed, A.E., Rashed, M.N., Mofty, A., 2003. Assessment of essential and toxic elements in some kinds of vegetables. Ecotoxicol Environ Saf 55, 251–260. https://doi.org/10.1016/S0147-6513(03)00026-5

Moskalyk, R.R., Alfantazi, A.M., 2003. Processing of vanadium: A review. Miner Eng. https://doi.org/10.1016/S0892-6875(03)00213-9

Moyo, N.A.G., Rapatsa, M.M., 2019. Trace Metal Contamination and Risk Assessment of an Urban River in Limpopo Province, South Africa. Bull Environ Contam Toxicol 102, 492–497. https://doi.org/10.1007/s00128-019-02564-7

Munyangane, P., Mouri, H., Kramers, J., 2017. Assessment of some potential harmful trace elements (PHTEs) in the borehole water of Greater Giyani, Limpopo Province, South Africa: possible implications for human health. Environ Geochem Health 39, 1201–1219. https://doi.org/10.1007/s10653-016-9887-0

Mahrous, S.S., Galil, E.A.A. and Mansy, M.S. (2022) “Investigation of modified orange peel in the removal of Cd2+, Co2+ and Zn2+ from wastewater,” Journal of Radioanalytical and Nuclear Chemistry, 331(2), pp. 985–997. https://doi.org/10.1007/s10967-021-08166-0.

Malan, M. *et al.* (2015) ‘Heavy metals in the irrigation water , soils and vegetables in the Philippi horticultural area in the Western Cape Province of South Africa’, *Environment Monitoring and Assessment*, 187(4085), pp. 2–8. doi: 10.1007/s10661-014-4085-y.

Manea, D. N., Ienciu, A. A., Ştef, R., Şmuleac, I. L., Gergen, I. I. & Nica, D. V. (2020). Health risk assessment of dietary heavy metals intake from fruits and vegetables grown in selected old mining areas—A case study: The Banat area of southern Carpathians. Int. J. Environ. Res. Public Health, 17, 1–19.

Marcinkowska, M., Barałkiewicz, D. (2016). Multi-elemental speciation analysis by advanced hyphenated technique – HPLC/ICP-MS: A review, Talanta, 161, 177 – 204.

Marcano, D. C., Kosynkin, D. V., Berlin, J. M., Sinitskii, A., Sun, Z., Slesarev, A., Alemany, L. B., Lu, W., & Tour, J. M. (2010). Improved Synthesis of Graphene Oxide. ACS Nano, 4(8), 4806-4814. https://doi.org/10.1021/nn1006368

Markiewicz, B., Komorowicz, I., Sajnóg, A., Belter, M., Barałkiewicz, D. (2015). Chromium and its speciation in water samples by HPLC/ICP-MS – technique establishing metrological traceability: A review since 2000, Talanta, 132, 814 – 828.

Matabane, D.L., Godeto, T.W. Mampa, R.M. Ambushe, A.A. (2021). Sequential Extraction and Risk Assessment of Potentially Toxic Elements in River Sediments, Minerals, 11, 1-18.

Mattusch, J., Wennrich, R., Schmidt, A. C. & Reisser, W. Determination of arsenic species in water, soils and plants. *Fresenius. J. Anal. Chem.* **366**, 200–203 (2000).

Mekonnen, K. N. *et al.* (2015) Assessment of potentially toxic elements in Swiss chard and sediments of Akaki River , Ethiopia, *Toxicological and Environmental Chemistry*, 96(10), pp. 1501–1515.

Menon, S. (201)6. Epidemiological study of clinical signs and symptoms of mercury poisoning in fish consumers residing in five villages along Thane Creek and Ulhas River Estuary near Mumbai, India. Nepals Journals Online. 14, 1.

Mishalanie, E. A., Lesnik, B., Araki, R., & Segall, R. (2016). Validation and Peer Review of U.S. Environmental Protection Agency Chemical Methods of Analysis. Washington DC: U.S. Environmental Protection Agency (EPA)

Mnyipika, S. H., Munonde, T. S., & Nomngongo, P. N. (2021). MnO2@Reduced Graphene Oxide Nanocomposite-Based Electrochemical Sensor for the Simultaneous Determination of Trace Cd(II), Zn(II) and Cu(II) in Water Samples. Membranes, 11(7), 517. https://doi.org/10.3390/membranes11070517

Mo, J., Yang, Q., Zhang, N., Zhang, W., Zheng, Y. & Zhang, Z. (2018). A review on agro-industrial waste (AIW) derived adsorbents for water and wastewater treatment. *J. Environ. Manage.* 227, 395–405.

Moldoveanu, S. C. & David, V. Parameters that Characterize HPLC Analysis. *Essentials Mod. HPLC Sep.* 53–83 (2013) doi:10.1016/B978-0-12-385013-3.00002-1.

Momina; Shahadat, M.; Isamil, S. Regeneration Performance of Clay-Based Adsorbents for the Removal of Industrial Dyes: A Review. *RSC Adv* **2018**, *8*, 24571–24587, doi:10.1039/C8RA04290J.

Montero, J.I.Z., Monteiro, A.S., Gontijo, E.S., Bueno, C.C., de Moraes, M.A. and Rosa, A.H. (2018). High efficiency removal of As (III) from waters using a new and friendly adsorbent based on sugarcane bagasse and corncob husk Fe-coated biochars. Ecotoxicology and environmental safety, 162, pp.616-624.

Morekhure-Mphahlele, R.; Focke, W.W.; Grote, W. Characterisation of Vumba and Ubumba Clays Used for Cosmetic Purposes. *S Afr J Sci* **2017**, *113*, 2–6, doi:10.17159/sajs.2017/20160105.

Moreno-Jiménez, E., Esteban, E. & Peñalosa, J. M. The fate of arsenic in soil-plant systems. *Rev. Environ. Contam. Toxicol.* **215**, 1–37 (2012).

Muchuweti, M., Birkett, J., Chinyanga, E., Zvauya, R., Scrimshaw, M.D., Lester, J. (2006). Heavy metal content of vegetables irrigated with mixtures of wastewater and sewage sludge in Zimbabwe: implications for human health, Agriculture, Ecosystems & Environment, 112 41-48.

Mudzielwana, R. Synthesis and Potential Application of Fe3+/Mn2+ Bimetal and Hexadecyltrimethylammonium Bromide (HDTMA-Br) Modified Clayey Soils for Arsenic Removal in Groundwater, University of Venda, 2019.

Nde, S.C., Mathuthu, M., Massoukou, R.Y.M., Bett, S.K., Richard, G., Oluwadamilare, O.P., 2021. Modelling the dynamics of the cancer risk due to potentially toxic elements in agricultural soils, in the upper Crocodile River catchment, North-West province, South Africa. Ecotoxicol Environ Saf 211, 1–13. https://doi.org/10.1016/j.ecoenv.2021.111961

Niño-Savala, A.G., Zhuang, Z., Ma, X., Fangmeier, A., Li, H., Tang, A., Liu, X., 2019. Cadmium pollution from phosphate fertilizers in arable soils and crops: An overview. Front Agric Sci Eng 6, 419–430. https://doi.org/10.15302/J-FASE-2019273

Niu, C., Dong, M., Niu, Y., 2023. Lead toxicity and potential therapeutic effect of plant-derived polyphenols. Phytomedicine 114, 1–11. https://doi.org/10.1016/j.phymed.2023.154789

Nsaka, N. C., Mccrindle, R. I. and Ambushe, A. A. (2018) Levels of potentially toxic metals in water , sediment and peat from Wonderfonteinspruit , North West Province , South Africa, *Journal of Environmental Science and Health, Part A*, 53(10), pp. 907–914. doi: 10.1080/10934529.2018.1462894.

Neeti, K. and Prakash, T. (2013). 'Effects of Heavy Metal Poisoning during Pregnancy', International Research Journal of Environment Sciences, 2(1), pp. 88–92.

Neha Gupta, Krishna Kumar Yadav, Vinit Kumar, Shiv Prasad, Marina M. S. Cabral-Pinto, Byong-Hun Jeon, Sandeep Kumar, Magda H. Abdellattif and Abdulmohsen Khalaf Dhahi Alsukaibia (2022). Investigation of Heavy Metal Accumulation in Vegetables and Health Risk to Humans From Their Consumption, Frontiers in Environmental Science, doi: 10.3389/fenvs.2022.791052

Nica, D. V., Bura, M., Gergen, I., Harmanescu, M. and Borden, D. M. (2012). Bioaccumulative and Concho logical assessment of heavy metal transfer in a soil-plant-snail food chain, Chemistry Central Journal, 6 (1): 55.

Nkuna, Z., Mamakoa, E., Mothetha, M. (2017). The important role of springs in South Africa's rural water supply: The case study of two rural communities in South Africa, Council for Scientific and Industrial Research (CSIR), South Africa.

Obijole, O.A., Gitari, M.W., Ndungu, P.G., Samie, A. (2019). Mechanochemically Activated Aluminosilicate Clay Soils and their Application for Defluoridation and Pathogen Removal from Groundwater, Int. J. Environ. Res. Public Health, 16, 654.

Obsa, A.L.; Shibeshi, N.T.; Mulugeta, E.; Workeneh, G.A. Bentonite/Amino-Functionalized Cellulose Composite as Effective Adsorbent for Removal of Lead: Kinetic and Isotherm Studies. *Results in Engineering* **2024**, *21*, doi:10.1016/j.rineng.2024.101756.

Ochieng, G.M., Seanego, E.S., Nkwonta, O.I. (2010). Impacts of mining on water resources in South Africa: A review, Scientific Research and Essays, 5, 3351 – 3357.

Olifant, G.E., Mavumengwana, V., Hümmelgen, I.A., Mamo, M.A. (2019). Understanding the sensing mechanism of carbon nanoparticles: MnO_2 –PVP composites sensors using in situ FTIR—online LCR meter in the detection of ethanol and methanol vapor, J. Mater. Sci. Mater. Electron, 30, 3552–3562.

Oliveira, H., 2012. Chromium as an Environmental Pollutant: Insights on Induced Plant Toxicity. J Bot 2012, 1–8. https://doi.org/10.1155/2012/375843

Ondo, N. *et al.* (2021) 'Phytoremediation Potential of Vetiver Grass (Vetiveria Zizanioides) in Two Mixed Heavy Metal Contaminated Soils from the Zoundweogo and Boulkiemde Regions of Burkina Faso (West Africa)', *Journal of Geoscience and Environment Protection*, 9, pp. 73–88. doi: 10.4236/gep.2021.911006.

Onyedikachi, U. B., Belonwu, C. D. and Wegwu, M. O. (2019). Health Risk Assessment of Chromium, Manganese and Arsenic through the Consumption of Food from Industrial Areas in South Eastern States of Nigeria. Annu. Res. Rev. Biol. 1–20 doi:10.9734/arrb/2019/v31i630067.

Oosthuizen, M., Wright, C., Matooane, M. and Phala, N. (2015). Human health risk assessment of airborne metals to a potentially exposed community: a screening exercise. Clean Air J. 25, 51–57.

Owolabi, I. A., Mandiwana, K. L. & Panichev, N. Speciation of chromium and vanadium in medicinal plants. *South African J. Chem.* **69**, 67–71 (2016).

Ozunu, A., 2015. Accumulation of heavy metals in soils and alluvial deposits of Lăpuş river, Maramures county, Romania, Article in Carpathian Journal of Earth and Environmental Sciences.

Prabawa, I.D.G.P.; Lestary, R.Y.; Hamdi, S.; Sunardi, S. Modified Physical Properties of Kaolin by Intercalation and Exfoliation Method. *IOP Conf Ser Mater Sci Eng* **2020**, *980*, doi:10.1088/1757-899X/980/1/012009.

Paerl, H.W., Otten, T.G., Kudela, R., 2018. Mitigating the Expansion of Harmful Algal Blooms Across the Freshwater-to-Marine Continuum. Environ Sci Technol 52, 5519–5529. https://doi.org/10.1021/acs.est.7b05950

Panda, G., Pobi, K.K., Gangopadhyay, S., Gope, M., Rai, A.K., Nayek, S., 2022. Contamination level, source identification and health risk evaluation of potentially toxic elements (PTEs) in groundwater of an industrial city in eastern India. Environ Geochem Health 44, 2685–2709. https://doi.org/10.1007/s10653-021-01071-1

Pant, R.R., Bishwakarma, K., Nepal, J., Paudel, S., Chand, M.B., Qaisar, F.U.R., Pal, K.B., Thapa, L.B., Wang, G., 2021. Seasonal Variations and Health Risk Assessment of Trace Elements in Seti River Basin, Gandaki Province, Nepal. Bull Environ Contam Toxicol 107, 441–448. https://doi.org/10.1007/s00128-021-03288-3

Pelcová, P., Ridošková, A., Hrachovinová, J., Grmela, J., 2021. Evaluation of mercury bioavailability to vegetables in the vicinity of cinnabar mine. Environmental Pollution 283, 1–10. https://doi.org/10.1016/j.envpol.2021.117092

Rahman, S.H., Khanam, D., Adyel, T.M., Islam, M.S., Ahsan, M.A., Akbor, M.A., 2012. Assessment of heavy metal contamination of agricultural soil around Dhaka Export Processing Zone (DEPZ), Bangladesh: Implication of seasonal variation and indices. Applied Sciences (Switzerland) 2, 584–601. https://doi.org/10.3390/app2030584

Randall, P.M., Chattopadhyay, S. (2013). Mercury contaminated sediment sites – An evaluation of remedial options. Environ. Res. 125, 131–149.

Raul, C., Bharti, V.S., Dar Jaffer, Y., Lenka, S. and Krishna, G. (2020). Sugarcane bagasse biochar: Suitable amendment for inland aquaculture soils. Aquaculture Research, 52(2), 643–654. doi:https://doi.org/10.1111/are.14922.

Rasheed, H., Slack, R. and Kay, P. (2016). Human health risk assessment for arsenic: A critical review. Crit. Rev. Environ. Sci. Technol. 46, 1529–1583.

Rathi, B.S., Kumar, P.S., Show, P.L. (2021). A review on effective removal of emerging contaminants from aquatic systems: Current trends and scope for further research. Journal of Hazardous Materials, 409. https://doi.org/10.1016/j.jhazmat.2020.124413.

Rockafellow-Baldoni, M., Spayd, S. E., Hong, J. Y., Meng, Q., Ohman-Strickland, P. and Robson, M. G. (2018). Arsenic exposure and cancer risk reduction with local ordinance requiring whole-house dual-tank water treatment systems. Hum. Ecol. Risk Assess. 24, 1256–1267.

Saadatkhah, N., Carillo Garcia, A., Ackermann, S., Leclerc, P., Latifi, M., Samih, S., Patience, G.S. and Chaouki, J. (2019). Experimental methods in chemical engineering: Thermogravimetric analysis—TGA. The Canadian Journal of Chemical Engineering, 98(1), 34–43. doi:https://doi.org/10.1002/cjce.23673.

Saini, R.K., Nile, S.H., Park, S.W., 2015. Carotenoids from fruits and vegetables: Chemistry, analysis, occurrence, bioavailability and biological activities. Food Research International 76, 735–750.

SANS, 2015. South African National Standards 241-1 Drinking water: part 1: microbiological, physical, aesthetic and chemical determinands., Second edition. ed. SABS, Pretoria.

SANS (2015) The South African National Standards (SANS) for drinking water.

Sarkar, B. et al. (2012). Bioreactive organoclay: A new technology for environmental remediation, Critical Reviews in Environmental Science and Technology, 42(5), pp. 435–488. doi: 10.1080/10643389.2010.518524.

Sarker, T.C., Azam, S.M.G.G., El-Gawad, A.M.A., Gaglione, S.A. and Bonanomi, G. (2017). Sugarcane bagasse: a potential low-cost biosorbent for the removal of hazardous materials. Clean Technologies and Environmental Policy, 19(10), pp.2343-2362.

Sarkheil, H. and Tavakoli, J. (2015). Oil-polluted water treatment using nano size bagasse optimized-isotherm study. European Online Journal of Natural and Social Sciences, 4(2), pp.392-412.

Schmidt, L., Landero, J.A., Santos, R.F., Mesko, M.F., Mello, P.A., Erico M. M., Flores, E.M.M., Caruso, J.A. (2017). Arsenic speciation in seafood by LC-ICP-MS/MS: method development and influence of culinary treatment, J. Anal. At. Spectrom., 32, 1490–1499.

Schmidt, M.P.; Siciliano, S.D.; Peak, D. Spectroscopic Quantification of Inner-and Outer-Sphere Oxyanion Complexation Kinetics: Ionic Strength and Background Cation Effect on Sulfate Adsorption to Hematite. *ACS Earth Space Chem* **2020**, *4*, 1765–1776, doi:10.1021/ACSEARTHSPACECHEM.0C00149/SUPPL_FILE/SP0C00149_SI_001.PDF.

Scott, D., Keoghan, J. M. and Allan, B. E. (1996). Native and low input grasses—a New Zealand high country perspective. Journal of Agricultural Research, 39, 499 – 512.

Selmi, T., Seffen, M., Celzard, A., Fierro, V. (2018). Effect of the adsorption pH and temperature on the parameters of the Brouers–Sotolongo models. Environmental Science and Pollution Research, 27(19), 23437–23446. doi:https://doi.org/10.1007/s11356-018-3835-8.

Shaheen, N., Irfan, N. M., Khan, I. N., Islam, S., Islam, M. S. and Ahmed, M. K. (2016). Presence of heavy metals in fruits and vegetables: health risk implications in Bangladesh. *Chemosphere*, 152, 431 – 438.

Sharafi, K., Yunesian, M., Nodehi, R. ., Mahvi, A. . & Pirsaheb, M. (2019). A systematic literature review for some toxic metals in widely consumed rice types (domestic and imported) in Iran: Human

health risk assessment, uncertainty and sensitivity analysis - ScienceDirect. Ecotoxicol. Environ. Saf. 176, 64–75.

Sharma, R. K., Agrawal, M. and Marshall, F. M. (2008). Heavy metal (Cu, Zn, Cd and Pb) contamination of vegetables in urban India: a case study in Varanasi. Environmental Pollution, 154, 254–263.

Sharma, S. D. (2020). Risk assessment via oral and dermal pathways from heavy metal polluted water of Kolleru lake - A Ramsar wetland in Andhra Pradesh, India. Environ. Anal. Heal. Toxicol. 35, e2020019.

Singh, U.K., Ramanathan, A.L., Subramanian, V., 2018. Groundwater chemistry and human health risk assessment in the mining region of East Singhbhum, Jharkhand, India. Chemosphere 204, 501–513. https://doi.org/10.1016/j.chemosphere.2018.04.060

Signes-Pastor, A. J., Mitra, K., Sarkhel, S., Hobbes, M., Burló, F., De Groot, W. T. & Carbonell-Barrachina, A. A. Arsenic speciation in food and estimation of the dietary intake of inorganic arsenic in a rural village of West Bengal, India. *J. Agric. Food Chem.* **56**, 9469–9474 (2008).

Singh, R.; Bhateria, R. Experimental and Modeling Process Optimization of Lead Adsorption on Magnetite Nanoparticles via Isothermal, Kinetics, and Thermodynamic Studies. *ACS Omega* **2020**, *5*, 10826–10837, doi:10.1021/ACSOMEGA.0C00450/ASSET/IMAGES/LARGE/AO0C00450_0005.JPEG.

Sivakumar, A., Dai, L., Sahaya Jude Dhas, S., Martin Britto Dhas, S. A., Eniya, P., Suresh Kumar, R., & Almansour, A. I. (2024). Synthesis of crystalline graphite from disordered graphite by acoustic shock waves: Hot-spot nucleation approach. Applied Surface Science, 655, 159632. https://doi.org/https://doi.org/10.1016/j.apsusc.2024.159632

Ssemugabo, C., Bradman, A., Ssempebwa, J. C., Sillé, F. & Guwatudde, D. An assessment of health risks posed by consumption of pesticide residues in fruits and vegetables among residents in the Kampala Metropolitan Area in Uganda. *Int. J. Food Contam. 2022 91* **9**, 1–14 (2022).

Sternik, D.; Gładysz-Płaska, A.; Grabias, E.; Majdan, M.; Knauer, W. A Thermal, Sorptive and Spectral Study of HDTMA-Bentonite Loaded with Uranyl Phosphate. *J Therm Anal Calorim* **2017**, *129*, 1277–1289, doi:10.1007/S10973-017-6384-3/FIGURES/10.

Strawn, D.G. Sorption Mechanisms of Chemicals in Soils. *Soil Systems 2021, Vol. 5, Page 13* **2021**, *5*, 13, doi:10.3390/SOILSYSTEMS5010013.

Suciu, N.A., De Vivo, R., Rizzati, N., Capri, E., 2022. Cd content in phosphate fertilizer: Which potential risk for the environment and human health? Curr Opin Environ Sci Health 30. https://doi.org/10.1016/j.coesh.2022.100392

Sultana, M. S., Rana, S., Yamazaki, S., Aono, T. & Yoshida, S. Health risk assessment for carcinogenic and non-carcinogenic heavy metal exposures from vegetables and fruits of Bangladesh. *Cogent Environ. Sci.* **3**, (2017).

Sun, J., Hu, G., Yu, R., Lin, C., Wang, X. & Huang, Y. (2017). Human health risk assessment and source analysis of metals in soils along the G324 Roadside, China, by Pb and Sr isotopic tracing. Geoderma, 305, 293–304.

Tadesse, S.H. Application of Ethiopian Bentonite for Water Treatment Containing Zinc. *Emerg Contam* **2022**, *8*, 113–122, doi:10.1016/J.EMCON.2022.02.002.

Teng, Y., Jiao, X., Wang, J., Xu, W., Yang, J., 2009. Environmentally geochemical characteristics of vanadium in the topsoil in the Panzhihua mining area, Sichuan Province, China. Chinese Journal of Geochemistry 28, 105–111. https://doi.org/10.1007/s11631-009-0105-y

Tao, W. *et al.* (2023). Revealing the Chemical Nature of Functional Groups on Graphene Oxide by Integrating Potentiometric Titration and Ab Initio Calculations. ACS Omega, 8, 24128–24679.

Taverniers, I., Loose, M. De and Bockstaele, E. Van (2004) 'laboratory . II . Analytical method validation and quality assurance', *Trends in Analytical Chemistry*, 23(8), pp. 1–18. doi: 10.1016/j.trac.2004.04.001.

Tchounwou, P. B., Yedjou, C. G., Patlolla, A. K. & Sutton, D. J. Heavy metal toxicity and the environment. *EXS* **101**, 133–164 (2012).

Tiwari, G. & Tiwari, R. Bioanalytical method validation: An updated review. *Pharm. Methods* **1**, 25 (2010).

Tseng, T. R., Yang, C. H., Lu, H. C., Liu, C. P., & Cheng, B. M. (2024). Analysis of Carbon Materials with Infrared Photoacoustic Spectroscopy. Anal Chem, 96(26), 10732-10737. https://doi.org/10.1021/acs.analchem.4c01797

Tulcan, R.X.S., Ouyang, W., Guo, Z., Lin, C., Cui, X., Hu, J., He, M., 2023. Industrial impacts on vanadium contamination in sediments of Chinese rivers and bays. Science of the Total Environment 873, 1–12. https://doi.org/10.1016/j.scitotenv.2023.162379

Tulcan, R.X.S., Ouyang, W., Lin, C., He, M., Wang, B., 2021. Vanadium pollution and health risks in marine ecosystems: Anthropogenic sources over natural contributions. Water Res 207, 1–12. https://doi.org/10.1016/j.watres.2021.117838

United States Environmental Protection Agency (2021) Field measurement of oxidation reducrion potential.

United States Environmental Protection Agency. 2010. Contract laboratory program for national functional guidelines for inorganic data review. Washington, USA: US EPA.

US EPA. Data Validation Standard Operating Procedures for Contract Laboratory Program US-EPA, Region 4, SESD, Athens, Georgia Inorganic Data By Inductively Coupled Plasma – Atomic Emission Spectroscopy And Inductively Coupled Plasma – Mass Spectroscopy. 1–35 (2011).

Vallius, H., 2015. Applying sediment quality guidelines on soft sediments of the Gulf of Finland, Baltic Sea. Mar Pollut Bull 98, 314–319. https://doi.org/10.1016/j.marpolbul.2015.06.036

Van Vuuren, L. (2014). Research builds body of knowledge to protect waterberg rivers, Water Wheel, 13(2), 8–11.

Varma, A.K. and Mondal, P. (2016) "Physicochemical Characterization and Pyrolysis Kinetic Study of Sugarcane Bagasse Using Thermogravimetric Analysis," Journal of Energy Resources Technology, Transactions of the ASME, 138(5), pp. 1–11. https://doi.org/10.1115/1.4032729.

Venter, A. D., Beukes, J. P., Gideon van Zyl, P., Josipovic, M., Jaars, K. & Vakkari, V. Regional atmospheric Cr(VI) pollution from the Bushveld Complex, South Africa. *Atmos. Pollut. Res.* **7**, 762–767 (2016).

Viprya, P., Kumar, D., & Kowshik, S. (2023). Study of Different Properties of Graphene Oxide (GO) and Reduced Graphene Oxide (rGO). Engineering Proceedings, 59(1), 84. https://doi.org/10.3390/engproc2023059084

Wackerlig, J. and Schirhagl, R. (2016). Applications of molecularly imprinted polymer nanoparticles and their advances toward industrial use: A review. Anal Chem. 88, 250–261.

Wahyuni, N.; Zissis, G.; Mouloungui, Z. Characterization of Acid Sites on Modified Kaolinite by FTIR Spectra of Pyridine Adsorbed. *AIP Conf Proc* **2018**, *2026*, doi:10.1063/1.5065002.

Wan Ngah, W. S. and Hanafiah, M. A. K. M. (2008). Removal of heavy metal ions from wastewater by chemically modified plant wastes as adsorbents: A review. Bioresour. Technol. 99, 3935–3948.

Wang, B. B. (2021) 'Research on drinking water purification technologies for household use by reducing total dissolved solids (TDS)', *PLoS ONE*, 16(9), pp. 1–14. doi:

10.1371/journal.pone.0257865.

Wang, S., Zhang, M., Li, B., Xing, D., Wang, X., Wei, C., Jia, Y. (2012). Comparison of mercury speciation and distribution in the water column and sediments between the algal type zone and the macrophytic type zone in a hypereutrophic lake (Dianchi Lake) in Southwestern China. Science of the Total Environment, 417-418, 204–213.

Wang, J., Hu, J., Hu, S., Gao, G., & Song, Y. (2020). A Novel Electrochemical Sensor Based on Electropolymerized Ion Imprinted PoPD/ERGO Composite for Trace Cd(II) Determination in Water. Sensors, 20(4), 1004. https://doi.org/10.3390/s20041004

Wang, L., Hu, J., Wei, W., Xiao, S., Wang, J., Song, Y., Li, Y., Gao, G., & Qin, L. (2023). An Electrochemical Sensor Based on Three-Dimensional Porous Reduced Graphene and Ion Imprinted Polymer for Trace Cadmium Determination in Water. Sensors, 23(23), 9561. https://doi.org/10.3390/s23239561

Wilbur, S., Abadin, H., Fay, M., Yu, D., Tencza, B. & Ingerman, L. *Wilbur, S., Abadin, H., Fay, M., Yu, D., Tencza, B. Toxicological Profile for Chromium. Atlanta (GA): US Department of Health and Human Services*. (Public Health Service, Agency for Toxic Substances and Disease Registry, 2012).

Witthuhn, B. et al. (2005). Sorption and biodegradation of 2,4-dichlorophenol in the presence of organoclays, Applied Clay Science. Elsevier, 28(1-4 SPEC. ISS.), 55–66. doi: 10.1016/j.clay.2004.01.003.

Witthuhn, B. et al. (2006) Organoclays for aquifer bioremediation: Adsorption of chlorobenzene on oganoclays and its degradation by Rhodococcus B528, in Water, Air, and Soil Pollution: Focus. Springer, pp. 317–329. doi: 10.1007/s11267-005-9025-y.

WHO, 2017. Guidelines for Drinking-water Quality FOURTH EDITION INCORPORATING THE FIRST ADDENDUM, 4th edition. ed.

WHO, 1988. Evaluation of certain food additives and contaminants : thirty-third report of the Joint FAO/WHO Expert Committee on Food Additives [meeting held in Geneva from 21 to 30 March 1988] [WWW Document]. Technical report series, Geneva. URL https://apps.who.int/iris/handle/10665/39252 (accessed 3.8.23).

World Health Organization (2017) *Guidelines for drinking water - quality*. 4th edn. Switzerland: World Health Organization (WHO).

World Health Organization. *WHO human health risk assessment toolkit: chemical hazards. World Health Organization*. (IPCS harmonization project document xv, 2010).

World Health Organisation (WHO). (1996). Guidelines for drinking water quality, http://www.drinkadria.eu/fileadmin/user_upload/FB1_Deliverable_Act_6.1_period2_Annex4_WHO_Guidelines_for_Drinking_-_water_Quality.pdf, (Accessed on 14/04/2018).

Wright, M.T., Belitz, K., 2010. Factors controlling the regional distribution of vanadium in groundwater. Ground Water 48, 515–525. https://doi.org/10.1111/j.1745-6584.2009.00666.x

Xiao, W., Zhang, Y., Li, T., Chen, B., Wang, H., He, Z. & Yang, X. Reduction Kinetics of Hexavalent Chromium in Soils and Its Correlation with Soil Properties. *J. Environ. Qual.* **41**, 1452–1458 (2012).

Xiao, S., Hu, J., Wang, J., Song, Y., Li, Y., Gao, G., & Qin, L. (2021, 25-29 April 2021). In-situ deposited ion-imprinted polymers for electrochemical detection of trace cadmium in water. 2021 IEEE 16th International Conference on Nano/Micro Engineered and Molecular Systems (NEMS).

Xu, Y. et al. (2018). Biochar modulates heavy metal toxicity and improves microbial carbon use efficiency in soil, Science of the Total Environment, 621, pp. 148–159. doi: 10.1016/j.scitotenv.2017.11.214.

Yan, S., Yu, W., Yang, T., Li, Q. and Guo, J. (2022). The Adsorption of Corn Stalk Biochar for Pb and Cd: Preparation, Characterization, and Batch Adsorption Study. Separations, 9(2), 1-22. doi:https://doi.org/10.3390/separations9020022.

Yang, J., Ma, S. and Zhou, J. (2018) 'Heavy metal contamination in soils and vegetables and health risk assessment of inhabitants in Daye , China', *Journal of International Medical Research*, 46(8), pp. 3374–3387. doi: 10.1177/0300060518758585.

Yang, J., Chen, L., Liu, L., Shi, W., Meng, X. (2014). Comprehensive risk assessment of heavy metals in lake sediment from public parks in Shanghai, Ecotoxicology and Environmental Safety, 102, 129-135.

Yang, L. et al. (2003). Chemical and Biological Regeneration of HDTMA-Modified Montmorillonite after Sorption with Phenol, Environmental Science and Technology. American Chemical Society, 37(21), pp. 5057–5061. doi: 10.1021/es0342493

Yap, P. L., Kabiri, S., Tran, D. N. H. & Losic, D. (2019). Selective and Highly Efficient Adsorption of Mercury. ACS Appl Mater Interfaces**,** 11, 6350–6362.

Yaradoddi, J.S., Banapurmath, N.R., Ganachari, S.V., Soudagar, M.E.M., Sajjan, A.M., Kamat, S., Mujtaba, M.A., Shettar, A.S., Anqi, A.E., Safaei, M.R., Elfasakhany, A., Haque Siddiqui, M.I. and Ali, M.A. (2021). Bio-based material from fruit waste of orange peel for industrial applications. Journal of Materials Research and Technology, 17. doi:https://doi.org/10.1016/j.jmrt.2021.09.016.

Yeasmin Nahar Jolly, Ashraful Islam and Shawkat Akbar (2013). Transfer of metals from soil to vegetables and possible health risk assessment, SpringerPlus, 2013, 2:385.

Yin, X., Ke, T., Zhu, H., Xu, P., Wang, H. (2023). Efficient Removal of Heavy Metals from Aqueous Solution Using Licorice Residue-Based Hydrogel Adsorbent. Gels, 9(7), 559–559. doi:https://doi.org/10.3390/gels9070559.

Yruela, I., 2009. Copper in plants: acquisition, transport and interactions. Functional Plant Biology 36, 409–430. https://doi.org/10.1071/FP08288

Yu, H., Zhang, B., Bulin, C., Li, R., Xing, R. (2016). High-efficient Synthesis of Graphene Oxide Based on Improved Hummers Method, Sci Rep 6, 36143.

Yu, L., Sun, L., Zhang, Q., Zhou, Y., Zhang, J., Yang, B., Xu, B., & Xu, Q. (2022). Nanomaterials-Based Ion-Imprinted Electrochemical Sensors for Heavy Metal Ions Detection: A Review. Biosensors, 12(12), 1096. https://doi.org/10.3390/bios12121096

Yue, C., Chong, K.C., Eng, C.C., Loh L.S. (2016). Utilization of Infused Tea Leaves for the Removal of Pb and Cd Ions from Aqueous Solution: Equilibrium and Kinetic Studies. 8(5), 568–582. doi:https://doi.org/10.4236/jwarp.2016.85047.

Zhang, W., Chen, Y., Qi, Y. & Hong, C. Seasonal variations of mercury levels and human health risk in vegetables from Arid Oasis (Shihezi city), Xinjiang, Northwest China. *Hum. Ecol. Risk Assess.* **24**, 122–136 (2018).

Zhang, Y., Liu, Y., Xu, W., Huang, W., Chen, T., Ding, H., Wang, B., & Yang, W. (2024). Novel electrochemical sensor based on rGO@TiO2 composite material and ion-imprinted polymer

modification for highly selective detection of cadmium ions in real samples. Ionics, 30(4), 2345-2355. https://doi.org/10.1007/s11581-024-05410-x

Zhang, Y., Xu, W., Liu, Y., Huang, W., & Yang, W. (2023). A novel electrochemical ion imprinting sensor modified with carbon nanocomposites and its high selectivity for cadmium ion detection in real samples. Polymer International, 72(12), 1096-1103. https://doi.org/10.1002/pi.6558

Zhu, J., Yin, H., Wang, Y., Wang, L., Geng, X., & Deng, Y. (2024). Conformational change-based fluorometric aptasensor for sensitive cadmium(<scp>ii</scp>) detection in fruits and vegetables. Analytical Methods, 16(34), 5826-5834. https://doi.org/10.1039/d4ay01333f

Zhu, R.; Zhou, Q.; Zhu, J.; Xi, Y.; He, H. Organo-Clays as Sorbents of Hydrophobic Organic Contaminants: Sorptive Characteristics and Approaches to Enhancing Sorption Capacity. *Clays Clay Miner* **2015**, *63*, 199–221, doi:10.1346/CCMN.2015.0630304.

Zondo, S., 2021. GROWING KWAZULU-NATAL TOGETHER Sources of heavy metals in agrochemicals.